



HAL
open science

3D Printing and Characterization of PLA Scaffolds for Layer-by-Layer BioAssembly in Tissue Engineering

Vera Guduric

► **To cite this version:**

Vera Guduric. 3D Printing and Characterization of PLA Scaffolds for Layer-by-Layer BioAssembly in Tissue Engineering. Human health and pathology. Université de Bordeaux, 2017. English. NNT : 2017BORD0858 . tel-01865824

HAL Id: tel-01865824

<https://theses.hal.science/tel-01865824>

Submitted on 2 Sep 2018

HAL is a multi-disciplinary open access archive for the deposit and dissemination of scientific research documents, whether they are published or not. The documents may come from teaching and research institutions in France or abroad, or from public or private research centers.

L'archive ouverte pluridisciplinaire **HAL**, est destinée au dépôt et à la diffusion de documents scientifiques de niveau recherche, publiés ou non, émanant des établissements d'enseignement et de recherche français ou étrangers, des laboratoires publics ou privés.

THESIS PRESENTED
TO OBTAIN THE GRADE OF

PhD

**OF THE UNIVERSITY OF BORDEAUX
AND THE UNIVERSITY OF NOVI SAD**

DOCTORAL SCHOOL OF LIFE AND HEALTH SCIENCES
SPECIALTY: CELLULAR BIOLOGY AND PATHOPHYSIOLOGY

By Vera GUDURIC

**3D Printing and Characterization of PLA Scaffolds for
Layer-by-Layer
BioAssembly in Tissue Engineering**

Thesis directors: Pr Sylvain CATROS and Dr Ognjan LUZANIN

Defended on the 13th of December 2017

Members of the jury:

Mr LESCLOUS Philippe	Professor	University of Nantes	President, Reporter
Mr PAUTHE Emmanuel	Professor	University of Cergy	Reporter
Mrs BLAZIC Larisa	Professor	University of Novi Sad	Member
Mrs KUHN Liisa	Associate professor	University of Connecticut	Member
Mr LUZANIN Ognjan	Associate professor	University of Novi Sad	Director
Mr CATROS Sylvain	Professor	University of Bordeaux	Director

Title: 3D Printing and Characterization of PLA Scaffolds for Layer-by-Layer BioAssembly in Tissue Engineering

Abstract:

Tissue Engineering (TE) is “an interdisciplinary field that applies principles of engineering and the life sciences toward development of biological substitutes that restore, maintain, or improve tissue function”. The First application of TE is to replace damaged tissues by artificial cell-materials products of tissue engineering (TE). Another TE application is to produce 2 or 3 dimensional (2D and 3D) models for biological and pharmacological *in vitro* studies. These models or tissue replacements can be fabricated using a combination of different interdisciplinary methods of medicine, biology, chemistry, physics, informatics and mechanics, providing specific micro-environment with different cell types, growth factors and matrix.

One of the major challenges of tissue engineering is related to limited cell penetration in the inner parts of porous biomaterials. Poor cell viability in the center of engineered tissue is a consequence of limited oxygen and nutrients diffusion due to insufficient vascular network within the entire construct. Layer-by-layer (LBL) BioAssembly is a new approach based on assembly of small cellularized constructs that may lead to homogenous cell distribution and more efficient three dimensional vascularization of large tissue engineering constructs.

Our hypothesis is that LBL Bioassembly approach is more suitable for bone regeneration than conventional tissue engineering approach. The primary objective of this thesis was to evaluate the advantages of LBL Bioassembly approach using 3D-printed polymer membranes seeded with human primary cells. We have evaluated the efficiency of vascular network formation *in vivo* within entire 3D tissue engineering construct using LBL bioassembly approach and comparing it to the conventional approach based on seeding of cells on the surface of massive 3D scaffolds. There was no significant difference in number of formed blood vessels in 3D at the outer parts of constructs implanted subcutaneously in mice 8 weeks post-implantation. But in the inner parts of implants which were not in direct contact with a host tissue, we could observe statistically more blood vessel formation when LBL bioassembly approach was used. This vascular network formation was more important in the case of co-cultures than mono-cultures of HBMSCs.

There were several secondary objectives in this work. The first was to fabricate cellularized 3D constructs for bone tissue engineering using poly(lactic) acid (PLA) membranes and human primary cells: human bone marrow stroma cells (HBMSCs) isolated from the bone marrow, and endothelial progenitor cells (EPCs) isolated from the umbilical cord blood. Then, we have compared different Additive manufacturing technologies to fabricate scaffolds: direct 3D printing (3DP) starting from PLA powder dissolved in chloroform and fused deposition modelling (FDM) using a commercial or a custom-made printer with different resolutions.

The custom-made printer equipped with 100 μm nozzle allowed the highest level of printing resolution concerning pores shape and size. In the meantime we evaluated different stabilization systems for layer-by-layer assembling of PLA membranes with human primary cells: the use of 3D printed PLA clips provided the most efficient stabilization to stack PLA membranes in 3D. Another advantage of this stabilization system is that it could be implanted together with LBL constructs. Then we investigated the most suitable cell culture system for such constructs and we observed more efficient cell proliferation and differentiation when co-culture system is used, comparing to mono-cultures.

LBL bioassembly approach seems to be suitable solution for efficient vascularization within entire large 3D tissue engineering constructs especially when co-cultures of mesenchymal and endothelial cells are used.

Keywords:

3D printing – Poly(lactic) acid – Layer-by-Layer BioAssembly – Bone Tissue Engineering – Biofabrication

Titre : Impression 3D et Caractérisation des Scaffolds en PLA pour Assemblage Couche par Couche en Ingénierie Tissulaire

Résumé :

L'Ingénierie tissulaire (IT) est un domaine interdisciplinaire qui applique les principes de l'ingénierie et des sciences de la vie au développement de substituts biologiques afin de restaurer, maintenir ou améliorer la fonction tissulaire. Sa première application consiste à remplacer les tissus endommagés par des produits cellulaires artificiels. Une autre application de l'IT est basée sur la production des modèles en 2 et 3 dimensions (2D et 3D) pour des études biologiques et pharmacologiques *in vitro*. Ces modèles ou remplacements de tissus peuvent être fabriqués en utilisant des différentes méthodes de médecine, biologie, chimie, physique, informatique et mécanique, fournissant un micro-environnement spécifique avec différents types de cellules, facteurs de croissance et matrice.

L'un des principaux défis de l'IT la pénétration cellulaire limitée dans les parties internes des biomatériaux poreux. Une faible viabilité cellulaire au centre du produit d'IT est la conséquence de la diffusion limitée d'oxygène et de nutriments du fait d'un réseau vasculaire insuffisant dans l'ensemble de la construction 3D. Le BioAssemblage couche-par-couche est une nouvelle approche basée sur l'assemblage de petites constructions cellularisées permettant une distribution cellulaire homogène et une vascularisation plus efficace dans des produits d'IT.

Notre hypothèse est que l'approche couche-par-couche est plus adaptée à la régénération osseuse que l'approche conventionnelle de l'IT. L'objectif principal de cette thèse était d'évaluer les avantages de l'approche couche-par-couche en utilisant des membranes de polymères imprimées en 3D etensemencées avec des cellules primaires humaines. Nous avons évalué l'efficacité de la formation du réseau vasculaire *in vivo* dans toute la construction 3D en utilisant cette approche et en la comparant à l'approche conventionnelle basée sur l'ensemencement des cellules sur la surface des scaffolds massives. Il n'y avait pas de différence significative dans le nombre de vaisseaux sanguins formés en 3D au niveau des parties externes des constructions implantées en site souscutanée chez des souris. Mais dans les parties internes des implants qui n'étaient pas en contact direct avec un tissu hôte, nous avons pu observer une formation des vaisseaux sanguins statistiquement plus efficace lorsque l'approche du bio-assemblage couche-par-couche a été utilisée. Cette formation de réseau vasculaire était plus importante dans le cas de co-cultures que de mono-cultures.

Il y avait plusieurs objectifs secondaires dans ce travail. Le premier était de fabriquer des constructions 3D cellularisées pour l'IT en utilisant des membranes d'acide polylactique (PLA) et des cellules primaires humaines : des cellules de stroma de moelle osseuse humaine (HBMSCs) isolées de la moelle osseuse et des cellules progénitrices endothéliales (EPCs)

isolées du sang du cordon ombilical. Ensuite, nous avons comparé différentes technologies de fabrication des scaffolds: impression 3D directe à partir de poudre de PLA et impression par fil fondu en utilisant une imprimante commerciale et une autre fabriquée sur mesure. L'imprimante sur mesure a permis le plus haut niveau de résolution d'impression spécialement adaptée à la forme et la taille des pores. Par ailleurs, nous avons évalué différents systèmes de stabilisation pour l'assemblage couche par couche : l'utilisation de clips en PLA imprimés en 3D a fourni une stabilisation plus efficace pour empiler les membranes PLA couche par couche. Un autre avantage de ce système de stabilisation est qu'il peut être implanté avec des implants. Ensuite, nous avons observé une prolifération et une différenciation cellulaire plus efficaces lorsque le système de co-culture était utilisé, en comparaison avec des monocultures.

L'approche du bioassemblage couche-par-couche semble être une solution appropriée pour une vascularisation efficace dans des structures 3D entières d'ingénierie tissulaire.

Mots clés :

Impression 3D printing – Acid Poly(lactic) – BioAssemblage Couche par Couche – Ingénierie Tissulaire Osseuse – Biofabrication

Résumé substantiel :

L'Ingénierie tissulaire (IT) est un domaine interdisciplinaire qui applique les principes de l'ingénierie et des sciences de la vie au développement de substituts biologiques afin de restaurer, maintenir ou améliorer la fonction tissulaire. La première application de l'IT consiste à remplacer les tissus endommagés par des produits cellulaires artificiels. Une autre application de l'IT est basée sur la production des modèles en 2 et 3 dimensions (2D et 3D) pour des études biologiques et pharmacologiques *in vitro*. Ces modèles ou remplacements de tissus peuvent être fabriqués en utilisant une combinaison de différentes méthodes interdisciplinaires de médecine, biologie, chimie, physique, informatique et mécanique, fournissant un micro-environnement spécifique avec différents types de cellules, facteurs de croissance et matrice extracellulaire.

L'un des principaux défis de l'ingénierie tissulaire est lié à la pénétration cellulaire limitée dans les parties internes des biomatériaux poreux. Une faible viabilité cellulaire au centre du produit d'ingénierie tissulaire est la conséquence de la diffusion limitée d'oxygène et de nutriments, du fait d'un réseau vasculaire insuffisant dans l'ensemble de la construction 3D. Le BioAssemblage couche-par-couche est une nouvelle approche basée sur l'assemblage de petites constructions cellularisées permettant une distribution cellulaire homogène et une vascularisation tridimensionnelle plus efficace dans des constructions d'ingénierie tissulaire.

L'objectif général de cette thèse était d'évaluer l'intérêt de réaliser des assemblages couche par couche de membranes de polymère cellularisées pour favoriser la prolifération et la différenciation cellulaire, en comparaison à la fabrication « conventionnelle » d'une construction d'ingénierie tissulaire composée de scaffolds massifs ensemencés avec des cellules souches primaires : des cellules de stroma de moelle osseuse humaine (HBMSCs) isolées de la moelle osseuse et des cellules progénitrices endothéliales (EPCs) isolées du sang du cordon ombilical. Plus spécifiquement, nous avons caractérisé *in vitro* et *in vivo* des constructions couche par couche fabriquées préparées avec des scaffolds en forme de membranes cellularisées. Ces scaffolds ont été fabriqués par le prototypage rapide (PR) et ensemencés avec des mono- et co-cultures de cellules primaires humaines. Nous avons également évalué l'effet de cette organisation 3D sur la formation de tissus par rapport aux méthodes conventionnelles décrites précédemment.

Les objectifs secondaires étaient liés au processus de fabrication des scaffolds en forme de membranes et plusieurs expériences ont été menées pour:

- Fabriquer des membranes PLA poreuses en utilisant deux technologies différentes de PR : impression 3D directe en utilisant la poudre de PLA et impression par dépôt de fil fondu (FDM) en utilisant un filament de polymère thermoplastique de PLA.
- Caractériser les propriétés physico-chimiques des scaffolds de PLA et observer s'ils ont été affectés par le processus FDM.
- Évaluer la viabilité, la prolifération et la différenciation cellulaires *in vitro* des monocultures et des co-cultures avant un assemblage en 3D, sachant que les HBMSCs

peuvent se différencier vers lignées ostéogéniques et que les EPCs ensemencés avec elles en co-cultures induisent une communication entre des cellules en produisant une matrice extracellulaire avec une sécrétion des facteurs de croissance. Les EPCs stimulent la différenciation ostéoblastique des HBMSC lorsqu'ils sont ensemencés dans des co-cultures en même temps [164].

- Garder les membranes au fond des puits de culture cellulaire pendant l'ensemencement et stabiliser les bio-assemblages couche par couche. Il était parfois difficile de réaliser les ensemencements cellulaires sur les membranes car celles-ci flottaient dans le milieu de culture, il était donc nécessaire de maintenir les assemblages couche par couche compacts, sans déplacement de couches au cours du temps (changement du milieu de culture) avant que les cellules ne produisent leur matrice extracellulaire. Cette stabilisation des assemblages couche par couche est également importante pour implanter les matériaux.
- Caractériser *in vivo* l'effet d'un système de culture cellulaire (contrôle sans cellules, mono- et co-culture) et l'organisation 3D des cellules et des membranes PLA (bio-assemblage couche par couche et un scaffold massif) sur la formation du réseau vasculaire 8 semaines après l'implantation chez les souris immunodéficientes.

La réalisation des objectifs de cette thèse est divisée en trois parties.

La première partie a été consacrée aux expériences *in vitro* pour évaluer la prolifération, la différenciation et la migration des cellules souches humaines en 2D et 3D en utilisant l'approche couche par couche pour assembler des membranes de PLA imprimées en 3D et cellularisées. Toutes les évaluations ont été réalisées sans aucune modification du biomatériau et sans addition des composants ostéogéniques ou des facteurs de croissance. La qualité d'impression des membranes a été évaluée par la microscopie électronique à balayage (MEB) ainsi que la forme des cellules ensemencées. Toutes les cellules avaient une morphologie attendue en mono- et en co-cultures et elles maintenaient la viabilité pendant 14 jours en 2D. Les différenciations ostéoblastique et endothéliales ont été confirmées par des expressions des marqueurs précoces : phosphatase alcaline (PAL) et facteur von Willebrand (vWF), respectivement. La prolifération cellulaire en mono-cultures de HBMSCs et en co-cultures était significativement plus élevée après 14 jours en 2D. Deux différentes évaluations ont été réalisées en 3D avec des membranes de PLA cellularisées et superposées couche par couche dans cette première partie : la caractérisation de phénotype ostéoblastique et l'observation de la migration des cellules entre les couches de PLA. Une différenciation ostéoblastique a été confirmée par la qPCR en montrant aucune différence significative dans l'expression des gènes ostéoblastiques entre des constructions couche par couche avec des différentes positions des EPCs en 3D. Les EPCs avaient le même effet sur la différenciation ostéoblastique quand elles ont été ensemencées en co-cultures avec des HBMSCs dans toutes les couches ou en mono-cultures dans les couches alternées. Enfin, des observations en microscopie à 2 photons des assemblages couches par couches avec des co-cultures des cellules taguées dans des couches alternées ont montré une migration des EPCs entre des couches après 14 jours.

Les expériences réalisées dans la première partie présentaient certaines limites. Les diamètres de pores des membranes PLA étaient entre 165 μm et 375 μm montrant l'impossibilité de

contrôler complètement leur taille. Au cours des expériences de culture cellulaire, les membranes de PLA flottaient dans des milieux de culture, il était donc nécessaire de les stabiliser avec des anneaux en verre pendant l'ensemencement et des expériences *in vitro*. L'utilisation d'anneaux de stabilisation a permis de maintenir les membranes au fond des puits mais elles n'étaient pas toujours complètement stables. Les assemblages couche par couche ont été stabilisés de la même manière. Cette stabilisation n'a pas fourni de conditions stables pour les constructions 3D. Le deuxième inconvénient de ce système de stabilisation est qu'il n'est pas implantable avec des assemblages pour des études *in vivo*.

L'objectif principal de la seconde partie de cette thèse était d'évaluer l'effet de l'organisation 3D des cellules et des biomatériaux (PLA) sur le développement de la vascularisation dans les produits d'ingénierie tissulaire *in vitro* et *in vivo*. La conception des matériaux a été optimisée pour dépasser des limites de la première partie de la thèse. Nous avons également étudié les propriétés physico-chimiques des membranes de PLA avant et après l'impression 3D afin d'observer si le processus de fabrication avait un effet sur les différentes propriétés du polymère. La première limite de la première partie concernant la taille des pores d'irrégularité a été surmontée en changeant la méthode de fabrication. Dans la deuxième partie, nous avons utilisé une imprimante commerciale à l'impression par fil fondu (FDM) équipée d'une buse d'impression de 400 μm . Cette imprimante FDM a permis la fabrication de membranes et de scaffolds massifs avec une gamme de tailles des pores plus étroite (294 μm - 311 μm). Les observations au MEB ont montré une morphologie des membranes attendue. L'analyse par spectroscopie infrarouge (FTIR) n'a pas montré des changements importants dans les spectres après le processus de fabrication. Les résultats ont révélé que le processus d'impression 2D n'avait pas d'effet important sur la masse moléculaire ni sur la structure amorphe du PLA, ce qui a été confirmé par la chromatographie d'exclusion de taille (SEC) et la calorimétrie différentielle à balayage (DSC). L'analyse thermogravimétrique a montré qu'il n'y avait pas de dégradation thermique du PLA causée par le processus de fabrication. Les membranes de PLA imprimées ont été stabilisées dans des plaques de puits sur l'agarose par des supports imprimés en PLA. Ces supports ont permis de garder les membranes stables dans le milieu de culture cellulaire pendant l'ensemencement et la culture pendant 3 jours avant l'assemblage couche par couche. Puis, des assemblages 3D ont été stabilisés avec des clips en PLA imprimés également en 3D. Ces clips ont maintenu ensemble 4 membranes superposées. Comme ce système de stabilisation était fabriqué en utilisant le même biomatériau que les membranes, il pouvait être stérilisé de la même manière en rayon γ et pouvait être implantés par voie sous-cutanée chez des souris avec des assemblages couche par couche. Ce système de stabilisation a facilité la manipulation des assemblages. Les membranes de PLA n'étaient pas cytotoxiques 24h après stérilisation par irradiation aux rayons γ . La différenciation des cellules ostéoblastiques et endothéliales dans toutes les couches des assemblage 3D a été étudiée et confirmée en observant les expressions de la PAL et du vWF, respectivement. Les cellules ont montré une différenciation attendue avec une distribution homogène dans toutes les couches. La caractérisation du phénotype par la qPCR a confirmé la différenciation ostéoblastique par l'expression de gènes ostéoblastiques.

Après ces premières évaluations *in vitro*, une étude *in vivo* a été réalisée. Nous avons implanté des assemblages couche par couche contenant soit des mono cultures de HBMSCs, soit des co-cultures de ces cellules avec des EPC. Nous avons également implanté des scaffold massifs ayant les mêmes dimensions que des assemblages couche par couche, contenant les mêmes types de cellules. Des échantillons témoins sans de cellules pour les deux types de scaffolds ont été également implantés. Les implants ont été réalisés en site sous-cutané chez des souris immunodéficientes. 8 semaines plus tard, des échantillons ont été inclus dans la résine et nous avons réalisé des coupes histologiques et un marquage une immunohistochimique pour la localisation de cellules humaines dans des implants. Une coloration au trichrome de Goldner a été réalisée et les vaisseaux sanguins ont été quantifiés sur ces coupes. Nous avons évalué l'efficacité de la formation du réseau vasculaire *in vivo* dans toute la construction 3D d'ingénierie tissulaire en utilisant cette approche et en la comparant à l'approche conventionnelle basée sur l'ensemencement des cellules sur la surface des scaffolds 3D massives. Il n'y avait pas de différence significative dans le nombre de vaisseaux sanguins formés en 3D au niveau des parties externes des constructions couche par couche implantées. Par contre, dans les parties internes des implants qui n'étaient pas en contact direct avec un tissu hôte, nous avons pu observer une formation des vaisseaux sanguins statistiquement plus efficace lorsque l'approche du bio-assemblage couche-par-couche a été utilisée. Cette formation de réseau vasculaire était plus importante dans le cas de co-cultures que de mono-cultures de HBMSCs.

Nous avons décidé ensuite d'améliorer le processus de la fabrication de membranes en termes de résolution d'impression. Cette étude est réalisée dans la troisième partie de cette thèse. Le prototype d'une nouvelle imprimante a été assemblé en collaboration avec le Technoshop à l'IUT de Bordeaux. Cette nouvelle imprimante contenait une buse d'extrusion de 100 μm qui n'existe pas sur le marché. Elle possédait une résolution mécanique élevée et un plateau receveur chauffant. Un logiciel spécifique a été conçu avec cette imprimante, permettant la conception rapide et facile des membranes pour assemblage couche par couche avec des pores perpendiculaires, prêtes pour l'impression. Nous avons utilisé le filament de PLA mais obtenu d'un autre fournisseur que celle de la deuxième partie de la thèse. Des membranes ayant trois tailles de pores différentes ont été imprimées : 150 μm , 200 μm et 250 μm et les dimensions des pores obtenues étaient légèrement plus petites que prévu. Les informations sur les dimensions des pores ont été obtenues par des observations microscopiques. La caractérisation physico-chimique des membranes imprimées a été réalisée. Nous avons constaté que le processus d'impression 3D induisait des diminutions de la masse moléculaire de PLA et des températures de dégradation observées par la SEC et l'analyse thermogravimétrique, respectivement. Le procédé de fabrication FDM n'a pas modifié la structure semi-cristalline du polymère. Les propriétés mécaniques ont été testées en fonction de la taille des pores des membranes et nous avons pu observer qu'il n'y avait pas d'effet de la taille des pores sur les propriétés mécaniques des scaffolds. Après la stérilisation aux rayons γ , les scaffolds n'ont montré aucune cytotoxicité vis-à-vis des HBMSCs. Ces cellules ont montré une viabilité élevée et une distribution homogène indépendamment de la taille des pores.

La technique FDM semble plus appropriée pour la fabrication de membranes en PLA que l'impression 3D directe en termes de résolution et de possibilité de créer facilement des différents systèmes de stabilisation. L'imprimante fabriquée sur mesure a permis le plus haut niveau de résolution d'impression spécialement adaptée à la forme et la taille des pores. Par ailleurs, l'utilisation de clips en PLA imprimés en 3D a fourni une stabilisation implantable et plus efficace pour empiler les membranes PLA couche par couche. Ensuite, la prolifération et la différenciation cellulaire ont été plus efficaces lorsque le système de co-culture était utilisé, en comparaison avec des mono-cultures. L'approche du bioassemblage couche-par-couche semble être une solution appropriée pour une vascularisation efficace dans des structures 3D entières d'ingénierie tissulaire. Cette approche pourrait convenir à différentes applications d'ingénierie tissulaire, car la vascularisation des produits d'ingénierie tissulaire reste un point critique pour plusieurs applications.

“Have the courage to follow your heart and intuition. They somehow already know what you truly want to become. Everything else is secondary.”

Steve Jobs

Acknowledgements

First of all, I would like to thank the members of the jury for doing me the honor of reading and evaluating the results of my three-years research.

Thank you, Sylvain, for responding positively to my e-mail three years ago and welcoming me to your project without even knowing me. Thank you for trusting in my work, for all the help during these three years, for making it possible for me to participate at numerous international conferences, which enriched my scientific knowledge. Thank you for teaching me to be a serious scientist and for the confidence and the opportunity to stay at the laboratory for another year.

Thank you, Ognjan, for your decision to support my numerous scholarship applications and for believing in my capacities from the very beginning. Thank you for your good will to continue having me as your collaborator.

Thank you, ReINETTE, for everything you taught me and for all your advice on how to obtain different grants and scholarships. Thank you for all the nice and funny moments during the breaks from work.

This thesis would not be the same without enormous help from internship students. Thank you, Agathe, Maxime and Joanna for all the pleasant moments and your hard work, which was essential for my research.

Thank you, Patrick, for all your IT help, for your humor in the morning and for your enormous help and the logistics of presents and surprises! Thank you for being here to find a solution for all kinds of problems!

Thank you, MatMat, for the translations of my letters and for all your help at all parts of a day. Thank you for all the funny unforgettable moments at the lab and after work. Je suis contente :D

Thank you, Robs, for your patience! Thank you for being always here to help and for all the jokes every day! I also have to thank for that week in January when we are the same age!

Brunito chikito preciocito! Thank you for your smile, for all the nice moments from my very first day at the lab, for all the fun, for listening to me and advising me! Thank you for all Saturday mornings at the market! Bejos

I have to thank you, Hugo, for being here to talk when there was a problem or just to listen and for all the advice in cases of doubt. Thank you also for all the funny Spanish moments during lunch breaks and for your company during our unforgettable NC adventure!

I would also like to thank the entire Biofabrication team of Biotis for useful scientific advice. Thanks to Raphaël, Claire, Adrien, Murielle, Jérôme, Davit, Nathalie, Damien, Olivia.

Thank you, Betty and Victor, for all your smiles, your good vibes and positive energy every single day!

Thank you to all the people at Biotis for all their help and for being part of this three-year adventure. Thanks to Jean-Christophe, Nicolas, Audrey, Carole, Juju, Olivier, Delphine, Sylvie, Sophie, Yoann, Laure, Mathilde, Sindhu...

Thank you my friends, Cams and Gat! Thank you for all “soirées filles/sushis” and meals “chez Nache”! Thank you for all the “mots fléchés” sessions and for being my French teachers. Thank you for being here when it was easy and fun and especially when it was hard. Thank you for supporting caprices of “une Serbe”. Thank you for every single day of your presence! Thank you for being Cams and Gat!

Thank you, my dear Serbs (and one Montenegrin). Thank you, Karajić, for your unconditional friendship. Thank you, Stefane and Saša, for all the great help after working hours. Thank you, Nikola, for all the parties which helped to collect positive energy. Thank you all for making me feel at home in Bordeaux.

Thank you, Vesna, for the beautiful friendship, for your understanding, for being a good listener and for all your advice.

My dearest brother, thank you for knowing me best in the world. Thank you for all the words, for all the listening and non-listening. Thank you for sticking out until the end. Thank you for believing in me!

Finally, my deepest thanks to my parents without whose support all of this would not have been possible. Thank you for believing in me! Thank you for all the sacrifices you made so I can finish this dissertation. Thank you for everything you did not have because my requirements and problems were more important than your needs. Thank you for all the advice and your presence. Thank you for making it possible for me to learn and work on what I wanted!

CONTENTS

LIST OF FIGURES	3
LIST OF TABLES	5
LIST OF ABBREVIATIONS	6
INTRODUCTION	7
1. TISSUE ENGINEERING	8
1.1. GENERAL CONCEPT	8
1.2. METHODOLOGICAL PRINCIPLES	8
2. BONE TISSUE ENGINEERING	10
2.1. BONE PHYSIOLOGY	10
2.2. NATURAL BONE HEALING	12
2.2.1. EMBRYONIC BONE FORMATION	12
2.2.2. BONE HEALING AFTER FRACTURE	14
2.3. BONE GRAFTS	17
2.4. BONE HEALING IN THE PRESENCE OF BIOMATERIALS	18
2.4.1. SPECIFICITIES OF BONE TISSUE ENGINEERING SCAFFOLDS	18
2.4.2. BIOMATERIALS FOR BONE TISSUE ENGINEERING SCAFFOLDS	19
2.4.3. CONVENTIONAL FABRICATION METHODS FOR BONE SCAFFOLDS	23
2.4.4. CELLS FOR BONE TISSUE ENGINEERING	23
2.4.5. GROWTH FACTORS FOR BONE TISSUE ENGINEERING	24
2.5. VASCULARIZATION TECHNIQUES	24
3. 3D PRINTING FOR BONE TISSUE ENGINEERING	26
3.1. TECHNOLOGIES FOR BONE TISSUE ENGINEERING SCAFFOLD FABRICATION	26
3.1.1. STEREO LITHOGRAPHY (SLA)	26
3.1.2. SELECTIVE LASER SINTERING (SLS)	28
3.1.3. POWDER-BASED 3D PRINTING	29
3.1.4. EXTRUSION TECHNIQUES	29
3.1.4.1. Direct 3D printing	29
3.1.4.2. <i>Fused Deposition Modeling (FDM)</i>	32
3.1.4.3. <i>3D Plotting</i>	34

3.1.5. ELECTROSPINNING	35
3.2. POLY-LACTIC ACID FOR 3D PRINTING	37
3.3. BIOFABRICATION FOR BONE TISSUE ENGINEERING	40
3.4. BIOASSEMBLY AS A NEW APPROACH FOR SCAFFOLD CELLULARIZATION	41
THESIS OBJECTIVES	50
RESULTS	52
FIRST PART	53
DIRECT 3D PRINTING OF POLY(LACTIC) ACID MEMBRANES AND THEIR BIOLOGICAL CHARACTERIZATION	53
SECOND PART	76
FUSED DEPOSITION MODELING TECHNIQUE FOR FABRICATION OF POLY(LACTIC) ACID MEMBRANES AND THEIR PHYSICOCHEMICAL AND BIOLOGICAL CHARACTERIZATION	76
THIRD PART	108
DEVELOPING THE PROTOTYPE OF FDM PRINTER WITH HIGH RESOLUTION	108
CONCLUSIONS AND PERSPECTIVES	130
SCIENTIFIC COMMUNICATIONS	135
BIBLIOGRAPHY	142
ANNEX	157

LIST OF FIGURES

Figure 1 : Conventional tissue engineering steps	9
Figure 2 : Mandibular bone micro and macro structure	11
Figure 3 : Bone remodeling process	12
Figure 4 : Mechanism of intramembranous ossification	13
Figure 5: Mechanism of endochondral ossification	14
Figure 6 : Natural bone healing process	16
Figure 7 : Cell colonization limit related to the oxygen and nutrients diffusion within large porous 3D scaffold	25
Figure 8 : Stereolithography technique	27
Figure 9 : Selective Laser Sintering technique	28
Figure 10 : Powder-based 3D printing technique	30
Figure 11 : Direct 3D printing technique	31
Figure 12 : Fused Deposition Modeling technique	33
Figure 13 : 3D plotting technique	34
Figure 14 : Electrospinning technique	36
Figure 15 : Effect of the molecular weight and L-stereoisomer content on the glass transition temperature of PLA	38
Figure 16 : Biofabrication and its contribution in tissue engineering and regenerative medicine.	40
Figure 17 : Biofabrication technologies for tissue engineering	41
Figure 18 : Cell-sheet scaffold-free biofabrication	42
Figure 19 : Stacking and destacking of LBL constructs for analyses	43

Figure 20 : 2 approaches for cell seeding onto PCL membranes44

Figure 21 : Quantification of proliferation of MG63 cells on PCL electrospun scaffolds45

Figure 22 : Design of preparation of LBL assemblies of ADSCs-leaden PCL/gelatin membranes46

Figure 23 : Micro-computed (μ CT) images of rat calvarial defects 12 weeks after implantation46

Figure 24 : Illustration of entire process to produce LBL assemblies of cellularized electrospun PCL membranes48

Figure 25 : . The effect of parallel and perpendicular stacking of cellularized membranes on formation of vascularized dermal tissue49

LIST OF TABLES

Table 1 : Physical properties and applications of natural bone tissues compared to degradable and non-degradable biomaterials	22
Table 2 : Different fields of biomedical applications of PLA	39

LIST OF ABBREVIATIONS

μ-CT	Micro Computed Tomography	LBL	Layer-by-Layer
2D	Two dimensions	MSC	Mesenchymal stem cells
3D	Three dimensions	OCN	Osteocalcein
3DP	3 dimensional printing	P	Phosphorus
ABS	Acrylonitrile butadiene styrene	PCL	Polycaprolactone
ADSC	Adipose derived stem cells	PEG	Polyethyleneglycol
ALP	Alkaline Phosphatase	PGA	Poly(glycolic) acid
BMP	Bone Morphogenic Protein	PLA	Poly(lactic) acid
BTE	Bone Tissue Engineering	PLGA	Poly(lactic-co-glycolic) acid
Ca	Calcium	PLLA	Poly(L-lactic) acid
CAD	Computer Aided Design	PMMA	Poly(methyl methacrylate)
CAM	Computer Aided Manufacturing	PP	Polypropylene
CaP	Calcium Phosphate	PTH	Parathyroid Hormone
CO ₂	Carbon dioxide	RM	Regenerative Medicine
COL	Collagen	RNA	Ribonucleic acid
DNA	Deoxyribonucleic acid	RP	Rapid Prototyping
ECM	Extracellular Matrix	Runx2	Runtrelated transcription factor 2
EPC	Endothelial Progenitor Cells	SLA	Stereolithography
ESC	Embryonic Stem Cells	SLS	Selective Laser Sintering
EVOH	Ethylene-co-vinyl alcohol	SVF	Stromal Vascular Fraction
FDA	Food and Drug Administration	TCP	Tricalcium Phosphate
FDM	Fused Deposition Modeling	TE	Tissue Engineering
H	Hydrogen	TGF	Transforming Growth Factor
HA	Hydroxyapatite	THF	Tetrahydrofuran
HBMSC	Human Bone Marrow Stroma Cells	TIPS	Thermally Induced Phase Separation
HUVEC	Human Umbilical Vein Endothelial Cells	TNF	Tumor Necrosis Factor
IGF	Insulin-like Growth Factor	UV	Ultra Violet
iPS	Induced Pluripotent Stem Cells	VEGF	Vascular Endothelial Growth Factor

INTRODUCTION

1. TISSUE ENGINEERING

Different pathological situations can occur in patients such as trauma, cancer or infection that can induce large bone defects in different parts of the body. These defects can not be repaired by natural healing processes and they require involvement of new technologies such as tissue engineering.

1.1. General concept

The global concept of Tissue Engineering, as defined by Langer and Vacanti [1] can be applied for different applications. Thus, TE methods can be used to fabricate artificial cell/materials assemblies to replace damaged tissue in regenerative medicine [2–4], but it can also be used to produce 2 or 3 dimensional (2D and 3D) models for biological and pharmacological *in vitro* studies [5]. These models can find applications in basic cell-cell [6] and/or cell-biomaterial studies [7]. Organ-on-a-chip engineered systems are used for drug screening [8]. Out of these TE applications, damaged tissue regeneration has been chosen as a subject of this thesis research.

The role of all tissue engineering methods is to provide the micro-environmental tissue-specific conditions to the target tissue concerning the cell type, growth factors and organic or inorganic matrix. Tissue engineering represents a combination of different interdisciplinary methods of medicine, biology, chemistry, physics, informatics and mechanics.

1.2. Methodological principles of tissue engineering

Conventional TE steps imply first, retrieving of patient cells (Figure 1. 1) and their culture in order to amplify and/or differentiate them (Figure 1. 2) to tissue specific cell lineage; then these cells (with or without growth factors) can be seeded or embedded onto degradable and biocompatible biomaterial (scaffold) (Figure 1. 3), and the whole composite material is cultured in a 3D environment (Figure 1. 4) for maturation. The last step would be the implantation of the 3D tissue-engineered construct in the patient (Figure 1. 5) [9]. Tissue Engineering has already been used to produce artificial human tissues for different clinical applications such as skin [10–13], bone [14,15], cartilage [16], blood vessels [17], kidney [18] and bladder [19] reconstruction.

Implantation of cells specific to the target tissue is usually performed to favor surrounding tissue penetration in the inner parts of tissue-engineered constructs. The choice of the cell source depends on the target tissue. Cell differentiation is performed in 2D *in vitro* in

most of the cases. But 2D cell culture system does not provide efficient conditions to reproduce the actual functionality of living tissues [20]. The 3D organization of cells, biomolecules and biomaterials enhances the formation of specific microenvironment, allowing cell-to-cell communication, extracellular matrix (ECM) formation, growth factor production and controlled diffusion of oxygen and nutrients as well as waste product elimination needed after implantation [21]. The cells used in regenerative medicine are usually autologous to avoid immune rejection after implantation.

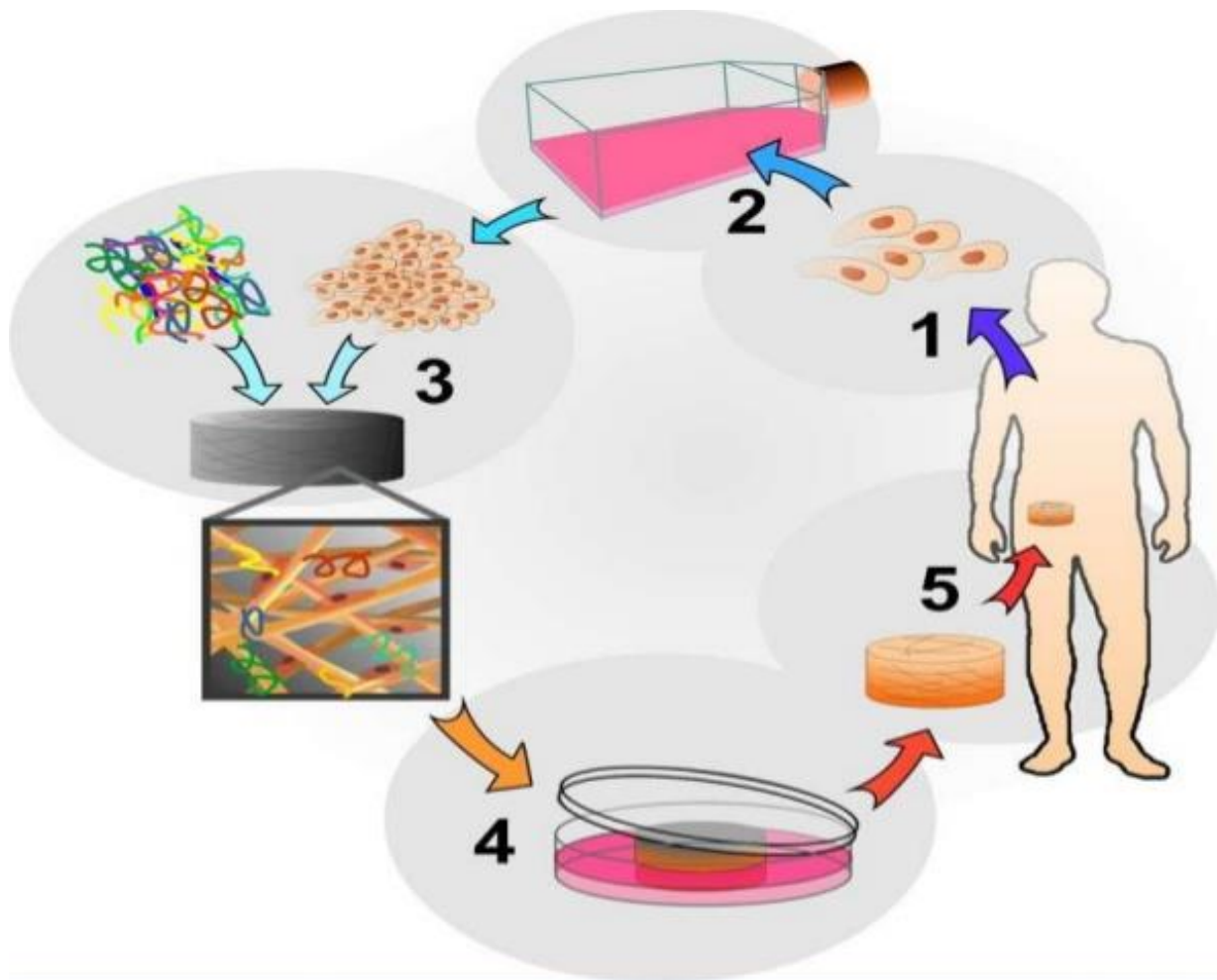


Figure 1. Conventional tissue engineering steps from Blitterswijk [9]

2. BONE TISSUE ENGINEERING

2.1. Bone physiology

Bone is a hierarchically organized tissue with a macrostructure of several millimeters scale and a microstructure of about 100 μm scale. The macrostructure is represented by cortical and cancellous bone, while the microstructure is composed of bone cells and extracellular matrix, including collagen and mineral components (Figure 2) [22]. Cortical bone represents 80 % of the total bone mass in an adult and it displays high mechanical strength due to its high density and low porosity. Cancellous bone is highly porous, which enables structural support, flexibility and metabolic activity, however it displays a reduced mechanical strength. Another important role of cancellous bone is the presence of bone marrow responsible for hematopoiesis [23]. Regarding microstructure, it is represented by osteons in cortical bone, which are composed of concentric layers surrounding a central haversian canal, whereas the cancellous bone is organized through trabecular struts (Figure 2). Extracellular matrix (ECM) in osteons (35 %) is mainly composed of mineral matrix and type 1 collagen, as well as proteoglycans, cytokines and growth factors and proteins, such as osteonectin and osteocalcin synthesized by osteoblasts. The mineral matrix represents 60 % of the bone volume and is mainly composed of hydroxyapatite crystals. The rest of bone contains water and osseous cells, such as osteoblasts, osteoclasts and osteocytes. Osteoclasts are responsible for bone resorption, while osteoblast are in charge of bone formation [24], both of these cells participating in the bone remodeling process.

Bone remodeling is a complex physiological process including different cell functions (Figure 3), allowing the constant adaptability of the bone [24] and the coupling between bone resorption and neoformation. Border cells that cover bone surface prohibit ECM contact with osteoclasts. Osteoclasts factors (PTH, vitamin D3 and PGE2) or inflammatory factors (interleukin-1 and -6 and α -TNF) cause retraction of border cells allowing the osteoclasts to reach ECM. The colonization of osteoclasts favored by preosteoclasts and monocytes induces the bone resorption phase followed by the polarization of the surface and releasing the H^+ ions by osteoclasts. This increased acidity causes HA crystals dissolution releasing Ca- and P-minerals and activation of proteolytic enzymes, such as collagenase, which degrades collagen. Then, inhibitors such as IGF-I or TGF- β induce the apoptosis of osteoclasts replaced by mononuclear macrophages in the inversion phase. The role of macrophages is to eliminate degraded ECM remnants. The last step of bone formation is osteoblast recruitment at the bottom of the resorption gap. During this phase, decreased osteoclasts inhibits osteoclastic precursors differentiation. Simultaneously, favored bone tissue formation inhibits adipogenic differentiation of mesenchymal cells. Osteoblasts fill the gap by applying a new collagen non-mineral matrix representing the osteoid tissue, which is going to be mineralized later. During the formation phase, osteoblasts synthesize alkaline phosphatase (ALP) enzyme, which is responsible for the hydrolysis of phosphoric esters inhibitors of mineralization. These cells synthesize growth factors

for their metabolism regulation as well as paracrine factors for regulation of surrounding cells (interleukine-1 or TGF- β) [25].

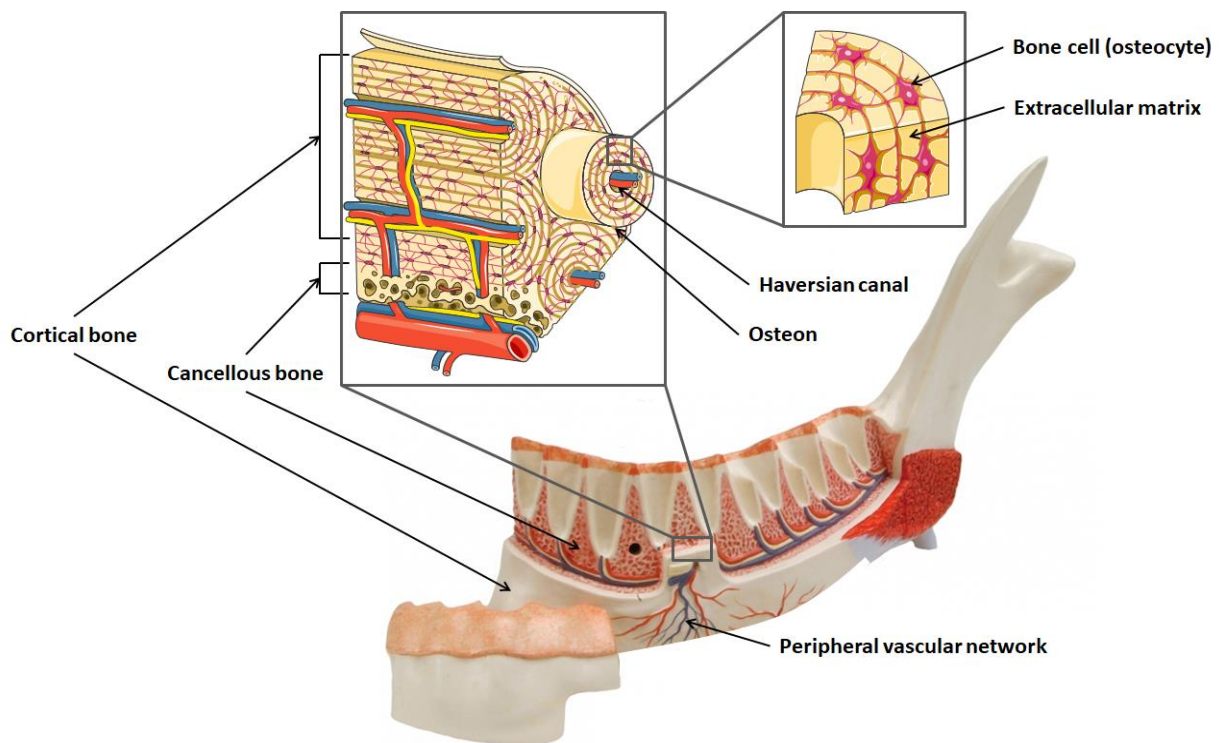


Figure 2. Mandibular bone micro and macro structure (from <https://humananatomy-lib.com>)

Regarding the complex structure of bone, any regenerative strategy must consider the replacement of each individual component and the adequate interrelation between these elements. Thus, it is necessary to find the best combination of biomaterial (with required architecture and mechanical properties), stem cells that can be differentiated in osteogenic lines and additional proteins and specific growth factors. Tissue engineering methods have been developed to find the best combination of these elements for tissue regeneration.

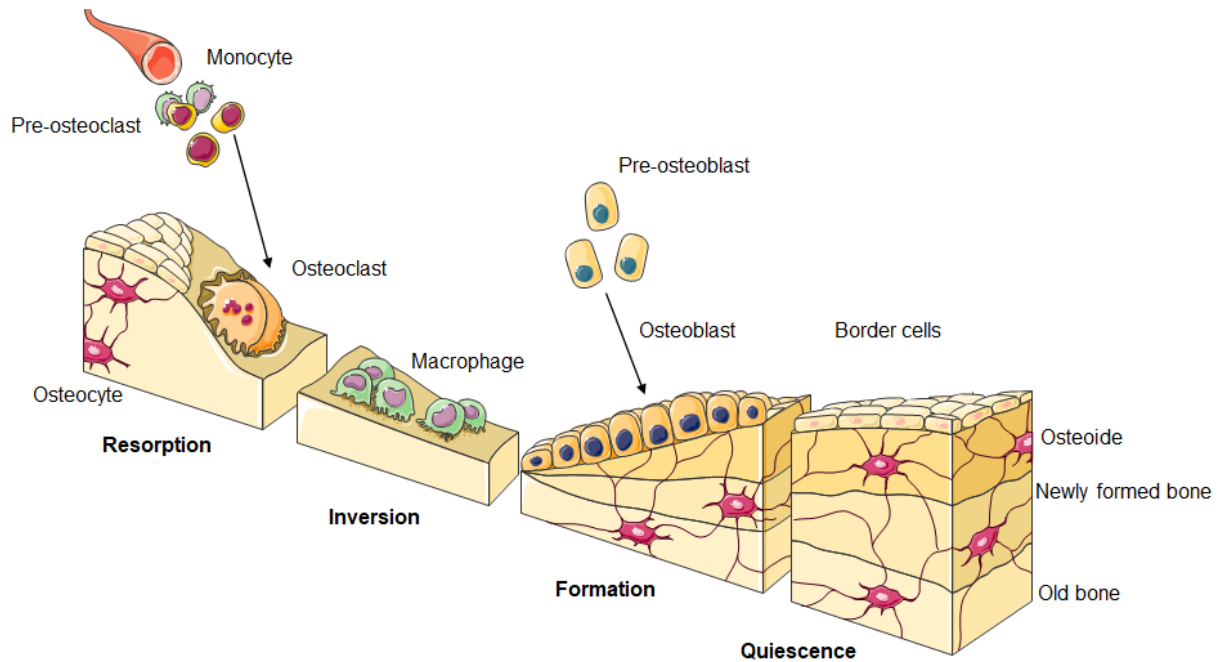


Figure 3. Bone remodeling process (from servier.com)

2.2. Natural Bone healing

2.2.1. Embryonic bone formation

Bone regeneration during bone repair after a lesion or osteogenesis occurs by replacement or remodeling of a pre-existent connective tissue. As some similarities exist between bone repair and embryonic bone formation, we have detailed below the process of bone formation during embryonic development.

There are two distinct mechanisms of bone formation:

- Intramembranous ossification – bone tissue is deposited directly into the connective tissue;
- Endochondral ossification – bone tissue replaces a pre-existent hyaline cartilage thanks to chondrocyte cells.

Osteoblasts are essential for bone regeneration. They differentiate from mesenchymal progenitor cells. During intramembranous ossification, mesenchymal progenitors differentiate

toward osteoblastic lineages. On the other side, they differentiate toward chondrocyte lineages and they become hypertrophic later, during endochondral ossification [26].

Intramembranous ossification concerns flat bones, such as skull bones. Ossification center is formed by grouped mesenchymal cells which differentiate into osteoblastic cells in the fibrous connective tissue membrane (Figure 4a). Nonmineralized matrix in the form of osteoid is secreted inside the synthesized fibrous tissue (Figure 4b). This osteoid tissue accumulates between blood vessels which form a random vascular network. After matrix mineralization process during couple of days connective tissue transforms in mineralized trabecular highly vascularized network (Figure 4c). Osteoblasts present in this mineralized bone matrix are in their terminal differentiation state and they acquire an osteocyte phenotype. Numerous ossification centers develop and merge later forming a network of anastomosed regions, to form the primary trabecular bone [27]. On the external surfaces, the connective tissue condenses and becomes the periosteum. Then a layer of compact bone is formed between the trabecular bone and the periosteum, which will be replaced by mature lamellar (cortical) bone. Finally, the spongy bone located between the two cortical bone laminae will be colonized by bone marrow (Figure 4d) [26].

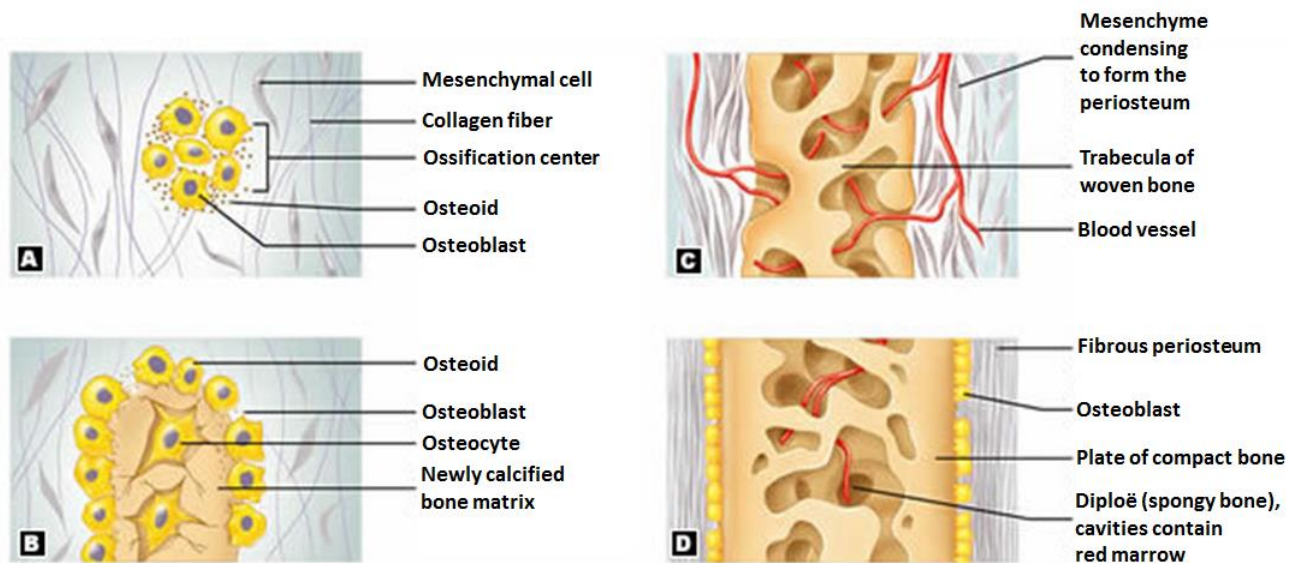


Figure 4. Mechanism of intramembranous ossification [28]

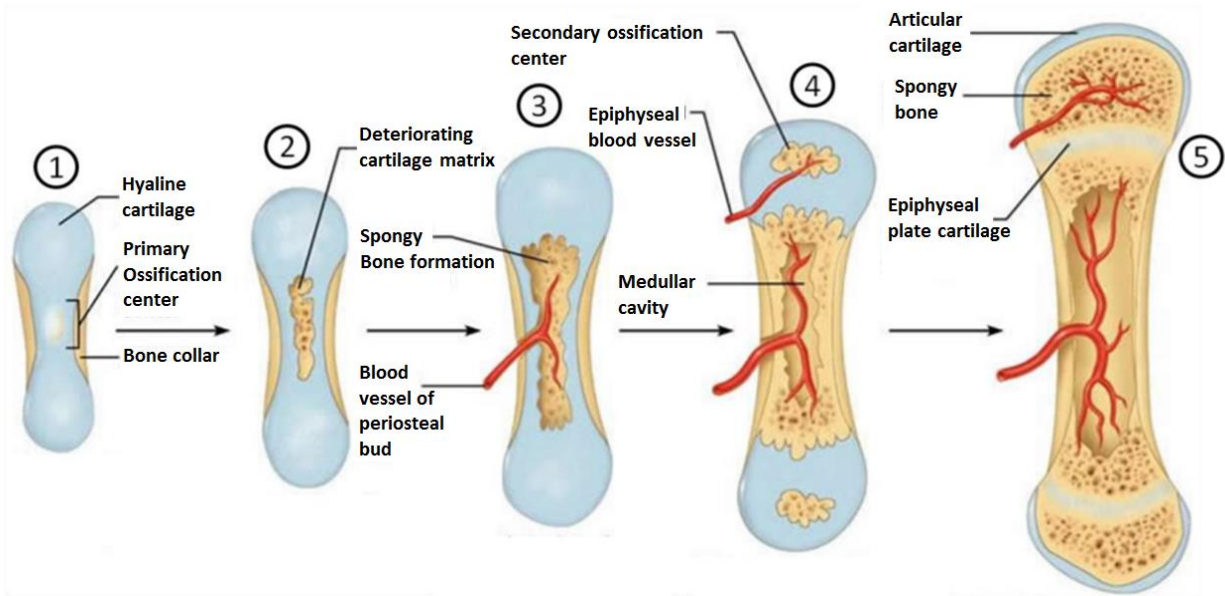


Figure 5. Mechanism of endochondral ossification [29]

Endochondral ossification develops within long bones and it starts from a cartilage (Figure 5). Chondrocyte cells synthesize extracellular matrix containing collagen type II in the ossification center. Then, they mature, hypertrophy and synthesize several angiogenic factors as well as a matrix mainly containing collagen type X. Among these angiogenic factors, VEGF stimulates vascular network formation. Inside of this primary ossification center the hypertrophic chondrocytes undergo apoptosis while the calcification of the matrix takes place. In the meantime, the internal perichondral cells express an osteogenic phenotype, forming a thin periosteal collar around the diaphysis. Then the blood vessels colonize the space previously occupied by the hypertrophic chondrocytes and they form a network towards extremities of the ossification center. Osteoprogenitor cells and hematopoietic stem cells reach the center of the calcified cartilage through the perivascular connective tissue surrounding the invasive blood vessels. Then, secondary ossification centers of secondary develop in the epiphyses. Finally, the long bone length growth depends on the interstitial hyaline cartilage growth whereas the center of the cartilage is gradually replaced by bone.

2.2.2. Bone healing after fracture

The most common bone lesion is a consequence of a fracture, often followed by a soft tissue lesion. It leads to a hemorrhage caused by muscle capillaries and vessels shear and a

tendon rip. Nerve damage can occur as well. The natural bone healing process includes 3 steps: 1) inflammation, 2) repair and 3) remodeling [30] (Figure 6).

1) Bone necrosis appears at the fracture site due to the cessation of bone vascular network in Haversian canals and a blood clot is formed to stop the bleeding. A couple of days later, the hemorrhage-induced blood clot is resorbed by macrophages, eliminating bone remains with osteoclasts. During the first week, a large part of the clot is invaded by blood vessels, developed from the periphery of the lesion, and a fibrous connecting tissue is gradually formed. Pluripotent bone marrow mesenchymal cells migrate to the periphery of the clot where early bone formation occurs [30].

2) Bone repair steps can last more than two months. After their migration in periphery of the lesion, stem cells differentiate into fibroblasts and osteoblasts thanks to the vascularization of the periphery of the clot. The first steps of reparation are the resorption of the blood clot, then the vascularization of the callus. These steps are followed by osteoclast recruitment. Cells from Haversian canal form resorption cones. Nutrients from new blood vessels allow multipotent cell supply to ensure cell renewal. At the same time, the outer callus formed from periosteum, continues to grow toward the fracture site. The internal callus is simultaneously formed in the medullar cavity and it grows toward outer regions of the fracture site. Resorption cones reach the fracture site and ends if the fractured bone [30].

3) Several weeks after a fracture, internal callus growth induces bone ends “sealing” and beginning of bone remodeling. It can last for several months.

Natural bone healing is limited to small defects because large and segmental defects impeded normal biomechanics and structural stability [31]. In the case of large bone defects, different biomaterials can be used to support bone healing.

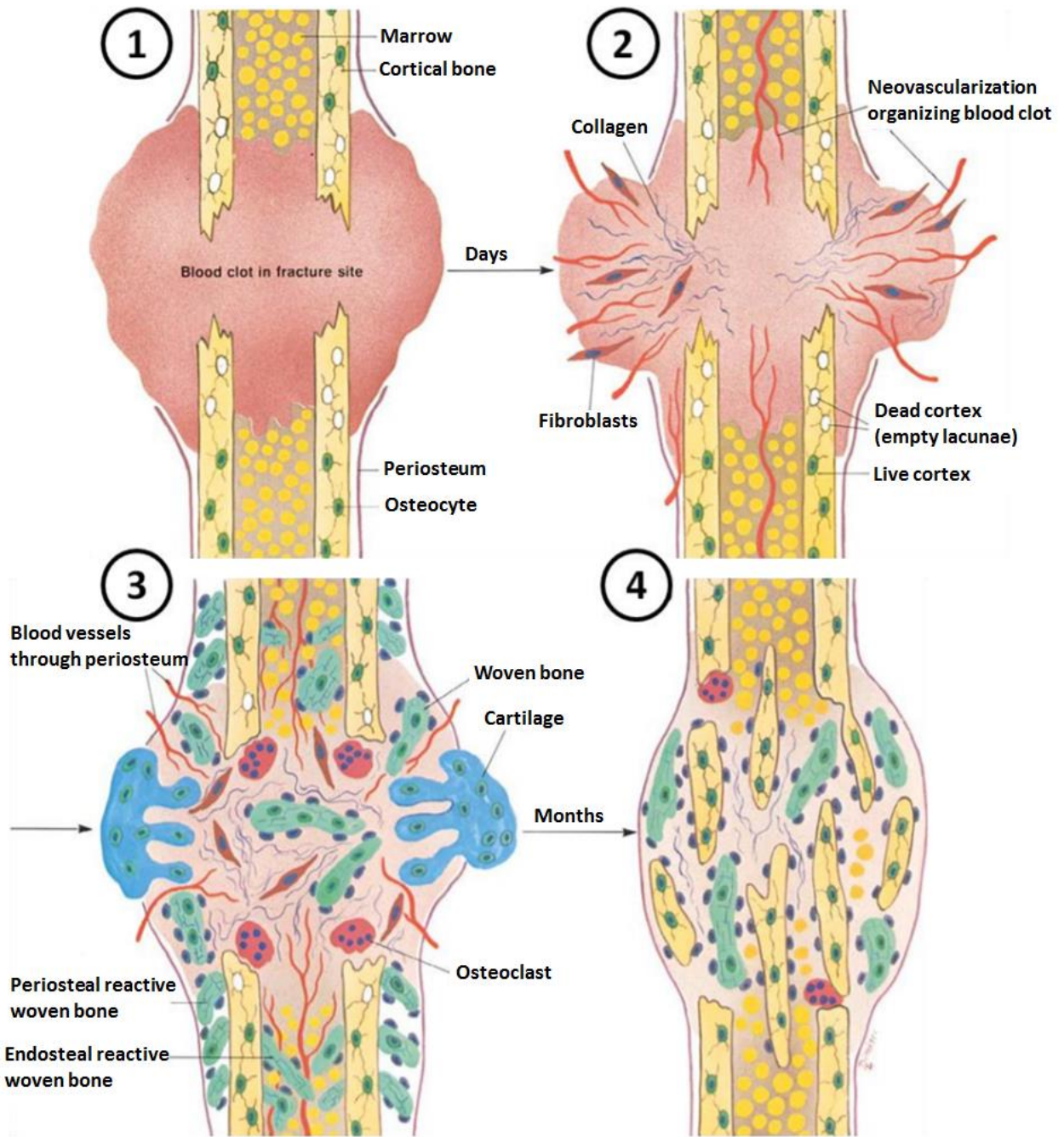


Figure 6. Natural bone healing process [28]

2.3. Bone grafts

Small defects in horizontal and/or vertical dimension can be repaired by the physiological healing process. Different pathological conditions such as trauma, cancer or infection can cause larger bone defects that require a surgical intervention for bone reconstruction. The treatment of such clinical situations is based on the surgical implantation of a graft that can be an autograft, an allograft [32], a xenograft or a synthetic graft, in order to increase the volume of repaired bone by providing a favorable environment for bone repair.

Autograft is taken in the same patient and it is currently the gold standard thanks to its osteogenic, osteoinductive and osteoconductive properties. The advantages of autografts are fulfil healing by bone tissue genesis thanks to its high osteogenic properties. Another benefit of the use of autograft is the absence of immune rejection [33]. The most common autograft is harvested from the iliac crest, providing a large amount of autologous cortical-cancellous bone [34]. Cortical graft possesses high initial mechanical strength, which reduces 6 months after implantation, while initially weaker porous cancellous graft gain strength over time. Iliac crest autograft is rich in progenitor cells directly correlating with bone healing [35]. It displays increased expression of BMPs, BMP receptors and other factors, compared to proximal tibia or humerus bone [36]. The main limitations of using autograft are related to the limited quantity available, the morbidity associated with second surgical site at the same patient, the unpredictable bone resorption and the inconsistency of graft quality between patients [37].

Allograft represents an alternative to autografts. It belongs to the same species, meaning that the donor is another patient [35]. Allograft can be in different forms: frozen mineralized, frozen lyophilized and not demineralized, demineralized frozen lyophilized and defatted deproteinized bone [38,39]. The advantages of allografts compared to autografts are the absence of the donor site in the same patient, meaning a reduction of surgical steps, the availability of larger graft quantity and an osteoinductive potential for the demineralized bone [39]. Its limits rely on a possibility of pathogenic transmission and immune response, inconsistent integration and late resorption [40].

Xenograft comes from a different species. There are several donor sources like coral [41,42], equine [43] or bovine [44]. The advantages are the absence of the donor site in the same patient and the availability of larger graft quantity. The limitations compared to an autograft are the absence of osteoinduction and the theoretical possibility of pathogenic transmission and immune rejection.

2.4. Bone healing in the presence of biomaterials

Depending on the clinical demand, different biomaterials for bone healing can be of natural or synthetic origin. The current biomaterials used in clinical practice for bone tissue regeneration will be detailed in the part 2.4.1. Biomaterials are integrated in the healing process and resorbed or not depending on their composition. Depending on the shape of the material surface, level of resorption of matrix proteins or cell attachment efficacy can variate. Large contact surface between bone and biomaterial provides higher level of protein resorption and improves cell attachment [45]. Out of all biomaterials, only autografts naturally possess osteoinductive properties thanks to the presence of bone morphogenetic proteins (BMPs) inside them, which can stimulate differentiation of stem cells towards osteoblasts. It means that they can initiate bone formation independently of the specific environmental tissue of bone when implanted. CaP are osteoconductive materials meaning that they lead bone healing. Bone healing in macroporous biomaterials occurs in centripetal way from borders to the center [46]. Bone formation passes through the formation of a mesenchymal blastema which ossifies later.

The bioactivity of materials is important because of the surface dissolution, which releases phosphate and calcium ions from the mineral bone matrix [47].

These biomaterials should be used only in cases when it is not possible to reach a natural bone healing because they can slow it down and they can be encapsulated inside fibrous tissues [48].

2.4.1. Properties of bone tissue engineering scaffolds

The role of a scaffold for bone repair is to provide a suitable 3D architecture and mechanical properties to support bone formation. An important prerequisite of any biomaterial designed for tissue regeneration is its biocompatibility. As defined by Williams, the biocompatibility is “ability of a biomaterial to perform its desired function with respect to a medicinal therapy, without eliciting any undesirable local or systemic effects in the recipient or beneficiary therapy, but generating the most appropriate beneficial cellular or tissue response in that specific situation, and optimizing the clinically relevant performance of that therapy” [54]. The biocompatibility of materials can be verified by different *in vitro* tests, such as cell viability and proliferation [55,56].

Osteoconductive properties are another important requirement for bone tissue engineering scaffolds. Osteoconduction can be defined as “bone growth on a surface or down into pores, channels or pipes” supporting bone growth without blocking progression of new bone [49].

Some scaffolds display osteoinductive properties, meaning that “primitive, undifferentiated and pluripotent cells are somehow stimulated to develop into the bone-forming cell lineage” [49]. Osteoconduction is a passive process allowing bone formation on the biomaterial’s surface, while osteoinduction is an active process inducing the osteogenesis.

External shape and internal structure are next important properties of bone tissue engineering scaffolds. The outer shape has an effect on the interaction between the scaffold and the receiving site. The first process in the integration is its revascularization when it is in contact with the host tissue since it is a source of vascular elements and osteoprogenitor biomolecules. Contact surface of defect and implanted biomaterial should be as large as possible to enable the most efficient resorption of proteins and other elements from surrounding tissue.

Suitable internal architecture of bone tissue engineering scaffolds is represented by interconnected pores of specific size allowing cell proliferation and migration as well as more efficient vascularization and host tissue penetration. Bone scaffolds must be biocompatible and biodegradable and ideally, they should be degraded while the new tissue is formed [50]. These biomaterials must allow cell adhesion, proliferation and differentiation towards specific lineages. Ideally, bone scaffolds must possess interconnected pores of 100-300 μm to promote cell seeding and their attachment, cell colonization and migration in 3D and osteogenesis [51,52]. Smaller pores make cell migration difficult, but larger ones decrease mechanical properties of the scaffold [53].

Sufficient mechanical properties of scaffolds are required to support mechanical forces in implantation site. Biomaterial composition has an important effect on mechanical properties of the final scaffold. Biodegradation time of a scaffold can be controlled by the biomaterial composition as well.

Since final BTE scaffold should have numerous mentioned properties, their fabrication is sometimes difficult and complex process. It is not possible very often to obtain all desired properties within the same product using conventional methods. All conventional methods are not adapted for specific biomaterials use.

2.4.2. Biomaterials for bone tissue engineering scaffolds

There are different natural and synthetic biomaterials that find their role in scaffold fabrication. They can be made of hydrogels, calcium-phosphate, polymers or their combination [57]. As detailed before, bone tissue engineering (BTE) is based on the combination of a scaffold made of a biomaterial with required properties, cells capable to differentiate toward osteogenic lineages and growth factors. Scaffolds for BTE must have interconnected pores and a pore size

between 100 and 300 μm [58]. Biomaterials for scaffold fabrication must have osteoconductive properties.

Hydrogels are materials which contain about 90 % of water. Their degradation is induced by enzymes or hydrolysis. Their internal architecture is close to extracellular matrixes of majority of tissues and they can easily be produced [59]. They are easy to manipulate and injectable meaning that they are not invasive at implantation site [60]. They are usually used as carriers for stem cells in tissue engineering. The main disadvantage of hydrogels regarding their application in bone tissue engineering is their low mechanical properties [61]. Limits of natural hydrogels such as chitosane, collagen or pullulane in their availability are overcome by synthetic hydrogels. They can be produced in reproducible manner without limits in quantity, but they can induce an immunogenic reaction. Polyacrylates, polyethylene glycol (PEG) and polyphosphoesters are mostly used in bone tissue engineering applications [62].

There are several advantages to use synthetic grafts like the possibility to control internal and external shape and architecture, but also the absence of viral transmission [63]. The limitations of these materials relies on difficulties to control degradation kinetics and modalities (some synthetic materials produce excessive inflammatory reaction while degrading) [64].

Most of the biomaterials used for bone regeneration are made of Calcium Phosphates (CaPs) since their composition is very close to the mineral part of bone. The major content of bioceramics for bone tissue engineering CaP can be in different forms: tri-calcium phosphate (TCP), hydroxyapatite (HA), biphasic calcium phosphate (TCP-HA), bioglass and their combinations in different proportions modifying their properties [65]. These materials show strong bioactivity. They react with the receiving site by spontaneous adhesion to the bone tissue facilitating the attachment of osteoprogenitor cells and production of ECM [66,67] Bioglass can produce a bioactive HA layer in biological fluids which can connect to a biological tissue. They can also release Si ions to activate osteogenesis of cells. Some CaP ceramics have shown to be osteopromotive thanks to their micro and nano porosity [68]. This microporosity increases the exchange surface between cells and biological environment. Crystals in contact with biological fluids are able to dissolve, interact with biological ions, precipitate and form apatite crystals similar to that of bone. These crystals can favor proteins' absorption (BMPs), allowing cell orientation toward osteoblastic lineages [69]. These biomaterials provide suitable 3D environment for cell progenitors attachment, their proliferation and mineralized ECM synthesis [70]. HA and bioglass resorptions are slow [71] while β -TCP resorption is fast and it occurs by releasing phosphate and calcium ions allowing colonization of newly formed bone [72]. β -TCP has low mechanical properties and that is the reason why it is very often associated with HA [73]. HA stimulates differentiation of mesenchymal cells. Its porous structure corresponds to cancellous bone as an effective osteoconductive matrix leading to mineralization, remodeling and mature bone formation. It is very stable and not that soluble in water comparing to β -TCP [74]. HA can undergo osteointegration with neofomed tissue. Some ceramics might display

osteoinductive properties *in vivo* in certain conditions (implantation in muscles in large animals models) [75].

Some limits of bioceramics, such as mechanical properties and biodegradation time, could be overcome using biodegradable polymers. There is a wide range of thermoplastic FDA-approved polymers and co-polymers, and it's also possible to produce custom materials by combining different raw products for specific applications, suitable for different technologies for scaffold fabrication. They show high biocompatibility and tunable biodegradation time [76]. Synthetic polymers have unlimited availability and they are suitable for numerous fabrication methods allowing possibility to control finely porosity and pore size. Usual polymers used in bone tissue engineering are: poly(glycolic) acid (PGA), poly(lactic acid) (PLA), poly(lactic-co-glycolic) acid (PLGA) or polycaprolactone (PCL) [77]. Degradation of PLA, PGA and PLGA forms glycolic and lactic acid, which can be eliminated from a human body by regular metabolism process. But in case of higher concentrations are high, they can cause some inflammatory reactions [78]. Another limit of these materials in their reduced mechanical properties and bioactivity [79]. They possess good osteoconduction properties thanks to their good compatibility with MSC cells from different sources [80]. Biodegradation properties of such materials can be adjusted by different combinations of them in the form of co-polymers. PCL has been used very often for bone tissue engineering regarding its good compatibility with MSC cells from different sources [80], but it has been used in different composite formulations to improve mechanical properties for bone regenerations. PLA has promising osteoconductive properties [81,82] but it requires often a surface treatment to improve cell attachment. Additional surface treatment can be avoided by combining PLA with CaP or by co-polymerization with glycolide for example [83]. Physical properties of different biomaterials for bone tissue regeneration compared to natural bone are given in the Table 1 [84].

Combination of polymers with calcium phosphates (CaPs) can overcome different limitations of these materials [83]. These composite materials have improved osteoinductive, osteoconductive and mechanical properties. Mostly used polymers in composite materials are collagen, chitosane, PLGA and PLA [85–87]. Collagene-HA composites stimulate osteogenic differentiation of human MSCs *in vitro* and bone neof ormation *in vivo* [88]. Osteoconductive and osteoinductive capacities of biomaterial have been shown with HA nanoparticles dispersed in pullulane-dextrane polysaccharides [89]. Different contents of β -TCP particles incorporated in PLA for scaffold fabrication by electrospinning showed an effect on thermal and structural properties of material [86].

Table 1. Physical properties and applications of natural bone tissues compared to degradable and non-degradable biomaterials [84]

	Material type	Compressive strength (MPa)	Tensile strength (MPa)	Young's modulus (GPa)	Degradation time (months)	Application for bone regeneration
<i>Bone</i>	Human cortical	131-224	35-283	17-20	Natural bone	Autograft and allograft for defect filling, alveolar ridge augmentation
	Human cancellous	5-10	1.5-38	0.05-0.1	Natural bone	Augmentation, dental ridge preservation
Degradable material	Collagen	0.5-1	50-150	0.002-5	2-4	BMP carriers HA-composites, membranes for guided bone regeneration, BTE scaffolds
	Chitosan	1.7-3.4	35-75	2-18	4-6	Scaffolds, composites, vertical bone augmentation membranes, xerogels
	PGA	340-920	55-80	5-7	3-4	Internal fixation, graft material, scaffold, composite
	PLLA	80-500	45-70	2.7	>24	BMP carrier, scaffold, HA-composite
	D,L(PLA)	15-25	90-103	1.9	12-16	Fracture fixation, interference screws
	L(PLA)	20-30	100-150	2.7	>24	Fracture fixation, interference screws, scaffold, bone graft material
	PLGA	40-55	50-80	1.4-2.8	1-12	Interference screws, microspheres and BMP carriers, scaffolds, composites
	PCL	20-40	10-35	0.4-0.6	>24	Scaffolds, HA-composites
	HA	500-1000	40-200	80-110	>24	Scaffolds, composites, bone fillers (blocks and granules), pastes, vertebroplasty, drug delivery, coating
	TCP	154	25-80	60-75	>24	Bone fillers, injectable pastes, cements
Non degradable material	Titanium alloy	900	900-1000	110-127	No	Implants, plates, screws, BMP carriers, orthognathic surgery, mid-facial fracture treatment
	Stainless steel	500-1000	460-1200	180-205	No	Implants, plates, screws
	Bioglass	40-60	120-150	35	No	Bone defect fillers

2.4.3. Conventional fabrication methods for bone scaffolds

Several traditional methods exist to fabricate bone scaffolds with polymers, ceramics and their composites. In solvent-casting and particle leaching techniques polymer is dissolved in a solution with uniformly distributed specific size salt particles. Salt particles remain in matrix after solvent evaporation, immersed in water where salt leaches producing a porous structure [90,91]. Main limits of this technique is that it allows production of scaffolds only in the shape of flat sheets and tubes, and residues of cytotoxic solvents can be observed [92,93].

Lyophilization or freeze drying is a process where polymer is dissolved and the solution is cooled down below its freezing temperature. It leads to solidification of solvent and its evaporation by sublimation, leaving dry porous scaffold. Disadvantages of this technique are lengthy timescales, high energy consumption, the use of cytotoxic solvents and irregular small pore size [91,94].

Thermally Induced Phase Separation (TIPS) uses low temperatures. Polymer solution is quenched and undergoes liquid-liquid phase separation, forming polymer-rich and polymer-poor phases. The first one solidifies and the polymer-poor one is removed, thus leaving a porous nanofibrous network. Low temperatures favor bioactive molecules incorporation [63].

In gas foaming process, inert gas-foaming agents such as carbon dioxide or nitrogen are used to pressurize molded biodegradable polymers with water, producing sponge-like structures. Disadvantages of this technique rely on the use of excessive heat during compression molding, the apparition of pores that are not interconnected and nanoporous skin layer at the scaffold surface [63].

In general, the main issues of these methods are in limited control of internal structure (porosity) and in the use of organic solvents which can have a negative effect on cell viability or biological functions [90,91].

2.4.4. Cells for bone tissue engineering

Primary cells used in tissue engineering are different stem cells harvested from patients. They can differentiate toward different cell lineages. Mesenchymal stem cells (MSCs) possess the ability to differentiate into osteogenic cells. They can be isolated from several different sources like bone marrow, adipose tissue, periosteum, synovial fluid, peripheral blood [95]. Their number and osteogenic efficacy can depend on the source and cells isolated from bone marrow have shown the highest differentiation rate [80].

Embryonic stem cells (ESC) are undifferentiated cells derived from early embryonic stages. These cells are called "pluripotent" meaning that they have the potential to differentiate

into any cell type of the human body [96]. One of main characteristics of these stem cells is their low immunogenicity.

Induced pluripotent stem cells or iPS are stem cells isolated from skin fibroblasts. These cells are reprogrammed by genetic modification using 4 transcription factors: Oct4, Sox2, Klf4 and Myc. Murine and human iPS have the capacity to differentiate towards all cell types and have properties identical to those of embryonic stem cells [97].

2.4.5. Growth factors for bone tissue engineering

Growth factors have an important effect on stem cell differentiation and their integration with the biomaterial. Bone morphogenetic proteins-2 and -7 (BMP-2 and BMP-7) have already shown their efficacy in bone tissue engineering [98]. The major limitations of growth factor use are uncontrolled cell differentiation and acute inflammatory reaction that may occur after implantation [99].

2.5. Vascularization techniques

Even when the scaffolds are made of an adequate biomaterial and ideally designed, cell colonization in the inner parts of large 3D scaffolds is difficult to achieve. The limit of these large scaffolds relies in the difficulty to mimic tissue microarchitecture and micro-environmental conditions. Cell penetration is poor for scaffolds larger than 500 μm (Figure 7) and they remain close to the surface [100] because of insufficient diffusion of oxygen and nutrients and poor waste products elimination in the inner parts of the scaffolds [101,102]. This is directly caused by a lack of vascularization in the inner parts of scaffolds. Achieving a vascularization within the entire construct remains a major challenge in tissue engineering. This vascular network formation is essential for tissue maturation and its integration at the implantation site. It is not possible to control cell density and distribution in 3D using conventional tissue engineering approach based on seeding of cells on the surface of macroporous 3D massive scaffolds.

Vascularization of scaffolds is limited to small-size defects [103] so the development of a new vasculature in tissue-engineering products for regenerative medicine represents a major challenge [104]. There are different cell-based and scaffold-based approaches existing to favor the development of vascularization in the core of scaffolds for tissue engineering purposes [105,106]. Several groups have proposed to place the cellularized scaffold into a tissue culture bioreactor in order to favor cell penetration, proliferation, differentiation and tissue formation: different devices have been proposed and their common objective is to force fluid transfer in the core of massive scaffolds to allow cell to survive and to play their function [107]. One limitation

of such bioreactors is the control of numerous parameters important for the physiological culture environment, knowing that it should not be a steady state process and that culture and tissue-specific parameters change with time. It is also difficult to maintain sterility during the entire process [108].

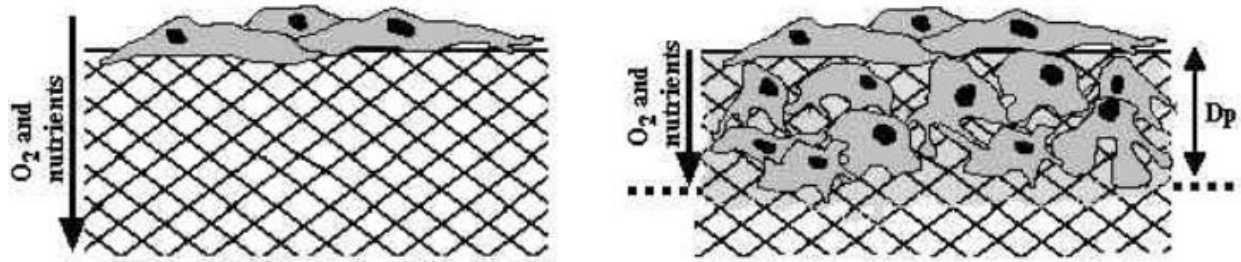


Figure 7. Cell colonization limit related to the oxygen and nutrients diffusion within large porous 3D scaffold [100]

In situ prevascularization is based on the use of the body as a natural bioreactor, by implanting the construct in an easily accessible and highly vascularized tissue, such as muscle, during several weeks, before the vascularized graft can be transferred to the recipient site. The main limitation of this approach is due to the multiple surgical steps required that increases the morbidity of the whole procedure [109].

3. 3D PRINTING FOR BONE TISSUE ENGINEERING

The main limits of conventional methods for bone tissue scaffold fabrication are the use of cytotoxic solvents and the limited control of internal architecture in terms of porosity and pore size. 3D printing technologies is a group of methods that can be used alternatively to produce scaffolds, in order to overcome some of the limitations of conventional methods.

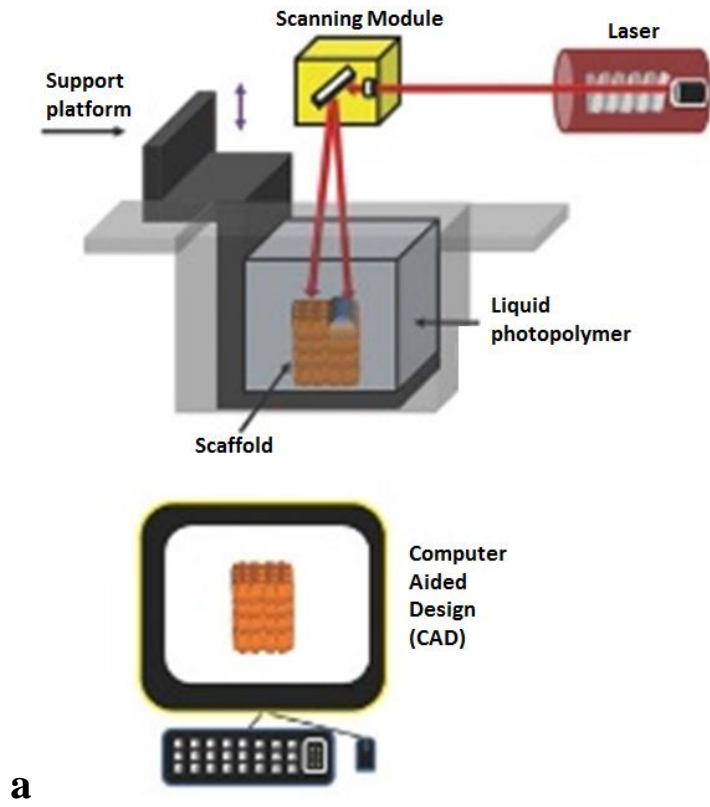
3.1. Technologies for bone tissue engineering scaffold fabrication

CAD/CAM technology has a role to overcome limits of conventional methods allowing a control of specific properties and producing final scaffolds of precise shape and microarchitecture with desired pore shape and size. These properties of scaffolds are reachable using CAD/CAM using RP. RP is of growing interest in the field of bone tissue scaffold fabrication since it enables fast 3D model fabrication with high resolution.

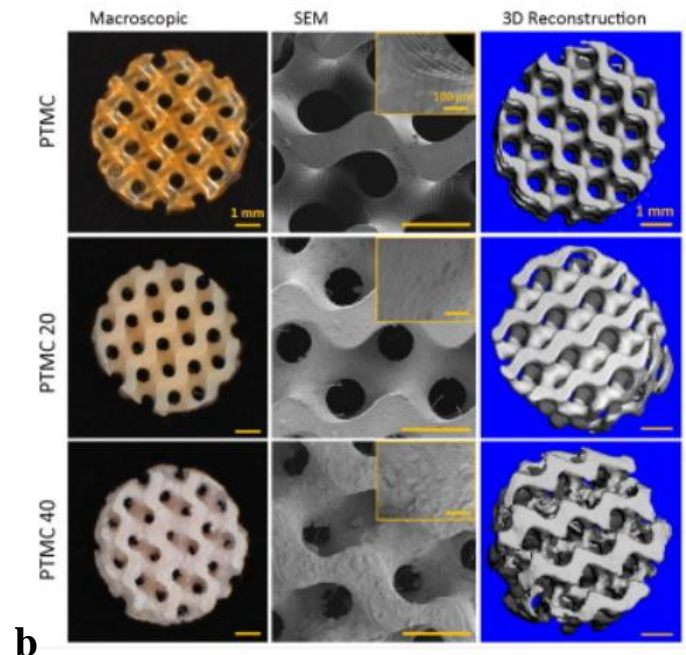
This technology enables also the production of patient-specific scaffold shapes using medical images made by Computed Tomography (CT). Dicom files obtained by these imaging procedures undergo processing treatment in order to obtain 3D model of the defect and/or scaffold to fill the defect. Then, 3D models obtained in this way can be exported to the STL file ready for pre-printing processing and RP fabrication process.

3.1.1. Stereolithography (SLA)

Stereolithography (SLA) is the first RP solid free form technique introduced primarily in the middle of 1980s to fabricate prototypes for automotive, aerospace and other industries [115]. It is based on the photo-polymerization of a resin using a UV laser (Figure 8a). The model is emerged in the resin chamber and the process is repeated layer-by-layer until the entire construct is produced. SLA has limited resolution since the heating of the model at the end might change the accuracy of the final structure [116]. The advantages of this technique are possibilities of multi-material fabrication [117]. This technique has been used to product scaffolds for soft tissues [118] and bone [119] (Figure 8b).



a



b

Figure 8. Stereolithography technique : a) Schematic representation of the SLA process [120], b) Microporous scaffolds of photo-crosslinkable poly(trimethylene carbonate) (PTMC) with 0, 20 and 40% of HA fabricated by SLA [119]

3.1.2. Selective Laser Sintering (SLS)

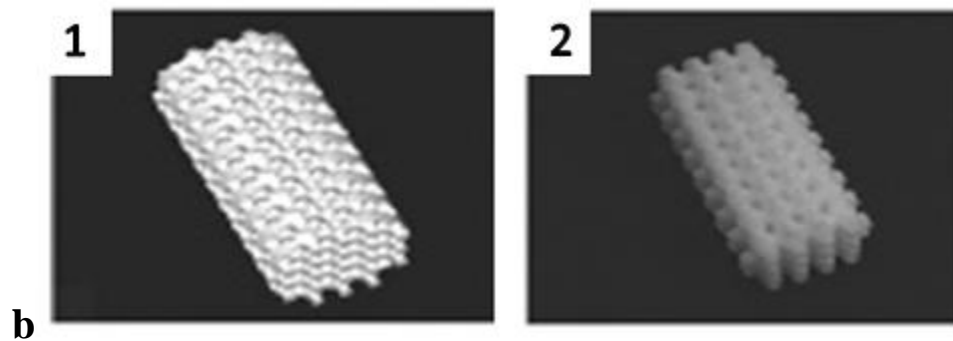
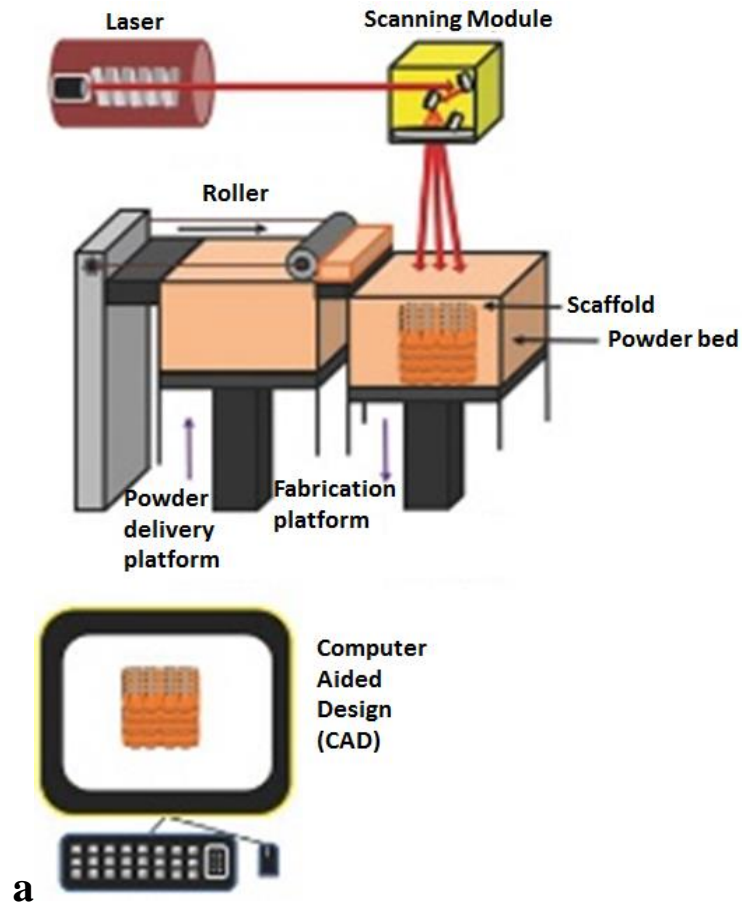


Figure 9. Selective Laser Sintering technique : a) Schematic representation of SLS process [120]; b) SLS scaffolds: 1) STL design file for porous scaffold, 2) PCL scaffold fabricated by SLS [121]

Selective Laser Sintering (SLS) is based on the sintering of a polymer powder by a CO₂ laser beam, while heating it above the transition temperature. The process is repeated layer-by-layer until the entire 3D model is finished. The model should be heated at the end to obtain the final density [122]. A high mechanical resistance of the scaffolds can be obtained. Another advantage of this technique is the possibility to obtain hierarchical structure, per example a multilayer scaffold for osteochondral repair containing different parts, from cartilage layer to subchondral layer (Figure 9) [123]. The main limitation of SLS is due to the high temperatures being used, which reduces the number of candidates biomaterials [116]. A post-processing of the model is needed to obtain final scaffold. This technique has been used to produce scaffold for the TE of cartilage [123] and bone [124,125].

3.1.3. Powder-based 3D Printing (3DP)

This technique is usually known as “3D printing”. It was developed at the Massachusetts Institute of Technology in 1995. It is based on the layer-by-layer spraying of a liquid binder onto a powder bed placed on a platform mounted on a Z-axis, which moves downwards following the shape information about each layer of 3D model. The binder bonds together the powder granules and after completing the first layer, the platform lowers and the process is repeated until the entire scaffold is printed (Figure 10) [126]. There are different types of powder, that may contain CaP for bone tissue engineering applications [127]. The limits of this method are due to particles aggregates formation, and also the expected pore size depends on the size of the powder particles [100].

3.1.4. Extrusion techniques

3.1.4.1. Direct 3D printing

This technique is based is based on the extrusion of a dissolved polymer, before the solidification occurs by the evaporation of the solvent. This technique allows the use different polymer concentration of the polymer for printing; Printing pressure, motor speed and nozzle diameter depend on the viscosity of the printing solution. Porosity and pore size depends on the material content as well (Figure 11) [128]. However, the polymer solvent is usually not biocompatible, so the materials must be rinsed extensively after fabrication.

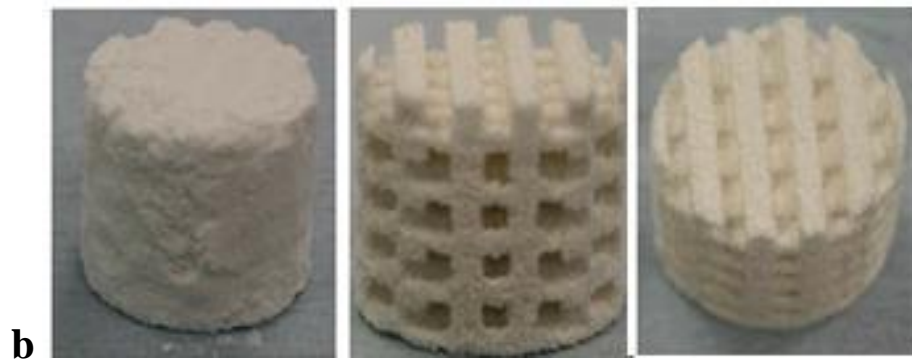
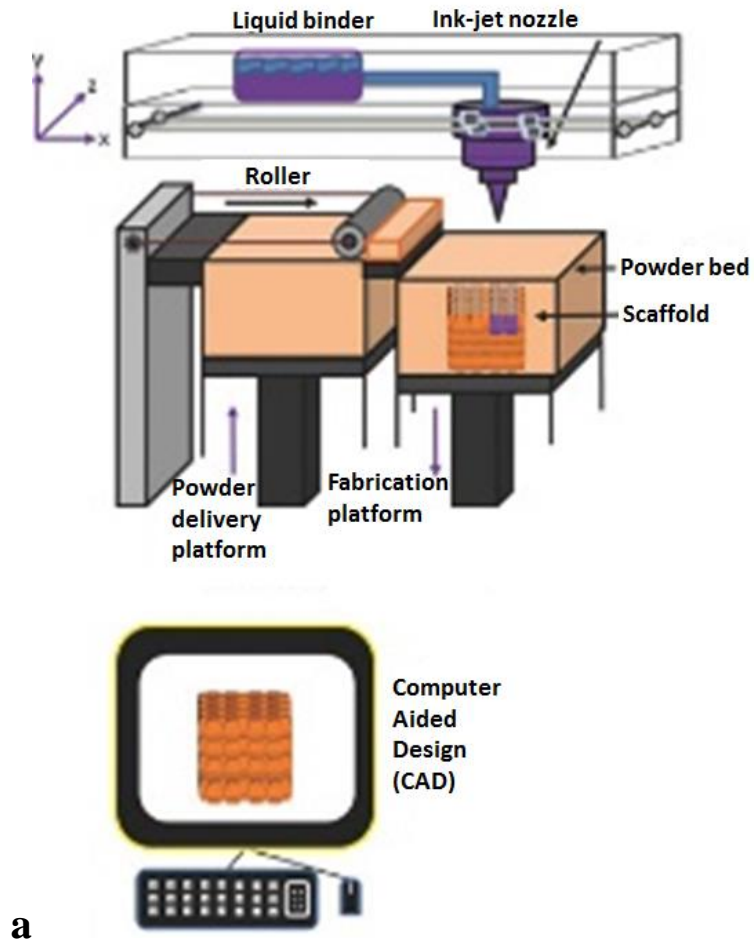


Figure 10. Powder-based 3D printing technique : a) Schematic illustration of powder-based 3D printing [120] and b) HA scaffolds fabricated by powder based 3DP [129]



a

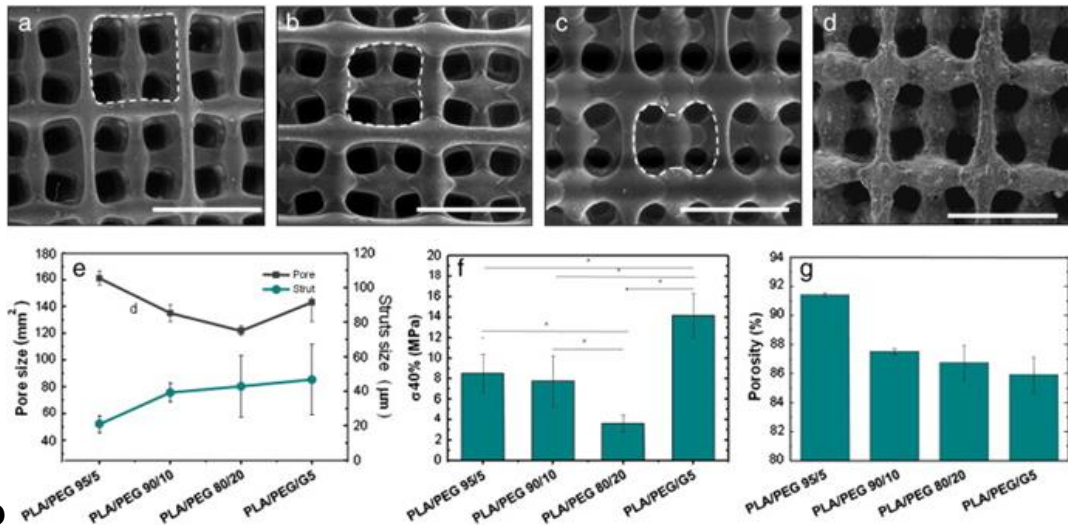


Figure 11. Direct 3D printing technique: a) Schematic illustration of direct 3DP technique; b) SEM images of PLA/PEG scaffolds fabricated by direct 3DP (PLA/PEG 95/5, PLA/PEG 90/10, PLA/PEG 80/20, PLA/PEG/G5. Scale bar is 500 μm) and effect of PEG content on pore and struts size (effect of PEG content on compressive strength at 40 % deformation and effect of PEG content on porosity)

3.1.4.2. Fused Deposition Modeling (FDM)

Fused Deposition Modeling (FDM) is a common technique for scaffold fabrication. It is based on the extrusion of a thermoplastic polymer at the temperature above its fusion point. The main parts of each FDM printer are the heated extrusion head, the nozzle and the receiving platform. Depending on the model, the platform can be moved in x,y or z directions. The platform can also be heated, which is important for some biomaterials printing, such as acrylonitrile butadiene styrene (ABS) per example, because they require a specific temperature to remain fixed on the platform until the end of the process. Extrusion head can move in x,y,z or x,z or y,z, which has an effect on the printing resolution. The nozzle diameter of commercial printers can range between 250 μm and 400 μm and the diameter of the filament is usually 1,75 mm. The thermoplastic filament is introduced inside a printing head, which is heated at a temperature just above the fusion temperature of the biomaterial. The melted filament passes through the nozzle to the receiving platform (Figure 12a). The process is repeated layer-by-layer until the 3D model is completed. As in all additive manufacturing processes, the information about size and shape of the final product are provided by the STL file of 3D model. Extruded filament solidifies by cooling. This technique is very adapted to fabricate porous scaffolds (Figure 12b). It enables high precision in terms of pore size and shape, with good control on their homogeneity.

For this method, the polymer must be prepared in the shape of a thread with precise diameter (1.75mm) because it has an impact printing accuracy. Moreover, as the thread is prepared by heating the raw material in a heated extruder, a degradation of the material might occur, thus a quality control must be performed at this step. It's the main limitation of this technique. Different combinations of printing parameters have an important effect on the quality of the final FDM product. Smaller nozzles provide more preciseness in terms of shape since extruded filament is thinner, but printing lasts longer. The thickness of the filament can be variated by the printing head heating temperature as well as printing speed. Higher temperature induces larger diameter of extruded filament, while higher speed decreases it.

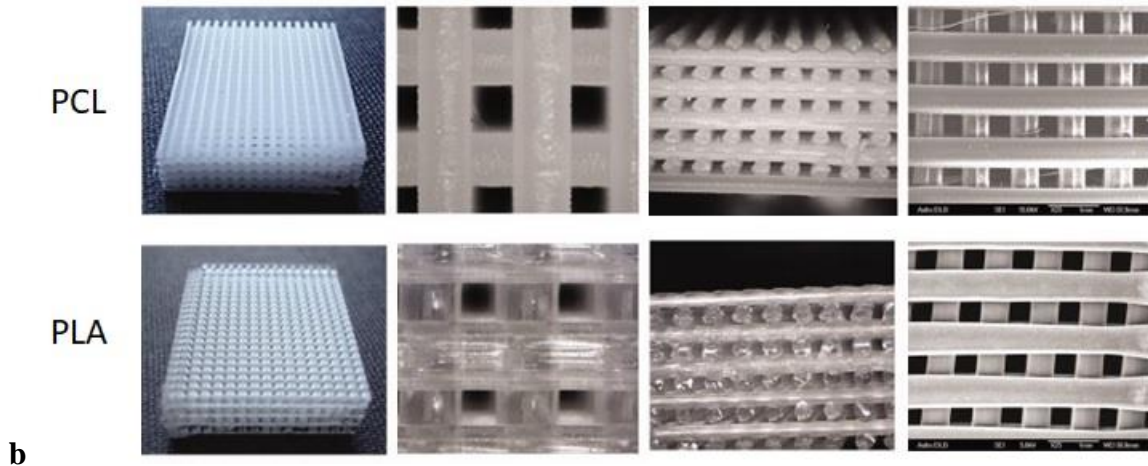
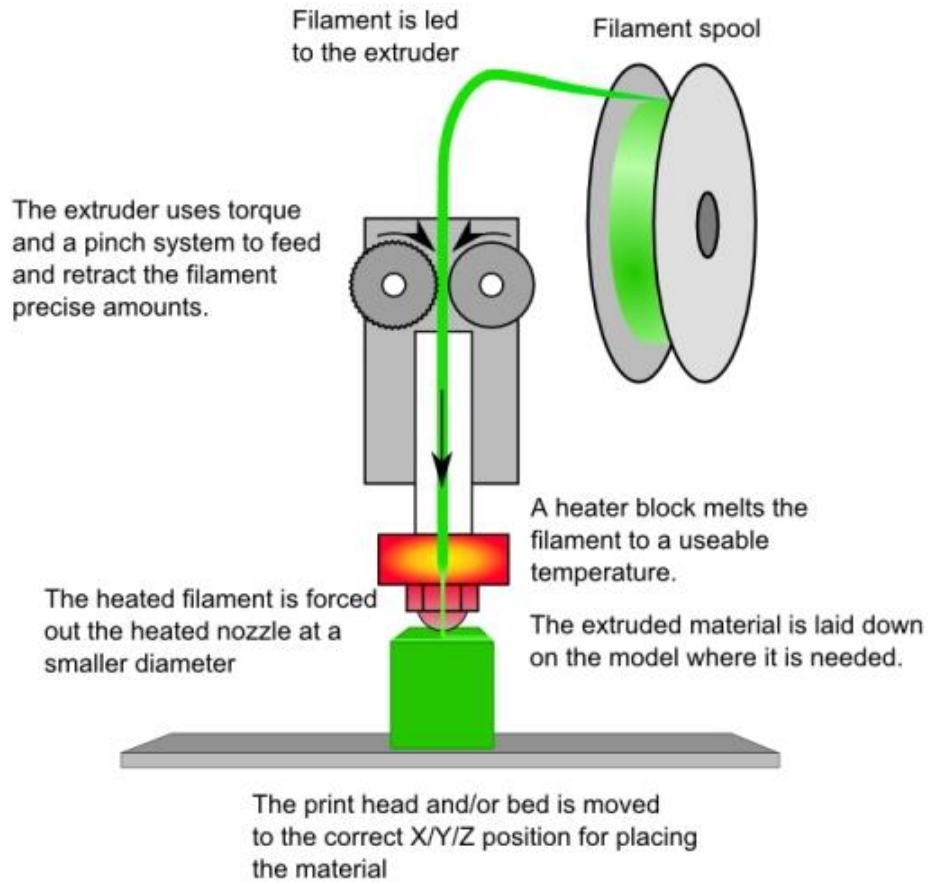


Figure 12. Fused Deposition Modeling technique : a) Schematic illustration of FDM printing process, b) PCL and PLA scaffolds in the shape of porous massive blocks [130]

3.1.4.3. 3D Plotting

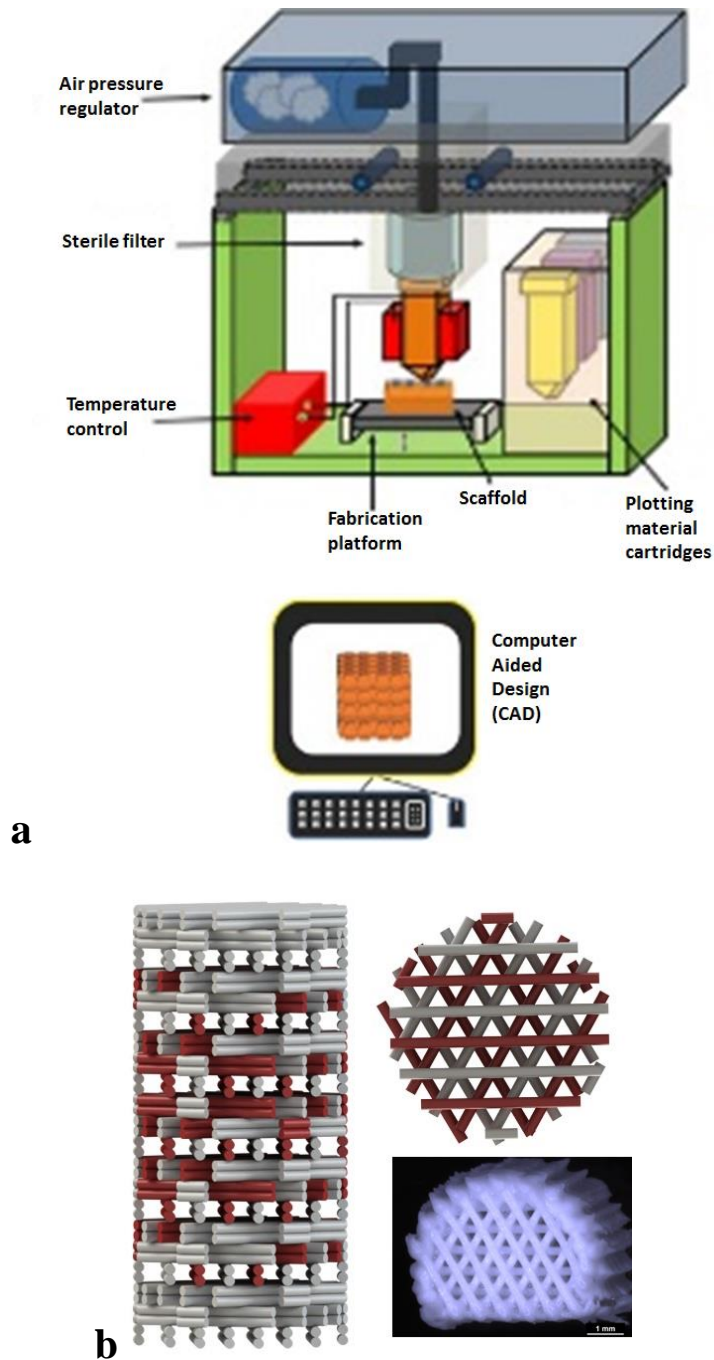


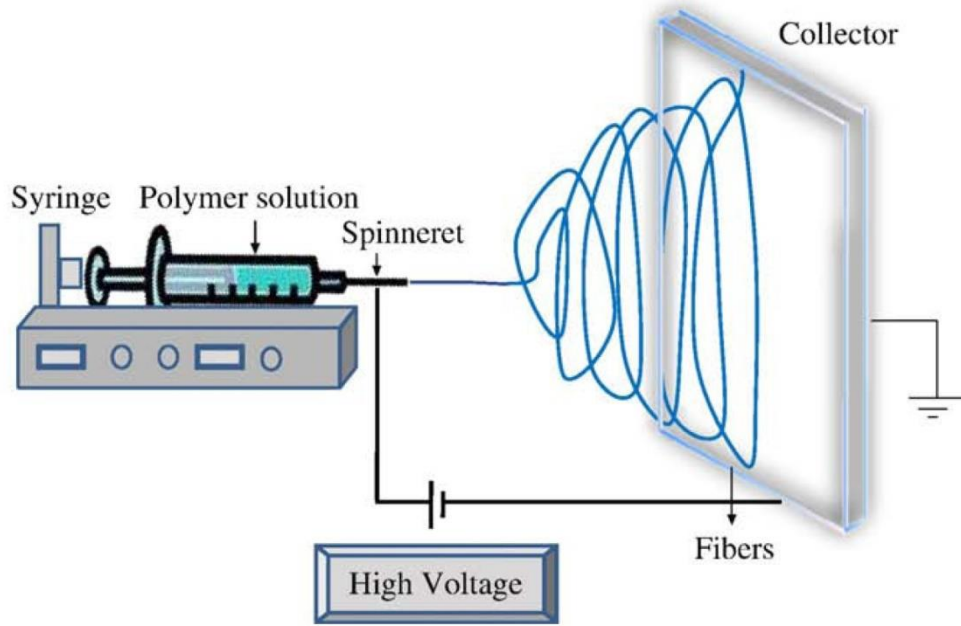
Figure 13. 3D plotting technique : a) Schematic representation of the 3D plotting technology [120], b) Schematic representation of biphasic scaffold design and photo of fabricated scaffold. Grey filaments represent CaP, while red ones represent growth factor loaded hydrogel [61]

3D plotting is technique which can be used for printing of “all pasty biomaterials, and therefore opens up many new options for manufacturing of bi- or multiphasic scaffolds or even tissue engineering constructs, containing e. g. living cells” [131]. It has been used often for CaP based scaffolds [61,132]. There are different types of printers using this technique, each of them having a different degree of complexity. In general, pasty material is placed in syringes. Pneumatic system produces air pressure to extrude the paste onto the receiving platform (Figure 13a). These printers can have numerous additional parts in order to provide fabrication of more complex scaffolds. Some of them have several printing heads, so they are able to print multi-phase scaffolds using different materials sequentially. It is possible to add cooling or heating systems depending on the biomaterial requests. The main advantage of this technique is the possibility to print different synthetic but also natural biological materials providing a wide range of tissue engineering applications (Figure 13b). The main limit is that printed materials require very often a post-processing to obtain final mechanical properties.

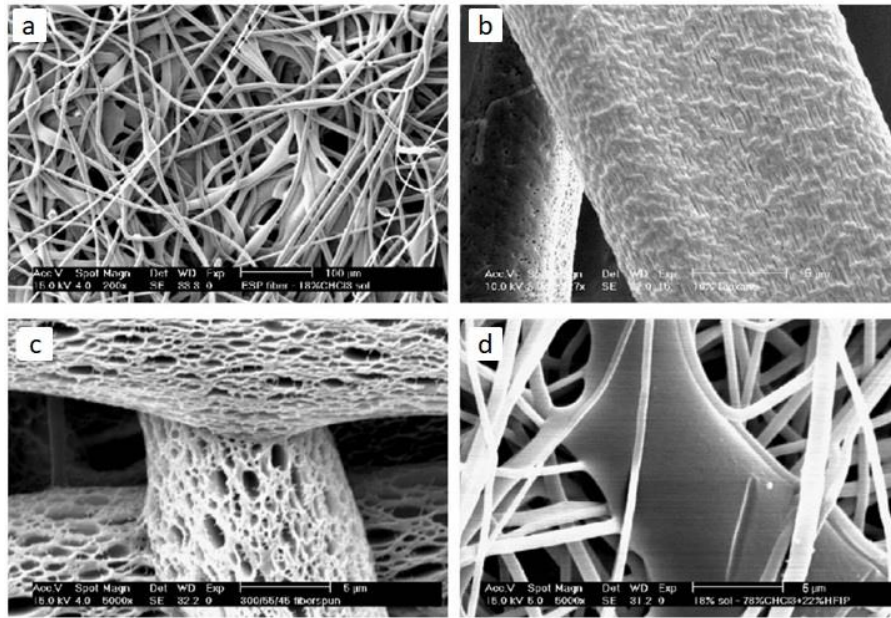
3.1.5. Electrospinning

Electrospinning is a technique used to fabricate membrane scaffolds and it's based on the spinning of a polymer solution in thin fibers collected on a support, under the action of a high voltage electric field [133]. The fiber diameter can variate depending on parameter combinations and it ranges between 250 nm [134] and 6 μm [113] with different micro- and nano-porosities. Different materials like PCL, PLA, PEG or PLGA might be used and they can be charged by different biomolecules to induce tissue regeneration, such as HA for bone applications per example [135]. Scaffolds in the shape of membranes or tubes can be obtained depending on the shape of the collector (Figure 14), however the materials obtained have usually low mechanical properties.

There is one more technique based on the same principle but using a polymer which melts by heating. The polymer solidifies by cooling. Melt-electrospun fiber can be in the range between 270 nm and 500 nm. High viscosity and low charge increase the variation in fiber diameter. Different polymers can be used for scaffold fabrication by melt electrospinning, such as poly(ethylene-co-vinyl alcohol) (EVOH), poly(methyl methacrylate) (PMMA), PCL, PEG, PLA or polypropylene (PP) [136].



a



b

Figure 14. Electrospinning technique : a) Schematic representation of the electrospinning technology and b) images of PEOT scaffolds (a) obtained by electrospinning using different solvents affecting pore morphology: (b) dioxane, (c) dichloromethane, (d) mixture of chloroform and HFIP [133]

3.2. Poly-Lactic Acid for 3D printing

Out of different biopolymers available for 3D printing, we have decided to use PLA as a material for scaffold fabrication for bone tissue engineering. PLA is a semi-crystalline or amorphous biopolymer with good osteoinductive properties and it is FDA-approved. Amorphous PLA is soluble in organic solvents: tetrahydrofuran (THF), benzene, dioxane, chlorinated solvents and acetonitrile, but crystalline PLA is soluble only in chlorinated solvents and benzene at high temperatures [137]. It is present in two enantiomers: L- and D-PLA, and depending on their ratios the mechanical properties of the polymer can variate as well as its biodegradation time. Increase of L-isomer quantity increases crystallinity and shear viscosity [138]. Thermal properties of PLA also depend on the L/D ratios as well as on the molecular weights. Glass transition temperature represents a range of temperatures over which glass transition occurs and it is always lower than melting temperature of a biomaterial. Glass transition is a reversible transition in amorphous materials. This temperature increases with molecular weight and L-isomer content (Figure 15). Glass transition temperature and melting temperature of PLA are approximately 55°C and 180 °C, respectively. Physicochemical properties of this co-polymer enable scaffold fabrication using different technologies and it has already been fabricated in forms of hydrogels, microspheres, blocks, fibers and membranes. PLA has already found its place in numerous biomedical applications (Table 2) [144].

Molecular weight has also an effect on the degradation time of the polymer: high molecular weight increases degradation time. Biodegradation represents a decomposition of the polymer to water and carbon dioxide. PLA degrades by hydrolysis and the degradation products (oligomers- are metabolized by cells. Furthermore, PLA can be used to produce scaffolds for Bone Tissue Engineering thanks to its thermal properties allowing its use for different fabrication technologies, such as extrusion for example. Mechanical properties and degradation time of PLA are lower than required for bone tissue engineering, but they can be improved by co-polymerization [139]. Low molecular weight PLA is good carrier of BMP, which is a biomolecule that induces a new bone formation on demineralized bone. But low weight PLA is limited to small defects because it degrades fast [140]. The addition of polyethylene glycol (PEG) in PLA could overcome this limit with bone regeneration in 2 weeks [141]. PLA can have other limits which can be overcome combining the polymer with different molecules. Intracellular degradation of PLA can cause an inflammatory response and that is why this polymer is often combined with bioglass or CaP [142]. Co-polymerization with glycolic acid increases degradation time and it is often use with L-PLA since it degrades very slowly [143].

HA or titanium (Ti) could improve tensile strength and stability of PLA [144]. PLA-based scaffold combined with HA, growth factors and MSCs, it has already gave good results in bone regeneration. In critical-size rat femoral segmental defects, spiral-wrapped electrospun scaffold with seeded MSCs and with a low dose of recombinant human bone morphogenetic protein-2 (rhBMP-2) resulted in laminated endochondral ossification templated by the scaffold

across the longitudinal span of the defect [145]. First application of PLA was for the repair of dogs' mandibular bone [146]. Addition of 15 % of HA in PLA 3D-printed scaffolds with shape recovery of 98 % was used for small bone defect[147]. Co-polymer of PLA with PEG scaffold promoted osteogenesis in rat femoral defect model and it was replaced by new bone within 2 months after complete biodegradation [98].

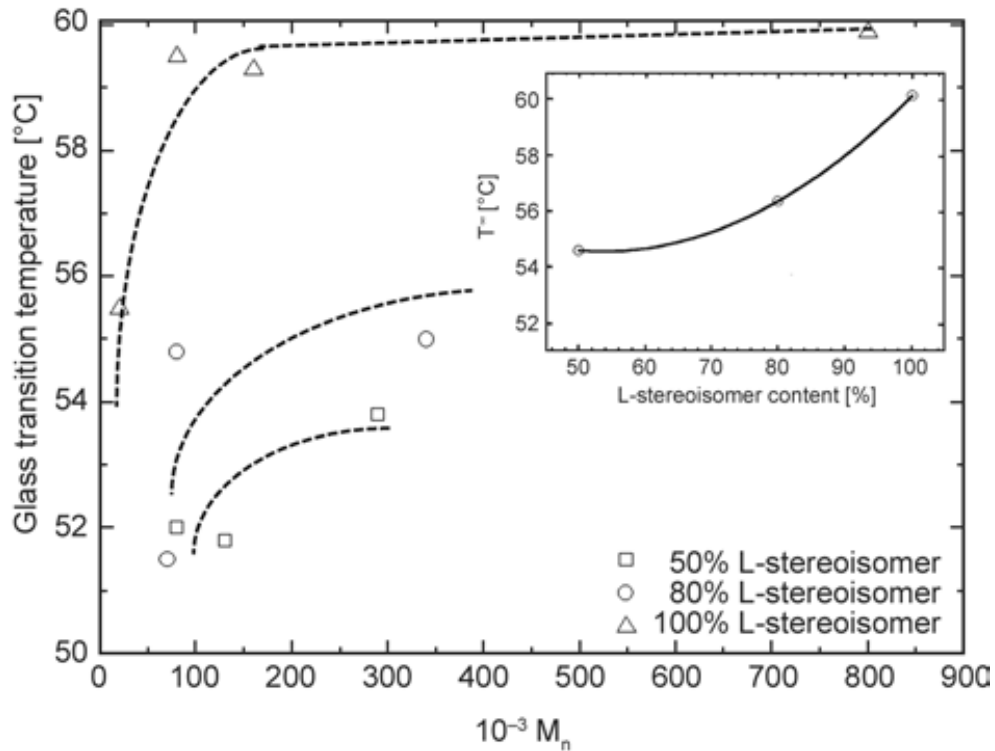


Figure 15. Effect of the molecular weight and L-stereoisomer content on the glass transition temperature of PLA [148]

As shown in the Table 2, PLA has been used in bone tissue regeneration in dentistry field, among the other fields. The use of PLA and its co-polymers or composite scaffolds provide low rigidity, controlled biodegradation and subsequent drug delivery [149]. To decrease alveolar bone resorption after tooth extraction PLA space fillers loaded with drugs could be used [150]. Depending on the type of PLA and scaffold fabrication technique, it is necessary to perform a surface treatment to improve cell attachment. For example, Polydopamine (PDA) coating of 3D printed PLA scaffolds has promoted cell adhesion and proliferation of hADSCs [151].

Table 2. Different fields of biomedical applications of PLA [144]

Field	Application
Orthopedic	Peripheral nerve and spinal cord injury regeneration Bioabsorbable screws Meniscus repair Guided bone regeneration
Cardiac	Chest wall reconstruction Stent - Synergy DES - Biolimus-eluting stent - Hybrid stent
Dentistry	Guided bone tissue regeneration (promotion of bone regeneration using a barrier membrane allowing for the repopulation of the osseous wound space [149]) Biocompatible space fillers (PLA fillers with drugs can help promote regeneration and maintain the original socket dimensions [152]. Synthetic PLA-PGA copolymer based filler was used during ridge preservation [153].
Plastic surgery	Suture Reconstructive surgery Dermal fillers Skin graft
General surgery	Hernia mesh
Gynecology	Stress incontinence mesh
Radiology	Theranostic imaging
Oncology	Drug delivery Intracranial delivery Nanoparticles – Intranasal delivery – Micelles – Thermoresponsive hydrogels – Vaccines – Transdermal delivery

3.3. Biofabrication for bone tissue engineering

“Biofabrication can be defined as the production of complex living and non-living biological products from raw materials such as living cells, molecules from extracellular matrices and biomaterials, dealing with science, engineering and technology”, where engineering part is related to the involvement of the Computed Aided Design-Computer Aided Manufacturing (CAD/CAM) [154]. Biofabrication technologies provide different applications in producing: 1) human tissues and organs for implantation, 2) extracorporeal living tissues (including devices), 3) *in vitro* 3D models of diseases for drug toxicity and drug discovery assays. Biofabrication is based on the combinations of cell and developmental biology (cells and tissue), materials sciences (biomaterials) and mechanical engineering (rapid prototyping (RP) through Computer Aided Design/Computer Aided Manufacturing (CAD/CAM) and additive manufacturing. It describes natural and technological processes in various disciplines, especially in tissue engineering and regenerative medicine (Figure 16). Challenges of biofabrication are cell survival during the fabrication process and the development of a vascularization, leading to tissue maturation through self-assembly. Mechanical engineering using RP technologies has an important role by controlling mechanical properties of the biomaterial (fabricated scaffolds suitable for tissue maturation). There are 4 different biofabrication technologies for preparation of tissue engineering constructs: single cell models, cellular aggregates models, bioprinted models and biofabricated models combining biomaterials and cells (Figure 17).

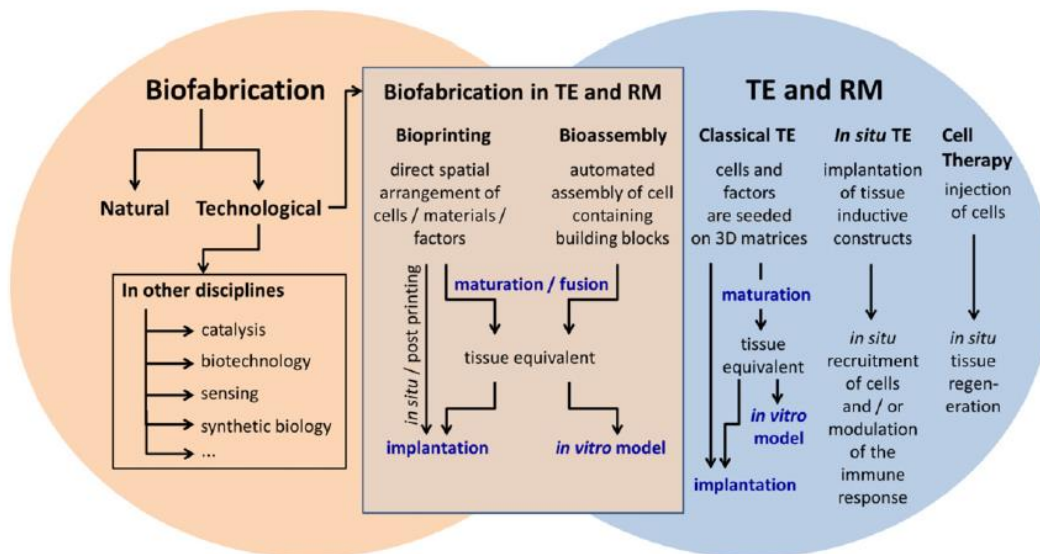


Figure 16. Biofabrication and its contribution in tissue engineering and regenerative medicine [111]

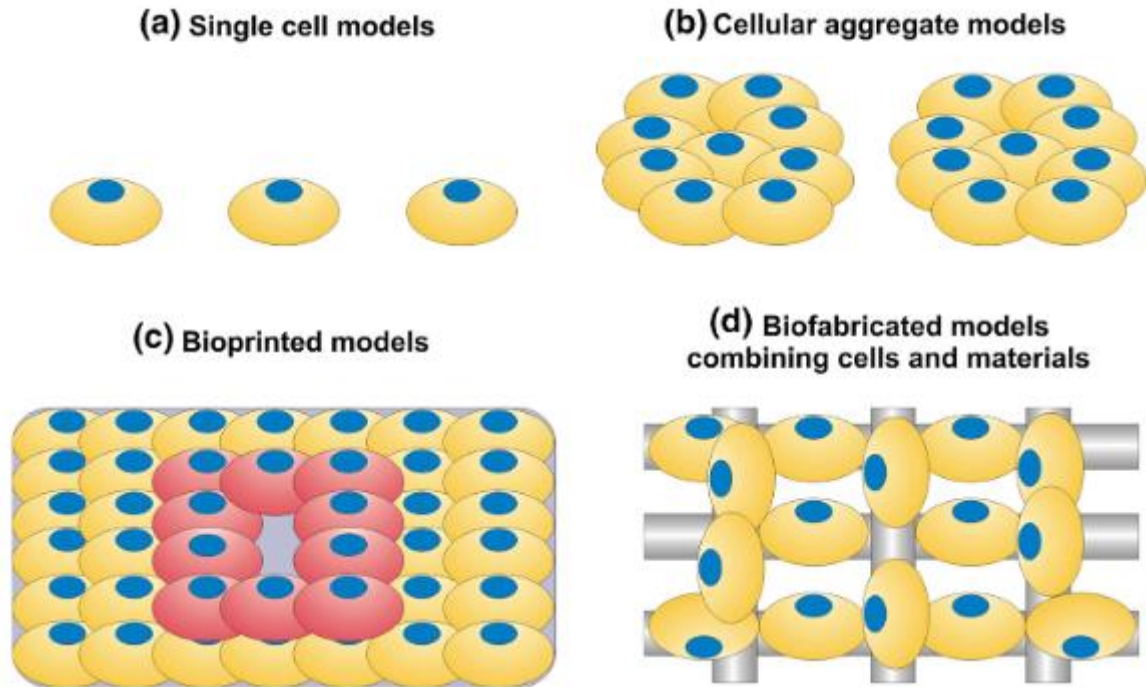


Figure 17. Biofabrication technologies for tissue engineering [155]

3.4. BioAssembly as a new approach for scaffold cellularization

To overcome some limits of conventional tissue engineering related to the difficulty to cellularize massive scaffolds for bone regeneration before implantation, different authors have proposed another approach by assembling cellularized membranes in tridimensional Layer-by-Layer (LBL) constructs [110,111,113,114,156,157]. This approach, known as BioAssembly, is based on “fabrication of hierarchical constructs with a prescribed 2D or 3D organization through automated assembly of pre-formed cell-containing fabrication units generated via cell-driven self-organization through preparation of hybrid cell-material building blocks” [111].

Layer-by-layer (LBL) BioAssembly implies the stacking of individual building blocks containing cells and an extracellular matrix. These cellularized scaffolds could have the shape of microporous membranes [112]. This enables a possibility to control the number and type of cells on each layer, leading to an homogeneous cell repartition and more efficient cell proliferation [113]. The stacking of layers containing different cell types should provide an effective control of cell colonization and efficient vascularization leading to expected cell differentiation. This

approach enables an easy manipulation of LBL assemblies with low level of cell damage, but insufficient 3D stabilization may occur in the case of thin scaffold membranes [114].

Layer by layer BioAssembly of cellularized membranes enables to control the cellular content of each layer of the final tissue engineering product.

Ren *et al.* have produced an engineering prevascularized 3D cell sheet constructs using HBMSCs and HUVECs. They superposed single cell sheets in the layer by layer manner forming final 3D product (Figure 18). HUVECs orientation toward network formation in 3D was promoted by HBMSCs *in vitro*. Blood vessel density was higher in these prevascularized constructs than in control groups after implantation in immunodeficient mice. These blood vessels were formed with host vascular network. This technology provides maximal cell-cell and cell-extracellular environment contact [158]. However, this approach has certain limits in terms of mechanical properties and low cell density [159].

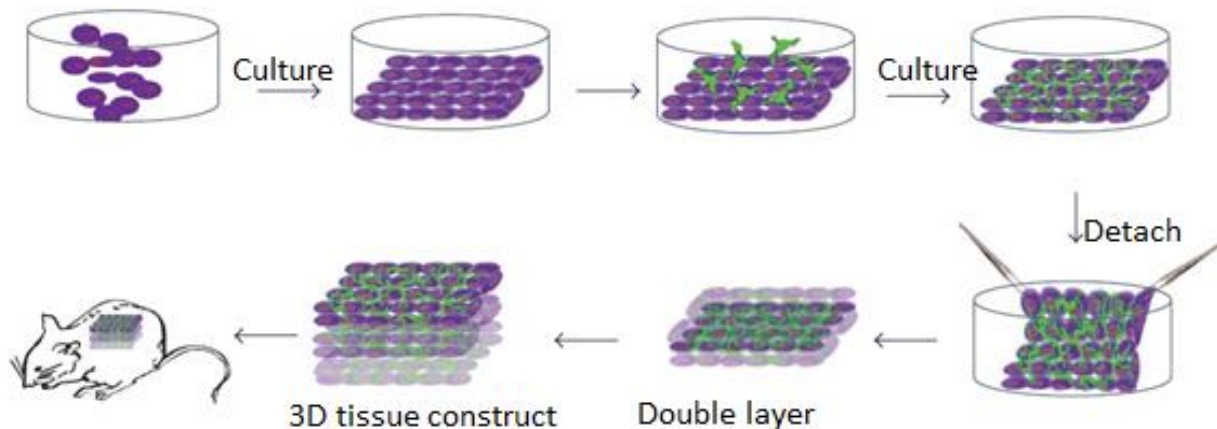


Figure 18. Cell-sheet scaffold-free biofabrication [160]

Derda *et al.* have shown that it was possible to control oxygen and nutrient gradients of 3D LBL constructs: they have fabricated LBL scaffolds including cells, and after 4 hours or 4 days, they have separated the different layers of the constructs and they have analyzed the molecular and genetic responses of each layer separately (Figure 19). They have used chromatography papers permeated with hydrogels to prove the concept. They have prepared different 3D constructs by stacking different number of layers, with HS-5 cells for *in vitro* and

Lewis lung cells for *in vivo* experiments with different cell densities in each layer. To produce suitable structures for oxygen and glucose diffusion, authors stacked eight papers of 200 μm -thick with the same cell density. After unstacking of constructs, the number of cells in inner layers was the same as the initial number of seeded cells, but the number of cells in the top layer was significantly higher. Cells in the inner layers had higher level of DNA damage. Distribution of cells depended on the cell type since their metabolic needs for oxygen and nutrients were different. Oxygen gradient was decreased in inner layers. The authors have performed the same analyses after *in vivo* implantation and they have observed similar patterns of cell survival in layers. The difference between *in vitro* and *in vivo* results was probably due to the influence of surrounding host cells that penetrated inside the implanted constructs. 3D constructs produced on this way by stacking membranes with different cell types and densities are suitable for fundamental cell biology, tissue engineering and drug development studies [161].

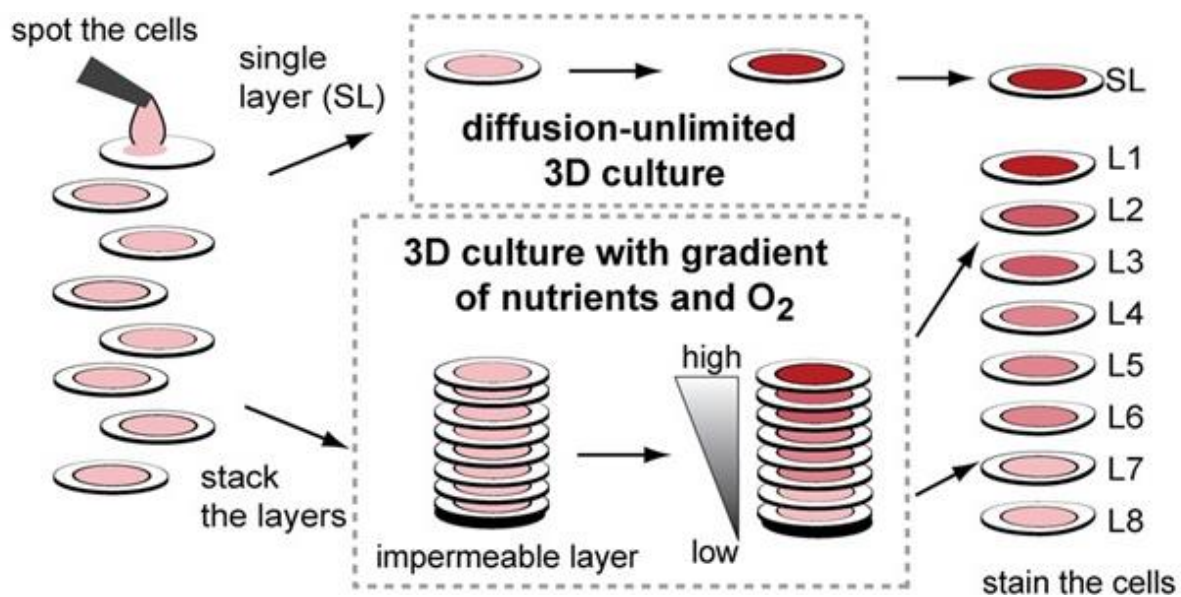


Figure 19. Stacking and unstacking of LBL constructs for analyses [161]

Catros *et al.* have evaluated cell proliferation in LBL BioAssembly constructs. They have used PCL membranes fabricated by electrospinning, which were seeded with MG63 cells transfected with Luciferase gene, to track cell proliferation through a quantification made on a photon-imager. The objective of the study was to evaluate the effect of the 3D organization of membrane scaffolds and cells on cell proliferation *in vitro*, and *in vivo* in calvarial defects in

mice. They have compared a construct of layer-by-layer stacked cellularized membranes (Figure 20a) to another construct containing cells seeded on the top of superposed membranes (Figure 203b). *In vitro* observations showed that the number of cells was similar in both types of constructs one day after cell seeding. Cell number was not significantly different in LBL bioassemblies during time, while in cell-seeded stacked membranes cell number decreased between 14 and 21 days of culture. A significant difference was observed between this approach and layer-by-layer stacked cellularized membranes for the same time points (Figure 21a). *In vivo* observations by photon-imager confirmed *in vitro* results. Cell proliferation was statistically more efficient for LBL assemblies than for seeded stacked membranes at all time points (Figure 21b). LBL approach using PCL seeded membranes provided a suitable environment for cell proliferation. This approach of using the scaffolds in the shape of membranes could be easily modified depending on the target tissue using different cell types, different biomaterials and scaffold fabrication methods for more complex tissue constructs [113].

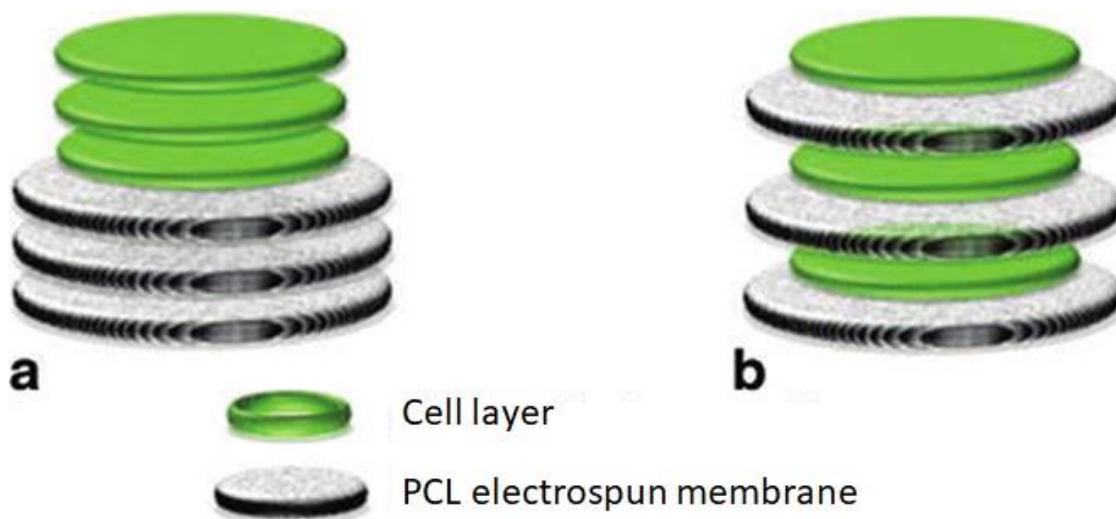


Figure 20. 2 approaches for cell seeding onto PCL membranes [113]

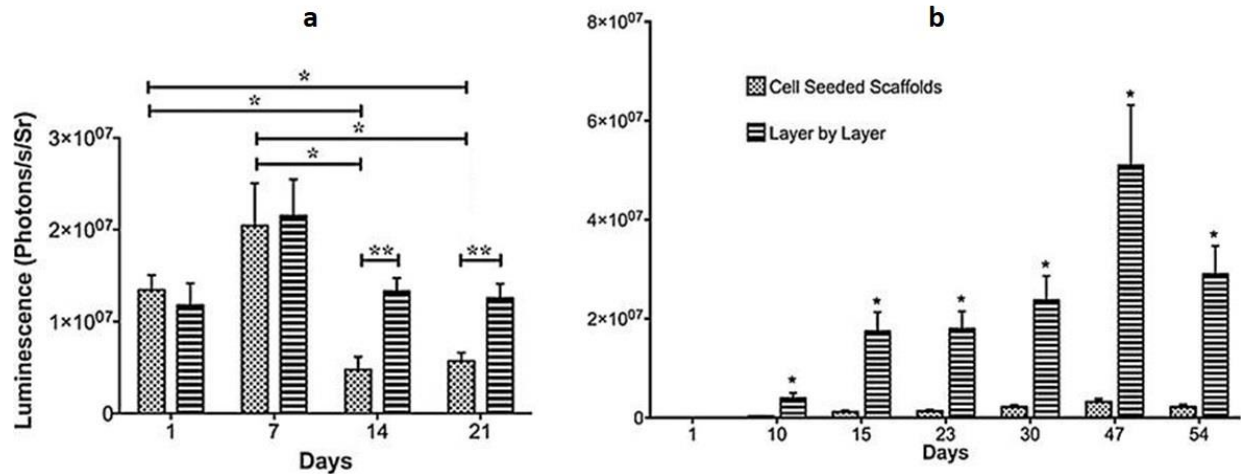


Figure 21. Quantification of proliferation of MG63 cells on PCL electrospun scaffolds a) *in vitro* and b) *in vivo* [113]

Another group have used the same principle of layer-by-layer assemblies using nanofibrous PCL/gelatin membranes fabricated by electrospinning, and seeded with adipose-derived stem cells ADSCs. The experiments were conducted *in vitro* and *in vivo* in rat calvarial defects. These PCL membranes were biocompatible with suitable physical properties for bone regeneration. They had adequate mechanical properties and improved cell adhesion provided by gelatin. Membranes were 70 μm thick and permeable to provide efficient oxygen and nutrients diffusion in 3D when cellularized scaffolds were assembled. Since ADSCs can differentiate toward osteogenic cells and produce extracellular matrix (ECM) followed by growth factor secretion, these cells were seeded in passage 4 onto membranes in osteogenic medium. The cells were seeded on both sides of the membranes in order to provide immediate contact of cells of all layers. After superposing of cellularized membranes to form layer-by-layer constructs, they were stabilized with stainless steel mesh clips. These clips had a role to disable any displacement of the membranes before sufficient extracellular matrix secretion for self-stabilization (Figure 22). Implantations of these constructs induced the filling of almost 90 % of a rat calvarial defect after 12 weeks (Figure 23c) with the highest bone mineral density, comparing to negative control groups (empty defects) (Figure 23a) or group with implanted LBL stacked membranes without cells (Figure 23b). Osteoblastic genes in this kind of 3D organization of cells and membranes showed more efficient expression, compared to control samples. Highly porous structure of membrane assemblies provided a suitable environment for ADSCs growth and proliferation in 3D and their differentiation toward osteogenic cell lineages. This 3D system promoted cell-to-cell and cell-to-tissue interactions which induced cell proliferation as well a high level of new tissue formation [156]. However, the authors have not included a massive scaffold control group in their experiment.

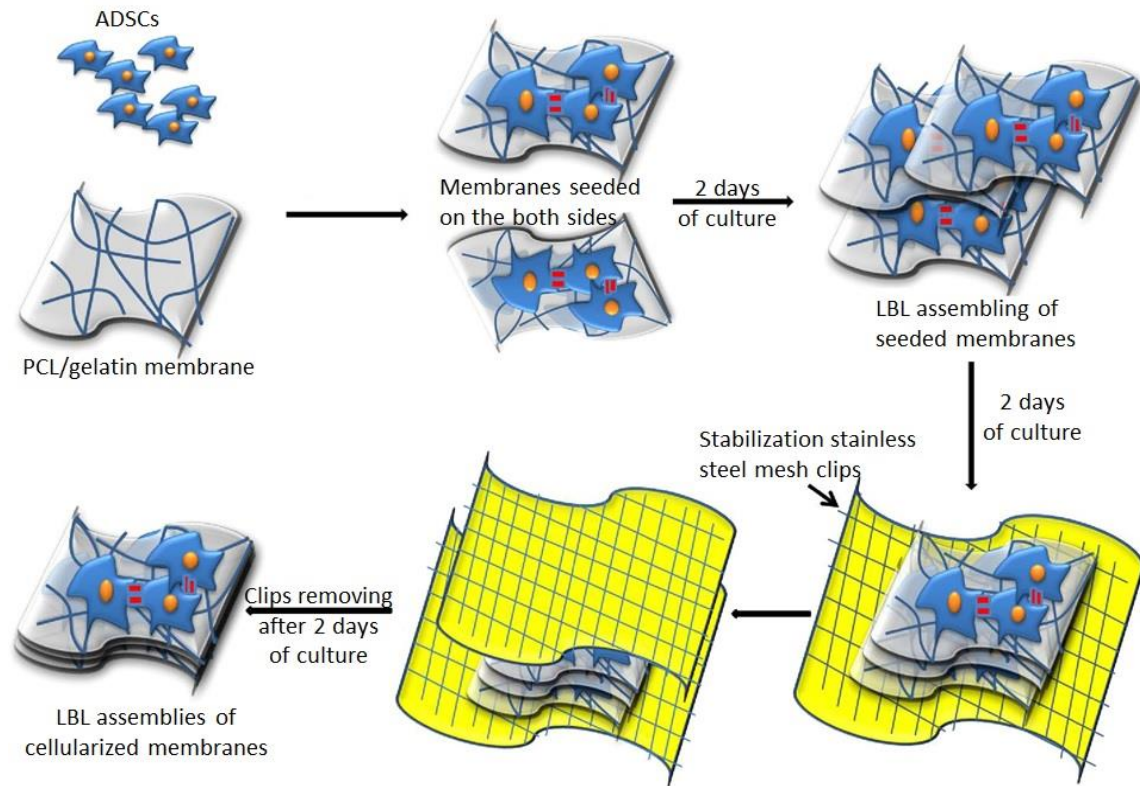


Figure 22. Design of preparation of LBL assemblies of ADSCs-lead PCL/gelatin membranes [156]

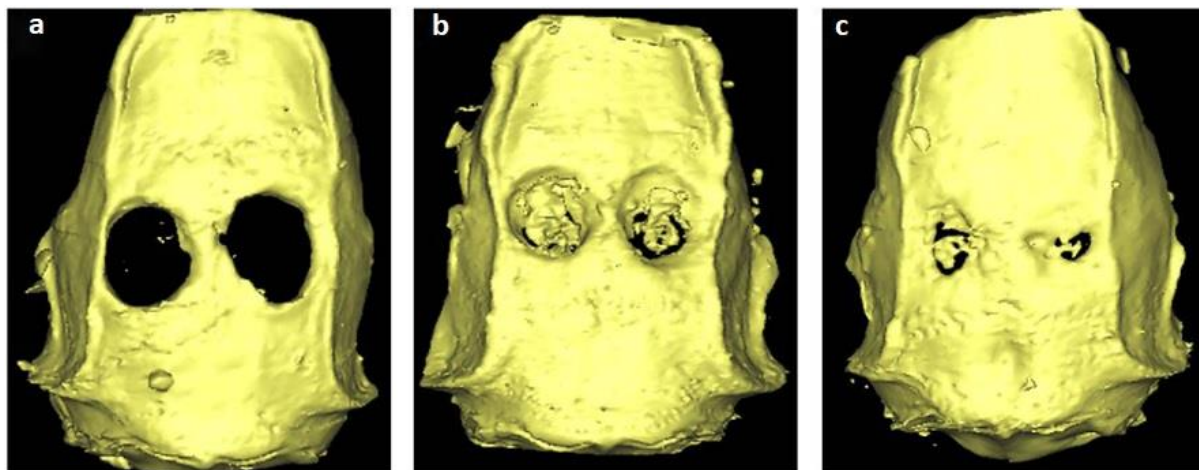


Figure 23. Micro-computed (μ CT) images of rat calvarial defects 12 weeks after implantation : a) control sample without any implantation, b) cell-free superposed membranes, c) ADSCs-laden LBL-stacked membranes [156]

Kim *et al.* have used the same principle of cellularized membranes stacking for muscle tissue engineering. PCL membranes were fabricated again by electrospinning. Authors have improved this membrane fabrication technique by using perpendicularly arranged aluminum strips in order to obtain well-oriented 800 nm fibers later fixed with frames (Figure 24i). Since LBL assembly provides the possibility to seed and control organization of different cell types within entire 3D construct, 3 cellularized membranes were combined in order to obtain skeletal muscle: endothelial and fibroblast layers by seeding C2C12 myoblasts, HUVECs and fibroblasts HS68, respectively (Figure 24ii-iv) [162]. The membranes were not designed like bone scaffolds because the architecture of the skeletal muscle tissue contains a dense bundle of uniaxially aligned myotubes. This fiber orientation enabled myotube orientation of C2C12 cells. Vascular membrane was enriched with matrigel to mimic microvascular system and endothelial tube-like formation was formed. The adaptability of this technique to produce tissue engineering constructs reflected in the possibility to stack membranes in perpendicular manner (Figure 25b). These 2 different ways to stack membranes did not have any important effect on vascular and tubular formation when stacking membranes seeded with HUVEC and HS68 (Figure 25). HUVEC membrane was in contact with fibroblast membranes in order to mimic vascularized tissue since fibroblasts produce angiogenesis growth factors. Thus it was confirmed in this experiment that the use of cellularized membranes provided possibility to control tissue microarchitecture and cell type within the entire 3D construct [162].

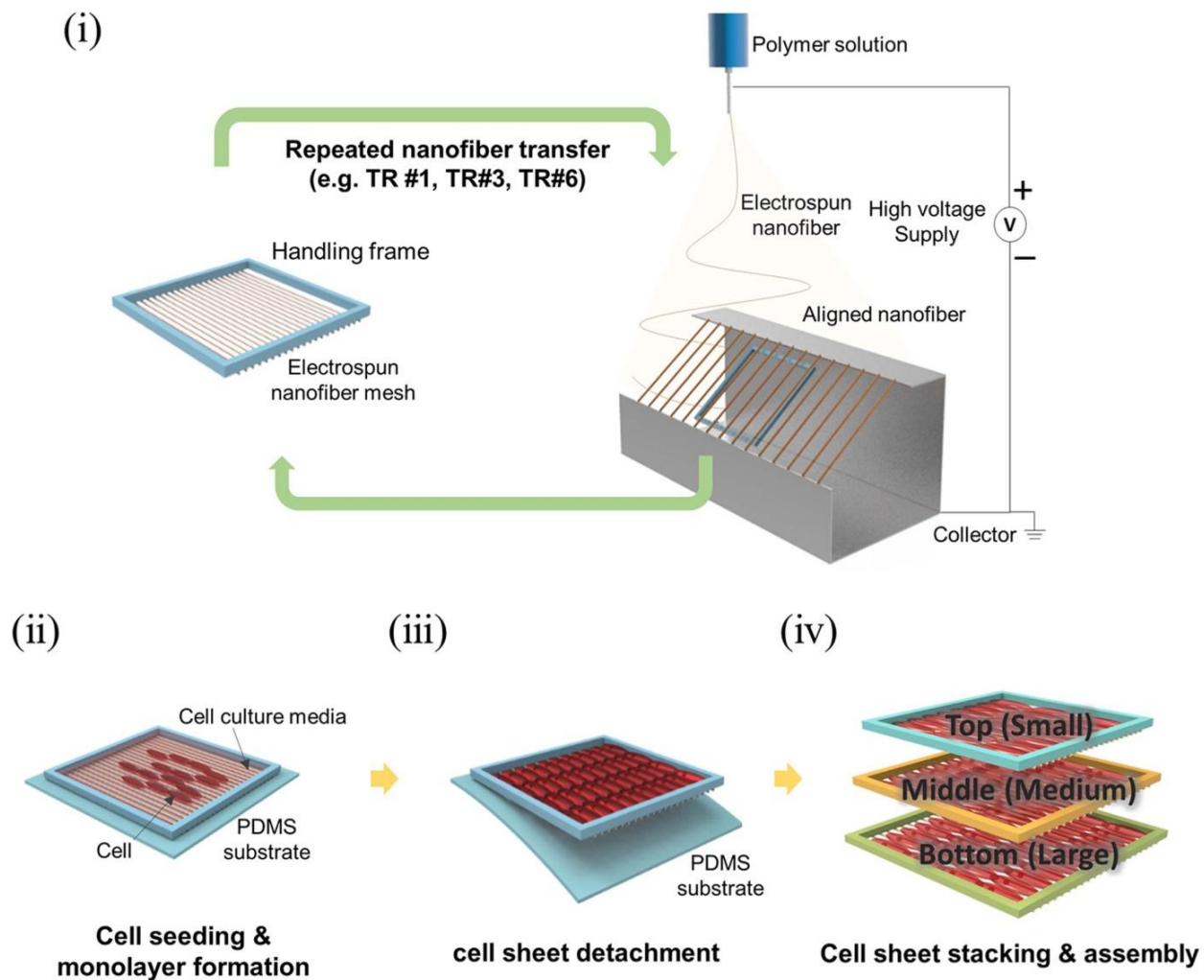


Figure 24. Illustration of entire process to produce LBL assemblies of cellularized electrospun PCL membranes : i) membrane fabrication by electrospinning, ii) seeding of cells onto PCL membranes placed on a PDMS substrate; iii) detachable cell sheets easy for manipulation, iv) LBL assembling of cellularized PCL membranes [162]

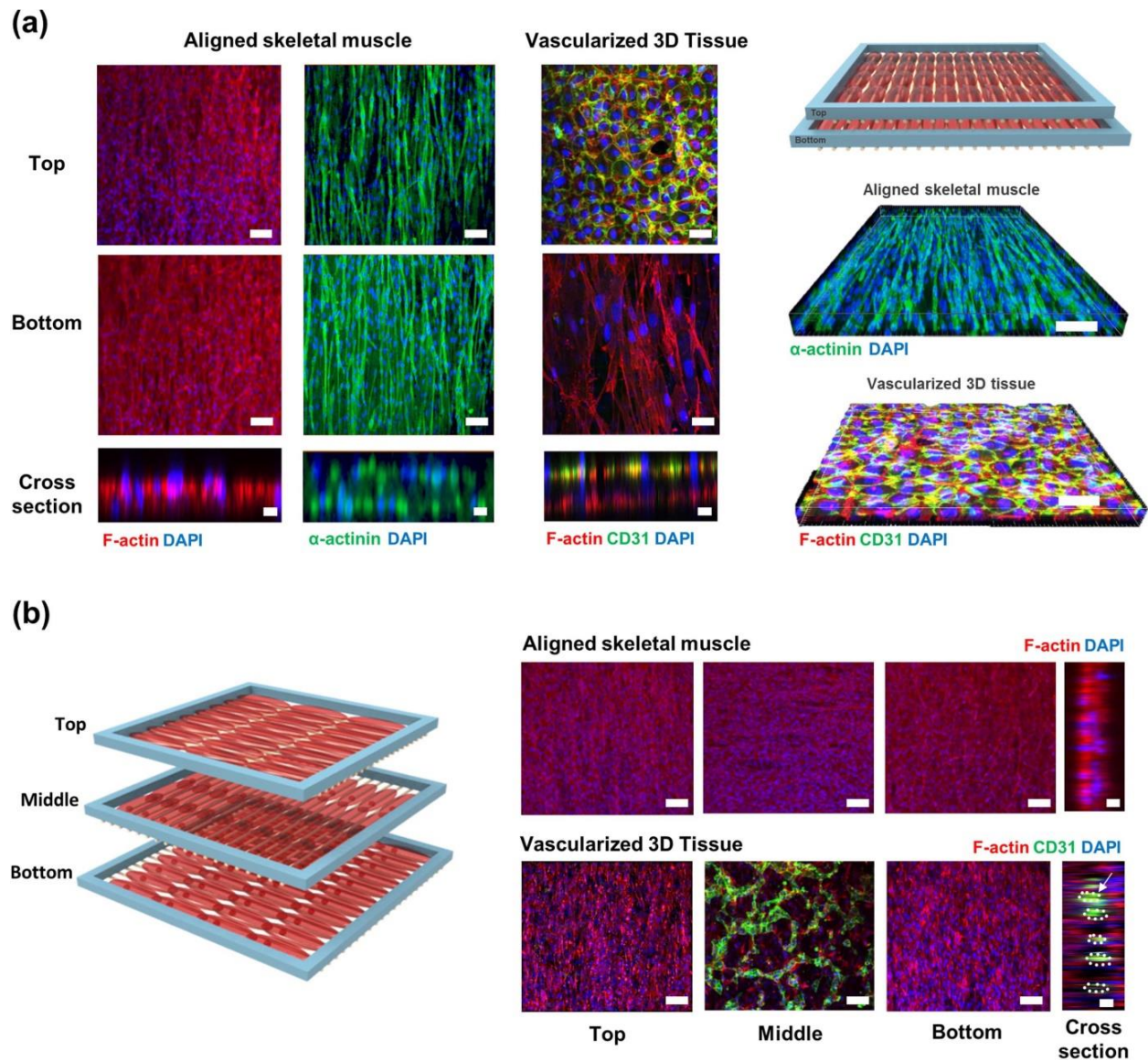


Figure 25. The effect of parallel and perpendicular stacking of cellularized membranes on formation of vascularized dermal tissue : a) parallel stacking of 2 membranes with HUVEC on the bottom and HS68 on the top membrane, b) perpendicular stacking of 3 membranes with HUVEC on the middle membrane and HS68 on the outer ones [162]

THESIS OBJECTIVES

The general objective of this doctoral thesis was to evaluate the fate of layer-by-layer assembly of cellularized polymer membranes for cell proliferation and differentiation, compared to “conventional” fabrication of a tissue-engineered construct composed of a massive scaffolds seeded with cells. More specifically, we have characterized *in vitro* and *in vivo* layer-by-layer constructs made of cellularized membrane scaffolds fabricated by RP and seeded with mono- and co-cultures of human primary cells. We have also evaluated the effect of this 3D organization on tissue formation compared to conventional methods described previously.

Secondary objectives were related to the membrane scaffold fabrication process, and several experiments were conducted to:

- Fabricate porous PLA membranes using two different RP technologies: direct 3D printing using starting PLA in powder form and Fused Deposition Modeling (FDM) using thermoplastic polymer filament of PLA.
- To characterize physico-chemical properties of PLA scaffolds and to observe if they were affected by FDM process.
- To evaluate *in vitro* cell viability, proliferation and differentiation for mono- and co-cultures before any 3D assembly, knowing that HBMSCs can differentiate toward osteogenic cell lineages and that EPCs from umbilical cord blood seeded with them in co-cultures induce cell-to-cell communication through ECM producing with growth factor secretion. EPCs stimulate osteoblastic differentiation of HBMSCs when seeded in co-cultures at the same time [163].
- To keep single membranes on the bottom of cell culture wells while seeding and to stabilize the LBL bioassemblies. This was difficult to perform cell seeding because the membranes were floating in cell culture medium, thus it was necessary to keep LBL assemblies compact, without moving of layers during time (culture media change) before cells produce ECM, which can provide sufficient stabilization to 3D constructs. This stabilization of LBL assemblies is important as well for implantation process.
- To characterize *in vivo* the effect of a cell culture system (cell-free, mono- and co-culture) and 3D organization of cells and PLA membranes (LBL bioassembly and large massive scaffold) on vascular network formation 8 weeks after implantation in immune-deficient mice since vascularization within large tissue engineering constructs is one of the most important challenge of tissue engineering.

RESULTS

FIRST PART:

**Direct 3D printing of poly(lactic) acid membranes and their
biological characterization**

**2D and 3D evaluations of PLA membranes seeded with human
primary cells**

A. INTRODUCTION

In order to obtain functional tissue engineering products, it is necessary to perform a 3D cell culture model. As discussed before, it has been frequently observed that cell migration inside 3D macroporous scaffolds is limited. Since cells have difficulties to penetrate in inner parts of large 3D scaffolds when seeded on their surfaces, layer-by-layer bioassembly might be a suitable approach to overcome this limitation.

The aim of this first set of *in vitro* experiments was to evaluate the proliferation, differentiation and migration of human primary cells isolated from bone marrow and umbilical cord blood in two and three dimensions using layer-by-layer approach to assemble cellularized 3D printed poly(lactic) acid membranes.

These evaluations were performed without any biomaterial coating, nor osteogenic components or growth factors supplementation. This first study can be separated in two parts: 2D and 3D evaluations.

2D evaluations

PLA membrane (scaffold) fabrication was performed at the Institute for BioEngineering of Catalonia (IBEC) in Barcelona, Spain. The scientific collaboration between IBEC laboratory and Biotis was initiated several years before through different projects in the field of bone tissue engineering. PLA was chosen for membrane fabrication because there was a strong experience in 3D printing of PLA using 3Dn-300, Sciperio/nScript (Inc. Orlando, Florida) at IBEC and this biomaterial has shown suitable mechanical and biological properties for bone tissue engineering [164].

2 types of human primary cells were used in this part: human bone marrow stroma cells (HBMSCs) and endothelial progenitor cells (EPCs). HBMSCs were chosen because of their high potential to differentiate toward osteoblastic cells and their source was established by an agreement between BioTis and University Hospital of Bordeaux. Bone marrow was collected from patients undergoing orthopedic surgeries. EPCs have already been used in co-cultures with HBMSCs, and it resulted in an increase of proliferation and differentiation of HBMSCs [165]. EPCs were isolated from umbilical cord blood harvested after birth deliveries (agreement with University hospital of Bordeaux). Beside co-cultures, human primary cells were seeded in mono-cultures as well in order to see their behavior on PLA.

Scanning Electron Microscopy (SEM) was used to collect qualitative information about material surface at high resolution. The scaffold fabrication quality was evaluated for pore size and shape. Then, the same technology was used to observe cell morphology at certain time

points after seeding onto PLA membranes. Cells had expected morphology in both, mono- and co-cultures and maintained cell viability during 14 days. Alkaline phosphatase (ALP) is an early osteoblastic marker and mesenchymal cells that differentiate toward osteoblastic lineages display violet granulation staining inside their cytoplasm [166]. Von Willebrand Factor (vWF) is a glycoprotein marker produced only by endothelial cells [167]. Expressions of these two markers showed cell differentiation toward osteoblastic and endothelial lineages during time

“CyQUANT® Cell Assay” allows easy, fast and sensitive cell proliferation quantification by the quantification of DNA synthesis. It showed that proliferation of HBMSCs and co-cultures was significantly higher after 14 days.

3D evaluations

Two different experiments were performed to evaluate cell behavior and their fate when cellularized PLA membranes are superposed in LBL 3D constructs: phenotype characterization and observation of cell migration between PLA layers.

Real Time Polymerase Chain Reaction (RT-qPCR) showed osteoblastic genes expressions in different types of LBL bioassemblies during time without significant difference between constructs with different position of EPCs in 3D.

EPCs had the same effect on osteoblastic differentiation when seeded in co-cultures with HBMSCs in all layers or in superposed alternating layers of mono-cultures. Then, 2 photon microscopy observations of LBL constructs containing co-cultures in alternating layers with tagged cells showed migration of EPCs between layers after 14 days.

ARTICLE 1

Layer-by-Layer Bioassembly of Cellularized Polylactic acid Porous Membranes for Bone Tissue Engineering

Vera GUDURIC, Carole METZ Robin SIADOUS, Reine BAREILLE, Riccardo LEVATO,
Elisabeth ENGEL, Jean-Christophe FRICAIN, Raphaël DEVILLARD, Ognjan LUZANIN,
Sylvain CATROS

*Accepted on the 15th of March 2017 and published in the Journal of Materials
Science: Materials in Medicine in May 2017*

1. INTRODUCTION

A typical bone tissue engineering (BTE) approach requires cells specific to the bone tissue, biochemical growth factors as well as porous biocompatible scaffold [1]. The role of the scaffold is to provide a support for cell proliferation and differentiation and it must possess specific features regarding pore diameters, porosity and microscopic dimensions, as well as adequate osteoconductive and osteoinductive properties [2]. There are different biomaterials being used for BTE nowadays, such as calcium phosphates, metals, hydrogels, polymers or their combination [3–9]. Different groups have recently used scaffolds made of polylactic acid (PLA) as a support for bone regeneration. Pure PLA scaffolds can be used [10,11] while coated PLA [12] and PLA-based composite materials have also been described [9,13–16]. The FDA has approved PLA for different biomedical applications, and it has proven adequate osteoconductive and osteoinductive properties for bone applications. Different types of human and animal cells have shown high ability to attach onto PLA scaffolds [17–19]. This polymer has been used to fabricate BTE scaffolds using several Rapid Prototyping (RP) methods, mostly by fused deposition modeling (FDM) [12], and 3D printing [20–22].

Conventional TE approach is based on the seeding of macroporous scaffold on its surface (“Top-Down” = TD), resulting in many cases in poor cell viability inside the scaffold, because it’s difficult for cells and nutrients to penetrate and survive in the core of the scaffold [23]. “Bioassembly” is based on self-induced assembly of cellularized building blocks and might also be called a “Bottom-Up” (BU) approach [24]. The main advantage of this approach is the possibility to seed different cell types onto one scaffold, which may lead to a homogeneous cell colonization and proliferation inside the scaffold. Layer-by-layer (LBL) assemblies of cellularized porous biomaterials may be used to fabricate cellularized constructs for bone tissue regeneration. The choice of the right order of layers plays an important role in order to obtain the best final implantable construct [25]. It was shown before that the combination of human bone marrow stromal cells (HBMSCs) and human umbilical vein endothelial cells (HUVECs) in alternating layers of cell sheets enables a high vascularization subcutaneously in mice [26]. Moreover, angiogenic factors secretion was augmented when alternates layers of mesenchymal stem cells and endothelial cells are stacked [27]. It was shown previously that it is possible to control the microenvironment inside the scaffold when using LBL approach since it enables the control of each layer accurately [28]. Another experiment based on LBL paper-stacking using ADSCs (Adipose Derived Stem Cells) and PCL/gelatin *in vivo* has shown that the LBL approach gave a promising osteogenic-related gene expressions [29]. We have already tested this method with MG63 cells transduced with Luciferase gene and PCL electrospun scaffold biopapers. Luciferase tracking with photon-imager displayed that cell proliferation was increased when the materials and cells were stacked layer-by-layer [30].

Concerning the cellular component of bone tissue engineering, it is already known that endothelial progenitor cells (EPCs) can modulate differentiation properties of mesenchymal

stem cells (MSCs) in a coculture system [31]. PLA has already been used as a scaffold for MSCs and EPCs isolated from the rat [32] but there are no data available for the coculture of human endothelial and osteoblastic cells on this material. The use of PLA scaffold membranes to support cell culture could improve the manipulation and mechanical properties of such constructs.

The aim of this work was to build PLA membranes cellularized with human osteoprogenitors and endothelial progenitor cells and to evaluate its properties *in vitro* in 2- and 3-dimensions

2. MATERIALS AND METHODS

2.1. Preparation of PLA membranes

PLA membranes were fabricated at the Institute for Bioengineering of Catalonia (IBEC) by direct 3D printing method, an additive RP method based on the extrusion of PLA dissolved in chloroform through a nozzle. We have used a 3Dn-300, Sciperio/nScript (Inc. Orlando, Florida) printer for this study. The PLA solution was prepared by dissolving a Poly(95L/5DL) lactic acid (Corbion Purac) in chloroform (5% w/v) at 45°C during 24h and then syringes of 5mL were filled, closed with paraffin film and stored at -20°C before use. The printing process was controlled using a tuned motor speed and pressure, in order to be adapted to viscosity of the solution. The motor speed was 3 mm/s and the pressure was between 40-80 psi. G27 nozzles were used for extrusion. In order to be used for experiments, raw membranes (4cm²) were cut with a tissue punch into 8mm diameter circles.

Before cell culture experiments, PLA membranes were rinsed with phosphate buffered saline (PBS) 0.1 < pH 7.4 (Gibco) and sterilized in a solution of ethanol 70% (v/v) during 30 minutes. Then, the membranes were rinsed twice with PBS. A small amount of 2% agarose (A9539-250G Sigma-Aldrich, St Louis, MO, USA) prepared in PBS was placed in each well before placing the membranes in order to prevent cell adhesion on tissue culture plastic (TCP). The membranes were rinsed with culture media during 24h before seeding the membranes with cells. All experiments were performed in 48 well plates (Corning Inc – Life Sciences, Durham, NC, USA).

2.2. Cell isolation and tagging

Two types of human primary cells were used in this study: Human Bone Marrow Stromal Cells (HBMSCs) were isolated from bone marrow retrieved during surgical procedures (Experimental Agreement with CHU de Bordeaux, Etablissement Français du Sang, agreement CPIS 14.14). Cells were separated into a single suspension by sequential passages through syringes fitted with 16-, 18- or 21-gauge needles. After the centrifugation of

15 minutes at 800g without break at room temperature, the pellet was resuspended with α -Essential Medium (α -MEM; Invitrogen) supplemented with 10% (v/v) fetal bovine serum (FBS) [33]. Endothelial Progenitor Cells (EPCs) were isolated from 30 μ L of diluted cord blood (Experimental Agreement with CHU de Bordeaux, Etablissement Français du Sang, agreement CPIS 14.14) in 1X PBS and 2mM ethylene diaminetetraacetic acid (EDTA, Sigma-Aldrich, St Louis, MO, USA). 15 mM of Histopaque solution (Sigma-Aldrich) was added. Then centrifugation was performed at 400g for 30 minutes and the ring of nuclear cells was removed and washed several times with 1X PBS and 2nM EDTA. At the end, cells were cultured in endothelial cell growth medium-2 (EGM-2, Lonza-Verviers, France) with supplements from the kit and 5% (v/v) FCS (GIBCO Life Technologies, Karlsruhe, Germany) on a 12-well cell plate. The cell plate was coated with collagen type I (Rat Tail, BD Biosciences). Non adherent cells were removed at Day 1 and media was changed every other day [34]. The medium for endothelial cells growth contained 5% FBS, 0,1% human epidermal growth factor (hEGF), 0,04% Hydrocortison, 4% human fibroblastic growth factor-b (hFGF-b), 0,1% vascular endothelial growth factor (VEGF), 0,1% R3 insulin-like growth factor-1 (R3-IGF-1) 0,1% ascorbic acid, 0,1% gentamicin, amphotericin B (GA) (Lonza-Verviers, France). Both, HBMSCs and EPCs were incubated in a humidified atmosphere of 95% air, 5% CO₂ at 37°C. The culture medium was changed every other day.

To evaluate the cell migration during LBL 3D experiments, both types of cells were tagged with fluorescent proteins. HBMSCs were tagged with green fluorescent protein (GFP) which exhibits a green fluorescence when exposed to light in the blue or ultraviolet range. EPCs were tagged with Td-Tomato, which exhibits a red fluorescence when exposed to the light in green range [35]. The lentiviral vectors contained GFP or Td-Tomato protein gene under the control of the MND (for GFP) or phosphoglycerate kinase (PGK) promoter (for Td-Tomato) for cell labeling. 2x10⁵ freshly trypsinized HBMSCs ou EPCs (low subculturing) in suspension were mixed with 6x10⁶ viral particles (MOI for GFP: 15; MOI for Td-Tomato: 30) for viral transduction (multiplicity of infection). After 24 h in culture, virus-containing medium was replaced by a fresh one to provide the cell growth. Medium was changed every other day.

2.3. Cell seeding and Characterization in 2D

2.3.1. Cell seeding in 2D

PLA membranes were stabilized on the agarose with glass rings in order to avoid the floating of membranes in the culture media. HBMSCs and EPCs were seeded onto membranes as mono- (HBMSCs 50.000 cells/cm², EPCs 100.000 cells/cm²) and co-cultures (HBMSCs 25.000/cm² + EPCs 50.000 cells/cm²). Culture media were changer every other day.

All 2D experiments were performed on PLA membranes seeded with different combinations of human primary cells (1 seeded membrane = 1 sample). Examined time points were Day 1, Day 3, Day 7, Day 14 and Day 21.

2.3.2. Cell Characterization in 2D

2.3.2.1. Live-Dead assay

The viability of the cells seeded on PLA membranes was tested by Live-Dead assay (LD, Life Technologies), which was based on acetoxymethylester of calcein (Calcein-AM) and ethidium homodimer-1 (EthD-1) [36]–[38]. Calcein-AM was cleaved in the cytoplasm by esterase and thus indicated live cells showing the green fluorescence. EthD-1 enters cells with damaged membranes and binds to nucleic acids, producing a red fluorescence of dead cells. The assay was performed by removing the culture media, rinsing the seeded PLA membrane with Hanks' balanced salt solution (HBSS, GIBCO) and addition of the solution of Calcein-AM and EthD-1 diluted in Hanks'. The solution was incubated during 15 minutes in a humidified atmosphere of 95% air, 5% CO₂ at 37°C. Fluorescence was observed with confocal scanning microscopy (Leica, TSC SPE DMI 4000B) with LAS-AF (Leica Advanced Suite-Advanced Fluorescence) software.

2.3.2.2. Quantification of the area covered by cells

Live-Dead images obtained by confocal microscope were used to calculate areas covered by live or dead cells by ImageJ (<https://imagej.nih.gov/ij/>). Five images (4 close to the borders at the ends of perpendicular axes and one in the middle) were used for each condition (mono- or co-cultures) and each time point (total of 45 images). Color channels (green and red) were split for each image and percentage of covered areas were calculated for each color. Statistical analyses were performed with GraphPad Prism 6 software using a 2way ANOVA and Bonferroni tests.

2.3.2.3. Scanning Electron Microscopy

Cell morphology was observed with a microscope Hitachi, S-2500 Scanning Electron Microscope (SEM). After 14 days of cell culture onto PLA membranes, the samples were fixed with paraformaldehyde (PFA) 4% and dehydrated in graded ethanol (EtOH) solution (30%, 50%, 70%, 90%, 100%) and then in dexamethylsilazan and air dried, followed by gold coating. The accelerating voltage used for the observation was 12kV and the samples were observed with magnification x80 and x200. Pictures were acquired using MaxView® and SamX® softwares.

2.3.2.4. *CyQuant assay*

Cell proliferation on PLA was evaluated with CyQuant® Cell Assay kit (In vitrogen C7026). This assay was based on fluorescent quantification of one protein which binds to cell DNA. The culture media was removed at each time point and culture plates were frozen and kept at -80°C to process all samples together. Finally, all plates were left at the room temperature for thawing. The lysis solution was first added in all samples and then 200µl of the buffer were added following the manufacturer's instructions. All samples were transferred in 96 well plates and mixed for 2-5 minutes in dark. The fluorescence of the solutions was measured at 480nm and 520nm using Victor X3 2030 Perkin Elmer.

2.3.2.5. *Immunofluorescent analysis*

The EPCs mono-cultures and the co-cultures HBMSCs+EPCs on PLA membranes were fixed with 4% (w/v) Paraformaldehyd (PFA) at 4°C during 15 min and permeabilized with Triton X-100 0.1 % (v/v) during 10 min. Endothelial phenotype was observed using intracellular marker von Willebrand Factor (vWF). The samples were incubated 1h in PBS containing 1% (w/v) Bovine serum albumin (BSA, Eurobio, France) before incubation with primary antibody. VWF primary antibody (Rabbit) was diluted in PBS 1X with 0.5 % (w/v) BSA at 1/300 (Dako, Glostrup, Denmark). The primary antibody was incubated 1.5 hour at the room temperature. Then, the cells were rinsed with PBS and incubated with the secondary antibody: Alexa 488-conjugated goat anti-rabbit IgG diluted at 1/300. Subsequently, cells were washed with PBS and incubated with the nuclear probe DAPI (4', 6'-diamino-2-phenylindole, FluoProbes 5 mg ml⁻¹, dilution 1:5000) for 10 min at room temperature, in order to label the nucleus in blue. The lasers used were 488 nm (green), 561 nm (red) and 405 nm (blue). The observations were performed at 100x magnification and the pictures were taken every 2.4 µm in "z" orientation. The 3D reconstruction was performed with LAS-AF (Leica Advanced Suite-Advanced Fluorescence) software.

2.3.2.6. *Alkaline phosphatase (ALP) assay*

Intracellular ALP activity was detected as an early osteoblastic marker. We have used the Ackerman technique, which is based on conversion of a colorless p-nitrophenyl phosphate to a colored p-nitrophenol (Sigma diagnostic kit, Aldrich). Three different conditions were tested: 1) mono-culture (HBMSCs) with induction media (α -MEM + 1/1000 dexamethasone, 1/10000 ascorbic acid, 1/100 β -glycerolphosphate, Iscove's Modified Dulbecco (IMDM, GIBCO), 10% SVF); 2) mono-culture (HBMSCs) without induction media (α -MEM alone) and 3) co-cultures (α -MEM + EGM-2 50/50). The samples were fixed with 4% (v/w) PFA during 10 min at 4°C. Then the samples were stained with alkaline dye (Fast blue RR salt supplemented with Naphtol AS-MX phosphate alkaline solution 0.25%, Sigma Aldrich) away

from light during 30 min. The observations were performed with an optical microscope (Leica DMI 3000 B) connected with a digital camera (Leica DFC 425C).

2.4. Layer-by-Layer assembly of cellularized membranes in 3D

2.4.1 Layer-by-Layer Assembly

After seeding the PLA membranes in 2D using HBMSCs or EPCs or cocultures of HBMSCs and EPCs, the membranes were stacked Layer-by-Layer (LBL) to obtain a 3D composite material (**Figure 1**).

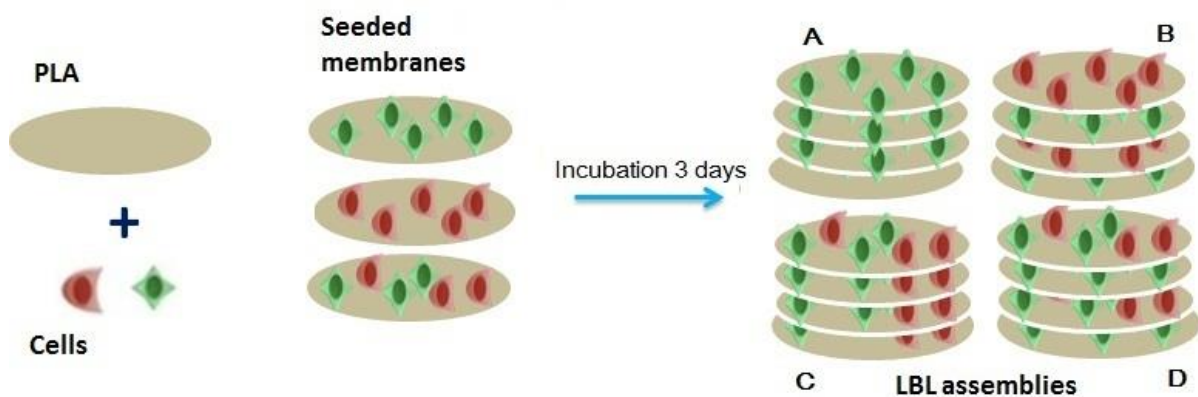


Figure 1. LBL bio-assembly of PLA membranes seeded with human cells. A – HBMSCs/ HBMSCs/ HBMSCs/ HBMSCs; B – HBMSCs/EPCs/HBMSCs/EPCs; C – Cocultures/ Cocultures/ Cocultures/ Cocultures; D – HBMSCs/Coculture/HBMSCs/Coculture

These 3D constructs were prepared by assembling 4 PLA membranes seeded with human primary cells (HBMSCs alone or coculture of HBMSCs and EPCs) after 3 days of culture in 2D. We prepared 4 different types of 3D constructs: A samples consisted of 4 membranes seeded with HBMSC, B samples had alternating layers of monocultures of HBMSCs and EPCs, C samples were constructed with co-culture membranes and D samples had alternating layers of mono-cultures of HBMSCs and co-cultures (**Figure 1**). LBL constructs were first characterized by observing the migration of tagged endothelial cells inside the LBL constructs using 2 photons microscopy, then the osteoblastic differentiation of the LBL 3D constructs was evaluated using Quantitative Polymerase Chain Reaction (qPCR).

2.4.2. Quantitative real-time polymerase chain reaction (QPCR)

Osteoblastic differentiation was examined on 3 different types of LBL constructs: HBMSCs in all 4 layers of 3D constructs, HBMSCs/EPCs/HBMSCs/EPCs and cocultures in all 4 layers (Figure 1 A, B, C). Total RNA was extracted using the RNeasy Total RNA kit (Qiagen, AMBION, Inc. Austin, Texas, USA), as indicated by the manufacturer and 1µl was used as the template for single-strand cDNA synthesis, using the Superscript pre-amplification system (Gibco) in a 20 ml final volume, containing 20 mM Tris-HCl, pH 8.4, 50 mM KCl, 2.5 mM MgCl₂, 0.1 mg/ml BSA, 10 mM DTT, 0.5 mM of each dATP, dCTP, dGTP and dTTP, 0.5 mg oligo(dT)₁₂₋₁₈ and 200 U reverse transcriptase. After incubation at 42°C for 50 min, the reaction was stopped at 70°C for 15 min. cDNA (5 µl) diluted at a 1:80 ratio was loaded onto a 96-well plate. Real-time PCR amplification was performed using the SYBR-Green Supermix (2´ iQ 50 mM KCl, 20 mM Tris-HCl, pH 8.4, 0.2 mM each dNTP, 25 U/ml iTaq DNA polymerase, 3 mM MgCl₂, SYBR Green I and 10 nM fluorescein, stabilized in sterile distilled water). Primers of investigated genes (**Table 1**) were used at a final concentration of 200 nM. Data were analysed using iCycler IQ software and compared by the $\Delta\Delta CT$ method. Q-PCR was performed in triplicate for PCR yield validation. Results of relative gene expressions for LBL B and LBL C on the 7th day of culture were expressed to relative gene expression levels of LBL A. Each Q-PCR was performed in triplicate. Data were normalized to P0 (ribosomal protein) mRNA expression for each condition and was quantified relative to Runx2, ALP, OCN and type I collagen (Col1) gene expression. Statistical analysis was performed by Mann Witney test in order to compare the expressions of different gens for B and C LBL constructs.

Table 1. Primers of investigated genes

Genes	Primers
ubiquitary ribosomic protein P0	forward 5'-ATG CCC AGG GAA GAC AGG GC-3' reverse 5'-CCA TCA GCA CCA CAG CCT TC-3'
ALP	forward 5'-AGC CCT TCA CTG CCA TCC TGT-3' reverse 5'-ATT CTC TCG TTC ACC GCC CAC-3'
COL1A1	forward 5'-TGG ATG AGG AGA CTG GCA ACC-3' reverse 5'-TCA GCA CCA CCG ATG TCC AAA-3'
Runx2	forward 5'-TCA CCT TGA CCA TAA CCG TCT-3' reverse 5'-CGG GAC ACC TAC TCT CAT ACT-3'
OCN	forward 5'-ACC ACA TCG GCT TTC AGG AGG-3' reverse 5'-GGG CAA GGG CAA GGG GAA GAG-3'

3. RESULTS

3.1. Cell culture onto a PLA substrate membrane

3.1.1. Scaffolds membranes features and Cell Morphology

The PLA membranes were 100 μm thick and pores diameter was 200 μm . SEM observations showed the external structure of PLA membranes and struts organization, which revealed that pore size was ranged between 165 and 375 μm (Figure 2A). Considering the PLA membranes loaded with cells, we have observed different cell morphologies of the mono- and co-cultures (Figure 2B): HBMSCs showed elongated and highly-branched morphology. EPCs were small, rounded cells with filopodia towards PLA membranes. Cells in co-cultures were elongated and branched and covered the membrane pores.

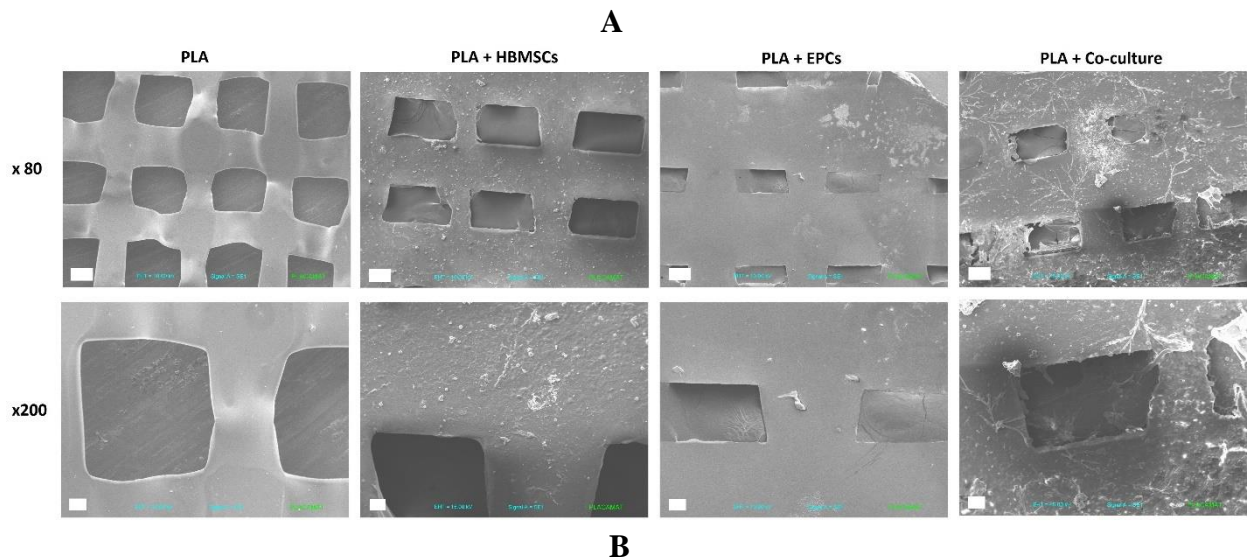


Figure 2. Scanning Electron Microscopy at D14: (control PLA membrane without cells, HBMSCs: Human Bone Marrow Stromal Cells, EPCs: Endothelial Progenitor Cells, Co-cultures of HBMSCs and EPCs on the PLA). Scale is 100 μm for x80 images and 30 μm for x200 images.

3.1.2. Cell viability

Live-Dead experiments were performed in 2D cell culture onto PLA membranes (Figure 3A). In general, we have observed a large amount of living cells after 14 days of culture. Most of the cells were alive at day 1, with the highest survival rates in mono-cultures of HBMSCs. Few EPCs were present on PLA membranes at Day 1. Coculture samples showed similar cell viability as mono-cultures of HBMSCs at the day 1. After 7 days of

culture, we observed higher density of live cells in HBMSCs mono-culture samples, which maintained until the day 14. Regarding mono-cultures of EPCs, we did not observe any significant difference in qualitative observations of live and dead cells after 7 days, but their population was much dense at the day 14. Coculture samples showed a large amount of live cells after 7 days, which maintained until the day 14. After 14 days, the co-cultures (HBMSCs + EPCs) have shown the highest cell survival.

3.1.3. Quantification of the area covered by cells

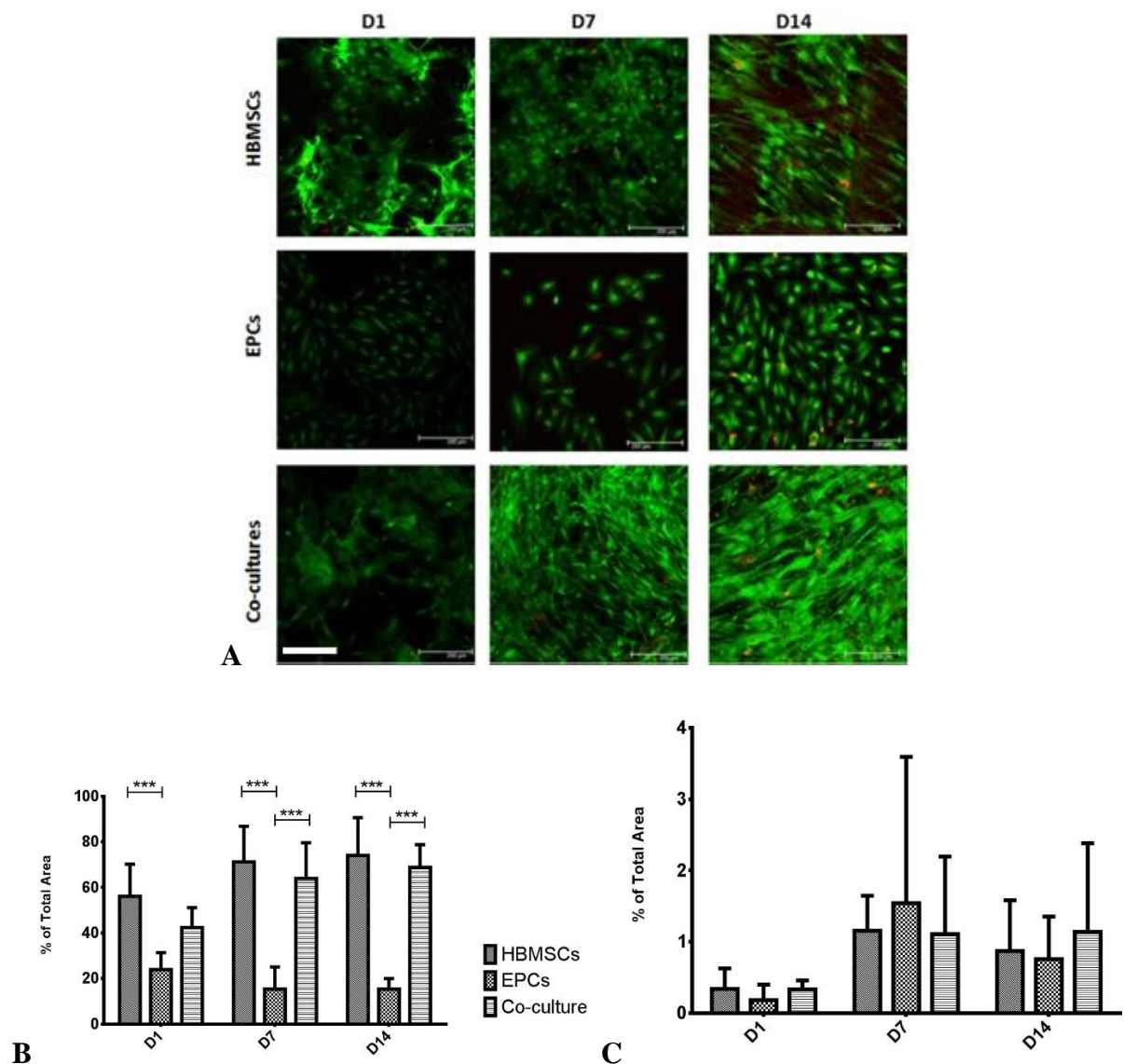


Figure 3. A – Qualitative images of the L/D assay at Day 1, 7 and 14. The scale is 200μm and it is the same for all images; B – Statistical results of the % of total area covered by live cells calculated from five different spots of one scaffold. ***p<0.001; C - Statistical results of the % of Total area covered by dead cells calculated from five different spots of one scaffold

The pictures obtained with confocal microscope after Live-Dead assay have been used to quantify the areas covered by live or dead cells, using ImageJ[®] software. Since the Calcein-AM colors the cytoplasm of live cells and the EthD-1 colors the nucleus of dead cells, we could not compare the surfaces covered by live to the surfaces covered by dead cells, so we compared live or dead cells in the function of different cell conditions. Percentages of total areas of live and dead cells are shown in Figure 3B and 3C respectively. At the day 1, the most of the surface covered by live cells was observed in HBMSCs mono-culture samples and it increased with time. The surface of live cells in co-culture systems increased with time as well. Mono-cultures of EPCs did not show an important increase in the surface covered by live cells. There was significantly less EPCs live surface in all conditions compared to HBMSCs and co-cultures. Regarding dead cells quantification, no significant difference was observed between all conditions. The highest surface covered by dead cells was observed in EPCs mono-culture samples after 7 days.

3.1.4. Cell proliferation (CyQuant)

In test samples, cell proliferation assays in 2 dimensions displayed a global increase of DNA synthesis in all samples with time (Figure 4). There was no any significant difference observed in the proliferation of EPCs in mono-culture samples during time. DNA synthesis was significantly increased between 7 and 14 days of culture for HBMSCs on the PLA. After 14 days of culture, a significant difference was observed in cell proliferation of co-cultures. Control results (TCP) confirm the significant increase in cell proliferation for all samples after 14 days of culture.

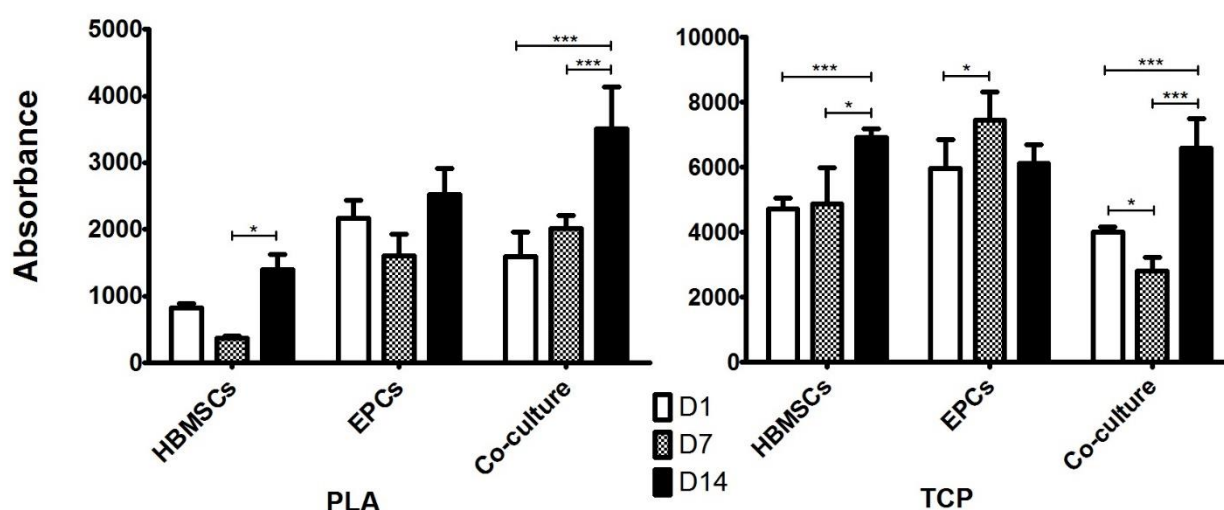


Figure 4. Cell proliferation during 14 days of culture on PLA membranes: Mono- and Co-cultures on PLA. Control experiments were done on Tissue Culture Plastic (TCP). * $p < 0.05$, ** $p < 0.001$, *** $p < 0.0001$

3.1.5. Cell differentiation

Endothelial phenotype was characterized by the intracellular marker Von Willebrand Factor (vWF) [39]. DAPI was used to label the nucleus in blue [40]. The vWF (green) and the DAPI (blue) staining were maintained in mono- and co-cultures on PLA during 14 days. Mono-cultures of EPCs on PLA showed a different organization than co-cultures on PLA membranes (Figure 5 A).

Osteoblastic phenotype was evaluated using alkaline phosphatase (ALP) staining. ALP expression was positive in both, mono- and co-cultures (Figure 5 B).

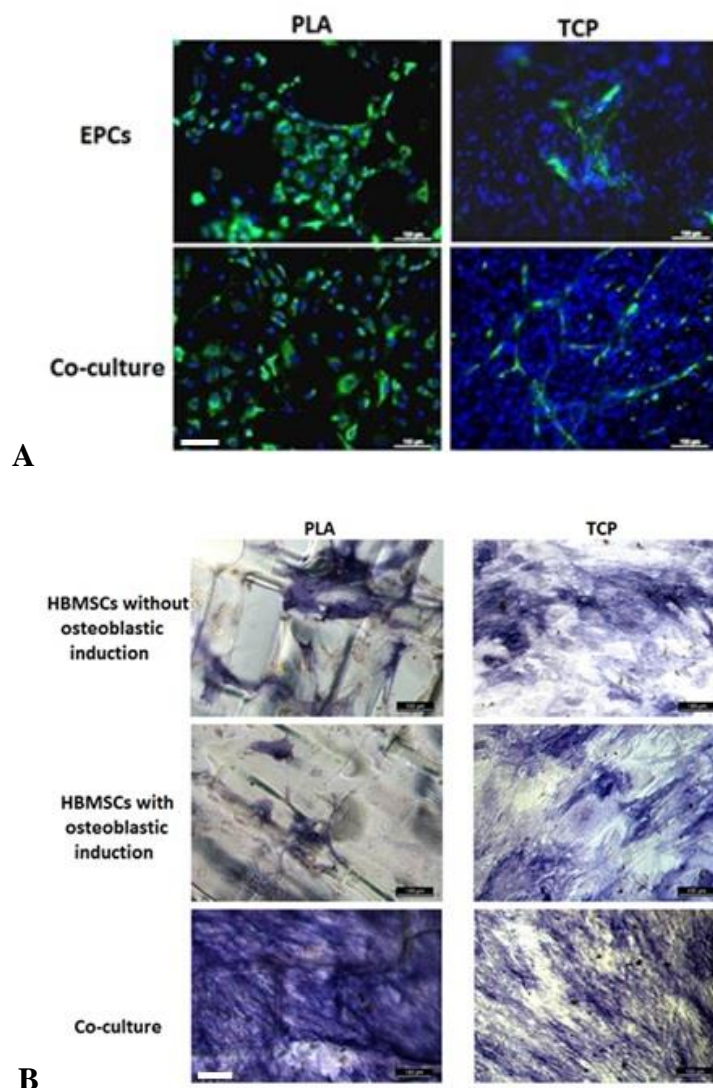


Figure 5. Cell differentiation in 2D mono and co-cultures on PLA membranes. The scale is 100 μ m and it is the same for all images: A - endothelial differentiation (vWF in green and DAPI in blue) at Day 14.; B - osteoblastic differentiation on Day 14. (PLA: Poly-Lactic Acid membranes; TCP: Tissue Culture Plastic)

3.2. Use of cellularized PLA membranes for LBL Bio-Assembly

In aim to obtain preliminary results for LBL Bio-Assembly we have characterized the osteoblastic phenotype in 3D constructs as well as the cell repartition in 3D.

3.2.1. Phenotype characterization in 3D constructs

The relative osteoblastic gene expressions at the 7th day of culture of two types of LBL constructs, with different positions of HBMSCs and EPCs in layers., The experiment was performed with LBL constructs with alternating layers of mono-cultures of HBMSCs and EPCs and LBL constructs with co-culture layers. Phenotype characterization was tested for relative gene expression of ALP, RunX2, OCN and Col1 as osteoblastic markers (Figure 6 A). LBL construct made of mono-cultures of HBMSCs were used as a control group.

3.2.2. Observation of 3D LBL Composite Materials by 2-photons microscopy

This experiment was performed in aim to observe the repartition of cells (EPCs) in 3D in LBL constructs. LBL composite materials were prepared to be observed after 14 days of culture using 2 photons confocal microscopy (2P). The tested sample had alternating layers of monoculture of HBMSCs-GFP and co-cultures (HBMSCs-GFP + EPCs-TdT). We could observe all 4 layers of 3D constructs and endothelial cells (red fluorescence) were present in all layers (Figure 6 B).

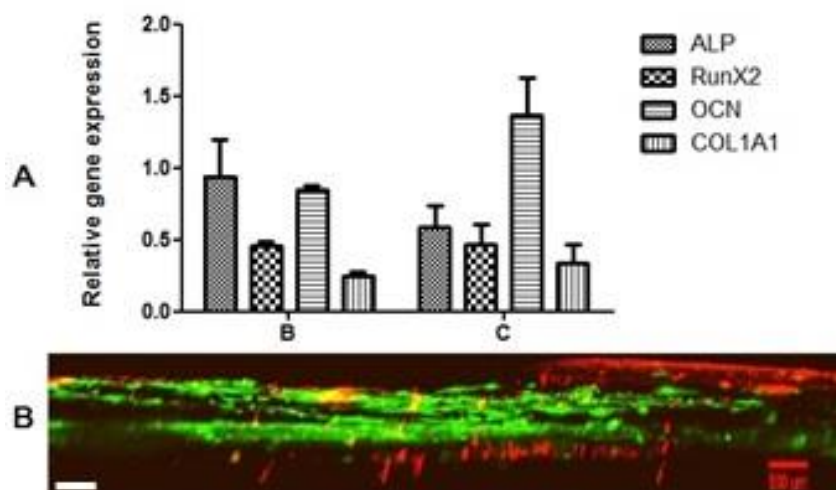


Figure 6. 3D LBL constructs. A - Osteoblastic differentiation (qPCR) of cells in 3D LBL B and C types of constructs on Day 7 in comparison to the A type; B – Cell colonization inside the LBL D constructs (HBMSCs-GFP in green color and EPCs-TdT in red fluorescence). The scale is 500 μm.

4. DISCUSSION

PLA used for this work has already been characterized by Serra *et al.* [41]. PLA membranes fabricated by 3D printing had an expected morphology and a pore size suitable for tissue engineering [42]. Human primary cells seeded on these PLA porous membranes have shown the morphology expected in these culture conditions.

A large amount of living cells were present on PLA membranes after 14 days of culture, especially in the case of co-cultures. There were much more membrane areas covered by live than by dead cells. The highest percentage of live cells was present in co-culture systems and it increased with time, which confirmed results obtained by SEM. The presence of both types of cells provided better conditions for cell survival. There were significantly less live EPCs in all conditions compared to HBMSCs and co-cultures. However, the quantification of dead cells surface is not fully reliable as they usually detach from their substrate.

The amount of DNA was higher for EPCs during the first week of culture, which was expected since we have seeded more EPCs at day 0 because they are much smaller than HBMSCs. Cells proliferated more significantly on the plastic of the cell culture dish (TCP) than on the PLA, what was expected since cells prefer the plastic more than a scaffold. There were no significant differences observed during the in co-culture control samples because cell achieved their confluence very fast thanks to the cell-to-cell communication and the growth factor secretion, which was not the case on mono-culture samples. This process was a little bit slower in test co-culture samples on PLA during 7 days, but it was changed after 14 days of culture. The reason is most likely in cell-to-cell interaction through growth factors (BMP-2, VEGF, IGF) production in co-cultures [43]. The proliferation in mono-culture samples was decreased after 7 days of culture probably because cells need more time to be adapted to the PLA than in control samples. But the proliferation was increased after 14 days, with a significant difference for HBMSCs.

EPCs were located only on struts of the PLA membranes and they formed a homogenous “grid line” shape after 14 days of culture. Co-cultures showed a higher density of cells and a lower density of vWF than mono-cultures

ALP expression was positive in both, mono- and co-cultures, which displayed early osteoblastic differentiation. The mono-cultures of HBMSCs on PLA showed similar ALP level with or without osteoblastic induction after 14 days. ALP was concentrated on the struts of the membranes. In the co-cultures performed on PLA, ALP staining covered all the surface of the membranes and pores. The ALP expression was especially high for co-cultures, which has already been described using co-cultures of HBMSCs and EPCs [44], probably because of the higher production of the extracellular matrix.

We have observed that the highest cell proliferation and viability in 2D on PLA appeared in the case of co-culture system. Then we have performed Layer-by-Layer Bioassembly of cellularized membranes in 3D: All tridimensional LBL constructs were made

of 4 layers of PLA membranes seeded with human primary cells. Even if we have used glass rings to stabilize the 3D constructs in culture plates, the materials were difficult to manipulate. Other groups have proposed to use of stainless steel mesh clips to stabilize the LBL constructs after the assembly [29]. Since we could observe the most efficient cell proliferation in co-culture samples in 2D, we decided to test osteoblastic genes expressions in culture samples with combination of 2 cell types with their different organization in aim to see if their 3D organization has an influence in osteoblastic differentiation. Control sample was mono-culture HBMSCs LBL construct (without EPCs). We have observed that OCN and ALP had the highest relative gene expression for both LBL types. It was expected since it has already been known that they genes are expressed earlier than others. The expressions of RunX2 and Col1 were lower. But we have not observed any significant difference between the 2 different LBL constructs concerning the expression of osteoblastic genes. There was no difference between 2 different types of LBL constructs containing EPCs.

Since the positions and different combinations of HBMSCs with EPCs in layers did not play an important role in osteoblastic differentiation, we have done new LBL constructs to observe the colonization of cells inside the layers. Cells were tagged in order to observe their migration between layers of PLA. The HBMSCs were tagged by GFP (green fluorescence) and EPCs were tagged by Td Tomato (red fluorescence). The tested 3D construct had alternating layers of monocultures HBMSCs-GFP and co-cultures HBMSCs-GFP + EPCs-TdT. Red color was present in all layers meaning that EPCs have probably migrated inside the LBL constructs.

5. CONCLUSIONS AND PERSPECTIVES

Fabrication of thin porous PLA membranes by direct 3D printing was successfully performed. Evaluations of viability, phenotypes maintain and proliferation of human primary cells cultured on PLA were positive: Cell proliferation increased with time in both, mono- and co-culture conditions. The level of ALP expression was higher in co-culture systems. We successfully made LBL constructs by assembling 4 layers of cellularized PLA membranes. Experiments of these 3D constructs have shown an osteoblastic differentiation after 7 days of culture as well as the cell colonization inside the constructs. This showed the potential of LBL approach to promote a homogenous cell distribution inside the scaffold. 3D experiments have shown that LBL bio-assembly enables better cell proliferation and differentiation into the scaffold than conventional BTE. Results obtained indicate that LBL approach could be suitable for bone tissue engineering, in order to promote homogenous cell distribution into the scaffold.

Acknowledgements

The authors wish to thank the French Institute in Belgrade, Serbia, via Campus France agency. 2-photon observations were done at Bordeaux Imaging Center, France.

Key words: biofabrication, layer-by-layer, bone tissue engineering, PLA, porous scaffold, 3D printing

Bibliography

- [1] G. Arealis and V. S. Nikolaou, "Bone printing: new frontiers in the treatment of bone defects," *Injury*, vol. 46 Suppl 8, pp. S20-22, Dec. 2015.
- [2] F. J. O'Brien, "Biomaterials & scaffolds for tissue engineering," *Mater. Today*, vol. 14, no. 3, pp. 88–95, Mar. 2011.
- [3] H. Oliveira *et al.*, "The proangiogenic potential of a novel calcium releasing biomaterial: Impact on cell recruitment," *Acta Biomater.*, vol. 29, pp. 435–445, Jan. 2016.
- [4] T. Feng, Y. Liu, Q. Xu, X. Li, X. Luo, and Y. Chen, "[In vitro experimental study on influences of final degradation products of polyactic acid on proliferation and osteoblastic phenotype of osteoblast-like cells]," *Zhongguo Xiu Fu Chong Jian Wai Ke Za Zhi Zhongguo Xiufu Chongjian Waikexue Zazhi Chin. J. Reparative Reconstr. Surg.*, vol. 28, no. 12, pp. 1525–1529, Dec. 2014.
- [5] E. Saito, D. Suarez-Gonzalez, W. L. Murphy, and S. J. Hollister, "Biomimetic coating increases bone formation by ex vivo BMP-7 gene therapy in rapid prototyped poly(L-lactic acid) (PLLA) and poly(ϵ -caprolactone) (PCL) porous scaffolds," *Adv. Healthc. Mater.*, vol. 4, no. 4, pp. 621–632, Mar. 2015.
- [6] L. Ciocca, F. De Crescenzo, M. Fantini, and R. Scotti, "CAD/CAM and rapid prototyped scaffold construction for bone regenerative medicine and surgical transfer of virtual planning: a pilot study," *Comput. Med. Imaging Graph. Off. J. Comput. Med. Imaging Soc.*, vol. 33, no. 1, pp. 58–62, Jan. 2009.
- [7] F. Mangano *et al.*, "Maxillary ridge augmentation with custom-made CAD/CAM scaffolds. A 1-year prospective study on 10 patients," *J. Oral Implantol.*, vol. 40, no. 5, pp. 561–569, Oct. 2014.
- [8] N. K. Nga, T. T. Hoai, and P. H. Viet, "Biomimetic scaffolds based on hydroxyapatite nanorod/poly(D,L) lactic acid with their corresponding apatite-forming capability and

biocompatibility for bone-tissue engineering,” *Colloids Surf. B Biointerfaces*, vol. 128, pp. 506–514, Apr. 2015.

[9] T. Lou, X. Wang, G. Song, Z. Gu, and Z. Yang, “Fabrication of PLLA/ β -TCP nanocomposite scaffolds with hierarchical porosity for bone tissue engineering,” *Int. J. Biol. Macromol.*, vol. 69, pp. 464–470, Aug. 2014.

[10] D. D’Alessandro *et al.*, “Processing large-diameter poly(L-lactic acid) microfiber mesh/mesenchymal stromal cell constructs via resin embedding: an efficient histologic method,” *Biomed. Mater. Bristol Engl.*, vol. 9, no. 4, p. 045007, Aug. 2014.

[11] A. Zamparelli *et al.*, “Growth on poly(L-lactic acid) porous scaffold preserves CD73 and CD90 immunophenotype markers of rat bone marrow mesenchymal stromal cells,” *J. Mater. Sci. Mater. Med.*, vol. 25, no. 10, pp. 2421–2436, Oct. 2014.

[12] C.-T. Kao, C.-C. Lin, Y.-W. Chen, C.-H. Yeh, H.-Y. Fang, and M.-Y. Shie, “Poly(dopamine) coating of 3D printed poly(lactic acid) scaffolds for bone tissue engineering,” *Mater. Sci. Eng. C Mater. Biol. Appl.*, vol. 56, pp. 165–173, Nov. 2015.

[13] Y. Hu, S. Zou, W. Chen, Z. Tong, and C. Wang, “Mineralization and drug release of hydroxyapatite/poly(L-lactic acid) nanocomposite scaffolds prepared by Pickering emulsion templating,” *Colloids Surf. B Biointerfaces*, vol. 122, pp. 559–565, Oct. 2014.

[14] M. Ding, S. S. Henriksen, D. Wendt, and S. Overgaard, “An automated perfusion bioreactor for the streamlined production of engineered osteogenic grafts,” *J. Biomed. Mater. Res. B Appl. Biomater.*, May 2015.

[15] Q. Lian, P. Zhuang, C. Li, Z. Jin, and D. Li, “[Mechanical properties of polylactic acid/beta-tricalcium phosphate composite scaffold with double channels based on three-dimensional printing technique],” *Zhongguo Xiu Fu Chong Jian Wai Ke Za Zhi Zhongguo Xiu fu Chongjian Waikē Zazhi Chin. J. Reparative Reconstr. Surg.*, vol. 28, no. 3, pp. 309–313, Mar. 2014.

[16] A. Ronca *et al.*, “Large defect-tailored composite scaffolds for in vivo bone regeneration,” *J. Biomater. Appl.*, vol. 29, no. 5, pp. 715–727, Nov. 2014.

[17] K. Hamad, “Properties and medical applications of polylactic acid: A review,” *Express Polym. Lett.*, vol. 9, no. 5, pp. 435–455, Mar. 2015.

[18] P. Vidyasekar, P. Shyamsunder, S. K. Sahoo, and R. S. Verma, “Scaffold-free and scaffold-assisted 3D culture enhances differentiation of bone marrow stromal cells,” *In Vitro Cell. Dev. Biol. Anim.*, vol. 52, no. 2, pp. 204–217, Feb. 2016.

[19] J. Huang *et al.*, “Evaluation of the novel three-dimensional porous poly (L-lactic acid)/nano-hydroxyapatite composite scaffold,” *Biomed. Mater. Eng.*, vol. 26 Suppl 1, pp. S197-205, 2015.

- [20] R. A. Giordano, B. M. Wu, S. W. Borland, L. G. Cima, E. M. Sachs, and M. J. Cima, "Mechanical properties of dense polylactic acid structures fabricated by three dimensional printing," *J. Biomater. Sci. Polym. Ed.*, vol. 8, no. 1, pp. 63–75, 1996.
- [21] C. R. Almeida, T. Serra, M. I. Oliveira, J. A. Planell, M. A. Barbosa, and M. Navarro, "Impact of 3-D printed PLA- and chitosan-based scaffolds on human monocyte/macrophage responses: unraveling the effect of 3-D structures on inflammation," *Acta Biomater.*, vol. 10, no. 2, pp. 613–622, Feb. 2014.
- [22] T. Serra, M. A. Mateos-Timoneda, J. A. Planell, and M. Navarro, "3D printed PLA-based scaffolds: a versatile tool in regenerative medicine," *Organogenesis*, vol. 9, no. 4, pp. 239–244, Oct. 2013.
- [23] S. Schlaubitz *et al.*, "Pullulan/dextran/nHA macroporous composite beads for bone repair in a femoral condyle defect in rats," *PloS One*, vol. 9, no. 10, p. e110251, 2014.
- [24] J. Groll *et al.*, "Biofabrication: reappraising the definition of an evolving field," *Biofabrication*, vol. 8, no. 1, p. 013001, 2016.
- [25] B. N. Sathy, U. Mony, D. Menon, V. K. Baskaran, A. G. Mikos, and S. Nair, "Bone Tissue Engineering with Multilayered Scaffolds-Part I: An Approach for Vascularizing Engineered Constructs In Vivo," *Tissue Eng. Part A*, vol. 21, no. 19–20, pp. 2480–2494, Oct. 2015.
- [26] L. Ren *et al.*, "Preparation of three-dimensional vascularized MSC cell sheet constructs for tissue regeneration," *BioMed Res. Int.*, vol. 2014, p. 301279, 2014.
- [27] A. Nishiguchi, M. Matsusaki, Y. Asano, H. Shimoda, and M. Akashi, "Effects of angiogenic factors and 3D-microenvironments on vascularization within sandwich cultures," *Biomaterials*, vol. 35, no. 17, pp. 4739–4748, Jun. 2014.
- [28] R. Derda *et al.*, "Paper-supported 3D cell culture for tissue-based bioassays," *Proc. Natl. Acad. Sci. U. S. A.*, vol. 106, no. 44, pp. 18457–18462, Nov. 2009.
- [29] W. Wan *et al.*, "Layer-by-layer paper-stacking nanofibrous membranes to deliver adipose-derived stem cells for bone regeneration," *Int. J. Nanomedicine*, vol. 10, pp. 1273–1290, 2015.
- [30] S. Catros *et al.*, "Layer-by-layer tissue microfabrication supports cell proliferation in vitro and in vivo," *Tissue Eng. Part C Methods*, vol. 18, no. 1, pp. 62–70, Jan. 2012.
- [31] L. Wen *et al.*, "Role of Endothelial Progenitor Cells in Maintaining Stemness and Enhancing Differentiation of Mesenchymal Stem Cells by Indirect Cell-Cell Interaction," *Stem Cells Dev.*, vol. 25, no. 2, pp. 123–138, Jan. 2016.

- [32] K. Eldesoqi *et al.*, “Safety evaluation of a bioglass-polylactic acid composite scaffold seeded with progenitor cells in a rat skull critical-size bone defect,” *PloS One*, vol. 9, no. 2, p. e87642, 2014.
- [33] J. Vilamitjana-Amedee, R. Bareille, F. Rouais, A. I. Caplan, and M. F. Harmand, “Human bone marrow stromal cells express an osteoblastic phenotype in culture,” *In Vitro Cell. Dev. Biol. Anim.*, vol. 29A, no. 9, pp. 699–707, Sep. 1993.
- [34] N. B. Thebaud, R. Bareille, M. Remy, C. Bourget, R. Daculsi, and L. Bordenave, “Human progenitor-derived endothelial cells vs. venous endothelial cells for vascular tissue engineering: an in vitro study,” *J. Tissue Eng. Regen. Med.*, vol. 4, no. 6, pp. 473–484, Aug. 2010.
- [35] N. B. Thébaud *et al.*, “Labeling and qualification of endothelial progenitor cells for tracking in tissue engineering: An in vitro study,” *Int. J. Artif. Organs*, vol. 38, no. 4, pp. 224–232, Apr. 2015.
- [36] K. R. Lau, R. L. Evans, and R. M. Case, “Intracellular Cl⁻ concentration in striated intralobular ducts from rabbit mandibular salivary glands,” *Pflüg. Arch. Eur. J. Physiol.*, vol. 427, no. 1–2, pp. 24–32, May 1994.
- [37] C. A. Poole, N. H. Brookes, and G. M. Clover, “Keratocyte networks visualised in the living cornea using vital dyes,” *J. Cell Sci.*, vol. 106 (Pt 2), pp. 685–691, Oct. 1993.
- [38] P. J. Vaughan, C. J. Pike, C. W. Cotman, and D. D. Cunningham, “Thrombin receptor activation protects neurons and astrocytes from cell death produced by environmental insults,” *J. Neurosci. Off. J. Soc. Neurosci.*, vol. 15, no. 7 Pt 2, pp. 5389–5401, Jul. 1995.
- [39] D. J. Metcalf, T. D. Nightingale, H. L. Zenner, W. W. Lui-Roberts, and D. F. Cutler, “Formation and function of Weibel-Palade bodies,” *J. Cell Sci.*, vol. 121, no. Pt 1, pp. 19–27, Jan. 2008.
- [40] A. T. Szczurek *et al.*, “Single molecule localization microscopy of the distribution of chromatin using Hoechst and DAPI fluorescent probes,” *Nucl. Austin Tex*, vol. 5, no. 4, pp. 331–340, Aug. 2014.
- [41] T. Serra, M. Ortiz-Hernandez, E. Engel, J. A. Planell, and M. Navarro, “Relevance of PEG in PLA-based blends for tissue engineering 3D-printed scaffolds,” *Mater. Sci. Eng. C*, vol. 38, pp. 55–62, May 2014.
- [42] S. Ahn, H. Lee, and G. Kim, “Functional cell-laden alginate scaffolds consisting of core/shell struts for tissue regeneration,” *Carbohydr. Polym.*, vol. 98, no. 1, pp. 936–942, Oct. 2013.
- [43] A. Aguirre, J. A. Planell, and E. Engel, “Dynamics of bone marrow-derived endothelial progenitor cell/mesenchymal stem cell interaction in co-culture and its

implications in angiogenesis,” *Biochem. Biophys. Res. Commun.*, vol. 400, no. 2, pp. 284–291, Sep. 2010.

[44] M. Grellier, L. Bordenave, and J. Amédée, “Cell-to-cell communication between osteogenic and endothelial lineages: implications for tissue engineering,” *Trends Biotechnol.*, vol. 27, no. 10, pp. 562–571, Oct. 2009.

SECOND PART:

Fused Deposition Modeling technique for fabrication of poly(lactic) acid membranes and their physicochemical and biological characterization

***In vitro* and *in vivo* evaluations of 3D layer-by-layer cellularized assemblies and the effect of cell culture system and its 3D organization with membranes on blood vessel formation**

A. INTRODUCTION

The previous experiments performed to produce membranes for Layer-by-Layer Biofabrication displayed some limits as described in the first article published:

- The pore diameters of the PLA membranes were comprised between 165 μm and 375 μm showing impossibility to completely control their size;
- During the cell culture experiments, the PLA membranes were floating in cell culture media so it was necessary to stabilize them with glass rings for *in vitro* cell seeding experiments. The use of glass rings allowed to keep the membranes on the bottom of wells but they were not always completely stable. 3D LBL assemblies were stabilized on the same way. This stabilization did not provide stable conditions for 3D constructs. Layers were moving sometimes during media changing. Stabilization of layers in 3D constructs during the first days after superposing of cellularized membranes is very important because it provides necessary conditions for cells while they synthesize matrix which will later keep the layers together. Second disadvantage of this stabilization system is that it is not implantable with assemblies for *in vivo* studies. It means that implantation can not be performed before sufficient synthesis of extracellular matrix which can provide sufficient stabilization in the host.

The primary objective of this second part was to evaluate the effect of 3D organization of cells and biomaterial (PLA) on the development of vascularization within tissue engineering products *in vitro* and *in vivo*.

Secondary objectives were to investigate physico-chemical properties of the PLA membranes. Finally, the design of the materials was optimized to overcome some limits of the previous study.

Some biofabrication and 3D printing techniques can cause some degradation of biomaterial or changes in its internal structure. Physico-chemical investigations of PLA used in this second part were performed in order to observe if the FDM process had an effect on the different properties of PLA. Scanning electron microscopy (SEM) was used to observe morphological properties of printed membranes and to measure the pore size obtained. Fourier Transformed Infra-Red Spectroscopy analysis showed limited changes in spectra after the fabrication process. The results revealed that 2D printing process did not have any important effect on molecular mass nor amorphous structure of PLA, which was investigated by Size Exclusion Chromatography (SEC) and Differential Scanning Calorimetry (DSC), respectively. Thermogravimetric analysis showed that there was no thermic degradation of the PLA caused by fabrication process.

The first mentioned limit concerning the irregularity pore size in the previous study (1st Article) was overcome by changing the fabrication method. In this second part, we used a Makerbot Replicator 2 Fused Deposition Modeling (FDM) printer equipped with a 400 μm printing nozzle. This FDM printer allowed the preparation of membranes and massive scaffolds with shorter pore size range (294 μm - 311 μm). Printed PLA membranes were stabilized in well plates on the agarose by 3D printed holders made of PLA. These holders

kept membranes stable without floating in cell culture media while seeding and culturing. Holders could be easily removed with tweezers before LBL assembling. LBL assemblies were stabilized with PLA 3D printed clips which kept 4 superposed membranes assembled tightly together. Since these clips were fabricated of the same biomaterial as membranes, they were sterilized on the same way and they could be implanted subcutaneously in mice together with assemblies. This stabilization system facilitated the manipulation of assemblies.

Some biomaterials can release cytotoxic biomolecules when they are in cell culture media. This is the reason why a cytotoxicity test was performed before all evaluation experiments. This test showed that PLA membranes were not cytotoxic 24h after sterilization by γ -rays irradiation.

Since the objective of the study was to evaluate the vascularization of tissue engineering products for bone tissue engineering applications, we investigated osteoblastic and endothelial cell differentiation in all layers of assemblies by observing the expressions of alkaline phosphatase (ALP) and von Willebrand factor (vWF), respectively. Cells showed expected differentiation with homogenous distribution in layers. Phenotype characterization by RT-qPCR confirmed osteoblastic differentiation through the expression of osteoblastic genes.

After these preliminary *in vitro* evaluations, an *in vivo* study was conducted. Implantations were performed subcutaneously in immunodeficient mice. We implanted LBL assemblies containing either mono-cultures of HBMSCs, or co-cultures of these cells with EPCs. We have also implanted massive scaffolds having same dimensions as LBL assemblies, containing the same cell types. Control cell-free samples for both types of scaffolds were implanted as well. Study was performed for N=8 samples. 8 weeks later, samples were embedded in resin, cut and immunostaining was performed for localization of human cells in implants. Goldner trichrome staining was performed to label blood vessels in order to quantify them. The results have shown that LBL bioassemblies provided more efficient conditions for vascular network formation within the whole 3D construct *in vivo*, especially when a co-culture system is used. This approach could be suitable for different tissue engineering applications as the vascularization of Tissue Engineering products remains a critical point for several applications.

ARTICLE 2

Layer-by-Layer BioAssembly of PLA membranes with co-culture system improves vascularization in vivo

Vera GUDURIC, Robin SIADOUS, Maxime SEIMBILLE, Reine BAREILLE, Sylvie REY, Noélie THÉABAUD, Damien LE NIHOANNEN, Jean-Christophe FRICAIN, Raphaël DEVILLARD, Ognjan LUZANIN, Sylvain CATROS

In preparation for submission in the Biomaterials Science

B. RESULTS

Abstract:

Layer-by-Layer (LBL) BioAssembly for Bone Tissue Engineering enables controlled cell distribution within the entire scaffold by assembling pre-formed cell-containing fabrication units. The objective of this study was to evaluate *in vivo* the vascularization within LBL bioassembled membranes with mono- and co-cultures of human primary cells and to compare it to the conventional approach using massive scaffolds. Poly(lactic) acid (PLA) scaffolds were fabricated by Fused Deposition Modeling. Physico-chemical and biological *in vitro* scaffold characterizations were performed. Membranes were seeded with mono-cultures of human bone marrow stroma cells (HBMSCs) or with co-cultures with endothelial progenitor cells (EPCs). Evaluations of early osteoblastic and endothelial differentiation were performed by the expressions of alkaline phosphatase (ALP) and von Willebrand's factor (vWF), respectively. Osteoblastic genes expressions (ALP and collagen type I-COL1) have also been evaluated. Then, 4 mono- or co-culture membranes were assembled in LBL constructs and implanted with cellularized massive scaffolds subcutaneously in immunodeficient mice. 8 weeks later, immunolabeling of human cells and quantification of vessels formed within implanted scaffolds were performed. Scaffold fabrication by Fused Deposition Modeling did not have any important effect on the polymer thermic degradation properties, molecular weight and amorphous structure. ALP and vWF were expressed in all layers of bioassemblies, showing an apparently homogeneous cell distribution. Human cells were observed in all layers of bioassemblies, but not in the inner parts of massive scaffolds, with higher rate in co-culture samples. The highest number of vessels was formed in co-culture LBL bioassemblies comparing to all the other samples. LBL bioassembly approach provides favorable conditions for homogenous cell distribution and vessel formation within the entire 3D scaffold comparing to the conventional approach.

1. INTRODUCTION

Tissue engineering aims (i) to produce tools for basic research in cell biology, (ii) to establish *in vitro* tissue models for drug testing or physiological studies, and finally (iii) to produce cellularized tissue equivalent products for regenerative medicine [1]. Depending on the target tissue, the scaffolds, the cells and their micro-environment must be tuned specifically. For bone tissue engineering applications, the scaffolds must possess adequate mechanical properties, their external and internal shape must be tailorable and the biological properties must be adapted to that of bone while biodegradation time of the scaffold should be adapted to the rate of new bone formation. In this process, the role of the scaffold is to provide physical and mechanical support for cell growth, proliferation and differentiation. It is important that scaffolds possess interconnected pores to facilitate cell penetration and migration in three dimensions (3D) and to allow nutrients, gas and waste products circulation [2]. For bone tissue engineering applications, there are different technologies for scaffold fabrication but 3D printing has many advantages over conventional methods of scaffold production: thanks to the sequential layer deposition of the biomaterial allowed by additive manufacturing techniques, a precise control of internal porosity can be obtained, and the external shape can be customized [3–5]. 3D printing (3DP) is the most common additive manufacturing technology used for scaffold fabrication. Out of all 3DP techniques, fused deposition modeling (FDM), also known as fused filament fabrication (FFF) had numerous successful applications in this field [6–8]. FFF is based on the deposition of melted polymer filament on the receiving platform following computer assisted information about the architecture of the final 3D model.

Scaffolds must be biodegradable and ideally should be resorbed in synergy with new tissue formation [9]. Different pure or chemically modified synthetic polymers have already been used in tissue engineering applications such as polycaprolactone (PCL) for bone [10–12] or acrylonitrile butadiene styrene (ABS) for tendon [13] and skin [14] tissue repair. Chemical modifications such as co-polymerization have an effect on the mechanical properties and the degradation time of the final scaffold. Poly(lactic acid) (PLA) is another polymer that has been used very often for vascular [15], cartilage [16,17] and bone tissue [18–21] applications. It displays favorable printing properties such as a low glass transition temperature (50-60 °C) and it does not require a heated printing bed. Despite these favorable properties, PLA is hydrophobic, which leads to difficult cell seeding and attachment, usually requiring a treatment of the scaffold before cell seeding [22]. PLA scaffolds have already been combined with adipose-derived stem cells (ADSCs) after their oxidation with atmospheric plasma oxidation [23], MC3T3-E1 cells after polydomapine [20] or chitosan [24] coating, and silk fibroin nanoparticles addition [25] for bone tissue engineering applications. Most of the studies using such PLA scaffolds have used cell mono-cultures. We have already shown that cell proliferation in 2D was more efficient when human bone marrow stroma cells (HBMSCs) and endothelial progenitor cells (EPCs) were seeded together in co-cultures on PLA scaffolds [26], which can be explained by growth factor production and extracellular matrix secretion [27].

The main limitation of large massive 3D scaffold-based tissue engineered constructs is related to poor cell penetration in the inner parts, because of the insufficient vascularization of these scaffolds. Consequently, a low diffusion of oxygen and nutrients and waste products elimination can be observed, leading to limited integration of these grafts in the long term [28]. Vascularization of scaffolds is limited to small-size defects [29] so the development of a new vasculature in tissue-engineering products for regenerative medicine represents a major challenge in the field of tissue engineering [30]. There are different cell-based and scaffold-based approaches existing to favor the development of vascularization in the core of scaffolds for tissue engineering purposes [31,32]. Several groups have proposed to favor cell penetration, proliferation, differentiation and tissues formation by placing the cellularized scaffold into a tissue culture bioreactor: different devices have been proposed and their common objective is to force fluid transfer in the core of massive scaffolds to allow cells to survive and to perform their function [33]. The use of bioreactors require the control of numerous parameters important for the physiological culture environment, knowing that it should not be a steady state process and that culture and tissue specific parameters change with time. Also it may be difficult to maintain sterility during the entire process [34]. *In situ* prevascularization is based on the use of the body as a natural bioreactor by implanting the construct in an easily accessible and highly vascularized tissue, such as muscle, during several weeks, before the vascularized graft can be transferred to the recipient site. The main limitation of this approach is that it requires several surgeries, so it increases the morbidity of the whole procedure [35]. The approach of “BioAssembly” has been developed to overcome these limitations [36,37]. It is based on “automated assembly of pre-formed cell-containing fabrication units in the final 3D form” [37]. This approach enables a homogeneous cell distribution in all parts of the engineered construct. Layer-by-layer (LBL) BioAssembly implies the stacking of cellularized scaffolds in the form of microporous membranes [38]. This enables a possibility to control the number and type of cells on each layer, and it leads to a homogeneous cell repartition and more efficient cell proliferation [39]. The stacking of layers containing different cell types should provide an effective control of cell colonization and efficient vascularization leading to expected cell differentiation. This approach enables an easy manipulation of LBL assemblies with low level of cell damage, but insufficient 3D stabilization may occur in the case of thin scaffold membranes [40].

The main objective of this study was to evaluate *in vivo* vascularization within 3D LBL scaffolds using cell mono- and co-cultures and to compare it to the vascularization occurring within massive scaffolds seeded with the same cell types (conventional tissue engineering approach). Secondary objectives were to characterize the physico-chemical properties of the scaffolds, to develop a specific stabilization system for LBL BioAssembly, and to evaluate *in vitro* cell differentiation towards osteoblastic and endothelial phenotype.

2. MATERIALS AND METHODS

2.1. Fabrication of microporous PLA massive scaffolds, membranes and stabilization “clips” by FDM

Macroporous PLA membranes, membrane holders (for cell seeding), clips (for stabilization of LBL constructs) and massive scaffolds, were designed in Rhinoceros software. Membranes and massive scaffolds were designed as objects with dimensions 17x17x0.5 mm and 17x17x2 mm respectively. Desired pore size was approximately 250 μm .

Completed 3D models were converted in .stl files for their fabrication by Fused deposition modeling (FDM) technology. We have used a Replicator 2 (MakerBot® Industries, LLC One MetroTech Center, 21st FI, Brooklyn, NY 11201 USA) FDM 3D printer and its slicer to prepare models for printing. PLA filament was purchased from MakerBot® Industries as well. In order to control and to obtain pore size of approximately 250 μm for the final scaffolds, the most adequate combination of different printing parameters were evaluated: layer thickness, extrusion speed, extrusion temperature, deposition angle, number of shells and Grid-Spacing-Multiplier (GSM). The GSM having the most stringent effect on pore size. Membranes were used for preparation of LBL assemblies. The role of PLA clips was to stabilize four assembled membranes in LBL constructs. Massive scaffolds were used for comparison with LBL assemblies.

For *in vitro* and *in vivo* cell culture experiments, 3D printed membranes were sterilized by gamma irradiation at 25 kGy (Gammacell 3000, MDS Nordion).

2.2. Physicochemical characterization of the PLA

All characterizations were performed on the PLA filament before 3D printing and on the printed scaffolds to determine if the fabrication process had an effect on certain physico-chemical properties of the polymer.

Scanning Electron Microscopy (SEM; JEOL JSM-6460LV, 20kV) was performed on microporous membranes to observe their morphological properties.

Fourier Transformed Infra-red Spectroscopy analysis (FTIR, ALPHA Bruker, Germany) with ATR single reflection diamond (Attenuated, Transmission total Reflection modulus) was performed for spectroscopic analysis of the polymer. The spectra were taken in the interval between 4000 and 400 cm^{-1} wavelengths with 4 cm^{-1} resolution. Each analyzed spectrum was obtained as a mean value of 24 recordings in order to insure reproducibility and accuracy of obtained data.

Molecular weight estimation was examined by size exclusion chromatography (SEC, Agilent Technologies, PL-GPC50 Plus; TOSOH TSK, G4000HXL). This technique is based on the separation of macromolecules depending on their hydrodynamic volumes. Macromolecule retention time in the column correlates with the molecular weight: the largest

molecules are first eluted. Once fitted, the calibration curve enables determination of molecular weight mean based on the hydrodynamic volume of macromolecules.

Polymer crystallinity determination was performed by differential scanning calorimetry (DSC, TA Instruments[®], DSC RCS). This technique measures heat exchanges between the sample and a reference. During a physical transformation as a transition phase, a certain heat quantity exchanges with the sample in order to maintain the same temperature as the reference. The machine determines absorbed heat quantity during an endothermic reaction or releases heat quantity during an exothermic reaction at the transition phase by measuring the heat flow between the sample and the reference.

Thermogravimetric analysis (TGA TA Instruments[®], TGA Q500) was used to determine polymer thermic degradation profile. This technique measures the sample weight variation as a function of time for one temperature profile.

2.3. Cell isolation

Two types of human primary cells were used. Human Bone Marrow Stromal Cells (HBMSCs) were isolated from bone marrow retrieved during surgical procedures (Experimental Agreement with CHU de Bordeaux, Etablissement Français du Sang, agreement CPIS 14.14). Cells were separated into a single suspension by sequential passages through syringes fitted with 16-, 18- or 21-gauge needles. After the centrifugation of 15 minutes at 800g without break at room temperature, the pellet was resuspended with α -Essential Medium (α -MEM; Invitrogen) supplemented with 10% (v/v) fetal bovine serum (FBS) (41). Human cord blood was obtained from healthy newborns (by agreement with Etablissement Français du Sang CPIS 14.14) after informed consent had been obtained from all parents of newborns. The study was performed conforming to the Declaration of Helsinki. Briefly, human cord blood was collected in citrate phosphate dextrose solution and EPCs were isolated as previously described (42). Cells were expanded over several passages using standard cell cultures procedures in complete EGM-2 MV (endothelial cell growth medium-2, Lonza) containing 5% Fetal Calf Serum (FCS). The stability of the endothelial phenotype during the expansion of these cells was regularly assessed by VE-cadherin (VEcad) and von Willebrand factor (vWF) staining (42).

2.4. Cytotoxicity assay

Eventual cytotoxicity of sterile membranes was evaluated according to the NF-EN-ISO 10993-5 standard with modifications, by measuring the metabolic activity and the cell viability of HBMSC and EPCs using a 3-(4-5 dimethylthiasol-2-yl) diphenyl tetrazolium (MTT) assay and a Neutral Red assay, respectively. For both assays, cell cultures medium extracts were prepared according to the EN 30993-5 European standard. Ratio of the immersed surface of the membrane and the volume of the extraction vehicle was 3 cm² / ml.

Membranes were put in contact with 1 ml of medium "Iscove's Modified Dulbecco's Medium" (IMDM) + Glutamax (Invitrogen[®], Cat No 31980-022). The assembly was then incubated during 3 days at 37 °C in a humidified atmosphere containing 5% CO₂ in air. The medium extracts were collected after one, two and three days and stored at 4 °C. For both MTT and Neutral Red assays, HBMSCs were plated at 10⁴ cells / cm² in 96-well plates and cultured during 72 hours to reach cell confluence. After removal of culture media, pure medium extracts were added. Triton 100X to 0.1% was used as a positive control and IMDM culture medium alone was used as negative control. The plates were incubated during 24 hours in a humidified atmosphere containing 5% CO₂ in air.

MTT (3- (4-5 dimethylthiasol-2-yl) diphenyl tetrazolium) is a yellow tetrazolium salt in aqueous solution at neutral pH. It reduces to blue formazan crystals by mitochondrial succinate dehydrogenases of the living cells. The amount of formazan generated from the cells after their incubation with extracts of material is proportional to their metabolic activity. After 24 hours of contact, the culture medium was removed and the cell layer was washed with Hank's solution (Gibco[®], Cat No. 14065-049). The stock solution of MTT (Sigma-Aldrich Co, Cat No M2128; 5 mg / ml in 0.1 M PBS, pH = 7.4) was diluted (20% in IMDM without phenol red (Gibco[®], Cat No. 21056-023)) and 125 µl of this solution was added in each well. After 3 hours of incubation at 37 °C in a humidified atmosphere containing 5% CO₂ in air, the supernatant was removed and formed formazan crystals were dissolved by addition 100 µl of dimethyl sulfoxide (DMSO; Sigma-Aldrich Co, Cat No. D5879-1L). The intensity of the staining was quantified by measuring the absorbances at 540 nm using a spectrophotometer (Perkin Elmer[®], 2030 Multilabel Reader VictorTMX3).

Neutral Red is a vital dye which fixes by electrostatic bonding to the anionic sites of lysosomal matrix. Any decrease in the incorporation of the dye means an alteration of the membrane integrity resulting in cell death. Thus, the intensity of the color is proportional to the number of living cells. After 24 hours of contact, the culture medium was removed and the cell layer was washed with Hank's solution. The Neutral Red (Sigma-Aldrich Co, N4648) was diluted (1,25% in IMDM supplemented with 10% FBS) and 100 µl of this solution was added in each well. After 3 hours of incubation at 37 °C in a humidified atmosphere containing 5% CO₂ in air, the supernatant was removed and cells were lysed with 100 µl of a solution made of 1% acetic acid in 50% ethanol. The intensity of the staining was quantified by measuring the absorbances at 540 nm using a spectrophotometer (Perkin Elmer[®], 2030 Multilabel Reader VictorTMX3).

2.5. Preparation of cellularized layer-by-layer assemblies and massive scaffolds

PLA Membranes were seeded with human primary cells before their assembling in sandwich constructs for *in vitro* and *in vivo* experiments. Each PLA membrane was stabilized on the agarose with two 3D printed membrane holders to stabilize them in the bottom of the well. HBMSCs were seeded onto membranes as mono-cultures (HBMSCs 100.000 cells/cm²) or co-cultures in combination with EPCs (HBMSCs 50.000/cm² + EPCs 100.000 cells/cm²).

Culture media were changed every other day. We prepared 2 types of LBL constructs by assembling membranes 3 days after cell seeding. It resulted in the assembly of 4 mono-culture or 4 co-culture membranes, stabilized with two clips each (Figure 1). The assembling day was considered as the D0 for further experiments.

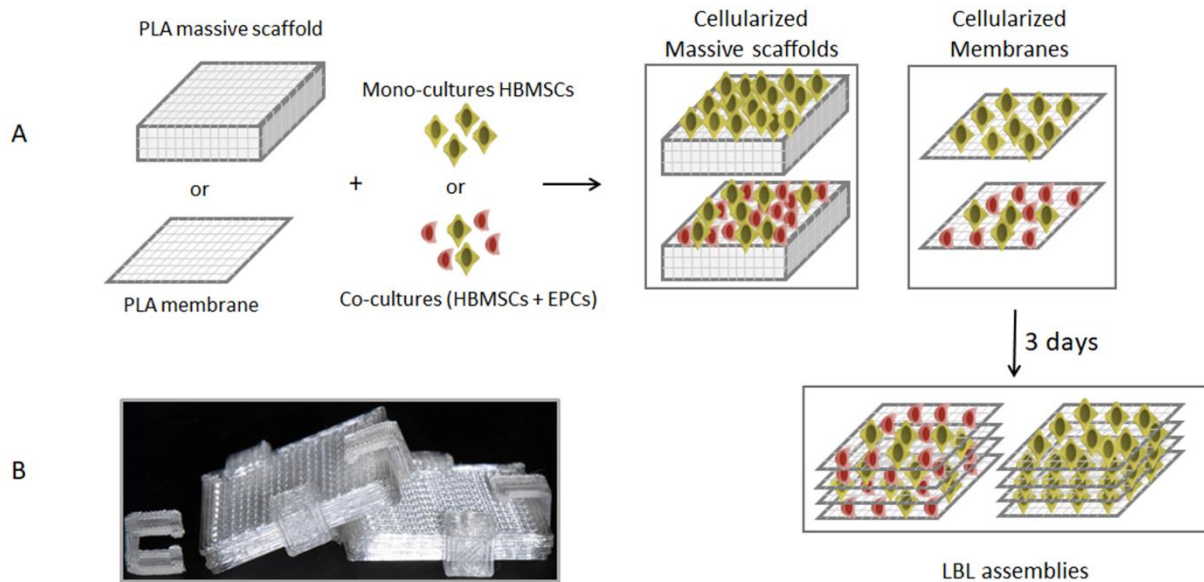


Figure 1. Cell seeding and LBL assemblies and cellularized massive scaffolds preparation. A: experimental design, B: Picture of LBL assemblies stabilized with clips

Cellularized massive scaffolds were prepared only for *in vivo* evaluations. Each scaffold was posed on the agarose in cell culture dishes. Cells were seeded on the surface of massive scaffolds either with 400.000 HBMSCs/cm² (in the case of mono-cultures) or 100.000 HBMSCs and 200.000 EPCs/cm² (in the case of co-cultures), which corresponded to the total number of cells present in 4 seeded membranes in LBL assemblies.

2.6. *In vitro* experiments

Qualitative evaluations of osteoblastic and endothelial differentiation of seeded cells were performed for N=3 after 14 days of culture. Endothelial differentiation was evaluated in co-culture LBL assemblies, while osteoblastic differentiation was evaluated in both, mono-

and co-culture 3D constructs. Quantitative evaluation of osteoblastic phenotype by RT-qPCR was performed for N=5 after 3, 7 and 14 days of culture.

2.6.1. Alkaline phosphatase (ALP) staining of HBMSCs

Alkaline phosphatase (ALP) staining was used as an early osteoblastic differentiation marker for *in vitro* experiments. The intracellular activity of this enzyme was investigated with Ackerman's technique (43) using a commercial kit (Sigma, 85L3R). In the presence of the naphthol-ASMX-phosphate substrate coupled with a diazonium salt (Fast-blue RR), ALP forms insoluble violet complex at active enzymatic sites. Cells with this activity possess intracellular purple granulations. LBL assemblies were washed with PBS 1X, dried and fixed with citrate-acetone mixture for 30 seconds at room temperature. Then, they were washed with tap water and dried again. After that, they were incubated in the coloration solution (2 ml of "fast blue" with 83 µl of naphthol) during 30 minutes in dark at room temperature. After washing with tap water, they were incubated with Mayer's solution during 10 minutes and washed with distilled water. At the end, all layers of LBL assemblies were separated and observed separately with binocular microscope.

2.6.2. Von Willebrand's Factor (VWF) immunolabelling of EPCs

Endothelial phenotype of EPCs was evaluated *in vitro* by *in situ* immunolabeling of von Willebrand factor. Sandwiches were washed with PBS 1X and fixated with paraformaldehyde (PFA) 4 % during 20 minutes at 4 °C. Then cells were permeabilized with Triton 0,1 % during 5 minutes at 4 °C and washed with PBS 1X. Non-specific peptide sites of cells were then saturated with PBS-bovine serum albumin (PBS-BSA) 1 % during 60 minutes at room temperature and washed with PBS 1X. For vWF immunolabeling, primary rabbit anti-human antibody (Cat N°A0082, DAKO®) was diluted (1/500) in PBS-BSA 0.5 % and used for the incubation of samples during 90 minutes at room temperature. Samples were washed twice with PBS 1X, secondary anti-rabbit antibody (Cat N°A11008, DAKO®) was diluted (1/250) in PBS-BSA 0,5 % and added for another 60 minutes incubation in dark. Samples were washed twice with PBS 1X and cell nuclei were labeled with DAPI (4',6'-diamidino-2-phenylindole; Cat N°E6758, Invitrogen®) diluted at 1/5000 in PBS 1X. LBL assemblies were washed with PBS 1X and observed with confocal microscope. For blue and green fluorescence 360 nm and 488 nm filters for excitation and 460 nm and 520 nm filters for emission were used, respectively. At the end, all layers of LBL assemblies were separated and observed separately with confocal microscope.

2.6.3. Osteoblastic phenotype characterization by RT-QPCR

Osteoblastic Gene Expression was examined in vitro on both types of LBL assemblies. Total RNA was extracted using the RNeasy Total RNA kit (Qiagen, AMBION, Inc. Austin, Texas, USA), as indicated by the manufacturer. Primers of investigated genes (ALP, and collagen type 1 (COL1)) were used at a final concentration of 200 nM (Table 1). Data were analysed using iCycler IQ software and compared by the $\Delta\Delta CT$ method. Q-PCR was performed in triplicate for PCR yield validation. Results of relative gene expressions for both types of LBL constructs on the 7th and 14th day of culture were expressed to relative gene expression levels of monoculture LBLs at the day 3. Data were normalized to the housekeeping gene RPLP0 (ribosomal protein) mRNA expression for each condition and was quantified relative to ALP and type I collagen (Col1) gene expression. Statistical analysis was performed by Mann Whitney test in order to compare the expressions of different genes for B and C LBL constructs.

Table 1. Primers of investigated genes

Genes	Primers
RPLP0	Forward CCTCGTGGAAGTGACATCGT Reverse ATCTGCTTGGAGCCCACATT
Col1	Forward TGGATGAGGAGACTGGCAACC Reverse TCAGCACCACCGATGTCCAAA
ALP	Forward GAATCTTCCCCAAGGGCCAA Reverse CTGGGAGGGTCAGATCCAGA

2.7. In vivo experiments

2.7.1. Subcutaneous implantations

Our composite materials were implanted subcutaneously in the back of 48 NOG SCID immunodeficient 8-week old male mice (IL2RG KO: Ho scid: Ho). 6 different conditions were implanted: LBL mono-culture (HBMSCs), massive scaffold mono-culture, LBL co-culture, massive scaffold co-culture, LBL control (cell-free) and massive scaffold control (cell-free) with N=8 for each group.

2.7.2. Preparation of histological samples

All mice were euthanatized 8 weeks post-implantation. The samples were retrieved and fixed in PFA during 12h and then left in EtOH 70 % until processing. Resin embedding was performed following the procedure given by the supplier (Technovit®, 9100 Methyl Methacrylate, Electron Microscopy Sciences, Hatfield, PA, USA). Histological sections of 10 µm were obtained with a microtome mounted with a C-Shape. Then the sections were dried and de-plastified prior staining and immunolabelling using the following protocol: Microscopic slides were immersed twice in metoxyethyl acetate (SIGMA-ALDRICH-308269-1L) during 20 minutes. Then, they were left in acetone twice during 5 minutes and at the end twice in the distilled water during 2 minutes.

2.7.3. Goldner Trichrome staining

Goldner trichrome staining is a three-color staining for distinguishing cells from surrounding connective tissue. Blood vessels are also easily observed with this staining method.

After deplastification, samples were hydrated with sequential baths of EtOH 70 %, EtOH 40 % and distilled water and then incubated in Weigert Hematoxyline solution during 15 minutes. After washing in tap water and distilled water, the incubation in Fushine/Ponceau solution was performed during 30 minutes. Next steps were washing in acetified water 1 %, incubation in Orange G/Molybdic solution during 8 minutes, washing in acetified water, incubation in Light green 3 % solution during 20 minutes and washing in acetified water. After deshydration in EtOH 70 % and EtOH 100 %. The slides were mounted with cover slips with Pertex glue (Histolab, 0081-FR). Slides were observed using Nikon Eclipse 80i microscope with the machine nanozoomer (BIC) allowing the observation of the whole slides with high resolution.

2.7.4. Immunolabelling of human cells: Anti-Mitofilin antibody

Anti-Mitofilin immunostaining was performed to label human cells implanted in the constructs. After deplastification, the antigen retrieval was performed with tris-EDTA-tween-2X tampon during 20 minutes at 95 °C. Then, samples were washed twice with PBS 1X, and H₂O₂ 35 % was added for endogenous peroxidases elimination during 5 minutes. Samples were washed twice with PBS 1X and covered with BSA 2 % during 30 minutes. Primary rabbit anti-human antibody (ab137057, Abcam, Paris, France) was diluted in BSA 1 % at 1/80 and used to cover samples at dark overnight at 4 °C. Negative control was also prepared by using BSA 1 % instead of primary antibody. The following day, samples were washed three times with PBS 1X and secondary anti-rabbit antibody was ½ diluted in BSA 1 % and added during 30 minutes at room temperature. Then, samples were washed three times with PBS 1X

and DAB was added during 9 minutes. Hemalun Mayer's staining was used to label nuclei. Slides were observed with Nikon Eclipse 80i microscope.

2.7.5. Blood Vessels Quantification

As the objective of this study was to evaluate the blood vessel distribution in the samples, depending on the type of cells used and on the method of cell seeding (massive scaffold vs LBL assembly), blood vessels observed in all samples were quantified. Vessels were counted for one section of each sample and expressed as number of vessels per mm² of PLA. Quantifications were performed for 2 types of histological sections: at the external parts of the samples and in the middle of the samples. In order to obtain samples in the middle, all resin blocks were cut in 2 halves and sections were performed in the same way.

2.7.6. Statistical analysis

Statistical analyses were performed by non-parametric t-test using Prism GraphPad.

3. RESULTS

3.1. Fabrication of microporous PLA blocks, membranes and clips

The printing parameters selected for scaffold fabrication are shown in Table 2. Pores of printed scaffolds ranged between 311 μm and 394 μm (Figure 2). PLA "clips" used to stabilize the membranes together were successfully printed as well.

Table 2. FDM parameters used for membranes and massive scaffolds printing

Layer thickness [mm]	Extrusion speed [m/s]	Extrusion temperature [°C]	Deposition angle [°]	Number of shells	GSM
0,2	60	230	90	2	1,8

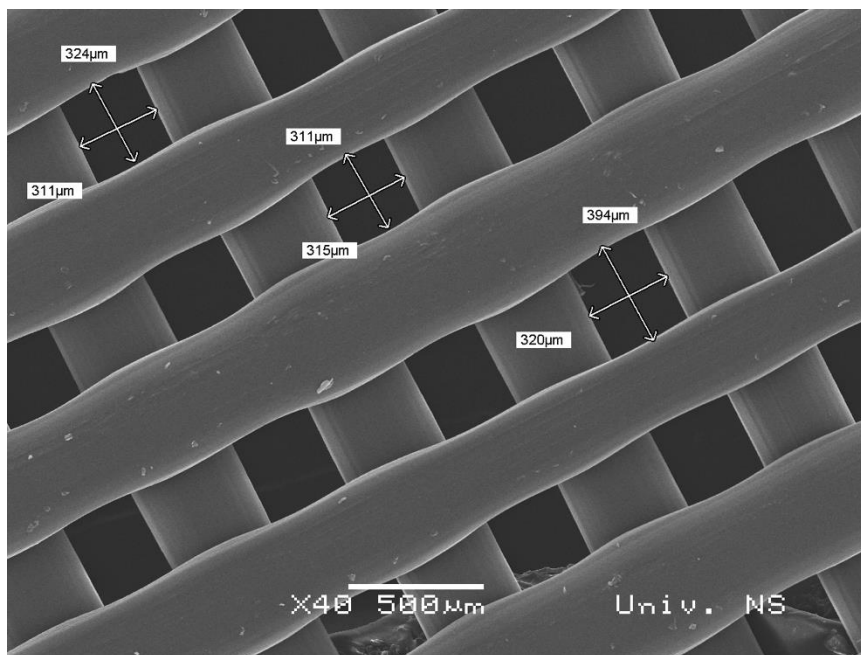


Figure 2. Scanning Electron Microscopy (SEM) observation of a PLA membrane (x40). The scale bar is 500 μm .

3.2. Physico-chemical characterization of PLA

FTIR revealed the presence of absorption maxima at wavelengths 2945, 1750, 1470, 1380, 1360 and 730 cm^{-1} before and after the fabrication process (Figure 3 – 1). Absorption maxima at wavelengths 2945 and 2866 cm^{-1} corresponded to the presence of C-H bonds of aliphatic carbohydrates, while 1750 cm^{-1} gives the information about the presence of C=O molecular group. Absorption maxima at wavelengths 1470, 1380, 1360 and 730 cm^{-1} come from deforming CH_3 and CH_2 symmetrical and asymmetrical vibrations, as well as from C=C-C bonds, respectively. CO_2 is responsible for absorption maxima at 2700 before FDM process.

Molecular weight measured by SEC did not change after printing (~ 120 kDa; Figure 3 – 2A and 2B): it showed that there was no degradation of the polymer during the scaffold fabrication process.

Glass transition, crystallization and fusion temperatures of PLA and measured by DSC before printing were 64, 122.58 and 144.68 $^\circ\text{C}$, respectively (Figure 3 – 3A). After the scaffold fabrication temperatures these temperatures remained the same (Figure 3 – 3B), meaning that the polymer maintained its amorphous structure.

Temperatures at the beginning and the end of the degradation of the PLA filament before printing were 293 $^\circ\text{C}$ and 367 $^\circ\text{C}$, respectively (Figure 3 – 4A). Scaffold fabrication

process had no effect on these temperatures, they were 294 °C and 366 °C (Figure 3 – 4B), meaning that the scaffold fabrication procedure did not induce a biomaterial degradation.

3.3. *In vitro* experiments

3.3.1. *Cytotoxicity of the PLA*

HBMSCs and EPCs reached about 100 % of metabolic activity (MTT) as well as 100 % of cell viability (NR) in the medium where PLA membranes were immersed during 24h after sterilization by γ irradiation (Figure 4).

3.3.2. *Osteoblastic differentiation of HBMSCs (ALP) and endothelial differentiation of EPCs (vWF)*

ALP and vWF markers were expressed in all layers of LBL constructs after 14 days *in vitro cell* culture (Figure 5). Regarding cell colonization, both cell types displayed a homogenous distribution in all layers of *in vitro* samples.

3.3.3. *Osteoblastic phenotype characterization*

Osteoblastic phenotype of cells cultured in LBL constructs *in vitro* was characterized by the expressions of an early (ALP) and late (COL1) osteoblastic genes (Figure 6, * $p < 0.05$; ** $p < 0.01$). Both genes were expressed in all samples after 3, 7 and 14 days of culture. The ALP expression was more significant for co-cultures at all time points comparing to mono-cultures. Expression of ALP in mono-cultures decreased after 14 days, while it remained stable for co-cultures. The expression of COL was statistically higher in co-cultures after 14 days than in all other samples.

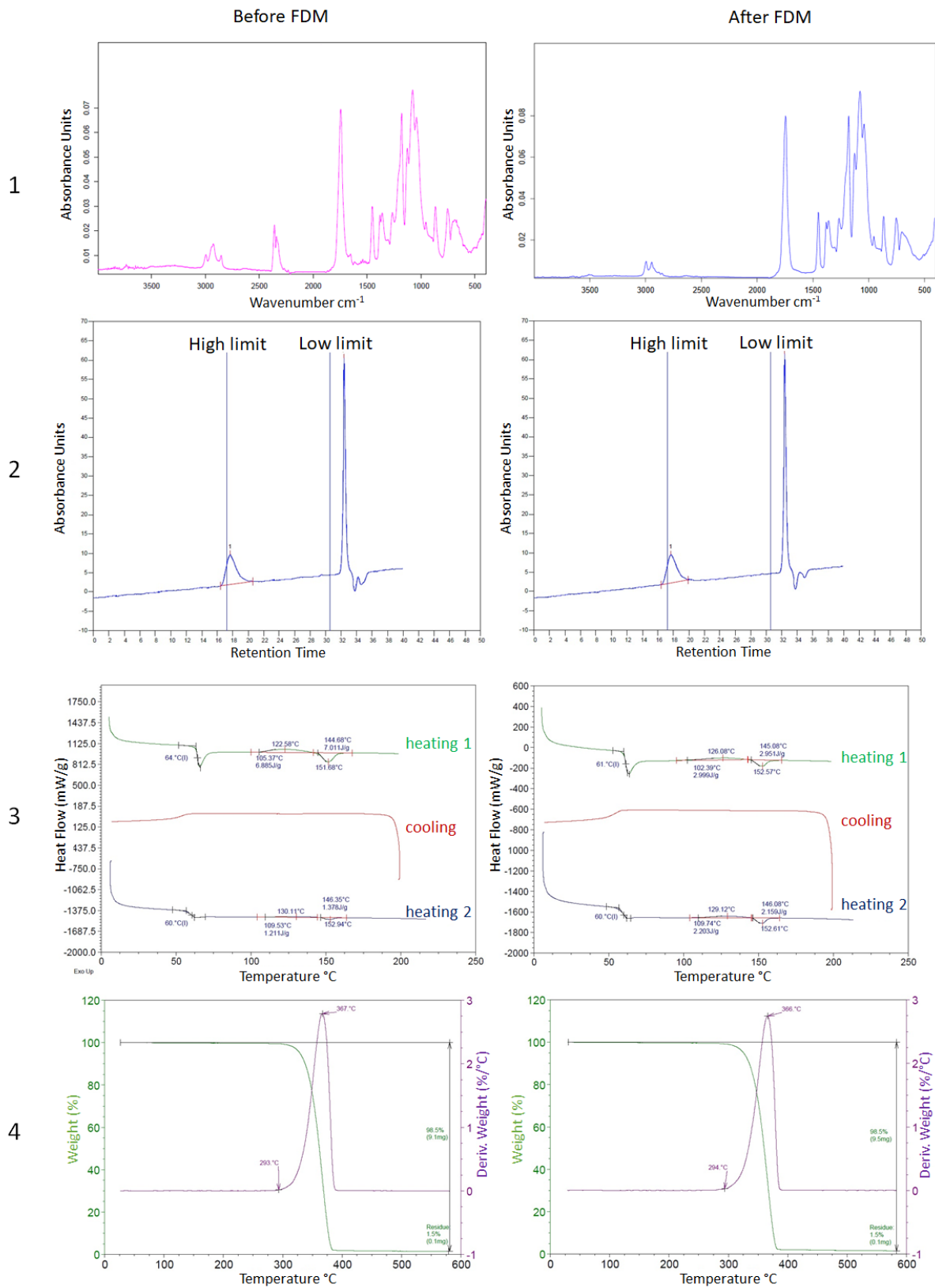


Figure 3. Physico-chemical characterization of PLA (A - filament before printing and B - printed membranes): 1 – Spectroscopic analysis (FTIR), 2 – Molecular weight estimation (size exclusion chromatography SEC), 3 – Polymer crystallinity determination (differential scanning calorimetry DSC), 4 – Polymer thermic degradation profile determination (thermogravimetric analysis)

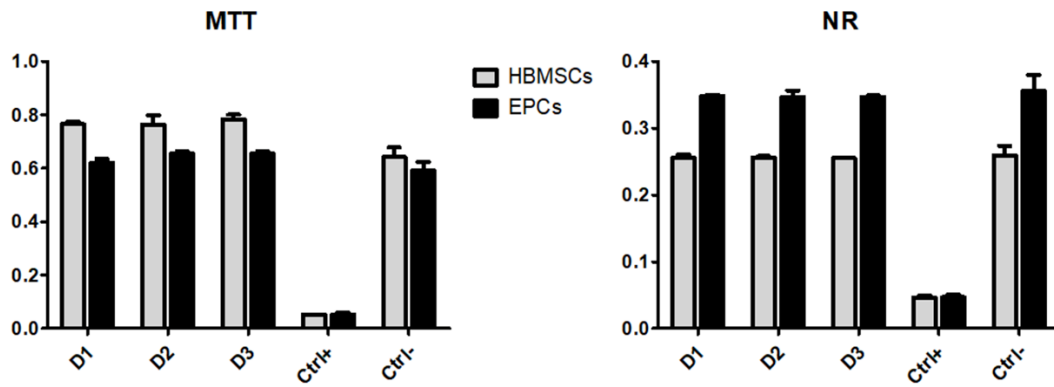


Figure 4. Cytotoxicity assays: Metabolic activity (MTT) and cell viability (NR) of HBMSCs and EPCs was not altered after direct contact with the conditioned medium produced with PLA membranes immersion)

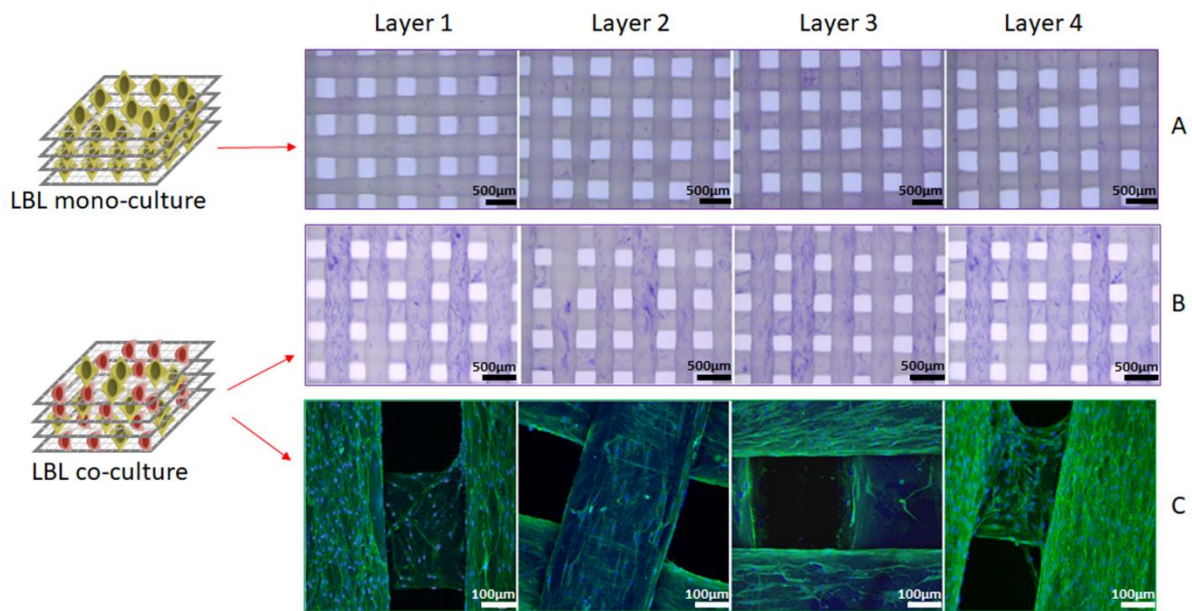


Figure 5. Expressions of early cell differentiation markers for all 4 layers of LBL assemblies after 14 days of culture: A) ALP expression in mono-cultures of HBMSCs, B) ALP expression in co-cultures (HBMSCs + EPCs), C) vWF expression in co-cultures (HBMSCs + EPCs). The scale bar is 500 μm for ALP and 100 μm for Vwf

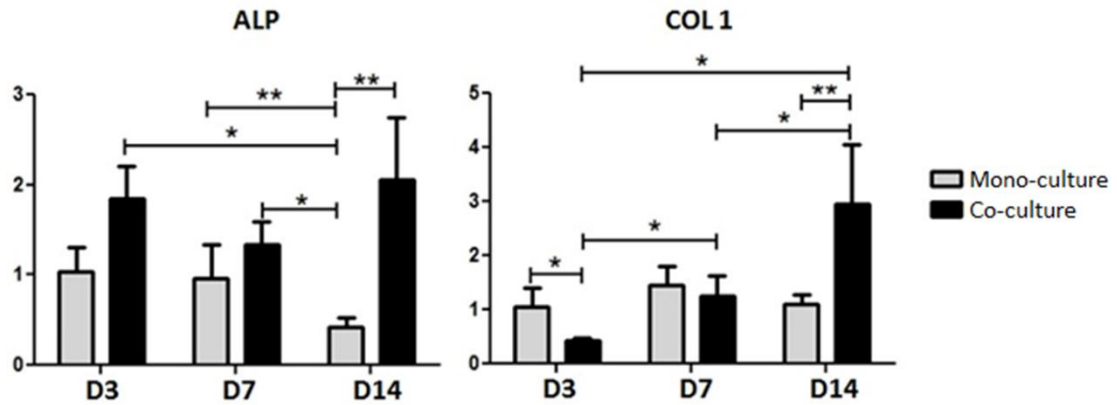


Figure 6. Osteoblastic phenotype characterization of LBL constructs with mono-cultures (HBMSCs) and co-cultures (HBMSCs+EPCs) *in vitro* by RT-qPCR. * $p<0.05$; ** $p<0.01$.

3.4. *In vivo* results

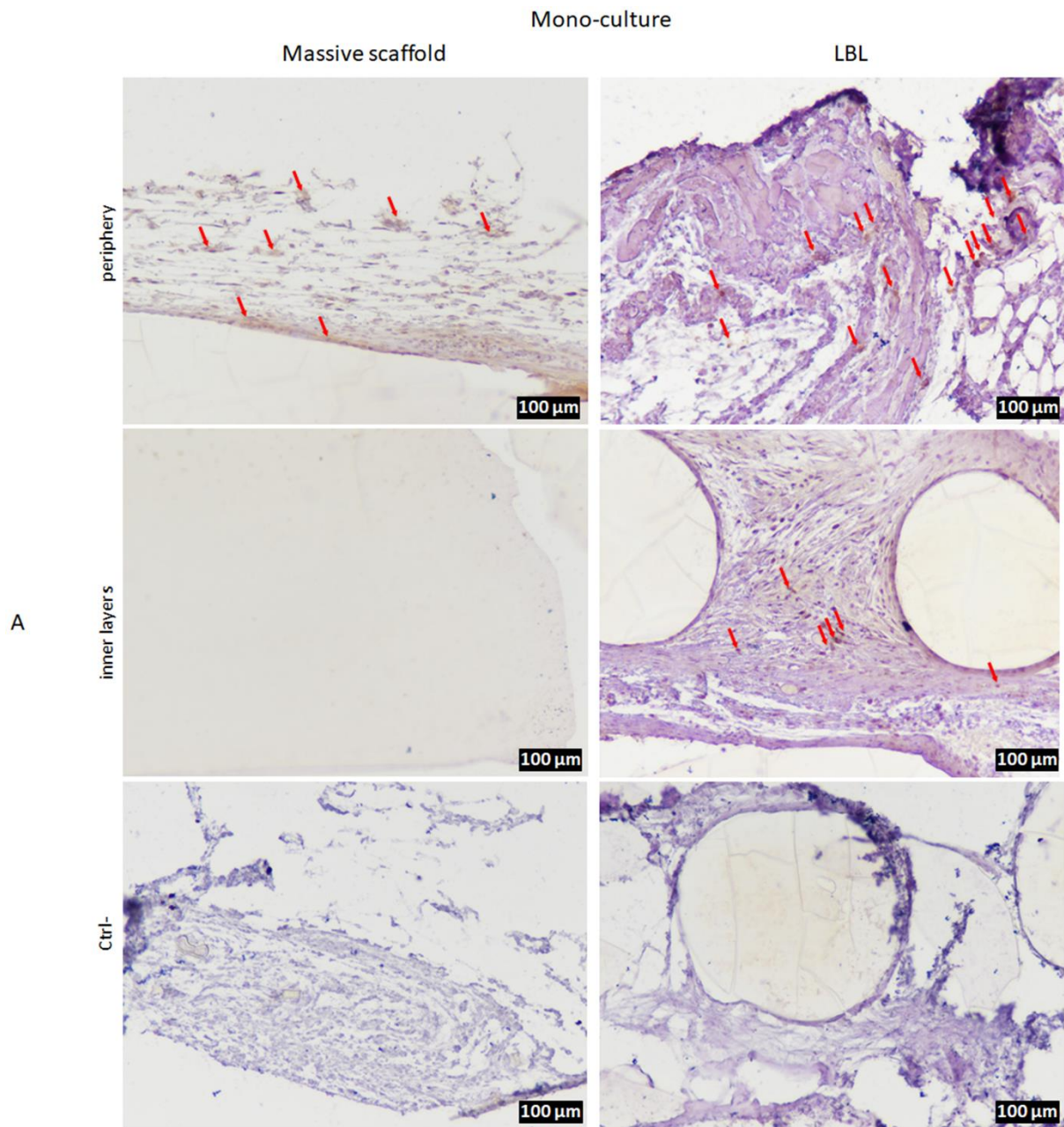
3.4.1. *Surgical outcomes and gross examination*

All animals survived the surgical procedure and the healing period was normal. Gross examination revealed that all the samples were well attached to the surrounding tissues. Concerning massive scaffolds, tissue was observed only at the peripheries. More tissue was observed in the case of LBL assemblies, especially in co-culture samples. Even if some clips had slightly moved, LBL assemblies were completely stable and there was no displacement of layers.

During the last step of resin embedding procedure, which implied vacuum air removing, some of the printed layers of massive scaffolds had detached. This was not observed in the case of LBL assemblies.

3.4.2. *Immuno-labeling of human cells*

The presence of the human cells implanted in the constructs was evaluated using Anti-Mitofilin antibody. There were no human cells observed in the inner parts of massive scaffolds with mono-cultures neither with co-cultures. On the other hand, human cells were present in the inner parts in both types of LBL assemblies (Figure 7) with apparently more cells in the case of co-cultures.



A

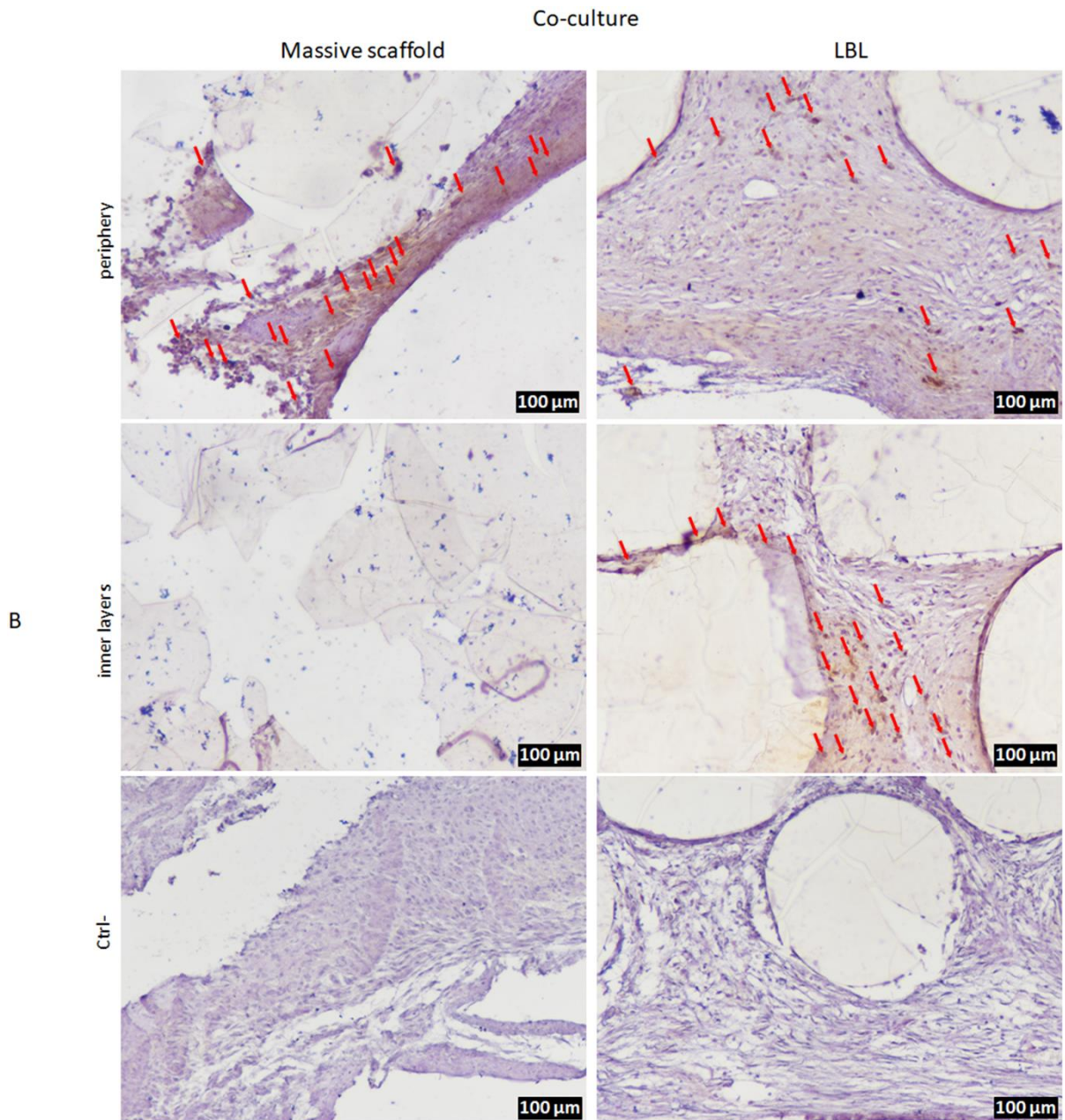


Figure 7. Immunolabelling of human cells with anti-mitofilin antibody in LBL assemblies and massive scaffolds. Human cells are indicated by red arrows. A- Mono-culture samples (HBMSCs), B- Co-culture samples (HBMSCs+EPCs). The scale bar is 100 µm.

3.4.3. Blood vessels formation: Goldner Trichrome staining

The presence of blood vessels was evaluated in the histological samples stained with Goldner Trichrome.

In the external part of the samples, we have observed the presence of blood vessels in all conditions and controls. In the inner parts of the samples, we have observed blood vessel formation only in co-culture LBL assemblies as well as strong host tissue penetration. Some host tissue penetration has been observed in mono-culture LBL samples as well. Images of samples are shown in the Figure 8 and blood vessels are marked with red arrows.

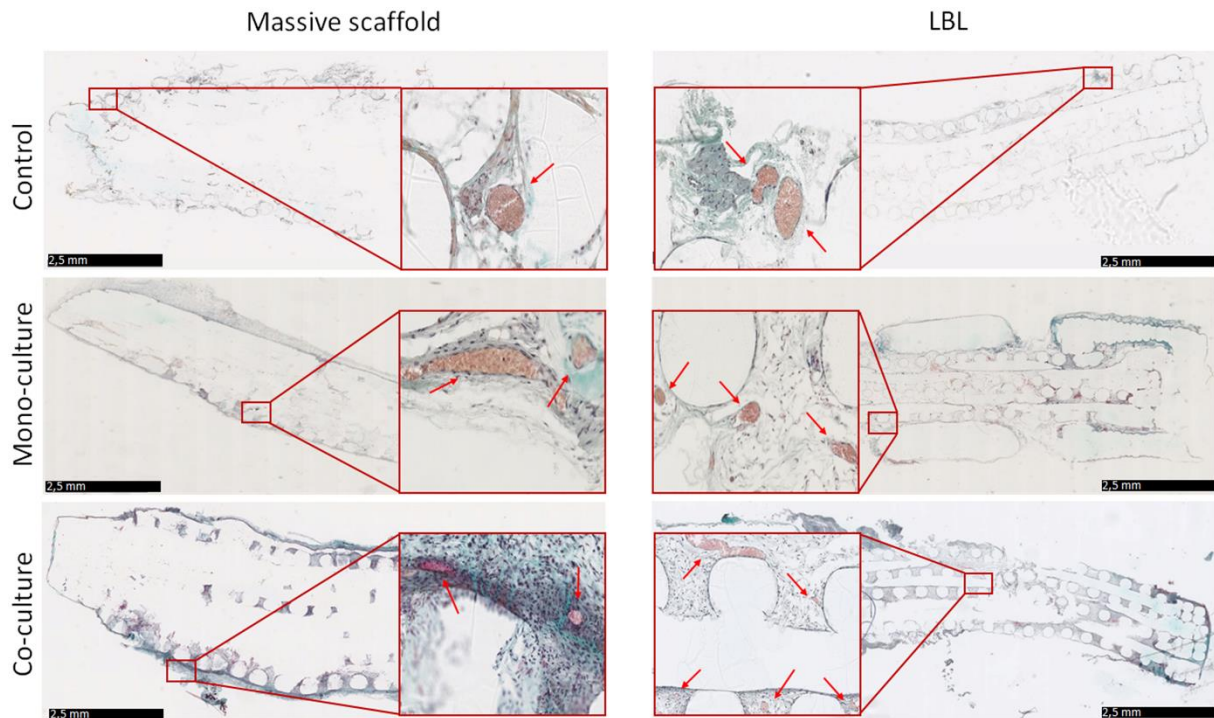


Figure 8. Blood vessels observed in samples after Goldner trichrome staining. Blood vessels are marked with red arrows. The scale bar is 2.5 mm.

3.4.4. Statistical analysis

At the edges of resin blocks, significant differences ($*p < 0.05$, $**p < 0.01$, $***p < 0.001$) were observed only between control samples. However, regarding the middle of the resin blocks, blood vessel formation was more efficient in LBL assemblies than in the massive scaffolds, especially in the case of co-cultures (Figure 9).

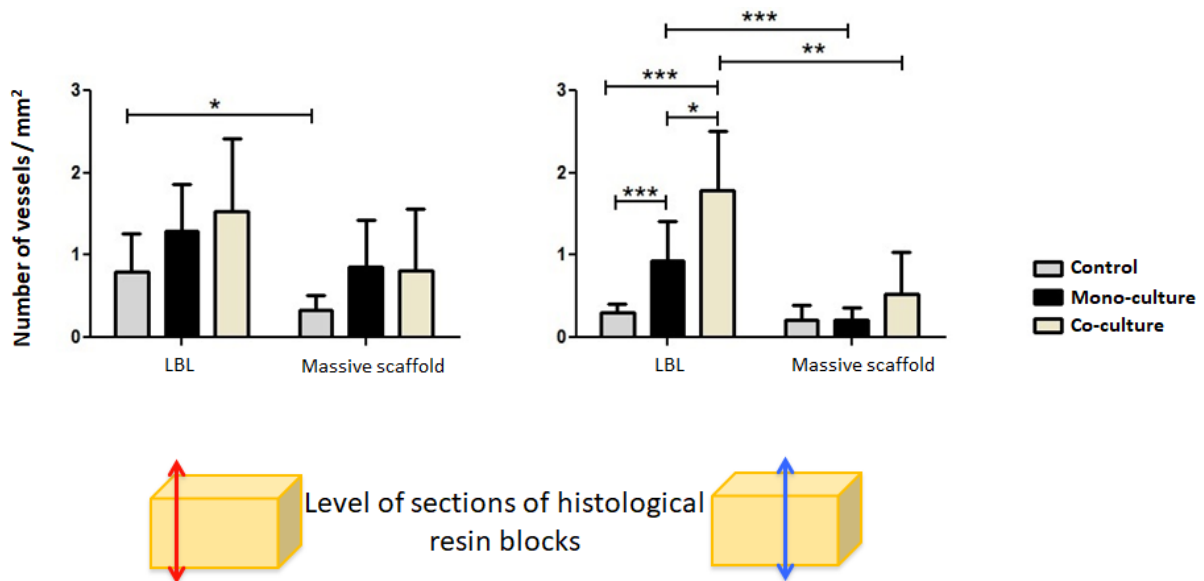


Figure 9. Quantification of blood vessels formed within the PLA implants without cells (control), with mono-cultures (HBMSCs) or co-cultures (HBMSCs+EPCs) at the external parts and in the middle of 3D constructs after 8 weeks *in vivo*. Statistical analysis was performed by non-parametric t-test, * $p < 0.05$, ** $p < 0.01$, *** $p < 0.001$)

4. DISCUSSION

One of the major current challenges in bone tissue engineering products is to obtain sufficient vascularization within massive 3D scaffolds, in order to allow homogeneous tissue formation into these biomaterials. In this study we have shown that the LBL bio-assembly of PLA membranes seeded with co-cultures of HBMSCs and EPCs provided an efficient platform to enhance vascularization *in vivo* in the core of these constructs, compared to conventional method of cell seeding inside massive scaffolds. Moreover, the fabrication process of PLA membranes by FDM did not affect the biomaterial properties.

Stabilization is an important part of LBL assemblies preparations in order to facilitate manipulation, to keep cells undamaged and to prevent movements of layers within the 3D constructs after implantation. Wan *et al.* have used stainless mesh clips under the first and on the top layer to provide stabilization during the culture before implantations [38]. Another group of authors used matrigel to glue layers between each other, but it did not enable sufficient stabilization [40]. We have already used glass rings on the top layer to disable the movements of layers during culture, but the glass rings were damaging top layer cells, the manipulation was difficult because the rings were not completely stable and this stabilization was not implantable avec LBL assemblies [26]. In this study we have used a new stabilization system which is easy to fabricate and manipulate and implantable with the LBL assemblies.

We have successfully printed PLA membranes, stabilization clips and massive 3D scaffolds. Pore size and shape can have an effect on the control of the release of polymer complexed material which can affect tissue regeneration [44]. Pores had an ordered cubic form, since it has been shown as the most suitable one for mesenchymal cell colonization [45]. Fabricated scaffolds had demanded characteristics with high reproducibility, concerning the 3D printing with a nozzle of 400 μm diameter. The obtained pore size was close to the expected and in the range of the size commonly used within scaffolds for bone tissue engineering applications [46].

FTIR revealed the difference of absorption maxima before and after 3DP, which indicated that 3D printing caused some degradation of PLA: small aliphatic carbohydrate groups were lost during the scaffold fabrication process. This small degradation did not have any important effect on the polymer thermic degradation properties, molecular weight and its amorphous structure, which was confirmed by TGA, SEC and DSC, respectively.

The gold standard for sterilization of medical implants in clinical practice is gamma irradiation at 25 kGy to prevent bacterial infection [47]. This sterilization method was used because it does not cause a degradation of PLA and it does not prevent an efficient attachment of osteoblastic cells comparing to other sterilization methods [48].

In some cases, biomaterials can release cytotoxic biomolecules in cell culture media while degrading: it could prevent cell attachment, proliferation and differentiation [49,50]. In these cases, it is necessary to rinse biomaterials prior cell seeding during time. Our membranes were not cytotoxic the first day after the γ irradiation toward HBMSCs or EPCs. Both types of cells reached 100 % of cell viability as well as metabolic activity when cultivated in the conditioned media with PLA membranes soaking.

In order to provide more efficient vascular network formation using this approach, previous studies have used a combination of different cell types seeded in each layer with [40] or without [51] scaffold support. The innovation of our work is in the use of co-cultures of mesenchymal and endothelial cells seeded together on each layer of LBL assemblies in order to compare the effect of different cell culture systems on blood vessel formation.

Since the thickness of our samples was 2 mm and PLA layers were not transparent, we could not observe all the layers together using a confocal microscope (for an early endothelial differentiation) or binocular microscope (for an early osteoblastic differentiation). So, the LBL assemblies were separated to observe each layer individually. All the samples were easily disassembled, except co-cultures after 14 days: It was difficult to separate these samples, probably due to the extracellular matrix deposition which increased mechanical stability of the LBL samples [52]. It was keeping the layers of co-culture LBL assembled together, even after removing the stabilization clips. Massive scaffolds were not examined *in vitro* because it was not possible to perform microscopy observations of the inner parts.

Early endothelial differentiation of cells in co-cultures was investigated after 14 days of culture. We observed high expression of ALP in all layers of LBL constructs with homogenous cell colonization of each layer. Early osteoblastic differentiation of seeded cells in mono-cultures and co-cultures was examined by the expression of alkaline phosphatase: it

was observed in all layers of both, mono-cultures and co-cultures after 14 days with homogenous distribution of cells. It seemed that this marker was more expressed in co-cultures comparing to mono-cultures even if there was twice less HBMSCs cells seeded at the beginning. It could be explained by the cell-to-cell communication through the growth factor secretion [27].

Rt-qPCR was used to obtain quantitative results concerning the expression of two osteoblastic genes in LBL mono- and co-culture constructs after 3, 7 and 14 days of culture. All gene expressions for different time points were expressed to relative gene expression levels of monoculture samples at the day 3. Since ALP is an early osteoblastic gene [53], it was expected that its expression would decrease during the time and this was observed in mono-culture samples. The expression of this gene was statistically more important in co-cultures after 14 days. It means that the presence of endothelial cells in co-culture systems has a positive effect on the differentiation of mesenchymal cells toward osteoblastic phenotype.

COL1 is a late osteoblastic gene and its expression is usually more significant after some time of culture since it is linked to the extracellular matrix secretion. The expression of this gene was augmented in co-cultures after 14 days. Regarding all results of phenotype characterization *in vitro*, we could observe again that the co-culture cell system of HBMSCs and EPCS onto PLA membranes enables better conditions for osteoblastic differentiation. We have already observed this trend using a 2D cell culture system [26], and we confirm here the same results in 3D.

Subcutaneous implantations *in vivo* were performed to observe the potential advantage of cellularized LBL assemblies compared to massive scaffolds (conventional tissue engineering approach) in terms of favoring the vascularization when they were surrounded by host tissue containing peripheral vascular network. Gross examination revealed that LBL assemblies were more compact after 8 weeks *in vivo* since they did not separate during the vacuum step of resin embedding, comparing to massive scaffolds. The host tissue penetrated and extracellular matrix was formed more efficiently in the case of LBL assemblies, which improved the stabilization of the whole construct.

In order to observe the fate of the implanted human cells in this animal model, we have used an Anti-mitofilin antibody for immunolabelling of human cells. Human cells were distributed in different parts of the samples depending on the constructs. Regarding the group of massive 3D scaffolds, human cells were present only in the outer parts of the implants in both cell culture system, but that there were more human cells in co-cultures. It means that this kind of 3D architecture did not provide favorable conditions for seeded cells penetration in the center of these scaffolds [54]. On the other hand, human cells were observed in the inner part of all LBL constructs with the distribution that seemed to be homogenous in all layers with more cells present in co-culture samples. LBL constructs provided more suitable and controlled environmental conditions for implanted cells comparing to massive 3D scaffolds allowing most likely more efficient oxygen and nutrients distribution in all parts of scaffolds [55]. The microenvironmental conditions appear to be more appropriate for cell survival and colonization in the case of co-cultures.

Goldner trichrome staining has already been used for collagen and blood vessels observations in another study [56]. We could observe some blood vessels on the outer surfaces of control and mono-culture massive scaffolds. They were not present in the inner parts probably because of the insufficient diffusion of oxygen. An important difference was observed in the case of LBL co-cultures where numerous blood vessels were observed within the entire constructs. We quantified the number of blood vessels formed at the peripheries and in the middle of samples in resin blocks. There was no significant difference observed in the number of blood vessels at the peripheries of resin blocks concerning the cell culture system in LBL assemblies. The difference was observed only in the case of control samples showing that LBL approach provides more efficient vascularization even without cell implantation. But regarding the central parts of resin blocks, we could observe statistically significant differences depending on the 3D structure of the scaffold as well as the cell culture system. Cell seeded massive scaffolds showed more efficient blood vessel formation than control samples. It means that the presence of human primary cells supported vascularization in the inner parts of scaffolds. In the case of mono-cultures, blood vessel formation was more important in the case of LBL bioassemblies comparing to massive scaffolds. This vascularization was more efficient in the case of co-cultures probably because of the improved growth factor production followed by host tissue penetration in the inner parts [57]. Co-culture system enabled favorable environment for blood vessel formation within the entire 3D bioassemblies. It means that the 3D organization of cells as well as used cell culture system have an important effect on the blood vessel formation.

5. CONCLUSIONS AND PERSPECTIVES

The development of blood vessels was more efficient in the case of LBL bioassembly approach using co-culture of HBMSCs and EPCs, compared to conventional tissue engineering approach using large 3D massive scaffolds.

This study confirmed *in vivo* our previous *in vitro* results, showing that co-culture system enables more suitable conditions for cell differentiation and colonization *in vitro* and cell colonization and blood vessel formation *in vivo*

The stabilization of LBL constructs has also been improved. Clips used in this work enabled a sufficient stabilization of 3D bioassemblies, which facilitate manipulation of LBL assemblies and which could be implanted together.

The perspectives of this study will be to develop the system by using a biomaterial more suitable for bone formation. Also, different arrangements of cells and biomolecules could be easily implemented to this 3D culture system for Bone Tissue Engineering applications.

Acknowledgements

We are grateful to Dr. Gérard Dimier, LCPO – Université de Bordeaux, for the chemical characterization of our scaffolds. This research was funded by a grant from “La Fondation des Gueules cassées” (57-2015), the ANR “Sandwich” (ANR-16-CE18-0009-01), French Embassy and French Institute in Serbia with CampusFrance.

Key words: biofabrication, bioassembly, vascularization, *in vivo*

References

1. Langer R, Vacanti JP. Tissue engineering. *Science*. **260**(5110), 920, 1993;
2. Phelps EA, Garcia AJ. Update on therapeutic vascularization strategies. *Regen. Med.* **4**(1), 65, 2009;
3. Lopa S, Piraino F, Kemp RJ, Di Caro C, Lovati AB, Di Giancamillo A, et al. Fabrication of multi-well chips for spheroid cultures and implantable constructs through rapid prototyping techniques. *Biotechnol. Bioeng.* **112**(7), 1457, 2015;
4. Ahlfeld T, Akkineni AR, Förster Y, Köhler T, Knaack S, Gelinsky M, et al. Design and Fabrication of Complex Scaffolds for Bone Defect Healing: Combined 3D Plotting of a Calcium Phosphate Cement and a Growth Factor-Loaded Hydrogel. *Ann. Biomed. Eng.* **45**(1), 224, 2017;
5. Yuan B, Zhou S-Y, Chen X-S. Rapid prototyping technology and its application in bone tissue engineering. *J. Zhejiang Univ. Sci. B.* **18**(4), 303, 2017;
6. Xu N, Ye X, Wei D, Zhong J, Chen Y, Xu G, et al. 3D artificial bones for bone repair prepared by computed tomography-guided fused deposition modeling for bone repair. *ACS Appl. Mater. Interfaces.* **6**(17), 14952, 2014;
7. Korpela J, Kokkari A, Korhonen H, Malin M, Närhi T, Seppälä J. Biodegradable and bioactive porous scaffold structures prepared using fused deposition modeling. *J. Biomed. Mater. Res. B Appl. Biomater.* **101**(4), 610, 2013;
8. Kim J, McBride S, Tellis B, Alvarez-Urena P, Song Y-H, Dean DD, et al. Rapid-prototyped PLGA/ β -TCP/hydroxyapatite nanocomposite scaffolds in a rabbit femoral defect model. *Biofabrication.* **4**(2), 025003, 2012;
9. Fleischer S, Dvir T. Tissue engineering on the nanoscale: lessons from the heart. *Curr. Opin. Biotechnol.* **24**(4), 664, 2013;
10. Groppo MF, Caria PH, Freire AR, Figueroba SR, Ribeiro-Neto WA, Bretas RES, et al. The effect of a hydroxyapatite impregnated PCL membrane in rat subcritical calvarial bone defects. *Arch. Oral Biol.* **82**, 209, 2017;

11. Xue R, Qian Y, Li L, Yao G, Yang L, Sun Y. Polycaprolactone nanofiber scaffold enhances the osteogenic differentiation potency of various human tissue-derived mesenchymal stem cells. *Stem Cell Res. Ther.* **8**(1), 148, 2017;
12. Fedore CW, Tse LYL, Nam HK, Barton KL, Hatch NE. Analysis of polycaprolactone scaffolds fabricated via precision extrusion deposition for control of craniofacial tissue mineralization. *Orthod. Craniofac. Res.* **20 Suppl 1**, 12, 2017;
13. Mozdzen LC, Rodgers R, Banks JM, Bailey RC, Harley BAC. Increasing the strength and bioactivity of collagen scaffolds using customizable arrays of 3D-printed polymer fibers. *Acta Biomater.* **33**, 25, 2016;
14. Cai H, Azangwe G, Shepherd DET. Skin cell culture on an ear-shaped scaffold created by fused deposition modelling. *Biomed. Mater. Eng.* **15**(5), 375, 2005;
15. Tung Y-T, Chang C-C, Ju J-C, Wang G-J. Fabrication of a reticular poly(lactide-co-glycolide) cylindrical scaffold for the in vitro development of microvascular networks. *Sci. Technol. Adv. Mater.* **18**(1), 163, 2017;
16. Revati R, Abdul Majid MS, Ridzuan MJM, Normahira M, Mohd Nasir NF, Rahman Y MN, et al. Mechanical, thermal and morphological characterisation of 3D porous *Pennisetum purpureum*/PLA biocomposites scaffold. *Mater. Sci. Eng. C Mater. Biol. Appl.* **75**, 752, 2017;
17. Su J-Y, Chen S-H, Chen Y-P, Chen W-C. Evaluation of Magnetic Nanoparticle-Labeled Chondrocytes Cultivated on a Type II Collagen-Chitosan/Poly(Lactic-co-Glycolic) Acid Biphasic Scaffold. *Int. J. Mol. Sci.* **18**(1), 2017;
18. Hao W, Jiang C, Jiang M, Wang T, Wang X. Osteogenic potency of dedifferentiated fat cells isolated from elderly people with osteoporosis. *Exp. Ther. Med.* **14**(1), 43, 2017;
19. Lu Y, Dong S, Zhang P, Liu X, Wang X. Preparation of a polylactic acid knitting mesh for pelvic floor repair and in vivo evaluation. *J. Mech. Behav. Biomed. Mater.* **74**, 204, 2017;
20. Zhao X, Han Y, Li J, Cai B, Gao H, Feng W, et al. BMP-2 immobilized PLGA/hydroxyapatite fibrous scaffold via polydopamine stimulates osteoblast growth. *Mater. Sci. Eng. C Mater. Biol. Appl.* **78**, 658, 2017;
21. Du L, Yang S, Li W, Li H, Feng S, Zeng R, et al. Scaffold composed of porous vancomycin-loaded poly(lactide-co-glycolide) microspheres: A controlled-release drug delivery system with shape-memory effect. *Mater. Sci. Eng. C Mater. Biol. Appl.* **78**, 1172, 2017;

22. Wagoner Johnson AJ, Herschler BA. A review of the mechanical behavior of CaP and CaP/polymer composites for applications in bone replacement and repair. *Acta Biomater.* **7**(1), 16, 2011;
23. Declercq HA, Desmet T, Dubruel P, Cornelissen MJ. The Role of Scaffold Architecture and Composition on the Bone Formation by Adipose-Derived Stem Cells. *Tissue Eng. Part A.* **20**(1–2), 434, 2014;
24. Xu T, Yang H, Yang D, Yu Z-Z. Polylactic Acid Nanofiber Scaffold Decorated with Chitosan Islandlike Topography for Bone Tissue Engineering. *ACS Appl. Mater. Interfaces.* **9**(25), 21094, 2017;
25. Chen B-Q, Kankala RK, Chen A-Z, Yang D-Z, Cheng X-X, Jiang N-N, et al. Investigation of silk fibroin nanoparticle-decorated poly(l-lactic acid) composite scaffolds for osteoblast growth and differentiation. *Int. J. Nanomedicine.* **12**, 1877, 2017;
26. Guduric V, Metz C, Siadous R, Bareille R, Levato R, Engel E, et al. Layer-by-layer bioassembly of cellularized polylactic acid porous membranes for bone tissue engineering. *J. Mater. Sci. Mater. Med.* **28**(5), 78, 2017;
27. Grellier M, Bordenave L, Amédée J. Cell-to-cell communication between osteogenic and endothelial lineages: implications for tissue engineering. *Trends Biotechnol.* **27**(10), 562, 2009;
28. Jaklenec A, Stamp A, Deweerd E, Sherwin A, Langer R. Progress in the tissue engineering and stem cell industry “are we there yet?” *Tissue Eng. Part B Rev.* **18**(3), 155, 2012;
29. Jain RK, Au P, Tam J, Duda DG, Fukumura D. Engineering vascularized tissue. *Nat. Biotechnol.* **23**(7), 821, 2005;
30. Rouwkema J, Khademhosseini A. Vascularization and Angiogenesis in Tissue Engineering: Beyond Creating Static Networks. *Trends Biotechnol.* **34**(9), 733, 2016;
31. Akintewe OO, Roberts EG, Rim N-G, Ferguson MAH, Wong JY. Design Approaches to Myocardial and Vascular Tissue Engineering. *Annu. Rev. Biomed. Eng.* **19**, 389, 2017;
32. Laschke MW, Menger MD. Prevascularization in tissue engineering: Current concepts and future directions. *Biotechnol. Adv.* **34**(2), 112, 2016;
33. Papadimitropoulos A, Piccinini E, Brachat S, Braccini A, Wendt D, Barbero A, et al. Expansion of human mesenchymal stromal cells from fresh bone marrow in a 3D scaffold-based system under direct perfusion. *PloS One.* **9**(7), e102359, 2014;
34. Oragui E, Nannaparaju M, Khan WS. The Role of Bioreactors in Tissue Engineering for Musculoskeletal Applications. *Open Orthop. J.* **5**, 267, 2011;

35. Laschke MW, Rücker M, Jensen G, Carvalho C, Mülhaupt R, Gellrich N-C, et al. Improvement of vascularization of PLGA scaffolds by inoculation of in situ-preformed functional blood vessels with the host microvasculature. *Ann. Surg.* **248**(6), 939, 2008;
36. Fricain J-C, De Olivera H, Devillard R, Kalisky J, Remy M, Kériquel V, et al. [3D bioprinting in regenerative medicine and tissue engineering]. *Med. Sci. MS.* **33**(1), 52, 2017;
37. Groll J, Boland T, Blunk T, Burdick JA, Cho D-W, Dalton PD, et al. Biofabrication: reappraising the definition of an evolving field. *Biofabrication.* **8**(1), 013001, 2016;
38. Wan W, Zhang S, Ge L, Li Q, Fang X, Yuan Q, et al. Layer-by-layer paper-stacking nanofibrous membranes to deliver adipose-derived stem cells for bone regeneration. *Int. J. Nanomedicine.* **10**, 1273, 2015;
39. Catros S, Guillemot F, Nandakumar A, Ziane S, Moroni L, Habibovic P, et al. Layer-by-layer tissue microfabrication supports cell proliferation in vitro and in vivo. *Tissue Eng. Part C Methods.* **18**(1), 62, 2012;
40. Kim MS, Lee B, Kim HN, Bang S, Yang HS, Kang SM, et al. 3D tissue formation by stacking detachable cell sheets formed on nanofiber mesh. *Biofabrication.* **9**(1), 015029, 2017;
41. Vilamitjana-Amedee J, Bareille R, Rouais F, Caplan AI, Harmand MF. Human bone marrow stromal cells express an osteoblastic phenotype in culture. *In Vitro Cell. Dev. Biol. Anim.* **29A**(9), 699, 1993;
42. Thebaud NB, Bareille R, Remy M, Bourget C, Daculsi R, Bordenave L. Human progenitor-derived endothelial cells vs. venous endothelial cells for vascular tissue engineering: an in vitro study. *J. Tissue Eng. Regen. Med.* **4**(6), 473, 2010;
43. Ackerman GA. Substituted naphthol AS phosphate derivatives for the localization of leukocyte alkaline phosphatase activity. *Lab. Investig. J. Tech. Methods Pathol.* **11**, 563, 1962;
44. Whang K, Tsai DC, Nam EK, Aitken M, Sprague SM, Patel PK, et al. Ectopic bone formation via rhBMP-2 delivery from porous bioabsorbable polymer scaffolds. *J. Biomed. Mater. Res.* **42**(4), 491, 1998;
45. Ferlin KM, Prendergast ME, Miller ML, Kaplan DS, Fisher JP. Influence of 3D printed porous architecture on mesenchymal stem cell enrichment and differentiation. *Acta Biomater.* **32**, 161, 2016;
46. Ramirez-Rodríguez GB, Montesi M, Panseri S, Sprio S, Tampieri A, Sandri M. Biom mineralized recombinant collagen-based scaffold mimicking native bone enhances mesenchymal stem cell interaction and differentiation. *Tissue Eng. Part A.* 2017;

47. Rihn JA, Irrgang JJ, Chhabra A, Fu FH, Harner CD. Does irradiation affect the clinical outcome of patellar tendon allograft ACL reconstruction? *Knee Surg. Sports Traumatol. Arthrosc. Off. J. ESSKA.* **14**(9), 885, 2006;
48. Valente T a. M, Silva DM, Gomes PS, Fernandes MH, Santos JD, Sencadas V. Effect of Sterilization Methods on Electrospun Poly(lactic acid) (PLA) Fiber Alignment for Biomedical Applications. *ACS Appl. Mater. Interfaces.* **8**(5), 3241, 2016;
49. Bordenave L, Chaudet B, Bareille R, Fernandez P, Amedee J. In vitro assessment of endothelial cell adhesion mechanism on vascular patches. *J. Mater. Sci. Mater. Med.* **10**(12), 807, 1999;
50. Pariente JL, Bordenave L, Bareille R, Rouais F, Courtes C, Daude G, et al. First use of cultured human urothelial cells for biocompatibility assessment: application to urinary catheters. *J. Biomed. Mater. Res.* **40**(1), 31, 1998;
51. Ren L, Ma D, Liu B, Li J, Chen J, Yang D, et al. Preparation of three-dimensional vascularized MSC cell sheet constructs for tissue regeneration. *BioMed Res. Int.* **2014**, 301279, 2014;
52. Engebretson B, Mussett ZR, Sikavitsas VI. Tenocytic extract and mechanical stimulation in a tissue-engineered tendon construct increases cellular proliferation and ECM deposition. *Biotechnol. J.* **12**(3), n/a, 2017;
53. Golub EE. Enzymes in mineralizing systems: state of the art. *Connect. Tissue Res.* **35**(1–4), 183, 1996;
54. Nguyen LH, Annabi N, Nikkhah M, Bae H, Binan L, Park S, et al. Vascularized Bone Tissue Engineering: Approaches for Potential Improvement. *Tissue Eng. Part B Rev.* **18**(5), 363, 2012;
55. Derda R, Laromaine A, Mammoto A, Tang SKY, Mammoto T, Ingber DE, et al. Paper-supported 3D cell culture for tissue-based bioassays. *Proc. Natl. Acad. Sci. U. S. A.* **106**(44), 18457, 2009;
56. Mai R, Kunert-Keil C, Grafe A, Gedrange T, Lauer G, Dominiak M, et al. Histological behaviour of zirconia implants: An experiment in rats. *Ann. Anat. - Anat. Anz.* **194**(6), 561, 2012;
57. Zhang X, Li J, Ye P, Gao G, Hubbell K, Cui X. Coculture of mesenchymal stem cells and endothelial cells enhances host tissue integration and epidermis maturation through AKT activation in gelatin methacryloyl hydrogel-based skin model. *Acta Biomater.* 2017;

THIRD PART:

Developing the Prototype of FDM Printer with High Resolution

**Physicochemical and Biological Characterization of Fabricated
Scaffolds**

A. INTRODUCTION

The fabrication of PLA membranes by FDM seemed to be more suitable than direct 3D printing in terms of resolution and possibility to easily create different stabilization systems. But we were wondering if it was possible to enhance the resolution of the printed membranes, based on the resolution of commercially available FDM printers. The most common extrusion nozzles of FDM printers measure 400 μm diameter. Other nozzle diameters such as 200 μm , 250 μm or 300 μm can easily be found. We wanted to assemble a new printer prototype containing an extrusion nozzle of 100 μm . This was performed in collaboration with Technoshop at the IUT of Bordeaux. This FDM printer (Microprint) had specific characteristics:

- Mechanical resolution: 25 μm in 3 axes (x;y;z);
- Printing object space: 100 mm in X, 100 mm in Y and 50 mm in Z;
- Z position sensor precision: 1 μm ;
- Printing Platform: Heating marble platform with a flatness tolerance of less than 0.005 mm;
- A brush cleans nozzle before each printing process;
- Printing head is equipped with 3 ventilators to maintain printing temperature;
- Printer can use any 1.75 mm thermoplastic filament.

A specific software was designed with this printer, allowing quick and easy design of membranes for LBL BioAssembly with perpendicular pores, ready for printing. It was possible to choose pore network shape and pore dimensions in the software.

This CAD/CAM system enabled production of PLA membranes with high resolution. Membranes having three different pore sizes were printed: 150 μm , 200 μm and 250 μm and obtained pore dimensions were slightly smaller than expected. Information about pores dimensions were obtained by microscopic observations.

Physico-chemical characterization of printed membranes was performed. We found that the 3D printing process induced decreases in both, PLA molecular weight and degradation temperatures observed by Size Exclusion Chromatography (SEC) and thermogravimetric analysis (TGA), respectively. FDM fabrication process did not change the semi-crystalline structure of the polymer. Mechanical properties were tested in function of pore size of membranes and we could observe that there was no effect of pore size on the mechanical properties of produced scaffolds.

Printed membranes were sterilized by γ irradiation prior to biological evaluations. After the sterilization, scaffolds did not exhibit any cytotoxicity towards human bone marrow stromal cells (HBMSC). After three and seven days of culture, HBMSC showed high viability and homogenous distribution irrespective of pore size.

These results suggest that FDM technology is a fast and reproducible technique that can be used to fabricate tridimensional custom-made scaffolds for tissue engineering.

ARTICLE 3

Characterization of Printed PLA Scaffolds for Bone Tissue Engineering

Agathe GRÉMARE, Vera GUDURIC, Reine BAREILLE, Valérie HÉROGUEZ, Simon LATOUR, Nicolas L'HEUREUX, Jean-Christophe FRICAIN, Sylvain CATROS, Damien LE NIHOANNEN

*Accepted for publication in Journal of Biomedical Materials Research Part A
in November 2017*

B. RESULTS

Abstract:

Autografts remain the gold standard for orthopedic transplantations. However, to overcome its limitations, bone tissue engineering proposes new strategies. This includes the development of new biomaterials such as synthetic polymers, to serve as scaffold for tissue production. The objective of this present study was to produce poly(lactic) acid (PLA) scaffolds of different pore size using fused deposition modeling (FDM) technique and to evaluate their physicochemical and biological properties. Structural, chemical, mechanical and biological characterizations were performed. We successfully fabricated scaffolds of three different pore sizes. However, the pore dimensions were slightly smaller than expected. We found that the 3D printing process induced decreases in both, PLA molecular weight and degradation temperatures, but did not change the semi-crystalline structure of the polymer. We did not observe any effect of pore size on the mechanical properties of produced scaffolds. After the sterilization by γ irradiation, scaffolds did not exhibit any cytotoxicity towards human bone marrow stromal cells (HBMSC). Finally, after three and seven days of culture, HBMSC showed high viability and homogenous distribution irrespective of pore size. Thus, these results suggest that FDM technology is a fast and reproducible technique that can be used to fabricate tridimensional custom-made scaffolds for tissue engineering.

Keywords:

Fused Deposition Modeling, PolyLactic Acid, Scaffolds, Physicochemical characterization, Biocompatibility

1. INTRODUCTION

Orthopedic surgical procedures involving bone grafting have increased in the last few decades making bone as one of the most transplanted tissue [1]. Autografts remain the gold standard solution. However, drawbacks such as limited tissue availability, pain, donor site morbidity and difficulty in producing anatomical shapes [2] have favored the development of engineered implants. Bone tissue engineering has thus become a promising approach to fabricate bone substitutes through the association of specific bone cells, growth factors and porous biocompatible scaffold [3]. An ideal scaffold for bone reconstruction should be (i) biocompatible and porous to support cell proliferation and differentiation, (ii) biodegradable to be gradually replaced by the host tissue, (iii) osteoconductive and osteoinductive and (iv) manufactured in a specific shape to precisely match complex bone defects [1].

Solid freeform fabrication techniques, also known as additive manufacturing (AM), have emerged as a new tool for the fabrication of 3D scaffolds for bone tissue engineering with well-defined and reproducible architectures, allowing the creation of an accurate 3D anatomic model of a specific bone tissue for a particular patient. Several techniques have been developed for AM such as stereolithography (SLA) [4], selective laser sintering (SLS) [5], three-dimensional printing (3DP) [6], fused deposition modeling (FDM) [7] for the production of custom, defect-matched constructs for bone repair [8]. FDM is the most commonly used technique in which the material, a filament, is melted, extruded and deposited to generate a three-dimensional structure in a layer-by-layer fashion with the benefit of controlling both the porosity and the pore size [9]. Another advantage of FDM technology is the ease to associate cells with these thin polymeric scaffolds resulting in a better cell colonization, proliferation and differentiation compared with a larger 3D structure which often includes an inner hypoxic central area avoiding deep cell colonization. Moreover, staked together, these populated scaffolds frequently aims to form a large 3D structure within an internal organization improving both cell communication and cell-material interactions *in vitro* and *in vivo* [10-12].

Biocompatible and biodegradable polymeric materials are commonly used for tissue engineering scaffolding [13]. Numerous degradable polymers such as acrylonitrile butadiene styrene (ABS), polycaprolactone (PCL), polylactic acid (PLA), polyglycolic acid (PGA), and chitosan can be used to fabricate 3D scaffolds [14]. In tissue engineering applications, ABS, PCL and PGA are used for bone, tendon and skin repair [15-18]. Composites polymeric materials like PCL-HA or PCL-TCP have also been produced by FDM and thus been used in bone tissue engineering for their mechanical and biochemical properties [19]. Chitosan is a well-known biodegradable polymer used to print scaffolds for tissue engineering purposes and has been shown to modulate the cytokine production by macrophage *in vitro* [20, 21]. PLA is a hydrophobic aliphatic polyester approved by the US Food and Drug Administration (FDA) for different biomedical and clinical applications [22]. PLA, because of its excellent biocompatibility, degradability, thermal stability and degradation of PLA, as well as low viscosity and thermoplastic properties, has been shown through numerous studies well-suited for the FDM technology [23]. Generally, the thermal stability and degradation properties of

PLA are dependent on the choice and distribution of stereoisomers within the polymers chains (L/D ratios) and molecular weights. Depending on the choice of pre-polymers and route of synthesis, a vast diversity of PLA can be achieved resulting in PLA with a broad range of physiochemical properties. The optical composition of PLA significantly affects crystallisation kinetics and the ultimate extent of crystallinity. In turn, the level of crystallinity developed is particularly influential on the PLA glass transition temperature (T_g), melting temperature (T_m) and degradation rate [24]. T_g and T_m of PLA are approximately 55 °C and 180 °C, respectively. PLA degrades by hydrolysis and degradation products in form of oligomers are metabolized by cells [25]. This material has often been used in skeletal tissue engineering [26, 27]. The degradation products of this polymer are not toxic. They are present in the human body and are removed by natural metabolic pathways [28]. Despite previous publications showing the possibility to associate printing PLA scaffolds with bone marrow cells, no study has been conducted on the reliability of the fabrication of porous scaffolds by FDM and to explore this influence of fabrication process on materials properties.

Thus, the aim of the present study was, to print PLA scaffolds with a custom-made FDM printer at high resolution and in a reproducible manner. We have characterized the physical properties of the printed scaffolds (pore size and thread diameter) and the reproducibility of the technique. Importantly, we also assessed whether both the printing process and the different porosities affected PLA chemical properties and PLA mechanical properties, respectively. Finally, we investigated the biocompatibility of printed PLA scaffolds towards human bone marrow cells (HBMSC).

2. MATERIALS AND METHODS

2.1. Scaffolds fabrication

Poly(lactic) acid filament (PLA; ESUN[®], natural, diameter 1.75mm) was used to fabricate scaffolds with a custom-made 3D printer, developed and assembled by “Technoshop” in the Technological Department at the Université of Bordeaux (IUT de Bordeaux, France). The working principle of this printer is based on FDM technology. Briefly, clump generator software[®] was used to create squared pores into a 3D object in a “stl” file format. The printing head was computer-controlled in three axes (x, y, z with a xy speed of 30 mm.s⁻¹) while extruding the PLA filament using the Repetier-Host software. A gear system guided the filament into the printing head, heated at a temperature above the PLA melting point (temperature near the nozzle was 186 °C). The melted PLA was then extruded through a 100 µm diameter stainless-steel nozzle onto a printing plate heated at 60 °C. Porous scaffolds were printed layer-by-layer in the form of squares surrounded by a dense PLA perimeter. We fabricated scaffolds with 4 different pore sizes (0, 150, 200, 250 µm). Prior to mechanical and biological evaluations, printed scaffolds were sterilized by gamma irradiation (25 kGy, 84 hours, room temperature; Nordion[®], GC 3000).

2.2. Structural characterization of the scaffolds after printing

Printed PLA scaffolds were observed using a binocular (Leica[®], MZ10F) and a scanning electron microscope (SEM; Hitachi[®], S-2500). To confirm the reliability of the printing technique, the expected pore size and thread diameter were compared with the actual pore and thread dimensions of printed scaffolds. For each pore size (150, 200 and 250 μm), three scaffolds were printed and four pictures were then taken per scaffold using binocular microscopy. After thresholding the images with ImageJ[®] software (NIH), a plug-in was written to automatically calculate pore dimensions (pore length and pore width were pooled) and thread diameter. Both for pore length and thread diameter, more than 330 measurements were realized per scaffold resulting in a total number of more than 1200 measurements.

2.3. Chemical characterization of the scaffolds before and after printing

PLA molecular weight estimation (size exclusion chromatography). After solubilization of the PLA in tetrahydrofuran (THF, 0.2 %), a pumping system associated with an injector introduced the sample into the column at a constant and reproducible rate (THF flow rate of 1 $\text{ml}\cdot\text{min}^{-1}$, at 40 °C and with polystyrene standard samples). Macromolecules were then detected by a refractive index detector at the exit of the column (Agilent Technologies, PL-GPC50 Plus; TOSOH TSK, G4000HXL).

Determination of the polymer thermal degradation profile (thermogravimetric analysis). The sample was placed in the balance system (under N_2 , with a heating rate of 10 $^{\circ}\text{C}\cdot\text{min}^{-1}$; TA Instruments[®], TGA Q500).

Determination of the polymer morphology (amorphous or crystalline parts) (differential scanning calorimetry). By measuring the difference in heat flow between the PLA and the reference, the amount of heat absorbed during a fusion endothermic phase transition or released during a crystallization exothermic phase transition during a transition process can be determined. Then, glass, melting and crystallization transition temperatures, as well as the enthalpies are measured (under N_2 with a gas flow of 25 $\text{ml}\cdot\text{min}^{-1}$, heating/cooling rate of 10 $^{\circ}\text{C}\cdot\text{min}^{-1}$; TA Instruments[®], DSC RCS).

2.4. Mechanical evaluation of the sterilized printed scaffolds

To investigate the possible influence of pore dimensions on mechanical properties of the printed PLA mesh, a uniaxial tensile test was performed on sterilized scaffolds. Five scaffolds were tested for each pore size (150, 200 and 250 μm). Two opposite sides of PLA dense perimeter were cut with a scalpel in their midsection. PLA scaffolds were attached by the two intact opposite sides of the perimeter with pneumatic grips (4 bars in grip pressure) of an Autograph AGS-X (Shimadzu[®]). Scaffolds were stretched at a speed of 10 mm / min until

failure. Maximal strength before rupture (F max) was then recorded using the Trapezium X[®] software.

2.5. Biological evaluation of the sterilized printed scaffolds

Isolation and culture of human bone marrow stromal cells (HBMSC). All human samples were collected in accordance with the French Ministry of Higher Education and Research and National Institute for Health and Medical Research (agreement DC-2008-412). Human bone marrow samples were collected during orthopedic surgeries. HBMSC were isolated and cultured [29]. Briefly, a single-cell suspension was obtained by sequential passages of the aspirate through 16-, 18-, and then 21-gauge needles. After centrifugation the pellet was resuspended in Minimum Essential Medium Alpha Modification (α -MEM; Gibco[®], Cat No. A10400-02), supplemented with 10% fetal bovine serum (FBS; Biowest[®]) and 0.1% plasmocin antibiotics (Invitrogen[®], Cat No. MPP-37-02A) and plated at a density of 5×10^5 cells / cm² onto 75 cm² tissue culture flasks and incubated at 37 °C in a humidified atmosphere containing 5% CO₂ in air. The culture medium was changed every 2 days, thereby removing non-adherent cells. After 11 days of culture, HBMSC were obtained [30].

2.5.1. Cytotoxicity evaluation

Sterile printed scaffolds cytotoxicity was evaluated according to the NF EN 30993-5 ISO 10993-5 standard, by measuring both HBMSC metabolic activity and HBMSC cellular viability using a 3-(4-5 dimethylthiasol-2-yl) diphenyl tetrazolium (MTT) assay and a Neutral Red assay, respectively. For both assays, medium extracts were prepared according to the NF EN 30993-5 ISO 10993-5 standard by incubating scaffolds in culture media with a ratio between the immersed surface of the scaffold and the volume of the medium (from 3 to 6 cm² / mL). Three scaffolds of each porosity were individually brought into contact with 1 mL of medium "Iscove's Modified Dulbecco's Medium" (IMDM) + Glutamax (Invitrogen[®], Cat No 31980-022). Scaffolds were incubated for 3 days at 37 °C in a humidified atmosphere containing 5% CO₂ in air. Medium extracts were collected after one (E1), two (E2) and three days (E3) and stored at 4 °C. For both MTT and Neutral Red assays, HBMSC were plated at 10^4 cells / cm² in 96-well plates and cultured during 72 hours to reach sub-confluence (80%). After removal of culture media, pure medium extracts (E1, E2 and E3) were added. Being recognized to induce a cytotoxic response in a reproducible way, Triton 100X (0.1%) was used as a positive control and IMDM culture medium alone was used as negative control. Plates were incubated during 24 hours in a humidified atmosphere containing 5% CO₂ in air. After 24 hours of incubation between cells with medium extracts, the culture medium was removed and the cell layer was washed with Hank's solution (Gibco[®], Cat No. 14065-049). The stock solution of MTT (Sigma-Aldrich Co, Cat No M2128; 5 mg / mL in 0.1 M PBS, pH = 7.4) was diluted (20% in IMDM without phenol red (Gibco[®], Cat No. 21056-023)) and 125 μ l of this solution was added in each well. After 3 hours of incubation at 37 °C in a

humidified atmosphere containing 5% CO₂ in air, the supernatant was removed and formed formazan crystals were dissolved in adding 100 µl of dimethyl sulfoxide (DMSO; Sigma-Aldrich Co, Cat No. D5879-1L). The intensity of the staining was quantified by measuring the absorbance at 540 nm using a spectrophotometer (Perkin Elmer[®], 2030 Multilabel Reader Victor[™]X3). After 24 hours of incubation between cells with medium extracts, the culture medium was removed and the cell layer was washed with Hank's solution. The Neutral Red (Sigma-Aldrich Co, N4638) was diluted (1.25% (w/v) in IMDM supplemented with 10% FBS) and 100 µl of this solution was added in each well. After 3 hours of incubation at 37 °C in a humidified atmosphere containing 5% CO₂ in air, the supernatant was removed and cells were lysed with 100 µl of a solution made of 1% acetic acid in 50% ethanol. The intensity of the staining was quantified by measuring the absorbance at 540 nm using a spectrophotometer (Perkin Elmer[®], 2030 Multilabel Reader Victor[™]X3).

2.5.2. Live/Dead assay

Human bone marrow stromal cells were seeded onto the surface of sterile PLA printed scaffolds (3 for each pore size) into 24-well plates at a final density of 10⁵ cells / cm² and incubated at 37 °C in a humidified atmosphere containing 5% CO₂ in air. Prior to experiment, each well was coated with 1 mL of agarose (Sigma-Aldrich Co, A9539; 2% (w/v) in 1X PBS) to avoid cell adhesion on the tissue culture plastic. Each scaffold was also stabilized with a glass ring crimped by agarose. After 3 and 7 days of culture, cell viability was determined using live/dead assay (Invitrogen[®], Cat No L3224). After 3 and 7 days of culture, medium was removed and PLA printed scaffold seeded with HBMSC were washed with Hank's solution. Scaffolds were then incubated with the live/dead assay staining solution at 37 °C in a humidified atmosphere containing 5% CO₂ in air. After 15 minutes of incubation, scaffolds were rinsed with Hank's solution. Fluorescent green and red stainings were visualized at 568 nm and 488 nm respectively for excitation and 600 nm and 520 nm for emission with fluorescence confocal microscope (Leica[®], TCS DMI 4000B).

2.5.3. Statistical analysis

Data are presented as representative images, representative experiments or as means ± standard deviation of the mean, with n indicating the number of independent samples or pictures. For the structural characterization (measured vs expected diameter of the thread) and the biological evaluation of the scaffolds, the differences were assessed by two-tailed one-sample t-test and accepted as statistically significant at p<0.05. For both the structural characterization (the 3 measured diameter threads) and the mechanical tests of the scaffolds, the differences were evaluated by non-parametric Kruskal-Wallis test and accepted as statistically significant at p<0.05.

3. RESULTS

3.1. Physical characterization of PLA printed scaffolds

PLA scaffolds were printed as a mesh with square pores in a solid frame (Fig. 1A). Scaffold total area was $0.67 \pm 0.04 \text{ cm}^2$ and the scaffold thickness was $206 \pm 4 \text{ }\mu\text{m}$ ($n = 6$). Macroscopic and microscopic observations using binocular (Fig. 1A) and scanning electron microscopy (Fig. 1B) of the scaffolds showed regular straight threads of PLA printed layer-by-layer in both horizontal and vertical directions with perpendicular crossings. To study whether the printing technology was precise and reproducible, we assessed pore size and thread diameter of printed scaffolds with predicted pore dimensions 150 (P150), 200 (P200) and 250 μm (P250) (Fig. 1C, 1D). Image analysis showed that pore sizes were statistically lower than the predicted values by $8 \pm 9 \%$ ($138 \pm 13 \text{ }\mu\text{m}$), $5 \pm 5 \%$ ($190 \pm 11 \text{ }\mu\text{m}$) and $5 \pm 5 \%$ ($237 \pm 14 \text{ }\mu\text{m}$) for P150, P200 and P250 respectively. Conversely, thread diameter was statistically higher by $16 \pm 9 \%$ ($116 \pm 9 \text{ }\mu\text{m}$), $17 \pm 8 \%$ ($117 \pm 8 \text{ }\mu\text{m}$) and $18 \pm 9 \%$ ($118 \pm 9 \text{ }\mu\text{m}$) than the predicted values (i.e. 100 μm in all cases) for P150, P200 and P250 μm respectively. Interestingly, these deviations from predicted values were not statistically different between the 3 groups ($p > 0.05$). Thus, while the printing process was reproducible (with SDs $< 10\%$ of measured values), printed scaffolds exhibited both a lower pore dimension and a higher diameter thread than the expected values.

3.2. Physicochemical and thermomechanical characterization of the PLA printed scaffolds

Size exclusion chromatography profiles indicated a decrease in 48 % of the PLA molecular weight from 100 kDa before printing to 54 kDa after printing (Fig. 2A). In addition, the thermal degradation curves showed a decreased in the values of both beginning and ending degradation temperatures from 293 °C and 370 °C before printing to 250 °C (-15 %) and 363 °C after printing, respectively. The decomposition of the material (around 100% mass loss) was obtained at 400 °C. Additionally, at the specific mass loss of 5% the degradation temperature is 326°C for the PLA before printing and only 280°C for the PLA after printing (Fig. 2B). Conversely, as shown on the “heating cycle 1” curves, the printing process did not apparently affect the phase change temperature profile of PLA and the crystallinity remains similar before and after printing with a degree of crystallinity of 23% and 24%, respectively. Nevertheless, a slight modification of both the glass transition temperature and the melting temperature was observed (Fig. 2C). Therefore, the printing process induced a shortening in PLA polymer chains and a decrease in degradation temperatures but the polymer retains an amorphous and crystalline character.

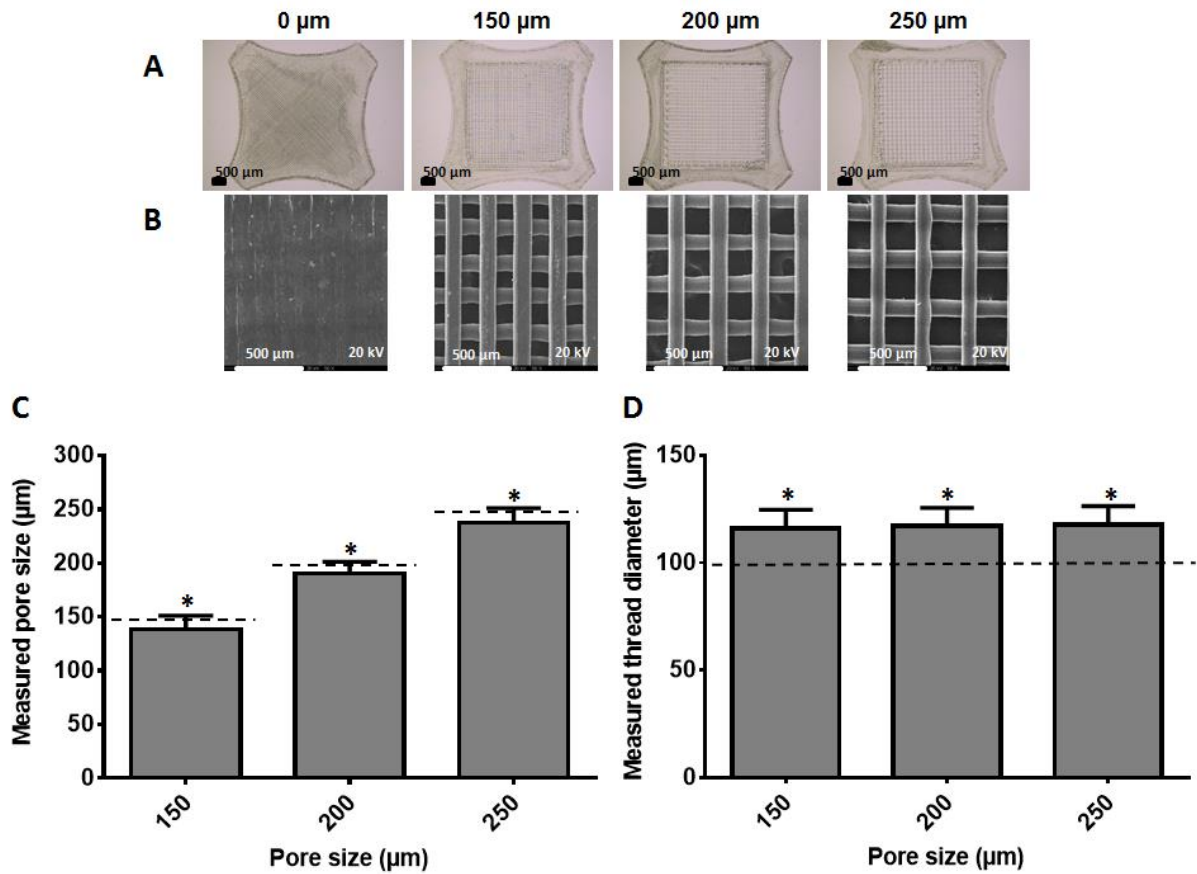


Figure 1. Structural and mechanical characterization of printed PLA scaffolds. Scaffolds with 0, 150, 200, 250 μm pore size were observed using binocular microscopy (A) and scanning electron microscopy (B). Printing reproducibility and accuracy were analyzed by quantification of both pore sizes (C) and thread diameter (D) determined by image analysis from binocular microscopy pictures. Dotted lines indicate the predicted values. Data are means \pm SD, $n = 3$ scaffolds and 4 pictures per scaffold, * $p < 0.05$ indicates significance compared to predicted values assessed by two-tailed one-sample t-test.

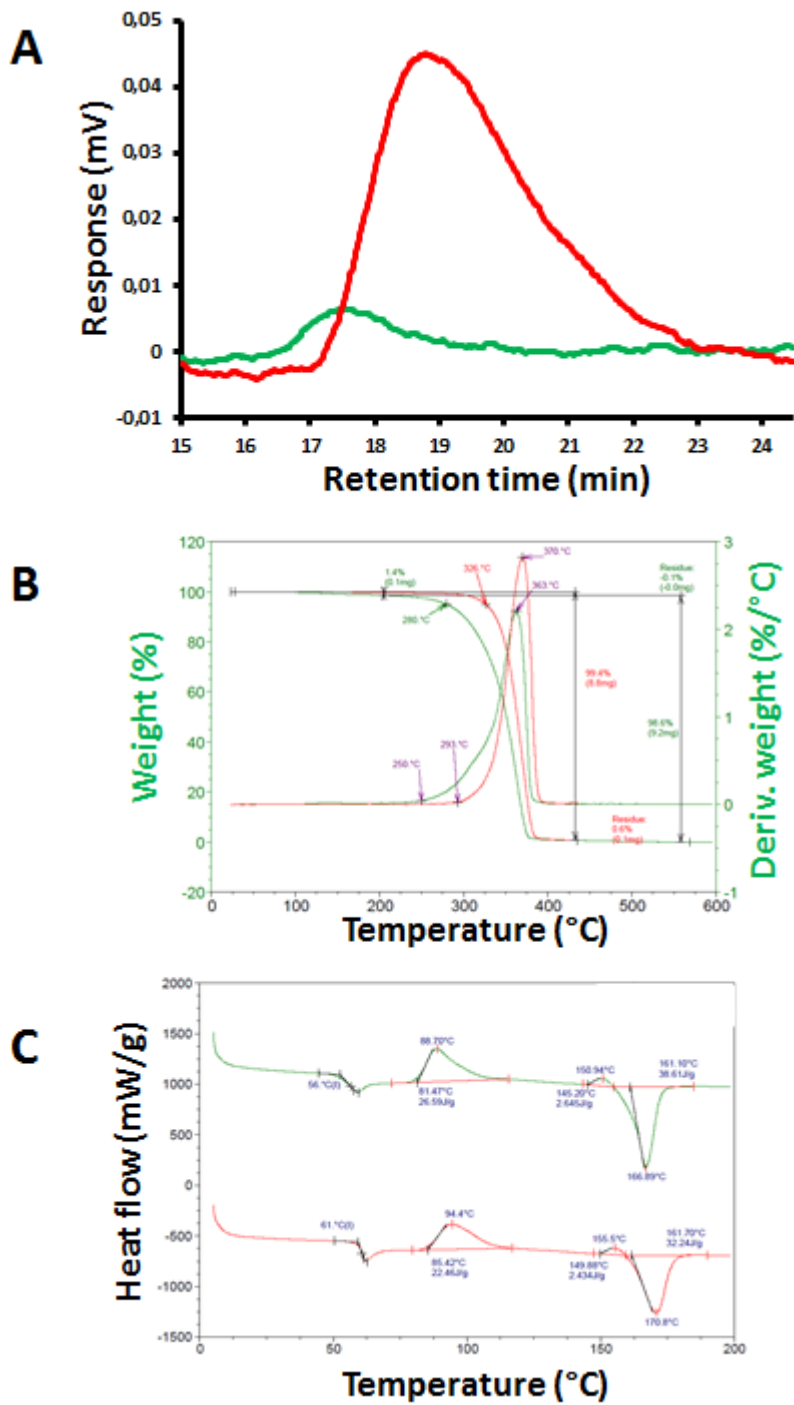


Figure 2. Physicochemical and thermomechanical characterizations of printed PLA scaffolds. Physicochemical and thermomechanical characterizations of PLA before and after 3D printing by FDM are displayed with red curves and with green curves, respectively. Results of size exclusion chromatography assay (A), of thermogravimetric analysis (B) and differential scanning calorimetric assay.

3.3. Mechanical properties of the sterilized PLA printed scaffolds

A similar breaking pattern was macroscopically observed for all tested scaffolds (Fig 3A). Tensile strengths of sterilized PLA mesh were assessed after cutting the frame. Sterile scaffolds with a pore dimension of 150, 200 and 250 μm did not exhibit statistically significant differences for ultimate tensile strength with values of 8 ± 2 N, 8 ± 1 N and 8 ± 1 N respectively (Fig. 3B). Thus, pore dimension did not affect the apparent ultimate strength of sterilized PLA printed scaffolds.

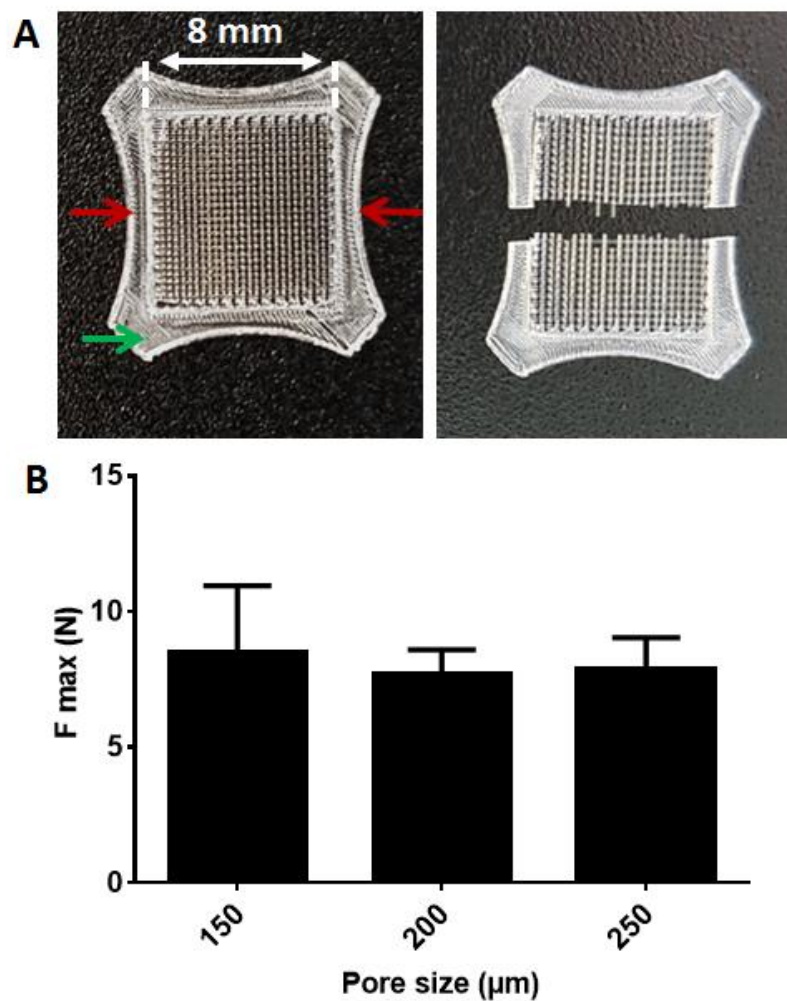


Figure 3. Mechanical evaluation of printed PLA scaffolds. Macroscopic image of a PLA printed scaffold preparation before a uniaxial tensile test (A, left panel) and a ruptured PLA printed scaffolds (A, right panel). Green arrow indicate the PLA dense perimeter of the scaffold and red arrows indicate scalpel cuts made on two opposite sides of PLA dense perimeter. Maximal strengths before rupture of gamma-sterilized PLA printed scaffolds with pore sizes of 150 μm , 200 μm and 250 μm , were determined using a uniaxial tensile test (after cutting sides of PLA dense perimeter) (B). Data are mean \pm SD, $n = 5$, no statistically significant difference was observed ($p > 0.05$).

3.4. Biological evaluation of the sterilized PLA printed scaffolds

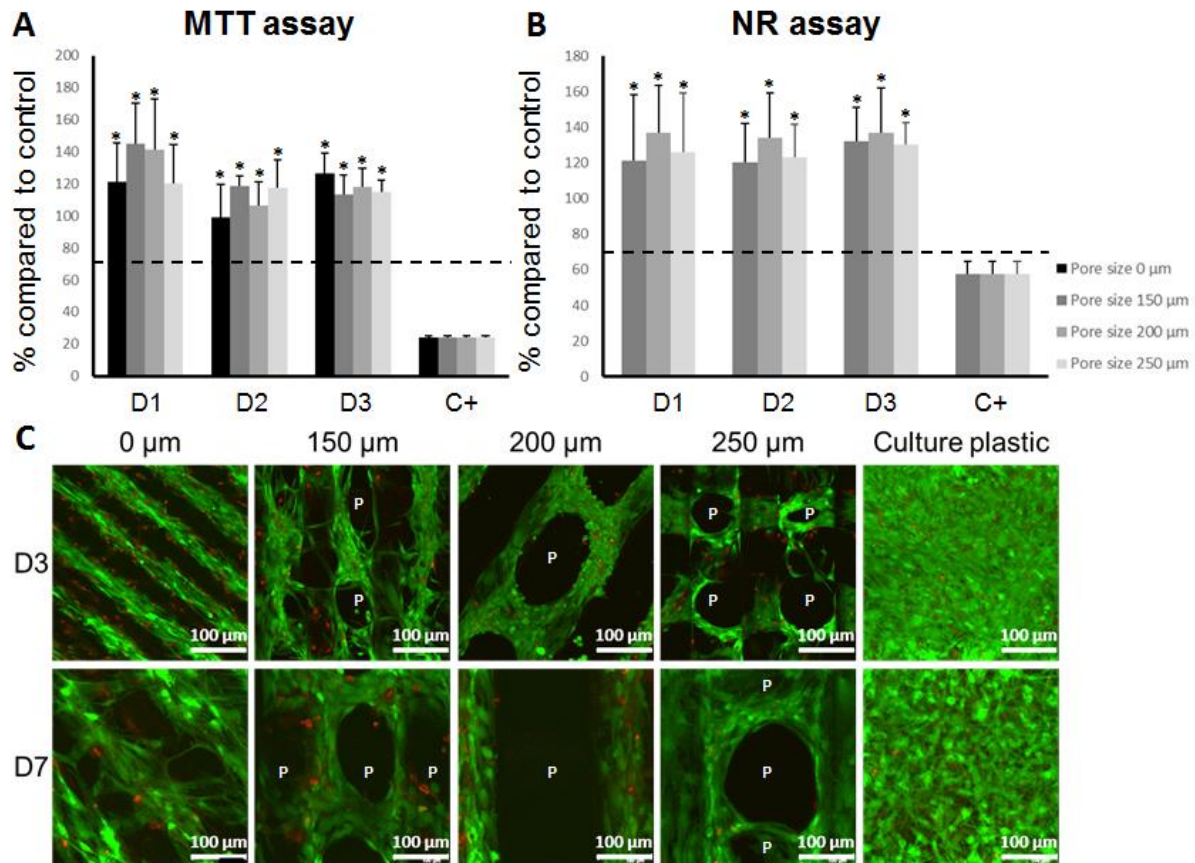


Figure 4. Biological evaluation of sterilized printed PLA scaffolds. Possible cytotoxic effect of PLA scaffolds toward HBMSC was evaluated using both MTT assay (A) and Neutral Red (NR) assay (B) and according to the NF-EN-ISO 10993-5 standard. Confluent HBMSC were cultured during 24h with medium previously incubated during 24 (D1), 48 (D2) and 72h (D3) with sterile scaffolds. Confluent HB<SC cultured during 24g with regular medium or with 0.1 % Triton 100X were used as negative control. On each graph, the dotted line indicated the limit (70 %) of cytotoxicity according to NF-EN-ISO 10993-5 standard. Data are mean \pm SD, $n = 3$, * $p < 0.05$ indicates significance assessed by two-tailed one-sample t-test, compared to the limit (70 %) of cytotoxicity. HBMSC colonization of sterilized PLA scaffolds was evaluated after 3 and 7 days of culture using fluorescent microscopy after live/dead staining (green/red) ($n = 3$) (C). P indicates pores within scaffolds.

Media extracts of printed scaffolds did not significantly affect either the metabolic activity or the cell viability of HBMSC, which remained significantly higher than 70% of control HBMSC cultures (Fig 4A, 4B). Thus, these results demonstrated the absence of cytotoxic effect of PLA printed scaffolds. We then examined cell viability of HBMSC plated onto printed scaffolds of different pore dimensions. After 3 and 7 days of culture, confocal microscopy pictures showed that HBMSC were predominantly alive (green fluorescence) with only rare dead (red) cells (Fig. 4C). Cells had spread throughout the mesh and moved in the pores of PLA scaffolds with pore sizes of 150, 200 and 250 μm . On non-porous scaffolds (0 μm), cells accumulated between PLA threads to form parallel lines of green viable cells. Taken together, these data show that sterile printed PLA scaffolds are suitable substrates for HBMSC culture.

4. DISCUSSION

In this study, we have shown that PLA threads can be successfully printed in scaffolds with different pore sizes. The size and the shape of the PLA printed scaffolds were maintained after cooling, and sufficient mechanical integrity was acquired to allow easy handling. We found that structural characteristics of the scaffolds measured were different from the predicted values entered in the printing software. We demonstrated that after the printing process, PLA maintained a semi-crystalline structure even if the polymer chains were shortened and thermal degradation profile was changed. Finally, we observed that not only were all sterilized printed scaffolds biocompatible, but they also allowed bone cell colonization.

In the field of solid freeform fabrication techniques, FDM is the most commonly used because of (i) its cost-effectiveness, (ii) its ability to use different materials, (iii) the printing resolution ranges from several hundred micrometers to a few micrometers and (iv) its possibility to fabricate of 3D implantable materials to exactly match patient's bone defect [31]. In our study, 200 μm thick PLA scaffolds with square pores were produced by a custom-made 3D printer based on this principle. However, because of temperatures reached during FDM printing, cells cannot be incorporated into the scaffolds during the fabrication process. For this reason, cells were seeded onto printed PLA scaffolds after the process. Numerous studies have suggested the importance of scaffold pore size in bone tissue engineering and have shown that they should be typically between 100 μm and 300 μm to allow cell penetration, migration, growth as well as an optimal tissue vascularization [32]. Thus, scaffolds with 3 different pore sizes were fabricated and scaffolds with no pore were used as a control. In this study, we demonstrate with SEM and binocular observations that all printed scaffolds exhibited statistically lower pore dimensions compared with predicted parameters. Similarly, thread diameter increased by about 17 % at all scaffold pore sizes and was also reproducible (with SDs < 10% of measured values). We hypothesize that the decrease in the pore sizes (around 12 μm for the three conditions) was due to the increase of the thread

diameter (around 16 μm for the three conditions), which was probably generated by its spreading during the printing process.

PLA is commonly used in bone tissue engineering for scaffold production and it is approved by the FDA for clinical applications [22]. As reported previously, the physicochemical properties of PLA were modified during the printing process [33]. Indeed, the use of high temperature in the printer head to melt the polymer reduced by half its molecular weight (from 100 kDa to 54 kDa). We observed that the printed PLA started to degrade at a temperature 15 % lower than before printing, which might be a direct consequence of the shortening of the polymer chains. However, the degree of crystallinity remains similar and the printed PLA retains an amorphous and crystalline character. One solution would be to reduce the temperature in order to limit the formation of short polymer chains but that requiring keeping the right solution viscosity [14].

Mechanical properties of formed scaffolds are of important for handling during the implantation process and can influence the remodeling of the tissue. Porous designs increase usable space of the scaffolds by increasing its surface area, however, pores can also be viewed as stress concentration sites that mechanically weaken the scaffold. In our system, increasing pore size decreased the number of thread on our PLA printed scaffolds with 31, 27 and 23 threads (measured in single orientation) for P150, P200 and P250, respectively. Our results demonstrate that, regardless of the porosity, PLA printed scaffolds displayed similar ultimate tensile forces (around 9.5 N). This may seem surprising since one would expect more threads to provide more strength. We hypothesize that the breakage of the scaffolds was initiated by a single (or a few) threads breaking first, then the remaining stress was concentrated on a neighboring threads creating a sort of chain reaction. This could suggest that all threads were not equally tensed during the test. Over all, the modification of pore size was insufficient to induce a significant difference of the mechanical properties of the scaffolds.

Thermoplastics that are widely used in biomedical applications will not survive a standard steam or dry heat sterilization. Since printing is not performed in sterile conditions all PLA printed scaffolds were sterilized by gamma irradiation (25 KGy) before their use for mechanical and biological tests. This method avoids significant degradation by PLA chain scission [34]. Possible changes of PLA properties changes after gamma-radiation sterilization were not studied here but the biocompatibility of sterilized PLA printed scaffolds was evaluated. Previous studies showed that PLA degradation releases acidic monomers (lactic acid) that cause inflammation and this property could affect cell attachment and behavior [9]. However, lactic acid is present in the human body and is removed by natural metabolic pathways [9]. Three methods used in this study revealed no cytotoxic effect of PLA on primary human bone marrow cells. These observations are consistent with Zhang *et al.* who showed “low” effect of PLA scaffolds on viability and metabolism of osteoblastic like cell line (MC3T3-E1) [35]. Similarly, Lee *et al.* demonstrated significant adherence and proliferation of human mesenchymal stem cells on PLA [36]. In this study, cell colonization was observed predominantly in the pits of the grooves created by the juxtaposition of the PLA

threads (P0) during the printing process. Additionally, we find that cellular alignment onto non-porous scaffolds which is parallel to PLA threads.

The success of a cell-populated scaffold implantation depends on two main parameters: scaffold design and cell incorporation [12]. To date, two methods of incorporating cells into scaffolds are being explored: (i) seeding of cells onto the surface of the scaffold following fabrication (top-down approach) and (ii) the incorporation of cells into the scaffold fabrication process (bottom-up approach). The small seeded PLA scaffolds produced in this study could be assembled to produce a larger volume scaffold like in the bottom up tissue engineering approach to achieve a homogeneous cells distribution in the final 3D construct [12]. Regardless of the method used to add cells to the 3D scaffolds, vascularization remains a great challenge in tissue engineering. The addition of endothelial progenitor cells would be a possible approach to initiate vasculogenesis before implantation [37]. Also, PLA is often used in association with calcium phosphate particles to improve bone regeneration [23]. Scaffolds loaded by calcium phosphate nanoparticles could be used to promote osteoblast activity and bone tissue formation [38].

Taken together, our results demonstrate that our method to produce scaffolds allows the printing of PLA scaffolds with a suitable and controlled pore size resolution in a highly reproducible way. Despite polymer modification induced by printing, printed scaffolds were biocompatible with HBMSC. In the context of bone regeneration, 3D printing of scaffolds has become one of the most innovative approaches in surgery to provide personalized patients treatments and our study proves the possibility of creating populated scaffolds with precise dimensions that could be later assembled in a larger tissue engineered construct for bone repair.

Acknowledgements and Funding

We are grateful to Dr. Gérard Dimier (Univ. Bordeaux, LCPO, CNRS UMR5629) for the chemical characterization of our scaffolds and to Ms Marine Garat for her technical assistance. This research was funded by “Gueules cassées” foundation (57-2015), the ANR “Sandwich” (ANR-16-CE18-0009-01).

References

1. Gomez, S., et al., Design and properties of 3D scaffolds for bone tissue engineering. *Acta biomaterialia*, 2016. 42: p. 341-50.
2. Kalk, W.W., et al., Morbidity from iliac crest bone harvesting. *Journal of oral and maxillofacial surgery : official journal of the American Association of Oral and Maxillofacial Surgeons*, 1996. 54(12): p. 1424-9; discussion 1430.
3. Langer, R., Tissue engineering. *Molecular therapy : the journal of the American Society of Gene Therapy*, 2000. 1(1): p. 12-5.
4. Lee, J.W., et al., Bone regeneration using a microstereolithography-produced customized poly(propylene fumarate)/diethyl fumarate photopolymer 3D scaffold incorporating BMP-2 loaded PLGA microspheres. *Biomaterials*, 2011. 32(3): p. 744-52.
5. Wiria, F.E., et al., Poly-epsilon-caprolactone/hydroxyapatite for tissue engineering scaffold fabrication via selective laser sintering. *Acta biomaterialia*, 2007. 3(1): p. 1-12.
6. Fielding, G.A., A. Bandyopadhyay, and S. Bose, Effects of silica and zinc oxide doping on mechanical and biological properties of 3D printed tricalcium phosphate tissue engineering scaffolds. *Dental materials : official publication of the Academy of Dental Materials*, 2012. 28(2): p. 113-22.
7. Park, S.A., S.H. Lee, and W.D. Kim, Fabrication of porous polycaprolactone/hydroxyapatite (PCL/HA) blend scaffolds using a 3D plotting system for bone tissue engineering. *Bioprocess and biosystems engineering*, 2011. 34(4): p. 505-13.
8. Chen, Q., et al., 3D Printing Biocompatible Polyurethane/Poly(lactic acid)/Graphene Oxide Nanocomposites: Anisotropic Properties. *ACS applied materials & interfaces*, 2017. 9(4): p. 4015-4023.
9. Zhang, H., et al., Three dimensional printed macroporous polylactic acid/hydroxyapatite composite scaffolds for promoting bone formation in a critical-size rat calvarial defect model. *Science and technology of advanced materials*, 2016. 17(1): p. 136-148.
10. Catros, S., et al., Layer-by-layer tissue microfabrication supports cell proliferation in vitro and in vivo. *Tissue engineering. Part C, Methods*, 2012. 18(1): p. 62-70.
11. Tiruvannamalai-Annamalai, R., D.R. Armant, and H.W. Matthew, A glycosaminoglycan based, modular tissue scaffold system for rapid assembly of perfusable, high cell density, engineered tissues. *PloS one*, 2014. 9(1): p. e84287.

12. Guduric, V., et al., Layer-by-layer bioassembly of cellularized polylactic acid porous membranes for bone tissue engineering. *Journal of materials science. Materials in medicine*, 2017. 28(5): p. 78.
13. Felfel, R.M., et al., In vitro degradation and mechanical properties of PLA-PCL copolymer unit cell scaffolds generated by two-photon polymerization. *Biomedical materials*, 2016. 11(1): p. 015011.
14. Serra, T., et al., Relevance of PEG in PLA-based blends for tissue engineering 3D-printed scaffolds. *Materials science & engineering. C, Materials for biological applications*, 2014. 38: p. 55-62.
15. Cai, H., G. Azangwe, and D.E. Shepherd, Skin cell culture on an ear-shaped scaffold created by fused deposition modelling. *Bio-medical materials and engineering*, 2005. 15(5): p. 375-80.
16. Mozdzen, L.C., et al., Increasing the strength and bioactivity of collagen scaffolds using customizable arrays of 3D-printed polymer fibers. *Acta biomaterialia*, 2016. 33: p. 25-33.
17. Groppo, M.F., et al., The effect of a hydroxyapatite impregnated PCL membrane in rat subcritical calvarial bone defects. *Archives of oral biology*, 2017. 82: p. 209-215.
18. Raeisdasteh Hokmabad, V., et al., Design and fabrication of porous biodegradable scaffolds: a strategy for tissue engineering. *Journal of Biomaterials Science, Polymer Edition*, 2017. 28(16): p. 1797-1825.
19. Chia, H.N. and B.M. Wu, Recent advances in 3D printing of biomaterials. *Journal of biological engineering*, 2015. 9: p. 4.
20. Li, G., et al., Direct writing of chitosan scaffolds using a robotic system. *Rapid Prototyping Journal*, 2005. 11(2): p. 90-97.
21. Almeida, C.R., et al., Impact of 3-D printed PLA- and chitosan-based scaffolds on human monocyte/macrophage responses: unraveling the effect of 3-D structures on inflammation. *Acta biomaterialia*, 2014. 10(2): p. 613-22.
22. Tyler, B., et al., Polylactic acid (PLA) controlled delivery carriers for biomedical applications. *Advanced drug delivery reviews*, 2016. 107: p. 163-175.
23. Senatov, F.S., et al., Mechanical properties and shape memory effect of 3D-printed PLA-based porous scaffolds. *Journal of the mechanical behavior of biomedical materials*, 2016. 57: p. 139-48.
24. Lunt, J., Large-scale production, properties and commercial applications of polylactic acid polymers. *Polymer Degradation and Stability*, 1998. 59(1): p. 145-152.

25. Hamad, K., et al., Properties and medical applications of polylactic acid: A review. *Express Polymer Letters*, 2015. 9(5).
26. Schagemann, J.C., et al., Poly-epsilon-caprolactone/gel hybrid scaffolds for cartilage tissue engineering. *Journal of biomedical materials research. Part A*, 2010. 93(2): p. 454-63.
27. Holloway, J.L., A.M. Lowman, and G.R. Palmese, Mechanical evaluation of poly(vinyl alcohol)-based fibrous composites as biomaterials for meniscal tissue replacement. *Acta biomaterialia*, 2010. 6(12): p. 4716-24.
28. Barbieri, D., et al., Controlling dynamic mechanical properties and degradation of composites for bone regeneration by means of filler content. *Journal of the mechanical behavior of biomedical materials*, 2013. 20: p. 162-72.
29. Vilamitjana-Amedee, J., et al., Human bone marrow stromal cells express an osteoblastic phenotype in culture. *In vitro cellular & developmental biology. Animal*, 1993. 29A(9): p. 699-707.
30. Guerrero, J., et al., Cell interactions between human progenitor-derived endothelial cells and human mesenchymal stem cells in a three-dimensional macroporous polysaccharide-based scaffold promote osteogenesis. *Acta biomaterialia*, 2013. 9(9): p. 8200-13.
31. Liu, A., et al., 3D Printing Surgical Implants at the clinic: A Experimental Study on Anterior Cruciate Ligament Reconstruction. *Scientific reports*, 2016. 6: p. 21704.
32. Tarafder, S., et al., Microwave-sintered 3D printed tricalcium phosphate scaffolds for bone tissue engineering. *Journal of tissue engineering and regenerative medicine*, 2013. 7(8): p. 631-41.
33. Gentile, P., et al., An overview of poly(lactic-co-glycolic) acid (PLGA)-based biomaterials for bone tissue engineering. *International journal of molecular sciences*, 2014. 15(3): p. 3640-59.
34. Farah, S., D.G. Anderson, and R. Langer, Physical and mechanical properties of PLA, and their functions in widespread applications - A comprehensive review. *Advanced drug delivery reviews*, 2016. 107: p. 367-392.
35. Zhang, Y., et al., [Biocompatibility of Porous Poly Lactic Acid/Bone Matrix Gelatin Composite Biomaterials for Bone Repair]. *Zhongguo xiu fu chong jian wai ke za zhi = Zhongguo xiufu chongjian waike zazhi = Chinese journal of reparative and reconstructive surgery*, 2016. 30(2): p. 251-7.
36. Salerno, A., et al., Bio-safe processing of polylactic-co-caprolactone and polylactic acid blends to fabricate fibrous porous scaffolds for in vitro mesenchymal stem cells

adhesion and proliferation. *Materials science & engineering. C, Materials for biological applications*, 2016. 63: p. 512-21.

37. Guerrero, J., et al., The use of total human bone marrow fraction in a direct three-dimensional expansion approach for bone tissue engineering applications: focus on angiogenesis and osteogenesis. *Tissue engineering. Part A*, 2015. 21(5-6): p. 861-74.
38. Oliveira, H., et al., The proangiogenic potential of a novel calcium releasing biomaterial: Impact on cell recruitment. *Acta biomaterialia*, 2016. 29: p. 435-45.

CONCLUSIONS AND PERSPECTIVES

This thesis work has been split in three parts presented in three scientific articles (accepted or in revision).

Poly(lactic) acid membrane fabrication

In all parts of the project, PLA porous membranes were successfully fabricated by different 3D printing techniques. The first technique used for membrane fabrication was direct 3D printing using syringes with PLA powder dissolved in chloroform. This technique allowed fast and repetitive fabrication of scaffolds. The polymer membranes solidified by evaporation of chloroform after printing. The toxic properties of chloroform represent the main disadvantage of this fabrication method. Another limit of direct 3D printing was the wide range of pore size observed, as the pores sizes were between 165 μm and 375 μm . As a majority of extrusion 3D printers, this one also has its own software allowing design of 3D structures without exporting a final 3D model into STL file. Design of membrane model consisted in information about shape, dimensions, distance between struts to form the pores, speed of displacement in X and Y directions and pressure applied on the syringe. Speed and extrusion pressure had a direct effect on the struts width and pore size.

Limits of the first fabrication method regarding toxic properties of chloroform and wide range of obtained pores were overcome in the second and the third part using Fused Deposition Modeling (FDM) technique. Commercial thermoplastic PLA filament was introduced in the heated printing head, and the membranes were successfully printed by extrusion of melted polymer. Printed membranes solidified by cooling of the polymer, meaning that there were no toxic evaporations. In the second part, pore size range was smaller than in the first one. Pores sizes were comprised between 294 μm and 311 μm . This printer used STL file but without asked dimensions of pores. The file was introduced as a square plate and pores were adjusted by changing the infill of the printed model. This technique allowed faster and more precise fabrication of PLA membranes. Nozzle of 400 μm diameter was used for extrusion of the filament. Regarding the diameter of the nozzle, struts could not be thinner than 200 μm .

The same FDM technique was used for membranes fabrication in the third part as well, but with the prototype printer prepared in collaboration with IUT, Bordeaux. This printer, equipped with 100 μm nozzle allowed even more precise membrane fabrication. Struts of membranes were thinner and pore size was more uniform. Beside the nozzle size that did not exist on the market, the heated receiving platform that was designed enabled easier printing of PLA. The software prepared for membrane fabrication using this printer enables easy and fast preparation of STL files of membrane models with different pore size. However, using this software, we can only design a rectangular shape for the pores. Some improvements should be performed to have a possibility to design triangular pores for example since this shape has showed better properties for cell attachment and migration in certain conditions [61].

Physicochemical properties of PLA before and after 3D printing

PLA is thermoplastic polymer meaning that its properties depend on temperature. Since FDM is a 3D printing technology that uses high temperatures above fusion temperatures of polymer, we investigated if this scaffold fabrication method had an effect on its different physicochemical properties. Two different PLA filaments were used with two FDM printers: Makerbot[®] PLA and Esun[®] PLA. The First difference between these two filaments was in the printing temperature: Makerbot[®] PLA was extruded at 235°C while Esun[®] PLA used much lower temperature of 186°C. This temperature difference comes probably because of different internal structure of polymers. Makerbot[®] PLA did not show any changes in thermal degradation properties or molecular weight after 3D printing probably because of its amorphous structure. But the same structural properties would probably cause low degradation time of this polymer. On the other hand, molecular weight of the Esun[®] PLA was reduced from 100 Kda to 54 Kda after FDM process. However, the thermal degradation profile did not change and the structure of the polymer remained semi-crystalline. Degradation temperatures decreased by 15 % and 2 %, which might be a direct consequence of the shortening of the polymer chains.

In vitro biological evaluations of PLA scaffolds

In the first part PLA membranes were sterilized in EtOH but for the experiments, we have performed γ irradiation, which is the commonly used method to sterilize medical devices. Both PLA filaments did not show any cytotoxic effect 24h after sterilization. The biological properties were evaluated in all three parts of this work using human primary cells. All scaffolds were compatible with cells showing good viability of HBMSCs and EPCs in 2D during time when seeded onto PLA membranes in mono-cultures. Viability was more efficient when these cells were seeded together in co-cultures. Osteoblastic and endothelial differentiations were evaluated in both, mono- and co-cultures in 2D by expressions of ALP and vWF respectively. These markers have shown cell differentiation in all layers of LBL BioAssemblies and it seemed that cell repartition was homogenous and more intense in the case of co-cultures. LBL bioassemblies provided suitable conditions for cell differentiation which was confirmed by the expression of osteoblastic genes investigated by RT-qPCR. Cell migration in 3D between layers was evaluated with fluorescent transduced cells after 14 days of culture.

In vivo study and vascularization evaluation

LBL assemblies and massive scaffolds seeded with mono-cultures of HBMSCs. After 8 weeks all samples were retrieved, embedded in resin and histological evaluations were performed to investigate human cell presence and blood vessel formation. Human cells were

present in outer parts of all samples in regions close to the surface. Regarding the inner parts, they were present only in LBL assemblies, with much more human cells in co-culture samples meaning that, in this experiment, this approach provided more suitable conditions for cell survival than conventional approach where cells are seeded on the surface of a massive scaffold. Even a large amount of MSCs were present in inner layers of mono-cultures, it did not provide suitable conditions for blood vessel formation. They were formed within the entire constructs only in the case of co-culture LBL samples meaning that this cell culture system provides more suitable conditions for vascular network formation and host tissue penetration.

Perspectives

In all parts of this thesis research rectangular shape of pores was used. It would be interesting to test different shapes, for example triangular, on cell viability, proliferation and differentiation in 2D. Triangular pores provide stronger mechanical properties and more stabilization of the printed large scaffolds [168]. But printing of triangular pores could have some disadvantages in terms of resolution. This kind of architecture is more sensitive for printing parameters. It usually requires lower speed and pressure meaning that printed filament is wider [61,87].

There are other types of human primary cell with a potential for osteoblastic differentiation which could be used in future experiments, such as ADSCs in co-cultures with EPCs or HUVECs. Advantage of ADSCs is that they can be obtained from abundant adipose tissue using minimally invasive procedure resulting in high number of cells [169]. Beside them, other cells such as preadipocytes, endothelial progenitor cells, pericytes, T cells and M2 macrophages can be derived from the stromal vascular fraction (SVF) obtained from the enzymatic digestion of fat tissue [170]. Osteogenic capacities of SVF are improved with biomaterial or BMP addition [171–173].

Cell proliferation was evaluated only *in vitro* in 2D. It was not possible to perform the same experiment in 3D because of the difficulty to collect cells from materials in inner layers. It would be possible to follow and quantify cell proliferation in 3D and *in vivo* using transduced cells such as HBMSCs-Luc and EPCs-TdT. These cells emit light that can be quantified by photon imager (in the presence of substrate for HBMSCs-Luc).

Degradation time is very important for biomaterials used in tissue engineering. This experiment was not performed because non-medical grade PLA was used so its clinical application is not possible. The use of medical grade polymer with the degradation time evaluation should be the first next step of this research.

Stabilization of layers in 3D assemblies during the first days after superposing of cellularized membranes is very important because it provides necessary conditions for cells while they synthesize matrix which will later keep the layers together. Second disadvantage of this stabilization system is that it is not implantable with assemblies for *in vivo* studies. It means that implantation can not be performed before sufficient synthesis of extracellular matrix which can provide sufficient stabilization in the host. Stabilization with glass ring used in the first part was not suitable and was not implantable. Improved stabilization in the second part using PLA clips enabled efficient stabilization of LBL assemblies and it was implantable with constructs. But this system can not be used for bone defects meaning that stabilization method should be improved. In the case of bone defects it would be necessary to fabricate stabilization system within the membranes such as there is no effect on the final shape of the implants.

The development of new materials is very important for improvement of tissue engineering procedures. Bioactivity toward osteogenic phenotype of materials can be improved by different modifications. Numerous combinations of biomaterials within polymer composites could provide control of degradation time, mechanical and osteoinduction properties. This could be achieved by adding of HA in PLA or co-polymer PLGA per example [174].

Different 3D printing methods could be implemented in future research based on this study. Per example Laser Assisted Bioprinting (LAB) of cells or extrusion of cells in hydrogels instead of manual seeding using pipettes. In these cases, membranes could be used as a receiving substrate for bioprinting (biopapers).

Finally, *in vivo* experiments should be performed to evaluate the bone regeneration capacities of such constructs using bone defect models. The first one applies rat calvarial defect. This animal model could be used for longitudinal observations of animals with *in vivo* μ -CT to follow bone regeneration. After euthanasia of animals and embedding in resin, blood vessel formation within constructs should be investigated as well as osteoid tissue formation. Next animal model could be large defect in minipig mandible with the application in alveolar bone regeneration to allow dental implants placement. Custom grafts of LBL assemblies could be fabricated from CT scanning of the defect.

SCIENTIFIC COMMUNICATIONS

PUBLICATIONS

1. Layer-by-Layer Bioassembly of Cellularized Polylactic acid Porous Membranes for Bone Tissue Engineering

Authors: **Vera GUDURIC**, Carole METZ, Robin SIADOUS, Reine BAREILLE, Riccardo LEVATO, Elisabeth ENGEL, Jean-Christophe FRICAIN, Raphaël DEVILLARD, Ognjan LUZANIN, Sylvain CATROS

Accepted on the 15th of March 2017 and published in the Journal of Materials Science: Materials in Medicine in May 2017; published online on the 6th of April 2017. Vol 28(5):78

DOI : 10.1007/s10856-017-5887-6

2. Characterization of 3D printed scaffolds for bone tissue engineering

Authors: Agathe GRÉMARE, **Vera GUDURIC**, Reine BAREILLE, Valérie HÉROGUEZ, Simon LATOUR, Nicolas L'HEUREUX, Jean-Christophe FRICAIN, Sylvain CATROS, Damien LE NIHOANNEN

Accepted for publication in Journal of Biomedical Materials Research Part A in November 2017.

DOI: 10.1002/jbm.a.36289

3. Layer-by-Layer BioAssembly and Co-culture Cell System Improve Vascularization of Scaffold-based Tissue Engineering

Authors : **Vera GUDURIC**, Robin SIADOUS, Maxime SEIMBILLE, Reine BAREILLE, Sylvie REY, Noélie THÉABAUD, Damien LE NIHOANNEN, Jean-Christophe FRICAIN, Raphaël DEVILLARD, Ognjan LUZANIN, Sylvain CATROS

Submitted in November 2017 in the Biofabrication, special issue from the World Conference on Biofabrication 2017 in Beijing, China

4. Investigating impact of five build parameters on the maximum flexural force in FDM specimens – A definitive screening design approach

Authors: Ognjan LUZANIN, Vera GUDURIC, Ivan RISTIC, Simon MUHIC

Accepted for publication in September 2016 in the Journal of Rapid Prototyping

DOI: 10.1108/RPJ-09-2015-0116

5. Odontologie et Ingénierie Tissulaire : La bioimpression au service de la régénération osseuse

Authors: Olivia KÉROUREDAN, Vera GUDURIC, Rawen SMIRANI, Murielle RÉMY, Hugo DE OLIVEIRA, Jean-Christophe FRICAIN, Adrien NAVEAU, Raphaël DEVILLARD, Sylvain CATROS

Published on the 19th of April 2017 in the Information Dentaire, Special Issue “Apport de la CFAO en Chirurgie Orale”, Vol. 16:38-44

6. Impression 3D en médecine régénératrice et ingénierie tissulaire

Authors: Jean-Christophe FRICAIN, Hugo DE OLIVEIRA, Raphaël DEVILLARD, Jérôme KALISKY, Murielle RÉMY, Virginie KÉRIQUEL, Damien LE NIHAUNNEN, Agathe GREMARE, Vera GUDURIC, Alexis PLAUD, Nicolas L’HEUREUX, Joëlle AMÉDÉE, Sylvain CATROS

Published in January 2017 in the Médecine/Sciences; Published online in the 25th of January 2017. Vol. 33:52-59

DOI: 10.1051/medsci/20173301009.

ORAL COMMUNICATIONS AT NATIONAL AND INTERNATIONAL CONFERENCES

2017	<p>Layer-by-layer Assembly of Poly(lactic) acid scaffolds seeded with human primary cells for bone tissue engineering: <i>in vitro</i> and <i>in vivo</i> study</p> <p><u>Vera Guduric</u>, Robin Siadous, Maxime Seimbille, Reine Bareille, Sylvie Rey, Jean-Christophe Fricain, Ognjan Luzanin, Sylvain Catros</p> <p>International Conference on Biofabrication, Beijing, China, October 2017</p>
	<p>3D Bioassembly of poly(lactic) acid scaffolds seeded with human primary cells for bone tissue engineering: <i>in vitro</i> and <i>in vivo</i> study.</p> <p><u>Vera Guduric</u>, Robin Siadous, Maxime Seimbille, Reine Bareille, Sylvie Rey, Benoît Rousseau, Jean-Christophe Fricain, Ognjan Luzanin, Sylvain Catros</p> <p>Journée scientifique de la Fr TecSan, IECB, Pessac, France, June 2017</p>
	<p><i>In vitro</i> and <i>in vivo</i> bioassemblage des scaffolds imprimés en 3D</p> <p><u>Vera Guduric</u>, Robin Siadous, Maxime Seimbille, Reine Bareille, Sylvie Rey, Benoît Rousseau, Ognjan Luzanin, Sylvain Catros</p> <p>Conference BIOMAT and materials for health, Ambleteuse, France, June 2017</p>
	<p>3D Bioassembly of poly(lactic) acid scaffolds seeded with human primary cells for bone tissue engineering: <i>in vitro</i> and <i>in vivo</i> study</p> <p><u>Vera Guduric</u>, Robin Siadous, Reine Bareille, Benoît Rousseau, Raphaël Devillard, Jean-Christophe Fricain, Ognjan Luzanin, Sylvain Catros</p> <p>19th French Days of Mineralized Tissues Biology (JFBTM), Lyon, France, May 2017</p>
	<p>3D Bioassembly of poly(lactic) acid scaffolds seeded with human primary cells for bone tissue engineering: <i>in vitro</i> and <i>in vivo</i> study</p> <p><u>Vera Guduric</u>, Robin Siadous, Reine Bareille, Benoît Rousseau, Raphaël Devillard, Jean-Christophe Fricain, Ognjan Luzanin, Sylvain Catros</p> <p>SVS Doctoral School Day, Pessac, France, April 2017</p>

2016	<p>In vitro and In vivo Evaluations of Layer-by-Layer Bioassembly Cellularized Scaffolds for Bone Tissue Engineering</p> <p>Vera Guduric, Robin Siadous, Reine Bareille, Benoît Rousseau, Raphaël Devillard, Jean-Christophe Fricain, Ognjan Luzanin, Sylvain Catros</p> <p>Annual conference of the International Society for Biofabrication 2016, Winston Salem, North Carolina, USA, October 2016</p> <p>Development of 3D printing technology to produce custom bone substitutes</p> <p>Agathe Gremare, <u>Vera Guduric</u>, Reine Bareille, Simon Latour, Valerie Héroguez, Jean-Christophe Fricain, Sylvain Catros, Damien Le Nihouannen</p> <p>Bordeaux Consortium for Regenerative Medicine (BxCRM), Bordeaux, France, October 2016</p> <p>Développement d'une technologie d'impression 3D pour la fabrication de substituts osseux sur mesure</p> <p>Agathe Grémare, <u>Vera Guduric</u>, Reine Bareille, Jean-Christophe Fricain, Sylvain Catros, Damien Le Nihouannen</p> <p>Congrès du Collège National des Enseignants en Sciences Biologiques Odontologiques (CNESBO), Sète, France, October 2016</p> <p>Layer-by-Layer Assemblies of Cellularized Poly(lactic acid) Scaffolds for Bone Tissue Engineering</p> <p><u>Vera Guduric</u>, Carole Metz, Robin Siadous, Reine Bareille, Riccardo Levato, Elisabeth Engel, Jean-Cristophe Fricain, Ognjan Luzanin, Sylvain Catros</p> <p>18th French Days of Mineralized Tissues Biology (JFBTM), Nancy, France, June 2016</p> <p>Layer-by-Layer assembly of Cellularized Poly(lactic acid) Substitutes for Bone Tissue Engineering</p> <p><u>Vera Guduric</u>, Robin Siadous, Reine Bareille, Carole Metz, Riccardo Levato, Elisabeth Engel, Jean-Cristophe Fricain, Ognjan Luzanin, Sylvain Catros</p> <p>Second Annual Tissue Engineering, Biofabrication and 3D-Bioprinting Conference, Boston, Massachusetts, USA, March 2016</p>
-------------	--

2015	<p>Layer-by-layer Microfabrication of Cellularized Poly (lactic acid) Constructs for Bone Tissue Engineering</p> <p><u>Vera Guduric</u>, Robin Siadous, Reine Bareille, Raphaël Devillard, Jean-Christophe Fricain, Ognjan Luzanin, Sylvain Catros</p> <p>Annual conference of the International Society for Biofabrication 2015, Utrecht, The Netherlands, November 2015</p> <p>Layer-by-Layer Biofabrication for Bone Tissue Engineering</p> <p><u>Vera Guduric</u>, Carole Metz, Robin Siadous, Reine Bareille, Riccardo Levato, Elisabeth Engel, Jean-Christophe Fricain, Sylvain Catros, Ognjan Luzanin</p> <p>8th Young Scientist Symposium, IECB, Pessac, France, May 2015</p>
-------------	--

POSTER COMMUNICATIONS AT NATIONAL AND INTERNATIONAL CONFERENCES

2016	<p><i>In vitro</i> and <i>In vivo</i> Evaluations of Layer-by-Layer Bioassembly Cellularized Scaffolds for Bone Tissue Engineering</p> <p><u>Vera Guduric</u>, Robin Siadous, Reine Bareille, Benoît Rousseau, Raphaël Devillard, Jean-Christophe Fricain, Ognjan Luzanin, Sylvain Catros</p> <p>1er Forum Franco-Québécois d'Innovation en Santé, Montreal, Canada, October 2016</p> <p>Layer-by-layer Bioassembly for Bone Tissue Engineering</p> <p><u>Vera Guduric</u>, Robin Siadous, Reine Bareille, Ognjan Luzanin, Jean-Cristophe Fricain, Raphaël Devillard, Sylvain Catros</p> <p>Workshop of the Regenerative Medicine, Talence, France, October 2016</p>
-------------	--

2016	<p>Layer-by-Layer Assemblies of Cellularized Poly (lactic acid) Scaffolds for Bone Tissue Engineering</p> <p><u>Vera Guduric</u>, Carole Metz, Robin Siadous, Reine Bareille, Riccardo Levato, Elisabeth Engel, Jean-Cristophe Fricain, Ognjan Luzanin, Sylvain Catros</p> <p>Journée scientifique de la Fr TecSan, Pessac, France, June 2016</p> <p>Développement d'une technologie d'impression 3D pour la fabrication de substituts osseux sur mesure</p> <p>Agathe Grémare, <u>Vera Guduric</u>, Reine Bareille, Jean-Christophe Fricain, Raphaël Devillard, Sylvain Catros, Damien Le Nihouannen</p> <p>Journée scientifique de la Structure Fédérative de Recherche Technologies pour la santé SFR (TecSan), Bordeaux, France, June 2016</p> <p>Développement d'une technologie d'impression 3D pour la fabrication de substituts osseux sur mesure</p> <p>Agathe Grémare, <u>Vera Guduric</u>, Reine Bareille, Jean-Christophe Fricain, Raphaël Devillard, Sylvain Catros, Damien Le Nihouannen</p> <p>18th French Days of Mineralized Tissues Biology (JFBTM), Nancy, France, Juin 2016</p> <p>Layer-by-Layer Biofabrication of Cellularized Porous Poly(lactic) Acid Membranes for Bone Tissue Engineering</p> <p><u>Vera Guduric</u>, Carole Metz, Robin Siadous, Reine Bareille, Riccardo Levato, Elisabeth Engel, Jean-Christophe Fricain, Ognjan Luzanin, Sylvain Catros</p> <p>SVS Doctoral School Day, Arcachon, France, April 2016</p>
2015	<p>A Layer-by-Layer Biofabrication for Bone Tissue Engineering</p> <p><u>Vera Guduric</u>, Carole Metz, Mathieu Maisani, Robin Siadous, Reine Bareille, Riccardo Levato, Elisabeth Engel, Jean-Christophe Fricain, Ognjan Luzanin, Sylvain Catros</p> <p>32nd Annual Meeting of the Canadian Biomaterials Society, Toronto, Ontario, Canada, May 2015</p>

BIBLIOGRAPHY

- [1] Langer R and Vacanti J 2016 Advances in tissue engineering *J. Pediatr. Surg.* **51** 8–12
- [2] Camp C L, Lebaschi A, Cong G-T, Album Z, Carballo C, Deng X-H and Rodeo S A 2017 Timing of Postoperative Mechanical Loading Affects Healing Following Anterior Cruciate Ligament Reconstruction: Analysis in a Murine Model *J. Bone Joint Surg. Am.* **99** 1382–91
- [3] Du J, Mei S, Guo L, Su Y, Wang H, Liu Y, Zhao Z, Wang S and Liu Y 2017 Platelet-rich fibrin/aspirin complex promotes alveolar bone regeneration in periodontal defect in rats *J. Periodontal Res.*
- [4] El-Rashidy A A, Roether J A, Harhaus L, Kneser U and Boccaccini A R 2017 Regenerating bone with bioactive glass scaffolds: A review of in vivo studies in bone defect models *Acta Biomater.*
- [5] Yamada K M and Cukierman E 2007 Modeling tissue morphogenesis and cancer in 3D *Cell* **130** 601–10
- [6] Acun A and Zorlutuna P 2017 Engineered myocardium model to study the roles of HIF-1 α and HIF1A-AS1 in paracrine-only signaling under pathological level oxidative stress *Acta Biomater.* **58** 323–36
- [7] Treiser M D, Liu E, Dubin R A, Sung H-J, Kohn J and Moghe P V 2007 Profiling cell-biomaterial interactions via cell-based fluororeporter imaging *BioTechniques* **43** 361–6, 368
- [8] Knowlton S and Tasoglu S 2016 A Bioprinted Liver-on-a-Chip for Drug Screening Applications *Trends Biotechnol.* **34** 681–2
- [9] Blitterswijk C V 2007 Tissue Engineering
- [10] Zhang W, Chen L, Chen J, Wang L, Gui X, Ran J, Xu G, Zhao H, Zeng M, Ji J, Qian L, Zhou J, Ouyang H and Zou X 2017 Silk Fibroin Biomaterial Shows Safe and Effective Wound Healing in Animal Models and a Randomized Controlled Clinical Trial *Adv. Healthc. Mater.* **6**
- [11] Zhu L, Zhou H, Sun Z, Lou W and Lang J 2013 Anatomic and sexual outcomes after vaginoplasty using tissue-engineered biomaterial graft in patients with Mayer-Rokitansky-Küster-Hauser syndrome: a new minimally invasive and effective surgery *J. Sex. Med.* **10** 1652–8
- [12] Priya S G, Jungvid H and Kumar A 2008 Skin tissue engineering for tissue repair and regeneration *Tissue Eng. Part B Rev.* **14** 105–18
- [13] Lee K H 2000 Tissue-engineered human living skin substitutes: development and clinical application *Yonsei Med. J.* **41** 774–9
- [14] Morrison D A, Kop A M, Nilasaroya A, Sturm M, Shaw K and Honeybul S 2017 Cranial reconstruction using allogeneic mesenchymal stromal cells: a phase 1 first-in-human trial *J. Tissue Eng. Regen. Med.*

- [15] Bajestan M N, Rajan A, Edwards S P, Aronovich S, Cevidanes L H S, Polymeri A, Travan S and Kaigler D 2017 Stem cell therapy for reconstruction of alveolar cleft and trauma defects in adults: A randomized controlled, clinical trial *Clin. Implant Dent. Relat. Res.*
- [16] Di Bella C, Duchi S, O'Connell C D, Blanchard R, Augustine C, Yue Z, Thompson F, Richards C, Beirne S, Onofrillo C, Bauquier S H, Ryan S D, Pivonka P, Wallace G G and Choong P F 2017 In-situ handheld 3D Bioprinting for cartilage regeneration *J. Tissue Eng. Regen. Med.*
- [17] Hibino N, McGillicuddy E, Matsumura G, Ichihara Y, Naito Y, Breuer C and Shinoka T 2010 Late-term results of tissue-engineered vascular grafts in humans *J. Thorac. Cardiovasc. Surg.* **139** 431–6, 436.e1-2
- [18] Kim I-H, Ko I K, Atala A and Yoo J J 2015 Whole kidney engineering for clinical translation *Curr. Opin. Organ Transplant.* **20** 165–70
- [19] Atala A, Bauer S B, Soker S, Yoo J J and Retik A B 2006 Tissue-engineered autologous bladders for patients needing cystoplasty *Lancet Lond. Engl.* **367** 1241–6
- [20] Haycock J W 2011 3D cell culture: a review of current approaches and techniques *Methods Mol. Biol. Clifton NJ* **695** 1–15
- [21] Lee J, Cuddihy M J and Kotov N A 2008 Three-dimensional cell culture matrices: state of the art *Tissue Eng. Part B Rev.* **14** 61–86
- [22] Katz J L, Yoon H S, Lipson S, Maharidge R, Meunier A and Christel P 1984 The effects of remodeling on the elastic properties of bone *Calcif. Tissue Int.* **36 Suppl 1** S31-36
- [23] Sikavitsas V I, Temenoff J S and Mikos A G 2001 Biomaterials and bone mechanotransduction *Biomaterials* **22** 2581–93
- [24] Jilka R L 2003 Biology of the basic multicellular unit and the pathophysiology of osteoporosis *Med. Pediatr. Oncol.* **41** 182–5
- [25] Negishi-Koga T and Takayanagi H 2012 Bone cell communication factors and Semaphorins *BoneKEy Rep.* **1** 183
- [26] Zelzer E and Olsen B R 2003 The genetic basis for skeletal diseases *Nature* **423** 343–8
- [27] Jabalee J, Hillier S and Franz-Odenaal T A 2013 An investigation of cellular dynamics during the development of intramembranous bones: the scleral ossicles *J. Anat.* **223** 311–20
- [28] Marieb E 2012 *Essentials of human anatomy & physiology* (San Francisco, CA: Benjamin Cummings)
- [29] Rubin R, Strayer D and Rubin E 2012 *Rubin's pathology : clinicopathologic foundations of medicine.*

- [30] Wang M, Yang N and Wang X 2017 A review of computational models of bone fracture healing *Med. Biol. Eng. Comput.* 1–20
- [31] Guerado E and Caso E 2017 Challenges of bone tissue engineering in orthopaedic patients *World J. Orthop.* **8** 87–98
- [32] Bićanić G, Crnogaća K, Aljinović A, Dubravčić I D and Delimar D 2015 USEFUL TECHNIQUE FOR ALLOGRAFT BONE HARVEST *Acta Clin. Croat.* **54** 326–9
- [33] Kim J, McBride S, Dean D D, Sylvia V L, Doll B A and Hollinger J O 2014 In vivo performance of combinations of autograft, demineralized bone matrix, and tricalcium phosphate in a rabbit femoral defect model *Biomed. Mater. Bristol Engl.* **9** 035010
- [34] Nkenke E, Weisbach V, Winckler E, Kessler P, Schultze-Mosgau S, Wiltfang J and Neukam F W 2004 Morbidity of harvesting of bone grafts from the iliac crest for preprosthetic augmentation procedures: a prospective study *Int. J. Oral Maxillofac. Surg.* **33** 157–63
- [35] Sheikh Z, Hamdan N, Ikeda Y, Grynaps M, Ganss B and Glogauer M 2017 Natural graft tissues and synthetic biomaterials for periodontal and alveolar bone reconstructive applications: a review *Biomater. Res.* **21** 9
- [36] Takemoto R C, Fajardo M, Kirsch T and Egol K A 2010 Quantitative assessment of the bone morphogenetic protein expression from alternate bone graft harvesting sites *J. Orthop. Trauma* **24** 564–6
- [37] Sudhakar K N V, Mohanty R and Singh V 2017 Evaluation of Donor Site Morbidity Associated with Iliac Crest Bone Harvest in Oral and Maxillofacial, Reconstructive Surgery *J. Clin. Diagn. Res. JCDR* **11** ZC28-ZC33
- [38] Cordaro L, Amadé D S and Cordaro M 2002 Clinical results of alveolar ridge augmentation with mandibular block bone grafts in partially edentulous patients prior to implant placement *Clin. Oral Implants Res.* **13** 103–11
- [39] Colombier M-L, Lesclous P and Tulasne J-F 2005 [Bone graft healing] *Rev. Stomatol. Chir. Maxillofac.* **106** 157–65
- [40] Egol K A, Nauth A, Lee M, Pape H-C, Watson J T and Borrelli J 2015 Bone Grafting: Sourcing, Timing, Strategies, and Alternatives *J. Orthop. Trauma* **29** Suppl 12 S10-14
- [41] Le P Y, Fricain J-C, Souillac V, Largeteau A and Schmitthaeusler R 2005 Coral purification method and coral thus obtained
- [42] Damien E and Revell P A 2004 Coralline hydroxyapatite bone graft substitute: A review of experimental studies and biomedical applications *J. Appl. Biomater. Biomech. JABB* **2** 65–73

- [43] Felice P, Piana L, Checchi L, Corvino V, Nannmark U and Piattelli M 2013 Vertical ridge augmentation of an atrophic posterior mandible with an inlay technique and cancellous equine bone block: a case report *Int. J. Periodontics Restorative Dent.* **33** 159–66
- [44] Felice P, Marchetti C, Iezzi G, Piattelli A, Worthington H, Pellegrino G and Esposito M 2009 Vertical ridge augmentation of the atrophic posterior mandible with interpositional bloc grafts: bone from the iliac crest vs. bovine anorganic bone. Clinical and histological results up to one year after loading from a randomized-controlled clinical trial *Clin. Oral Implants Res.* **20** 1386–93
- [45] Marco F, Milena F, Gianluca G and Vittoria O 2005 Peri-implant osteogenesis in health and osteoporosis *Micron Oxf. Engl.* **1993** **36** 630–44
- [46] Pothuaud L, Fricain J-C, Pallu S, Bareille R, Renard M, Durrieu M-C, Dard M, Vernizeau M and Amédée J 2005 Mathematical modelling of the distribution of newly formed bone in bone tissue engineering *Biomaterials* **26** 6788–97
- [47] Tenenbaum H, Cuisinier F, Fricain J-C and Lemaitre J 2005 Les Matériaux de Substitution Osseuse
- [48] Fénelon M, Masson-Regnault E and Catros S 2016 La cicatrisation osseuse en chirurgie orale *Réal. Clin.* 37–43
- [49] Albrektsson T and Johansson C 2001 Osteoinduction, osteoconduction and osseointegration *Eur. Spine J. Off. Publ. Eur. Spine Soc. Eur. Spinal Deform. Soc. Eur. Sect. Cerv. Spine Res. Soc.* **10** **Suppl 2** S96-101
- [50] Fleischer S and Dvir T 2013 Tissue engineering on the nanoscale: lessons from the heart *Curr. Opin. Biotechnol.* **24** 664–71
- [51] Perez R A and Mestres G 2016 Role of pore size and morphology in musculo-skeletal tissue regeneration *Mater. Sci. Eng. C Mater. Biol. Appl.* **61** 922–39
- [52] Karageorgiou V and Kaplan D 2005 Porosity of 3D biomaterial scaffolds and osteogenesis *Biomaterials* **26** 5474–91
- [53] Duan P, Pan Z, Cao L, He Y, Wang H, Qu Z, Dong J and Ding J 2014 The effects of pore size in bilayered poly(lactide-co-glycolide) scaffolds on restoring osteochondral defects in rabbits *J. Biomed. Mater. Res. A* **102** 180–92
- [54] Williams D F 2008 On the mechanisms of biocompatibility *Biomaterials* **29** 2941–53
- [55] Thi Hiep N, Chan Khon H, Dai Hai N, Byong-Taek L, Van Toi V and Thanh Hung L 2017 Biocompatibility of PCL/PLGA-BCP porous scaffold for bone tissue engineering applications *J. Biomater. Sci. Polym. Ed.* **28** 864–78

- [56] Wang X, Li G, Liu Y, Yu W and Sun Q 2017 Biocompatibility of biological material polylactic acid with stem cells from human exfoliated deciduous teeth *Biomed. Rep.* **6** 519–24
- [57] Chai F, Raoul G, Wiss A, Ferri J and Hildebrand H F 2011 [Bone substitutes: Classification and concerns] *Rev. Stomatol. Chir. Maxillofac.* **112** 212–21
- [58] Tarafder S, Balla V K, Davies N M, Bandyopadhyay A and Bose S 2013 Microwave-sintered 3D printed tricalcium phosphate scaffolds for bone tissue engineering *J. Tissue Eng. Regen. Med.* **7** 631–41
- [59] Drury J L and Mooney D J 2003 Hydrogels for tissue engineering: scaffold design variables and applications *Biomaterials* **24** 4337–51
- [60] Lee K Y, Alsberg E and Mooney D J 2001 Degradable and injectable poly(aldehyde guluronate) hydrogels for bone tissue engineering *J. Biomed. Mater. Res.* **56** 228–33
- [61] Ahlfeld T, Akkineni A R, Förster Y, Köhler T, Knaack S, Gelinsky M and Lode A 2017 Design and Fabrication of Complex Scaffolds for Bone Defect Healing: Combined 3D Plotting of a Calcium Phosphate Cement and a Growth Factor-Loaded Hydrogel *Ann. Biomed. Eng.* **45** 224–36
- [62] Maisani M, Pezzoli D, Chassande O and Mantovani D 2017 Cellularizing hydrogel-based scaffolds to repair bone tissue: How to create a physiologically relevant micro-environment? *J. Tissue Eng.* **8** 2041731417712073
- [63] Roseti L, Parisi V, Petretta M, Cavallo C, Desando G, Bartolotti I and Grigolo B 2017 Scaffolds for Bone Tissue Engineering: State of the art and new perspectives *Mater. Sci. Eng. C Mater. Biol. Appl.* **78** 1246–62
- [64] Lane J M, Tomin E and Bostrom M P 1999 Biosynthetic bone grafting *Clin. Orthop.* S107-117
- [65] Zijdeveld S A, Zerbo I R, van den Bergh J P A, Schulten E A J M and ten Bruggenkate C M 2005 Maxillary sinus floor augmentation using a beta-tricalcium phosphate (Cerasorb) alone compared to autogenous bone grafts *Int. J. Oral Maxillofac. Implants* **20** 432–40
- [66] Saijo H, Igawa K, Kanno Y, Mori Y, Kondo K, Shimizu K, Suzuki S, Chikazu D, Iino M, Anzai M, Sasaki N, Chung U and Takato T 2009 Maxillofacial reconstruction using custom-made artificial bones fabricated by inkjet printing technology *J. Artif. Organs Off. J. Jpn. Soc. Artif. Organs* **12** 200–5
- [67] Nguyen L H, Annabi N, Nikkhah M, Bae H, Binan L, Park S, Kang Y, Yang Y and Khademhosseini A 2012 Vascularized bone tissue engineering: approaches for potential improvement *Tissue Eng. Part B Rev.* **18** 363–82

- [68] Yuan H, Fernandes H, Habibovic P, de Boer J, Barradas A M C, de Ruiter A, Walsh W R, van Blitterswijk C A and de Bruijn J D 2010 Osteoinductive ceramics as a synthetic alternative to autologous bone grafting *Proc. Natl. Acad. Sci. U. S. A.* **107** 13614–9
- [69] Habibovic P, Yuan H, van der Valk C M, Meijer G, van Blitterswijk C A and de Groot K 2005 3D microenvironment as essential element for osteoinduction by biomaterials *Biomaterials* **26** 3565–75
- [70] Granja P L, De Jéso B, Bareille R, Rouais F, Baquey C and Barbosa M A 2005 Mineralization of regenerated cellulose hydrogels induced by human bone marrow stromal cells *Eur. Cell. Mater.* **10** 31-37; discussion 37-39
- [71] Ben Slama L 2005 [Autologous bone grafts, allografts and biomaterials] *Rev. Stomatol. Chir. Maxillofac.* **106** 133–5
- [72] Malhotra A and Habibovic P 2016 Calcium Phosphates and Angiogenesis: Implications and Advances for Bone Regeneration *Trends Biotechnol.* **34** 983–92
- [73] Cesarano J, Dellinger J G, Saavedra M P, Gill D D, Jamison R D, Grosser B A, Sinn-Hanlon J M and Goldwasser M S 2005 Customization of Load-Bearing Hydroxyapatite Lattice Scaffolds *Int. J. Appl. Ceram. Technol.* **2** 212–20
- [74] Sun L, Danoux C B, Wang Q, Pereira D, Barata D, Zhang J, LaPointe V, Truckenmüller R, Bao C, Xu X and Habibovic P 2016 Independent effects of the chemical and microstructural surface properties of polymer/ceramic composites on proliferation and osteogenic differentiation of human MSCs *Acta Biomater.* **42** 364–77
- [75] Habibovic P, Yuan H, van den Doel M, Sees T M, van Blitterswijk C A and de Groot K 2006 Relevance of osteoinductive biomaterials in critical-sized orthotopic defect *J. Orthop. Res. Off. Publ. Orthop. Res. Soc.* **24** 867–76
- [76] Cordonnier T, Sohier J, Rosset P and Layrolle P 2011 Biomimetic Materials for Bone Tissue Engineering – State of the Art and Future Trends *Adv. Eng. Mater.* **13** B135–50
- [77] Mondal D, Griffith M and Venkatraman S S 2016 Polycaprolactone-based biomaterials for tissue engineering and drug delivery: Current scenario and challenges *Int. J. Polym. Mater. Polym. Biomater.* **65** 255–65
- [78] García-Gareta E, Coathup M J and Blunn G W 2015 Osteoinduction of bone grafting materials for bone repair and regeneration *Bone* **81** 112–21
- [79] Shrivats A R, McDermott M C and Hollinger J O 2014 Bone tissue engineering: state of the union *Drug Discov. Today* **19** 781–6

- [80] Xue R, Qian Y, Li L, Yao G, Yang L and Sun Y 2017 Polycaprolactone nanofiber scaffold enhances the osteogenic differentiation potency of various human tissue-derived mesenchymal stem cells *Stem Cell Res. Ther.* **8** 148
- [81] Noreikaitė A, Antanavičiūtė I, Mikalayeva V, Darinskas A, Tamulevičius T, Adomavičiūtė E, Šimatonis L, Akramienė D and Stankevičius E 2017 Scaffold design for artificial tissue with bone marrow stem cells *Med. Kaunas Lith.* **53** 203–10
- [82] Serra T, Mateos-Timoneda M A, Planell J A and Navarro M 2013 3D printed PLA-based scaffolds: a versatile tool in regenerative medicine *Organogenesis* **9** 239–44
- [83] Dai Y, Li X, Wu R, Jin Y and Gao C 2017 Macrophages of Different Phenotypes Influence the Migration of BMSCs in PLGA Scaffolds with Different Pore Size *Biotechnol. J.*
- [84] Sheikh Z, Najeeb S, Khurshid Z, Verma V, Rashid H and Glogauer M 2015 Biodegradable Materials for Bone Repair and Tissue Engineering Applications *Materials* **8** 5744–94
- [85] Yunus Basha R, Sampath Kumar T S and Doble M 2015 Design of biocomposite materials for bone tissue regeneration *Mater. Sci. Eng. C Mater. Biol. Appl.* **57** 452–63
- [86] Siqueira L, Passador F R, Costa M M, Lobo A O and Sousa E 2015 Influence of the addition of β -TCP on the morphology, thermal properties and cell viability of poly (lactic acid) fibers obtained by electrospinning *Mater. Sci. Eng. C Mater. Biol. Appl.* **52** 135–43
- [87] Serra T, Planell J A and Navarro M 2013 High-resolution PLA-based composite scaffolds via 3-D printing technology *Acta Biomater.* **9** 5521–30
- [88] Danoux C B S S, Bassett D C, Othman Z, Rodrigues A I, Reis R L, Barralet J E, van Blitterswijk C A and Habibovic P 2015 Elucidating the individual effects of calcium and phosphate ions on hMSCs by using composite materials *Acta Biomater.* **17** 1–15
- [89] Fricain J C, Schlaubitz S, Le Visage C, Arnault I, Derkaoui S M, Siadous R, Catros S, Lalande C, Bareille R, Renard M, Fabre T, Cornet S, Durand M, Léonard A, Sahraoui N, Letourneur D and Amédée J 2013 A nano-hydroxyapatite--pullulan/dextran polysaccharide composite macroporous material for bone tissue engineering *Biomaterials* **34** 2947–59
- [90] Thavornyutikarn B, Chantarapanich N, Sitthiseripratip K, Thouas G A and Chen Q 2014 Bone tissue engineering scaffolding: computer-aided scaffolding techniques *Prog. Biomater.* **3** 61–102
- [91] Bajaj P, Schweller R M, Khademhosseini A, West J L and Bashir R 2014 3D Biofabrication Strategies for Tissue Engineering and Regenerative Medicine *Annu. Rev. Biomed. Eng.* **16** 247
- [92] Subia B, Kundu J and Kundu S C 2010 Biomaterial Scaffold Fabrication Techniques for Potential Tissue Engineering Applications

- [93] Tarun G, Ajay B, Bhawna K, Sunil K and Ravi J 2011 Scaffold: Tissue Engineering and Regenerative Medicine *IRJP* **2** 37–42
- [94] Zhu N and Chen X 2013 Biofabrication of Tissue Scaffolds
- [95] Fennema E M, Tchang L A H, Yuan H, van Blitterswijk C A, Martin I, Scherberich A and de Boer J 2017 Ectopic bone formation by aggregated mesenchymal stem cells from bone marrow and adipose tissue: A comparative study *J. Tissue Eng. Regen. Med.*
- [96] Hao Z, Song Z, Huang J, Huang K, Panetta A, Gu Z and Wu J 2017 The scaffold microenvironment for stem cell based bone tissue engineering *Biomater. Sci.* **5** 1382–92
- [97] Takahashi K and Yamanaka S 2006 Induction of pluripotent stem cells from mouse embryonic and adult fibroblast cultures by defined factors *Cell* **126** 663–76
- [98] Li X, Yi W, Jin A, Duan Y and Min S 2015 Effects of sequentially released BMP-2 and BMP-7 from PELA microcapsule-based scaffolds on the bone regeneration *Am. J. Transl. Res.* **7** 1417–28
- [99] Saito A, Suzuki Y, Ogata S-I, Ohtsuki C and Tanihara M 2004 Prolonged ectopic calcification induced by BMP-2-derived synthetic peptide *J. Biomed. Mater. Res. A* **70** 115–21
- [100] Sachlos E and Czernuszka J T 2003 Making tissue engineering scaffolds work. Review: the application of solid freeform fabrication technology to the production of tissue engineering scaffolds *Eur. Cell. Mater.* **5** 29-39; discussion 39-40
- [101] Ko H C H, Milthorpe B K and McFarland C D 2007 Engineering thick tissues--the vascularisation problem *Eur. Cell. Mater.* **14** 1-18; discussion 18-19
- [102] Griffith L G and Naughton G 2002 Tissue engineering--current challenges and expanding opportunities *Science* **295** 1009–14
- [103] Jain R K, Au P, Tam J, Duda D G and Fukumura D 2005 Engineering vascularized tissue *Nat. Biotechnol.* **23** 821–3
- [104] Rouwkema J and Khademhosseini A 2016 Vascularization and Angiogenesis in Tissue Engineering: Beyond Creating Static Networks *Trends Biotechnol.* **34** 733–45
- [105] Akintewe O O, Roberts E G, Rim N-G, Ferguson M A H and Wong J Y 2017 Design Approaches to Myocardial and Vascular Tissue Engineering *Annu. Rev. Biomed. Eng.* **19** 389–414
- [106] Laschke M W and Menger M D 2016 Prevascularization in tissue engineering: Current concepts and future directions *Biotechnol. Adv.* **34** 112–21
- [107] Papadimitropoulos A, Piccinini E, Brachat S, Braccini A, Wendt D, Barbero A, Jacobi C and Martin I 2014 Expansion of human mesenchymal stromal cells from fresh bone marrow in a 3D scaffold-based system under direct perfusion *PLoS One* **9** e102359

- [108] Oragui E, Nannaparaju M and Khan W S 2011 The Role of Bioreactors in Tissue Engineering for Musculoskeletal Applications *Open Orthop. J.* **5** 267–70
- [109] Laschke M W, Rücker M, Jensen G, Carvalho C, Mülhaupt R, Gellrich N-C and Menger M D 2008 Improvement of vascularization of PLGA scaffolds by inosculation of in situ-preformed functional blood vessels with the host microvasculature *Ann. Surg.* **248** 939–48
- [110] Fricain J-C, De Olivera H, Devillard R, Kalisky J, Remy M, Kériquel V, Le Nihounen D, Grémare A, Guduric V, Plaud A, L’Heureux N, Amédée J and Catros S 2017 [3D bioprinting in regenerative medicine and tissue engineering] *Med. Sci. MS* **33** 52–9
- [111] Groll J, Boland T, Blunk T, Burdick J A, Cho D-W, Dalton P D, Derby B, Forgacs G, Li Q, Mironov V A, Moroni L, Nakamura M, Shu W, Takeuchi S, Vozzi G, Woodfield T B F, Xu T, Yoo J J and Malda J 2016 Biofabrication: reappraising the definition of an evolving field *Biofabrication* **8** 013001
- [112] Wan W, Zhang S, Ge L, Li Q, Fang X, Yuan Q, Zhong W, Ouyang J and Xing M 2015 Layer-by-layer paper-stacking nanofibrous membranes to deliver adipose-derived stem cells for bone regeneration *Int. J. Nanomedicine* **10** 1273–90
- [113] Catros S, Guillemot F, Nandakumar A, Ziane S, Moroni L, Habibovic P, van Blitterswijk C, Rousseau B, Chassande O, Amédée J and Fricain J-C 2012 Layer-by-layer tissue microfabrication supports cell proliferation in vitro and in vivo *Tissue Eng. Part C Methods* **18** 62–70
- [114] Kim M S, Lee B, Kim H N, Bang S, Yang H S, Kang S M, Suh K-Y, Park S-H and Jeon N L 2017 3D tissue formation by stacking detachable cell sheets formed on nanofiber mesh *Biofabrication* **9** 015029
- [115] Melchels F P W, Feijen J and Grijpma D W 2010 A review on stereolithography and its applications in biomedical engineering *Biomaterials* **31** 6121–30
- [116] Catros S 2010 Etude de la Micro-Impression d’Eléments Biologiques par Laser pour l’Ingénierie du Tissu Osseux
- [117] Bajaj P, Chan V, Jeong J H, Zorlutuna P, Kong H and Bashir R 2012 3-D biofabrication using stereolithography for biology and medicine *Conf. Proc. Annu. Int. Conf. IEEE Eng. Med. Biol. Soc. IEEE Eng. Med. Biol. Soc. Annu. Conf.* **2012** 6805–8
- [118] Mondschein R J, Kanitkar A, Williams C B, Verbridge S S and Long T E 2017 Polymer structure-property requirements for stereolithographic 3D printing of soft tissue engineering scaffolds *Biomaterials* **140** 170–88
- [119] Guillaume O, Geven M A, Sprecher C M, Stadelmann V A, Grijpma D W, Tang T T, Qin L, Lai Y, Alini M, de Bruijn J D, Yuan H, Richards R G and Eglin D 2017 Surface-enrichment

with hydroxyapatite nanoparticles in stereolithography-fabricated composite polymer scaffolds promotes bone repair *Acta Biomater.* **54** 386–98

[120] Do A-V, Khorsand B, Geary S M and Salem A K 2015 3D Printing of Scaffolds for Tissue Regeneration Applications *Adv. Healthc. Mater.* **4** 1742–62

[121] Williams J M, Adewunmi A, Schek R M, Flanagan C L, Krebsbach P H, Feinberg S E, Hollister S J and Das S 2005 Bone tissue engineering using polycaprolactone scaffolds fabricated via selective laser sintering *Biomaterials* **26** 4817–27

[122] Pattanayak D K, Fukuda A, Matsushita T, Takemoto M, Fujibayashi S, Sasaki K, Nishida N, Nakamura T and Kokubo T 2011 Bioactive Ti metal analogous to human cancellous bone: Fabrication by selective laser melting and chemical treatments *Acta Biomater.* **7** 1398–406

[123] Du Y, Liu H, Yang Q, Wang S, Wang J, Ma J, Noh I, Mikos A G and Zhang S 2017 Selective laser sintering scaffold with hierarchical architecture and gradient composition for osteochondral repair in rabbits *Biomaterials* **137** 37–48

[124] Ding R, Wu Z, Qiu G, Wu G, Wang H, Su X, Yin B, Ma S and Qi B 2014 [Selective Laser Sintering-produced porous titanium alloy scaffold for bone tissue engineering] *Zhonghua Yi Xue Za Zhi* **94** 1499–502

[125] Kinstlinger I S, Bastian A, Paulsen S J, Hwang D H, Ta A H, Yalacki D R, Schmidt T and Miller J S 2016 Open-Source Selective Laser Sintering (OpenSLS) of Nylon and Biocompatible Polycaprolactone *PLoS One* **11** e0147399

[126] Lee J W, Kim J Y and Cho D-W 2010 Solid Free-form Fabrication Technology and Its Application to Bone Tissue Engineering *Int. J. Stem Cells* **3** 85–95

[127] Brunello G, Sivoletta S, Meneghello R, Ferroni L, Gardin C, Piattelli A, Zavan B and Bressan E 2016 Powder-based 3D printing for bone tissue engineering *Biotechnol. Adv.* **34** 740–53

[128] Serra T, Ortiz-Hernandez M, Engel E, Planell J A and Navarro M 2014 Relevance of PEG in PLA-based blends for tissue engineering 3D-printed scaffolds *Mater. Sci. Eng. C Mater. Biol. Appl.* **38** 55–62

[129] Cox S C, Thornby J A, Gibbons G J, Williams M A and Mallick K K 2015 3D printing of porous hydroxyapatite scaffolds intended for use in bone tissue engineering applications *Mater. Sci. Eng. C Mater. Biol. Appl.* **47** 237–47

[130] Korpela J, Kokkari A, Korhonen H, Malin M, Närhi T and Seppälä J 2013 Biodegradable and bioactive porous scaffold structures prepared using fused deposition modeling *J. Biomed. Mater. Res. B Appl. Biomater.* **101B** 610–9

- [131] Luo Y, Akkineni A R and Gelinsky M 2014 Three-dimensional plotting is a versatile rapid prototyping method for the customized manufacturing of complex scaffolds and tissue engineering constructs *Zhongguo Xiu Fu Chong Jian Wai Ke Za Zhi Zhongguo Xiufu Chongjian Waik Zazhi Chin. J. Reparative Reconstr. Surg.* **28** 279–85
- [132] Quade M, Knaack S, Akkineni A R, Gabrielyan A, Lode A, Rösen-Wolff A and Gelinsky M 2017 Central Growth Factor Loaded Depots in Bone Tissue Engineering Scaffolds for Enhanced Cell Attraction *Tissue Eng. Part A*
- [133] Moroni L, Licht R, de Boer J, de Wijn J R and van Blitterswijk C A 2006 Fiber diameter and texture of electrospun PEOT/PBT scaffolds influence human mesenchymal stem cell proliferation and morphology, and the release of incorporated compounds *Biomaterials* **27** 4911–22
- [134] Motamedi A S, Mirzadeh H, Hajiesmaeilbaigi F, Bagheri-Khoulenjani S and Shokrgozar M 2017 Effect of electrospinning parameters on morphological properties of PVDF nanofibrous scaffolds *Prog. Biomater.*
- [135] Amjadian S, Seyedjafari E, Zeynali B and Shabani I 2016 The synergistic effect of nano-hydroxyapatite and dexamethasone in the fibrous delivery system of gelatin and poly(l-lactide) on the osteogenesis of mesenchymal stem cells *Int. J. Pharm.* **507** 1–11
- [136] Muerza-Cascante M L, Haylock D, Hutmacher D W and Dalton P D 2015 Melt electrospinning and its technologization in tissue engineering *Tissue Eng. Part B Rev.* **21** 187–202
- [137] Garlotta D 2001 A Literature Review of Poly(Lactic Acid) *J. Polym. Environ.* **9** 63–84
- [138] Saeidlou S, Huneault M A, Li H and Park C B 2012 Poly (lactic acid) crystallization *Prog. Polym. Sci.* **37** 1657–1677
- [139] Zhang Q, Mochalin V N, Neitzel I, Knoke I Y, Han J, Klug C A, Zhou J G, Lelkes P I and Gogotsi Y 2011 Fluorescent PLLA-nanodiamond composites for bone tissue engineering *Biomaterials* **32** 87–94
- [140] Saito N and Takaoka K 2003 New synthetic biodegradable polymers as BMP carriers for bone tissue engineering *Biomaterials* **24** 2287–93
- [141] Chang P C, Liu B Y, Liu C M, Chou H H, Ho M H, Liu H C, Wang D M and Hou L T 2007 Bone tissue engineering with novel rhBMP2-PLLA composite scaffolds *J. Biomed. Mater. Res. - Part A* **81** 771–80
- [142] Ceccarelli G, Presta R, Benedetti L, Cusella De Angelis M G, Lupi S M and Rodriguez Y Baena R 2017 Emerging Perspectives in Scaffold for Tissue Engineering in Oral Surgery *Stem Cells Int.* **2017** 4585401

- [143] Willerth S M and Sakiyama-Elbert S E 2008 Combining stem cells and biomaterial scaffolds for constructing tissues and cell delivery *StemBook* (Cambridge (MA): Harvard Stem Cell Institute)
- [144] Tyler B, Gullotti D, Mangraviti A, Utsuki T and Brem H 2016 Polylactic acid (PLA) controlled delivery carriers for biomedical applications *Adv. Drug Deliv. Rev.* **107** 163–75
- [145] Kutikov A B, Skelly J D, Ayers D C and Song J 2015 Templated repair of long bone defects in rats with bioactive spiral-wrapped electrospun amphiphilic polymer/hydroxyapatite scaffolds *ACS Appl. Mater. Interfaces* **7** 4890–901
- [146] Tan L, Yu X, Wan P, Yang K, Tan L, Yu X, Wan P and Yang K 2013 Biodegradable Materials for Bone Repairs: A Review, Biodegradable Materials for Bone Repairs: A Review *J. Mater. Sci. Technol.* **29** 503–13
- [147] Senatov F S, Niaza K V, Zadorozhnyy M Y, Maksimkin A V, Kaloshkin S D and Estrin Y Z 2016 Mechanical properties and shape memory effect of 3D-printed PLA-based porous scaffolds *J. Mech. Behav. Biomed. Mater.* **57** 139–48
- [148] Hamad K, Kaseem M, Yang H W, Deri F and Ko Y G 2015 Properties and medical applications of polylactic acid: A review *EXPRESS Polym. Lett.* **9** 435–55
- [149] Gentile P, Chiono V, Tonda-Turo C, Ferreira A M and Ciardelli G 2011 Polymeric membranes for guided bone regeneration *Biotechnol. J.* **6** 1187–97
- [150] Thomas N G, Sanil G P, Rajmohan G, Prabhakaran J V and Panda A K 2011 Fabrication and anti-microbial evaluation of drug loaded polylactide space filler intended for ridge preservation following tooth extraction *J. Indian Soc. Periodontol.* **15** 260
- [151] Kao C-T, Lin C-C, Chen Y-W, Yeh C-H, Fang H-Y and Shie M-Y 2015 Poly(dopamine) coating of 3D printed poly(lactic acid) scaffolds for bone tissue engineering *Mater. Sci. Eng. C* **56** 165–73
- [152] Thomas N G, Sanil G P, Rajmohan G, Prabhakaran J V and Panda A K 2011 Fabrication and anti-microbial evaluation of drug loaded polylactide space filler intended for ridge preservation following tooth extraction *J. Indian Soc. Periodontol.* **15** 260
- [153] Tomlin E M, Nelson S J and Rossmann J A 2014 Ridge preservation for implant therapy: a review of the literature *Open Dent. J.* **8** 66–76
- [154] Mironov V, Trusk T, Kasyanov V, Little S, Swaja R and Markwald R 2009 Biofabrication: a 21st century manufacturing paradigm *Biofabrication* **1** 022001
- [155] Costa P F 2015 Biofabricated constructs as tissue models: a short review *J. Mater. Sci. Mater. Med.* **26** 156

- [156] Wan W, Zhang S, Ge L, Li Q, Fang X, Yuan Q, Zhong W, Ouyang J and Xing M 2015 Layer-by-layer paper-stacking nanofibrous membranes to deliver adipose-derived stem cells for bone regeneration *Int. J. Nanomedicine* **10** 1273–90
- [157] Guduric V, Metz C, Siadous R, Bareille R, Levato R, Engel E, Fricain J-C, Devillard R, Luzanin O and Catros S 2017 Layer-by-layer bioassembly of cellularized polylactic acid porous membranes for bone tissue engineering *J. Mater. Sci. Mater. Med.* **28** 78
- [158] Hannachi I E, Yamato M and Okano T 2009 Cell sheet technology and cell patterning for biofabrication *Biofabrication* **1** 022002
- [159] Guillotin B and Guillemot F 2011 Cell patterning technologies for organotypic tissue fabrication *Trends Biotechnol.* **29** 183–90
- [160] Ren L, Ma D, Liu B, Li J, Chen J, Yang D and Gao P 2014 Preparation of three-dimensional vascularized MSC cell sheet constructs for tissue regeneration *BioMed Res. Int.* **2014** 301279
- [161] Derda R, Laromaine A, Mammoto A, Tang S K Y, Mammoto T, Ingber D E and Whitesides G M 2009 Paper-supported 3D cell culture for tissue-based bioassays *Proc. Natl. Acad. Sci. U. S. A.* **106** 18457
- [162] Kim M S, Lee B, Kim H N, Bang S, Yang H S, Kang S M, Suh K-Y, Park S-H and Jeon N L 2017 3D tissue formation by stacking detachable cell sheets formed on nanofiber mesh *Biofabrication* **9** 015029
- [163] Thébaud N B, Siadous R, Bareille R, Remy M, Daculsi R, Amédée J and Bordenave L 2012 Whatever their differentiation status, human progenitor derived - or mature - endothelial cells induce osteoblastic differentiation of bone marrow stromal cells *J. Tissue Eng. Regen. Med.* **6** e51-60
- [164] Serra T, Mateos-Timoneda M A, Planell J A and Navarro M 2013 3D printed PLA-based scaffolds: a versatile tool in regenerative medicine *Organogenesis* **9** 239–44
- [165] Grellier M, Bordenave L and Amédée J 2009 Cell-to-cell communication between osteogenic and endothelial lineages: implications for tissue engineering *Trends Biotechnol.* **27** 562–71
- [166] Ackerman G A 1962 Substituted naphthol AS phosphate derivatives for the localization of leukocyte alkaline phosphatase activity *Lab. Investig. J. Tech. Methods Pathol.* **11** 563–7
- [167] Zanetta L, Marcus S G, Vasile J, Dobryansky M, Cohen H, Eng K, Shamamian P and Mignatti P 2000 Expression of Von Willebrand factor, an endothelial cell marker, is up-regulated by angiogenesis factors: a potential method for objective assessment of tumor angiogenesis *Int. J. Cancer* **85** 281–8

- [168] Lee J W, Kim K-J, Kang K S, Chen S, Rhie J-W and Cho D-W 2013 Development of a bone reconstruction technique using a solid free-form fabrication (SFF)-based drug releasing scaffold and adipose-derived stem cells *J. Biomed. Mater. Res. A* **101** 1865–75
- [169] Tsuji W, Rubin J P and Marra K G 2014 Adipose-derived stem cells: Implications in tissue regeneration *World J. Stem Cells* **6** 312–21
- [170] Astori G, Vignati F, Bardelli S, Tubio M, Gola M, Albertini V, Bambi F, Scali G, Castelli D, Rasini V, Soldati G and Moccetti T 2007 “In vitro” and multicolor phenotypic characterization of cell subpopulations identified in fresh human adipose tissue stromal vascular fraction and in the derived mesenchymal stem cells *J. Transl. Med.* **5** 55
- [171] Yoon E, Dhar S, Chun D E, Gharibjanian N A and Evans G R D 2007 In vivo osteogenic potential of human adipose-derived stem cells/poly lactide-co-glycolic acid constructs for bone regeneration in a rat critical-sized calvarial defect model *Tissue Eng.* **13** 619–27
- [172] Scherberich A, Müller A M, Schäfer D J, Banfi A and Martin I 2010 Adipose tissue-derived progenitors for engineering osteogenic and vasculogenic grafts *J. Cell. Physiol.* **225** 348–53
- [173] Mehrkens A, Saxer F, Güven S, Hoffmann W, Müller A M, Jakob M, Weber F E, Martin I and Scherberich A 2012 Intraoperative engineering of osteogenic grafts combining freshly harvested, human adipose-derived cells and physiological doses of bone morphogenetic protein-2 *Eur. Cell. Mater.* **24** 308–19
- [174] Tayton E, Purcell M, Aarvold A, Smith J O, Briscoe A, Kanczler J M, Shakesheff K M, Howdle S M, Dunlop D G and Oreffo R O C 2014 A comparison of polymer and polymer-hydroxyapatite composite tissue engineered scaffolds for use in bone regeneration. An in vitro and in vivo study *J. Biomed. Mater. Res. A* **102** 2613–24

ANNEX

SCHOLARSHIPS

French Government scholarship given by the Embassy of France in Belgrade in Serbia for PhD studies in co-mentorship in 2014.

AVIESAN travel scholarship to attend the “1er Forum Franco-Québécois d’Innovation en Santé” in Montreal, Canada, October 2016.

AUF scholarship to attend the 8th Young Scientist Symposium at IECB in Pessac, France, May 2015.

AWARDS

Travel award from the International Society for Biofabrication to attend the International Conference on Biofabrication 2017 in Beijing, China, October 2017.

The best oral communication award at the “Journée scientifique de la Fr TecSan” at IECB in Pessac in France, June 22nd 2017.

Rapid presentation award from BIOMAT Society at the “18th French Days of Mineralized Tissues Biology” (JFBTM) in Nancy, France, June 2016.

The best poster award at “Journée scientifique de la Fr TecSan” at IECB in Pessac, France, June 2016.

Layer-by-layer bioassembly of cellularized polylactic acid porous membranes for bone tissue engineering

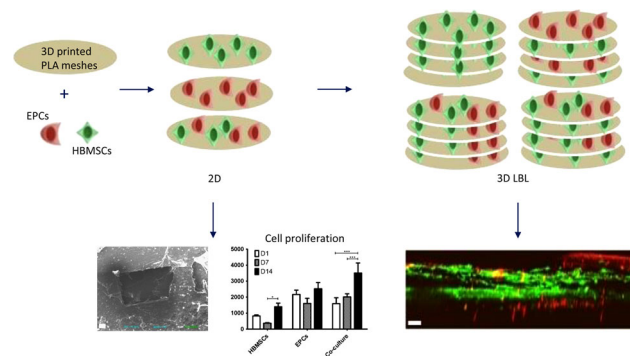
Vera Guduric^{1,2} · Carole Metz¹ · Robin Siadous¹ · Reine Bareille¹ · Riccardo Levato^{3,4} · Elisabeth Engel³ · Jean-Christophe Fricain¹ · Raphaël Devillard¹ · Ognjan Luzanin² · Sylvain Catros¹

Received: 6 November 2016 / Accepted: 15 March 2017
© Springer Science+Business Media New York 2017

Abstract The conventional tissue engineering is based on seeding of macroporous scaffold on its surface (“top–down” approach). The main limitation is poor cell viability in the middle of the scaffold due to poor diffusion of oxygen and nutrients and insufficient vascularization. Layer-by-Layer (LBL) bioassembly is based on “bottom–up” approach, which considers assembly of small cellularized blocks. The aim of this work was to evaluate proliferation and differentiation of human bone marrow stromal cells (HBMSCs) and endothelial progenitor cells (EPCs) in two and three dimensions (2D, 3D) using a LBL assembly of polylactic acid (PLA) scaffolds fabricated by 3D printing. 2D experiments have shown maintain of cell viability on PLA, especially when a co-culture system was used, as well as adequate morphology of seeded cells. Early osteoblastic and endothelial differentiations were observed and cell proliferation was increased after 7 days of culture. In 3D, cell migration was observed between layers of LBL constructs, as well as an osteoblastic differentiation. These results indicate that LBL assembly of PLA layers could be suitable for BTE, in order to promote homogenous cell distribution

inside the scaffold and gene expression specific to the cells implanted in the case of co-culture system.

Graphical Abstract



1 Introduction

A typical bone tissue engineering (BTE) approach requires cells specific to the bone tissue, biochemical growth factors as well as porous biocompatible scaffold [1]. The role of the scaffold is to provide a support for cell proliferation and differentiation and it must possess specific features regarding pore diameters, porosity and microscopic dimensions, as well as adequate osteoconductive and osteoinductive properties [2]. There are different biomaterials being used for BTE nowadays, such as calcium phosphates, metals, hydrogels, polymers or their combination [3–9]. Different groups have recently used scaffolds made of polylactic acid (PLA) as a support for bone regeneration. Pure PLA scaffolds can be used [10, 11] while coated PLA [12] and PLA-based composite materials have also been described [9, 13–16]. The FDA has approved PLA for different biomedical

✉ Sylvain Catros
sylvain.catros@u-bordeaux.fr

¹ Biotis, Inserm U1026, Université Bordeaux Segalen, 146 rue Léo-Saignat, Case 45, Bordeaux Cedex 33076, France

² Fakultet Tehnickih Nauka, Univerzitet u Novom Sadu, Trg Dositeja Obradovica 3, Novi Sad 21000, Serbia

³ Biomaterials for Regenerative Therapies Group, Institute for Bioengineering of Catalonia (IBEC), Barcelona, Spain

⁴ Department of Orthopedics, University Medical Center Utrecht, Utrecht, The Netherlands

applications, and it has proven adequate osteoconductive and osteoinductive properties for bone applications. Different types of human and animal cells have shown high ability to attach onto PLA scaffolds [17–19]. This polymer has been used to fabricate BTE scaffolds using several rapid prototyping (RP) methods, mostly by fused deposition modeling (FDM) [12], and 3D printing [20–22].

Conventional TE approach is based on the seeding of macroporous scaffold on its surface (“Top–Down” = TD), resulting in many cases in poor cell viability inside the scaffold, because it’s difficult for cells and nutrients to penetrate and survive in the core of the scaffold [23]. “Bioassembly” is based on self-induced assembly of cellularized building blocks and might also be called a “Bottom–Up” (BU) approach [24]. The main advantage of this approach is the possibility to seed different cell types onto one scaffold, which may lead to a homogeneous cell colonization and proliferation inside the scaffold. Layer-by-layer (LBL) assemblies of cellularized porous biomaterials may be used to fabricate cellularized constructs for bone tissue regeneration. The choice of the right order of layers plays an important role in order to obtain the best final implantable construct [25]. It was shown before that the combination of human bone marrow stromal cells (HBMSCs) and human umbilical vein endothelial cells (HUVECs) in alternating layers of cell sheets enables a high vascularization subcutaneously in mice [26]. Moreover, angiogenic factors secretion was augmented when alternates layers of mesenchymal stem cells and endothelial cells are stacked [27]. It was shown previously that it is possible to control the microenvironment inside the scaffold when using LBL approach since it enables the control of each layer accurately [28]. Another experiment based on LBL paper-stacking using adipose derived stem cells (ADSCs) and PCL/gelatin *in vivo* has shown that the LBL approach gave a promising osteogenic-related gene expressions [29]. We have already tested this method with MG63 cells transduced with Luciferase gene and PCL electrospun scaffold biopapers. Luciferase tracking with photon-imager displayed that cell proliferation was increased when the materials and cells were stacked layer-by-layer [30].

Concerning the cellular component of bone tissue engineering, it is already known that endothelial progenitor cells (EPCs) can modulate differentiation properties of mesenchymal stem cells (MSCs) in a coculture system [31]. PLA has already been used as a scaffold for MSCs and EPCs isolated from the rat [32] but there are no data available for the coculture of human endothelial and osteoblastic cells on this material. The use of PLA scaffold membranes to support cell culture could improve the manipulation and mechanical properties of such constructs.

The aim of this work was to build PLA membranes cellularized with human osteoprogenitors and endothelial

progenitor cells and to evaluate its properties *in vitro* in 2- and 3-dimensions

2 Materials and methods

2.1 Preparation of PLA membranes

PLA membranes were fabricated at the Institute for Bioengineering of Catalonia (IBEC) by direct 3D printing method, an additive RP method based on the extrusion of PLA dissolved in chloroform through a nozzle. We have used a 3Dn-300, Sciperio/nScript (Inc. Orlando, Florida) printer for this study. The PLA solution was prepared by dissolving a Poly(95 L/5DL) lactic acid (Corbion Purac) in chloroform (5% w/v) at 45 °C during 24 h and then syringes of 5 mL were filled, closed with paraffin film and stored at –20 °C before use. The printing process was controlled using a tuned motor speed and pressure, in order to be adapted to viscosity of the solution. The motor speed was 3 mm/s and the pressure was between 40 and 80 psi. G27 nozzles were used for extrusion. In order to be used for experiments, raw membranes (4 cm²) were cut with a tissue punch into 8 mm diameter circles.

Before cell culture experiments, PLA membranes were rinsed with phosphate buffered saline (PBS) 0.1 < pH 7.4 (Gibco) and sterilized in a solution of ethanol 70% (v/v) during 30 min. Then, the membranes were rinsed twice with PBS. A small amount of 2% agarose (A9539-250G Sigma-Aldrich, St Louis, MO, USA) prepared in PBS was placed in each well before placing the membranes in order to prevent cell adhesion on tissue culture plastic (TCP). The membranes were rinsed with culture media during 24 h before seeding the membranes with cells. All experiments were performed in 48-well plates (Corning Inc—Life Sciences, Durham, NC, USA).

2.2 Cell isolation and tagging

Two types of human primary cells were used in this study: human bone marrow stromal cells (HBMSCs) were isolated from bone marrow retrieved during surgical procedures (Experimental Agreement with CHU de Bordeaux, Etablissement Français du Sang, agreement CPIS 14.14). Cells were separated into a single suspension by sequential passages through syringes fitted with 16-, 18- or 21-gauge needles. After the centrifugation of 15 min at 800×g without break at room temperature, the pellet was resuspended with α -Essential Medium (α -MEM; Invitrogen) supplemented with 10% (v/v) fetal bovine serum (FBS) [33]. Endothelial Progenitor Cells (EPCs) were isolated from 30 μ L of diluted cord blood (Experimental Agreement with CHU de Bordeaux, Etablissement Français du Sang, agreement CPIS

14.14) in 1X PBS and 2 mM ethylene diaminetetraacetic acid (EDTA, Sigma-Aldrich, St Louis, MO, USA). 15 mM of Histopaque solution (Sigma-Aldrich) was added. Then centrifugation was performed at 400g for 30 min and the ring of nuclear cells was removed and washed several times with 1× PBS and 2 nM EDTA. At the end, cells were cultured in endothelial cell growth medium-2 (EGM-2, Lonza-Verviers, France) with supplements from the kit and 5% (v/v) FCS (GIBCO Life Technologies, Karlsruhe, Germany) on a 12-well cell plate. The cell plate was coated with collagen type I (Rat Tail, BD Biosciences). Non adherent cells were removed at Day 1 and media was changed every other day [34]. The medium for endothelial cells growth contained 5% FBS, 0.1% human epidermal growth factor (hEGF), 0.04% Hydrocortison, 4% human fibroblastic growth factor-b (hFGF-b), 0.1% vascular endothelial growth factor (VEGF), 0.1% R3 insulin-like growth factor-1 (R3-IGF-1) 0.1% ascorbic acid, 0.1% gentamicin, amphotericin B (GA) (Lonza-Verviers, France). Both, HBMSCs and EPCs were incubated in a humidified atmosphere of 95% air, 5% CO₂ at 37 °C. The culture medium was changed every other day.

To evaluate the cell migration during LBL 3D experiments, both types of cells were tagged with fluorescent proteins. HBMSCs were tagged with green fluorescent protein (GFP) which exhibits a green fluorescence when exposed to light in the blue or ultraviolet range. EPCs were tagged with Td-Tomato, which exhibits a red fluorescence when exposed to the light in green range [35]. The lentiviral vectors contained GFP or Td-Tomato protein gene under the control of the MND (for GFP) or phosphoglycerate kinase (PGK) promoter (for Td-Tomato) for cell labeling. 2×10^5 freshly trypsinized HBMSCs or EPCs (low sub-culturing) in suspension were mixed with 6×10^6 viral particles (MOI for GFP: 15; MOI for Td-Tomato: 30) for viral transduction (multiplicity of infection). After 24 h in culture, virus-containing medium was replaced by a fresh one to provide the cell growth. Medium was changed every other day.

2.3 Cell seeding and characterization in 2D

2.3.1 Cell seeding in 2D

PLA membranes were stabilized on the agarose with glass rings in order to avoid the floating of membranes in the culture media. HBMSCs and EPCs were seeded onto membranes as mono- (HBMSCs 50,000 cells/cm², EPCs 100,000 cells/cm²) and co-cultures (HBMSCs 25,000/cm² + EPCs 50,000 cells/cm²). Culture media were changed every other day.

All 2D experiments were performed on PLA membranes seeded with different combinations of human primary cells

(1 seeded membrane = 1 sample). Examined time points were Day 1, Day 3, Day 7, Day 14 and Day 21.

2.3.2 Cell characterization in 2D

2.3.2.1 Live-dead assay The viability of the cells seeded on PLA membranes was tested by Live-Dead assay (LD, Life Technologies), which was based on acetoxymethyl ester of calcein (Calcein-AM) and ethidium homodimer-1 (EthD-1) [36–38]. Calcein-AM was cleaved in the cytoplasm by esterase and thus indicated live cells showing the green fluorescence. EthD-1 enters cells with damaged membranes and binds to nucleic acids, producing a red fluorescence of dead cells. The assay was performed by removing the culture media, rinsing the seeded PLA membrane with Hanks' balanced salt solution (HBSS, GIBCO) and addition of the solution of Calcein-AM and EthD-1 diluted in Hanks'. The solution was incubated during 15 min in a humidified atmosphere of 95% air, 5% CO₂ at 37 °C. Fluorescence was observed with confocal scanning microscopy (Leica, TSC SPE DMI 4000B) with LAS-AF (Leica Advanced Suite-Advanced Fluorescence) software.

2.3.2.2 Quantification of the area covered by cells Live-Dead images obtained by confocal microscope were used to calculate areas covered by live or dead cells by ImageJ (<https://imagej.nih.gov/ij/>).

For each condition (mono- or co-cultures) and for each time point, we have selected five images (four close to the borders at the ends of perpendicular axes and one in the middle) to quantify the cell area covered by cells. This led to a total of 45 images quantified. Color channels (green and red) were split for each image and percentage of covered areas were calculated for each color. Statistical analyses were performed with GraphPad Prism 6 software using a two way ANOVA and Bonferroni tests.

2.3.3.3 Scanning electron microscopy Cell morphology was observed with a microscope Hitachi, S-2500 scanning electron microscope (SEM). After 14 days of cell culture onto PLA membranes, the samples were fixed with paraformaldehyde (PFA) 4% and dehydrated in graded ethanol (EtOH) solution (30, 50, 70, 90, 100%) and then in dex-amethylsilazan and air dried, followed by gold coating. The accelerating voltage used for the observation was 12 kV and the samples were observed with magnification ×80 and ×200. Pictures were acquired using MaxView® and SamX® softwares.

2.3.4.4 CyQuant assay Cell proliferation on PLA was evaluated with CyQuant® Cell Assay kit (In vitrogen C7026). This assay was based on fluorescent quantification

of one protein which binded to cell DNA. The culture media was removed at each time point and culture plates were frozen and kept at -80°C to process all samples together. Finally, all plates were left at the room temperature for thawing. The lysis solution was first added in all samples and then 200 μl of the buffer were added following the manufacturer's instructions. All samples were transferred in 96-well plates and mixed for 2–5 min in dark. The fluorescence of the solutions was measured at 480 and 520 nm using Victor X3 2030 Perkin Elmer.

2.3.5.5 Immunofluorescent analysis The EPCs monocultures and the co-cultures HBMSCs + EPCs on PLA membranes were fixed with 4% (w/v) Paraformaldehyd (PFA) at 4°C during 15 min and permeabilized with Triton X-100 0.1% (v/v) during 10 min. Endothelial phenotype was observed using intracellular marker von Willebrand Factor (vWF). The samples were incubated 1 h in PBS containing 1% (w/v) Bovine serum albumin (BSA, Eurobio, France) before incubation with primary antibody. VWF primary antibody (Rabbit) was diluted in PBS $1\times$ with 0.5% (w/v) BSA at 1/300 (Dako, Glostrup, Denmark). The primary antibody was incubated 1.5 h at the room temperature. Then, the cells were rinsed with PBS and incubated with the secondary antibody: Alexa 488-conjugated goat anti-rabbit IgG diluted at 1/300. Subsequently, cells were washed with PBS and incubated with the nuclear probe DAPI (4', 6'-diamino-2-phenylindole, FluoProbes 5 mg ml^{-1} , dilution 1:5000) for 10 min at room temperature, in order to label the nucleus in blue. The lasers used were 488 nm (green), 561 nm (red) and 405 nm (blue). The observations were performed at $100\times$ magnification and the pictures were taken every 2.4 μm in "z" orientation. The 3D reconstruction was performed with LAS-AF (Leica Advanced Suite-Advanced Fluorescence) software.

2.3.6.6 Alkaline phosphatase (ALP) assay Intracellular ALP activity was detected as an early osteoblastic marker. We have used the Ackerman technique, which is based on conversion of a colorless p-nitrophenyl phosphate to a colored p-nitrophenol (Sigma diagnostic kit, Aldrich). Three different conditions were tested: (1) mono-culture (HBMSCs) with induction media (α -MEM + 1/1000 dexamethasone, 1/10,000

ascorbic acid, 1/100 β -glycerolphosphate, Iscove's Modified Dulbecco (IMDM, GIBCO), 10% SVF); (2) mono-culture (HBMSCs) without induction media (α -MEM alone) and (3) co-cultures (α -MEM + EGM-2 50/50). The samples were fixed with 4% (v/w) PFA during 10 min at 4°C . Then the samples were stained with alkaline dye (Fast bluse RR salt supplemented with Naphtol AS-MX phosphate alkaline solution 0.25%, Sigma Aldrich) away from light during 30 min. The observations were performed with an optical microscope (Leica DMi 3000 B) connected with a digital camera (Leica DFC 425 $^{\circ}\text{C}$).

2.4 Layer-by-Layer assembly of cellularized membranes in 3D

2.4.1 Layer-by-layer assembly and seeding strategies

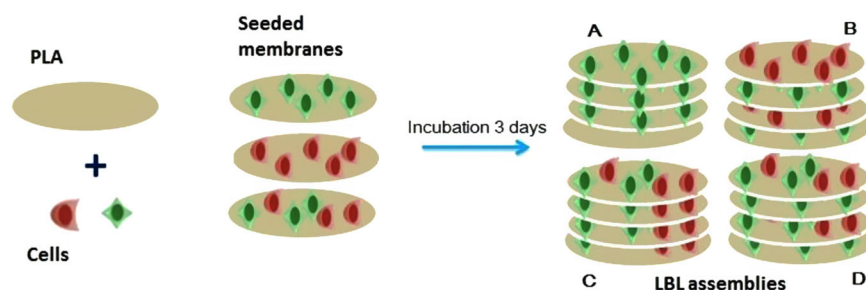
After seeding the PLA membranes in 2D using HBMSCs or EPCs or cocultures of HBMSCs and EPCs, the membranes were stacked Layer-by-Layer (LBL) to obtain a 3D composite material (Fig. 1).

These 3D constructs were prepared by assembling four PLA membranes seeded with human primary cells (HBMSCs alone or coculture of HBMSCs and EPCs) after 3 days of culture in 2D. We have prepared four different types of 3D constructs: Sample "A" consisted of four membranes seeded with HBMSC, samples "B" was made of alternating layers of monocultures of HBMSCs and EPCs, samples "C" were constructed with co-culture membranes and samples "D" had alternating layers of mono-cultures of HBMSCs and co-cultures (Fig. 1). LBL constructs were first characterized by observing the migration of tagged endothelial cells inside the LBL constructs using two photons microscopy, then the osteoblastic differentiation of the LBL 3D constructs was evaluated using quantitative polymerase chain reaction (qPCR).

2.4.2 Quantitative real-time polymerase chain reaction (QPCR)

Osteoblastic differentiation was examined on three different types of LBL constructs: HBMSCs in all four layers of 3D constructs, HBMSCs/EPCs/HBMSCs/EPCs and cocultures

Fig. 1 LBL bio-assembly of PLA membranes seeded with human cells. **a** HBMSCs/HBMSCs/HBMSCs/HBMSCs; **b** HBMSCs/EPCs/HBMSCs/EPCs; **c** Cocultures/Cocultures/Cocultures/Cocultures; **d** HBMSCs/Coculture/HBMSCs/Coculture



in all four layers (Fig. 1a–c). Total RNA was extracted using the RNeasy Total RNA kit (Qiagen, AMBION, Inc. Austin, Texas, USA), as indicated by the manufacturer and 1 µl was used as the template for single-strand cDNA synthesis, using the Superscript pre-amplification system (Gibco) in a 20 ml final volume, containing 20 mM Tris-HCl, pH 8.4, 50 mM KCl, 2.5 mM MgCl₂, 0.1 mg/ml BSA, 10 mM DTT, 0.5 mM of each dATP, dCTP, dGTP and dTTP, 0.5 mg oligo(dT) 12–18 and 200 U reverse transcriptase. After incubation at 42 °C for 50 min, the reaction was stopped at 70 °C for 15 min. cDNA (5 µl) diluted at a 1:80 ratio was loaded onto a 96-well plate. Real-time PCR amplification was performed using the SYBR-Green Supermix (2' iQ 50 mM KCl, 20 mM Tris-HCl, pH 8.4, 0.2 mM each dNTP, 25 U/ml iTaq DNA polymerase, 3 mM MgCl₂, SYBR Green I and 10 nM fluorescein, stabilized in sterile distilled water). Primers of investigated genes (Table 1) were used at a final concentration of 200 nM. Data were analysed using iCycler IQ software and compared by the ΔΔCT method. Q-PCR was performed in triplicate for PCR yield validation. Results of relative gene expressions for LBL B and LBL C on the 7th day of culture were expressed to relative gene expression levels of LBL A. Each Q-PCR was performed in triplicate. Data were normalized to P0 (ribosomal protein) mRNA expression for each condition and was quantified relative to Runx2, ALP, OCN and type I collagen (Col1) gene expression. Statistical analysis was performed by Mann Witney test in order to compare the expressions of different gens for B and C LBL constructs.

2.4.3 2 Photons microscopy (2PM)

2PM was used to obtain a large field of view of the samples in 3D (450 µm). We prepared 3D constructs with HBMSCs tagged with GFP and EPCs tagged with TdT in order to observe the colonization of cells inside the LBL constructs (Fig. 1d). The confocal microscope was a Leica DM6000 TSC SP5 MP. L5 filter was used for green and N3 filter for

red fluorescence. HCXIRAPO objective with immersion was used to observe the samples. Argon laser for HBMSCs GFP and DPSS 561 for EPCs TdT. Excitation for HBMSCs GFP was performed at 488 nm and for EPCs TdT at 561 nm wavelength.

3 Results

3.1 Cell culture onto a PLA substrate membrane

3.1.1 Scaffolds membranes features and cell morphology

The PLA membranes were 100 µm thick and pores diameter was 200 µm. SEM observations showed the external structure of PLA membranes and struts organization, which revealed that pore size was ranged between 165 and 375 µm (Fig. 2a). Considering the PLA membranes loaded with cells, we have observed different cell morphologies of the mono- and co-cultures (Fig. 2b): HBMSCs showed elongated and highly-branched morphology. EPCs were small, rounded cells with filopodia towards PLA membranes. Cells in co-cultures were elongated and branched and covered the membrane pores.

3.1.2 Cell viability

Live-Dead experiments were performed in 2D cell culture onto PLA membranes (Fig. 3a). In general, we have observed a large amount of living cells after 14 days of culture. Most of the cells were alive at day 1, with the highest survival rates in mono-cultures of HBMSCs. Few EPCs were present on PLA membranes at Day 1. Coculture samples showed similar cell viability as mono-cultures of HBMSCs at day 1. After 7 days of culture, we observed higher density of live cells in HBMSCs mono-culture samples, which was maintained until day 14. Regarding mono-cultures of EPCs, we did not observe any significant difference in qualitative observations of live and dead cells

Table 1 Primers of investigated genes

Genes	Primers
Ubiquitary ribosomic protein P0	Forward 5'-ATG CCC AGG GAA GAC AGG GC-3' Reverse 5'-CCA TCA GCA CCA CAG CCT TC-3'
ALP	Forward 5'-AGC CCT TCA CTG CCA TCC TGT-3' Reverse 5'-ATT CTC TCG TTC ACC GCC CAC-3'
COL1A1	Forward 5'-TGG ATG AGG AGA CTG GCA ACC-3' Reverse 5'-TCA GCA CCA CCG ATG TCC AAA-3'
Runx2	Forward 5'-TCA CCT TGA CCA TAA CCG TCT-3' Reverse 5'-CGG GAC ACC TAC TCT CAT ACT-3'
OCN	Forward 5'-ACC ACA TCG GCT TTC AGG AGG-3' Reverse 5'-GGG CAA GGG CAA GGG GAA GAG-3'

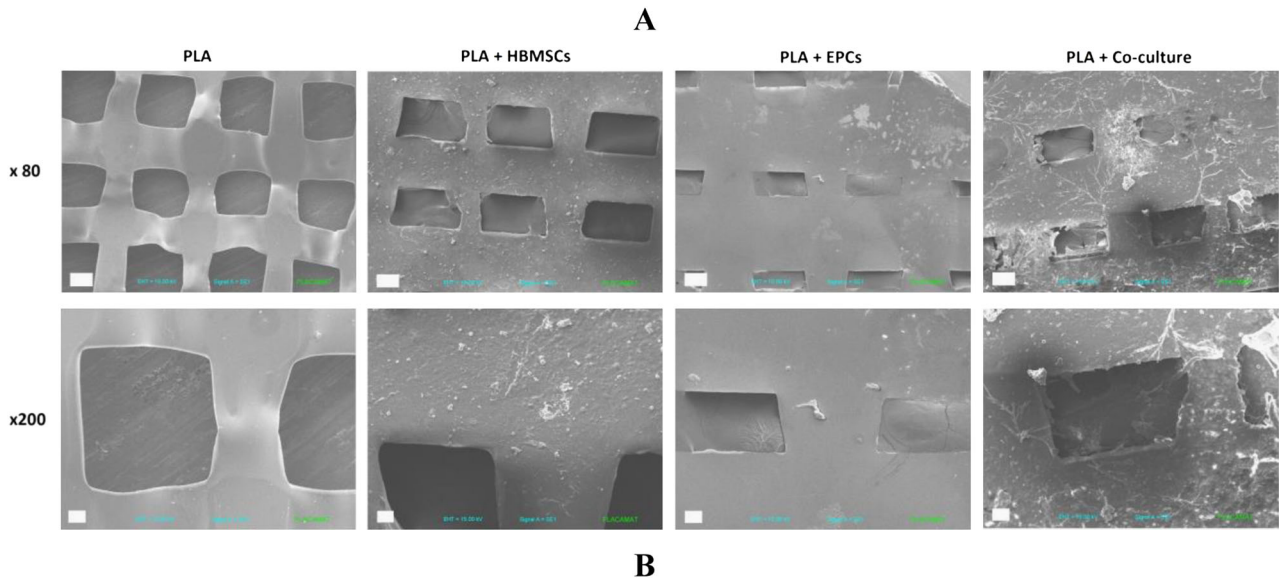


Fig. 2 Scanning electron microscopy at Day 14: PLA: control PLA membranes without cells; PLA + HBMSCs: human bone marrow stromal cells cultured on PLA membranes; PLA + EPCs: endothelial

progenitor cells cultured on PLA membranes; PLA + Co-cultures: cocultures of HBMSCs and EPCs on PLA membranes. Scale bar is 100 μm for $\times 80$ images and 30 μm for $\times 200$ images

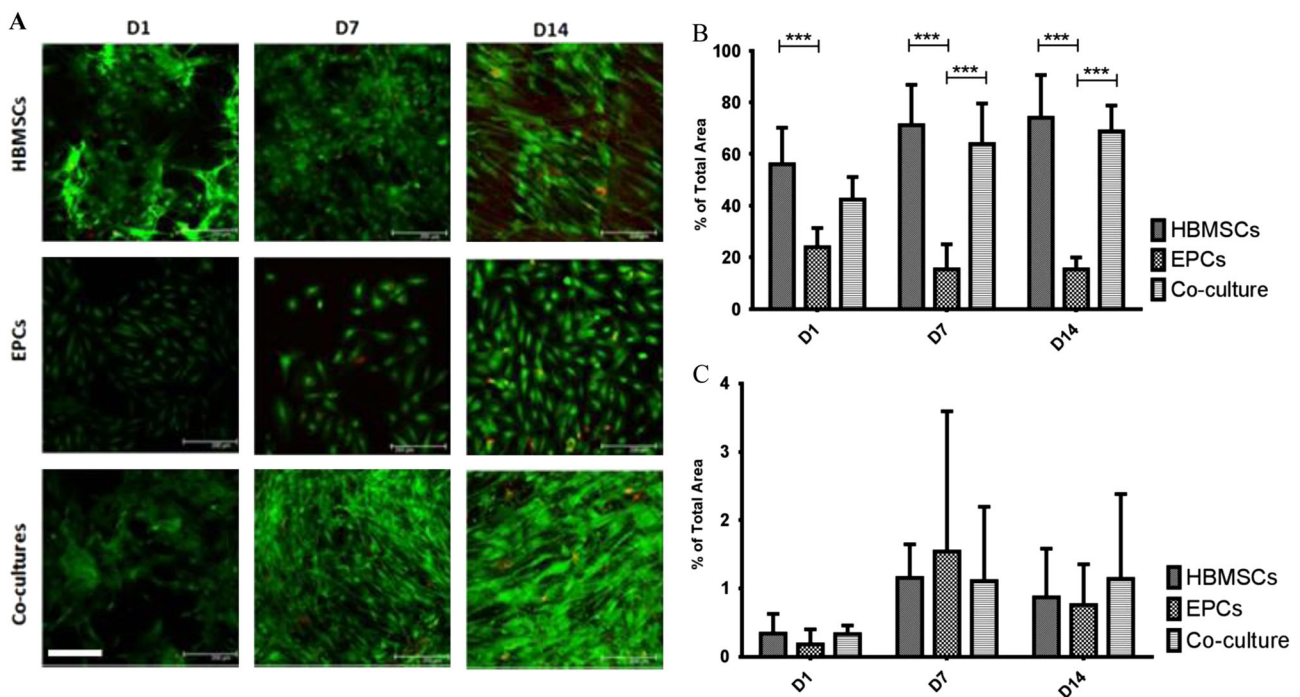


Fig. 3 **a** Qualitative images of the L/D assay at Day 1, 7 and 14. Scale bar is 200 μm for all images; **b** Statistical results of the % of total area covered by live cells calculated from five different spots of one

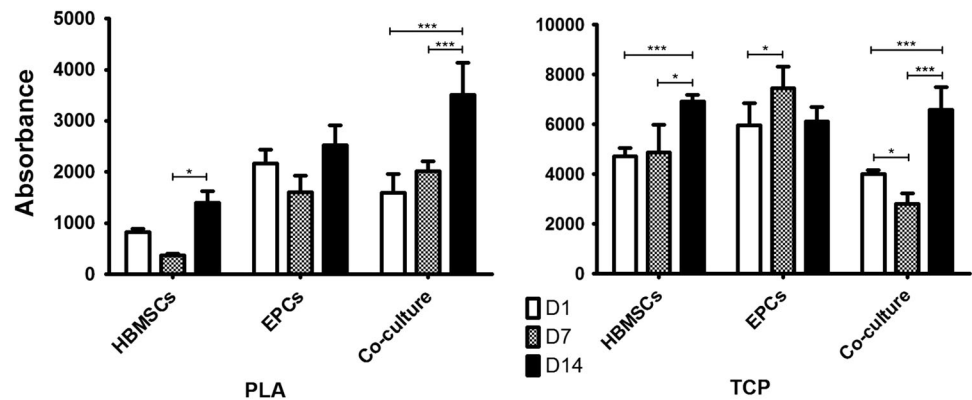
scaffold. *** $p < 0.001$; **c** Statistical results of the % of total area covered by dead cells calculated from five different spots of one scaffold

after 7 days, but their population was denser at day 14. Coculture samples showed a large amount of live cells after 7 days, which was maintained until the day 14. After 14 days, the co-cultures (HBMSCs + EPCs) have shown the highest cell survival.

3.1.3 Quantification of the area covered by cells

The pictures obtained with confocal microscope after Live-Dead assay have been used to quantify the areas covered by live or dead cells, using ImageJ[®] software. Since the

Fig. 4 Cell proliferation during 14 days of culture on PLA membranes: mono- and co-cultures on PLA. Control experiments were done on tissue culture plastic (TCP). * $p < 0.05$, ** $p < 0.001$, *** $p < 0.0001$



Calcein-AM colors the cytoplasm of live cells and the EthD-1 colors the nucleus of dead cells, we could not compare the surfaces covered by live to the surfaces covered by dead cells, so we have compared live or dead cells in function of different cell culture conditions. Percentages of total areas of live and dead cells are shown in Fig. 3b and c respectively. At day 1, most of the surface covered by live cells was observed in HBMSCs mono-culture samples and it increased with time. The surface of live cells in co-culture systems increased with time as well. Mono-cultures of EPCs did not show an important increase in the surface covered by live cells. There was significantly less EPCs live surface in all conditions compared to HBMSCs and co-cultures. Regarding dead cells quantification, no significant difference was observed between all conditions. The highest surface covered by dead cells was observed in EPCs mono-culture samples after 7 days.

3.1.4 Cell proliferation (CyQuant)

In test samples, cell proliferation assays in two dimensions displayed a global increase of DNA synthesis in all samples with time (Fig. 4). There was no significant difference in the proliferation of EPCs in mono-culture samples during time. DNA synthesis was significantly increased between 7 and 14 days of culture for HBMSCs on the PLA. After 14 days of culture, a significant difference was observed in cell proliferation of co-cultures. Control results (TCP) confirm the significant increase in cell proliferation for all samples after 14 days of culture.

3.1.5 Cell differentiation

Endothelial phenotype was characterized by the intracellular marker Von Willebrand Factor (vWF) [39]. DAPI was used to label the nucleus in blue [40]. The vWF (green) and the DAPI (blue) staining were maintained in mono- and co-

cultures on PLA during 14 days. Mono-cultures of EPCs on PLA showed a different organization than co-cultures on PLA membranes (Fig. 5a).

Osteoblastic phenotype was evaluated using alkaline phosphatase (ALP) staining. ALP expression was positive in both, mono- and co-cultures (Fig. 5b).

3.2 Use of cellularized PLA membranes for LBL bio-assembly

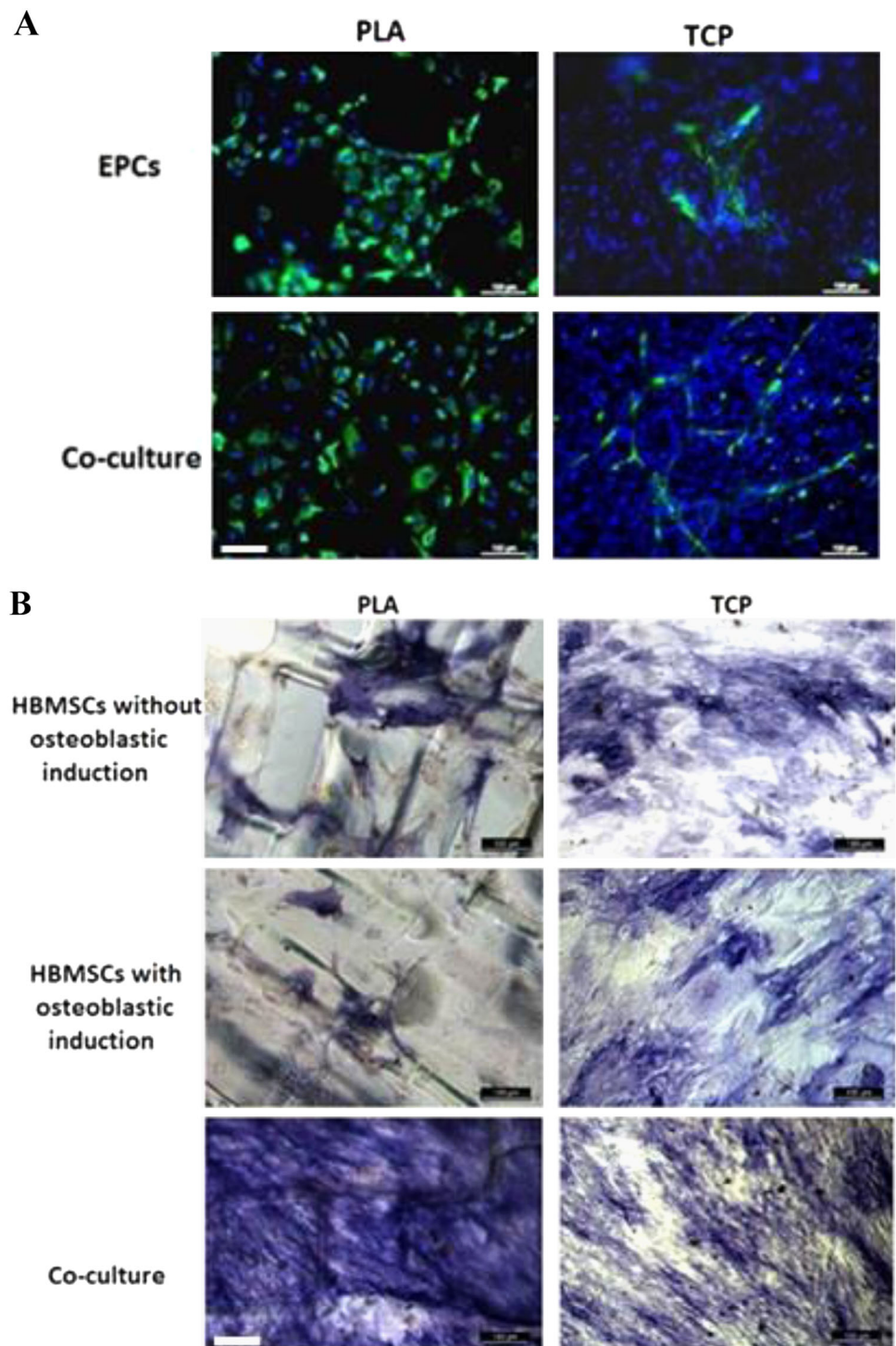
In aim to obtain preliminary results for LBL Bio-Assembly we have characterized the osteoblastic phenotype in 3D constructs as well as the cell repartition in 3D.

3.2.1 Phenotype characterization in 3D constructs

The relative osteoblastic gene expressions at the 7th day of culture of two types of LBL constructs, with different positions of HBMSCs and EPCs in layers., The experiment was performed with LBL constructs with alternating layers of mono-cultures of HBMSCs and EPCs and LBL constructs with co-culture layers. Phenotype characterization was tested for relative gene expression of ALP, RunX2, OCN and Col1 as osteoblastic markers (Fig. 6a). LBL construct made of mono-cultures of HBMSCs were used as a control group.

3.2.1.1 Observation of 3D LBL composite materials by 2-photon microscopy This experiment was performed in aim to observe the repartition of cells (EPCs) in 3D in LBL constructs. LBL composite materials were prepared to be observed after 14 days of culture using two photons confocal microscopy (2P). The tested sample had alternating layers of monoculture of HBMSCs-GFP and co-cultures (HBMSCs-GFP + EPCs-TdT). We could observe all four layers of 3D constructs and endothelial cells (red fluorescence) were present in all layers (Fig. 6b).

Fig. 5 Cell differentiation in 2D mono and co-cultures on PLA membranes. The scale is 100 μm and it is the same for all images: **a** endothelial differentiation (vWF in *green* and DAPI in *blue*) at Day 14.; **b** osteoblastic differentiation on Day 14. (PLA poly-lactic acid membranes; TCP tissue culture plastic) (color figure online)



4 Discussion

PLA used for this work has already been characterized by Serra et al. [41]. PLA membranes fabricated by 3D printing had an expected morphology and a pore size suitable for tissue engineering [42]. Human primary cells seeded on these PLA porous membranes have shown the morphology expected in these culture conditions.

A large amount of living cells were present on PLA membranes after 14 days of culture, especially in the case of co-cultures. There were much more membrane areas covered by live than by dead cells. The highest percentage of live cells was present in co-culture systems and it increased with time, which confirmed results obtained by SEM. The presence of both types of cells provided better conditions for cell survival. There were significantly less

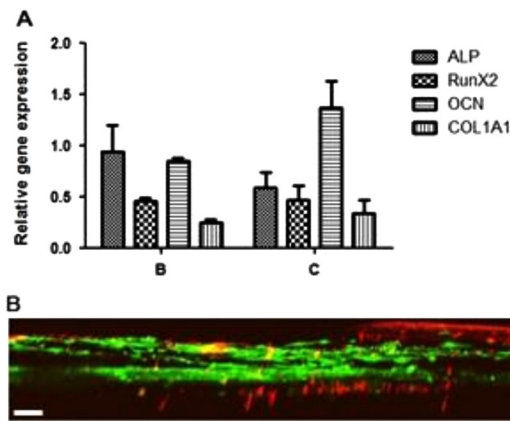


Fig. 6 3D LBL constructs. **a** Osteoblastic differentiation (qPCR) of cells in 3D LBL B and C types of constructs on Day 7 in comparison to the A type; **b** Cell colonization inside the LBL D constructs (HBMSCs-GFP in green color and EPCs-TdT in red fluorescence). The scale bar is 500 μ m (color figure online)

live EPCs in all conditions compared to HBMSCs and co-cultures. However, the quantification of dead cells surface is not fully reliable as they usually detach from their substrate.

The amount of DNA was higher for EPCs during the first week of culture, which was expecting since we have seeded more EPCs at day 0 because they are much smaller than HBMSCs. Cells proliferation was significantly higher in the positive controls (tissue culture plastic) than on the PLA samples, what was expected with this reference tissue culture surface. There were no significant differences observed during the co-culture control samples because cell achieved their confluence very fast thanks to the cell-to-cell communication and the growth factor secretion, which was not the case on mono-culture samples. This process was slower in test co-culture samples on PLA during 7 days, but it was changed after 14 days of culture. The reason is most likely related to cell-to-cell interaction through growth factors (BMP-2, VEGF, IGF) production in co-cultures [43]. The proliferation in mono-culture samples was decreased after 7 days of culture probably because cells need more time to be adapted to the PLA than in control samples. But the proliferation was increased after 14 days, with a significant difference for HBMSCs.

EPCs were located only on struts of the PLA membranes and they formed a homogenous “grid line” shape after 14 days of culture. Co-cultures showed a higher density of cells and a lower density of vWF than mono-cultures

ALP expression was positive in both, mono- and co-cultures, which displayed early osteoblastic differentiation. The mono-cultures of HBMSCs on PLA showed similar ALP level with or without osteoblastic induction after 14 days. ALP was concentrated on the struts of the membranes. In the co-cultures performed on PLA, ALP

staining covered all the surface of the membranes and pores. The ALP expression was especially high for co-cultures, which has already been described using co-cultures of HBMSCs and EPCs [44], probably because of the higher production of the extracellular matrix.

We have observed that the highest cell proliferation and viability in 2D on PLA appeared in the case of co-culture system. Then we have performed layer-by-layer bioassembly of cellularized membranes in 3D: All tridimensional LBL constructs were made of four layers of PLA membranes seeded with human primary cells. Even if we have used glass rings to stabilize the 3D constructs in culture plates, the materials were difficult to manipulate. Other groups have proposed to use of stainless steel mesh clips to stabilize the LBL constructs after the assembly [29]. Since we could observe the most efficient cell proliferation in co-culture samples in 2D, we decided to test osteoblastic genes expressions in culture samples with combination of 2 cell types with their different organization in aim to see if their 3D organization has an influence in osteoblastic differentiation. Control sample was mono-culture HBMSCs LBL construct (without EPCs). We have observed that OCN and ALP had the highest relative gene expression for both LBL types. It was expected since it has already been known that they genes are expressed earlier than others. The expressions of RunX2 and Col1 were lower. But we have not observed any significant difference between the two different LBL constructs concerning the expression of osteoblastic genes. There was no difference between two different types of LBL constructs containing EPCs.

Since the positions and different combinations of HBMSCs with EPCs in layers did not play an important role in osteoblastic differentiation, we have done new LBL constructs to observe the colonization of cells inside the layers. Cells were tagged in order to observe their migration between layers of PLA. The HBMSCs were tagged by GFP (green fluorescence) and EPCs were tagged by Td Tomato (red fluorescence). The tested 3D construct had alternating layers of monocultures HBMSCs-GFP and co-cultures HBMSCs-GFP + EPCs-TdT. Red color was present in all layers meaning that EPCs have probably migrated inside the LBL constructs.

5 Conclusions and perspectives

Fabrication of thin porous PLA membranes by direct 3D printing was successfully performed. Evaluations of viability, phenotypes maintain and proliferation of human primary cells cultured on PLA were positive: Cell proliferation increased with time in both, mono- and co-culture conditions. The level of ALP expression was higher in co-culture systems. We successfully made LBL constructs by

assembling four layers of cellularized PLA membranes. Experiments of these 3D constructs have shown an osteoblastic differentiation after 7 days of culture as well as the cell colonization inside the constructs. This showed the potential of LBL approach to promote a homogenous cell distribution inside the scaffold. 3D experiments have shown that LBL bio-assembly enables better cell proliferation and differentiation into the scaffold than conventional BTE. Results obtained indicate that LBL approach could be suitable for bone tissue engineering, in order to promote homogenous cell distribution into the scaffold.

Acknowledgements The authors wish to thank the French Institute in Belgrade, Serbia, via Campus France agency. 2-photon observations were done at Bordeaux Imaging Center, France.

Conflict of interest The authors declare that they have no conflict of interest.

References

1. Arealis G, Nikolaou VS. Bone printing: new frontiers in the treatment of bone defects. *Injury*. 2015;46(Suppl 8):S20–2.
2. O'Brien FJ. Biomaterials and scaffolds for tissue engineering. *Mater Today*. 2011;14(3):88–95.
3. Oliveira H, et al. The proangiogenic potential of a novel calcium releasing biomaterial: impact on cell recruitment. *Acta Biomater*. 2016;29:435–45.
4. Feng T, Liu Y, Xu Q, Li X, Luo X, Chen Y. In vitro experimental study on influences of final degradation products of polyactic acid on proliferation and osteoblastic phenotype of osteoblast-like cells. *J Repair Reconstr Surg*. 2014;28(12):1525–9.
5. Saito E, Suarez-Gonzalez D, Murphy WL, Hollister SJ. Bio-mineral coating increases bone formation by ex vivo BMP-7 gene therapy in rapid prototyped poly(L-lactic acid) (PLLA) and poly(ϵ -caprolactone) (PCL) porous scaffolds. *Adv Healthc Mater*. 2015;4(4):621–32.
6. Ciocca L, De Crescenzo F, Fantini M, Scotti R. CAD/CAM and rapid prototyped scaffold construction for bone regenerative medicine and surgical transfer of virtual planning: a pilot study. *Comput Med Imaging Graph*. 2009;33(1):58–62.
7. Mangano F, et al. Maxillary ridge augmentation with custom-made CAD/CAM scaffolds. A 1-year prospective study on 10 patients. *J Oral Implantol*. 2014;40(5):561–9.
8. Nga NK, Hoai TT, Viet PH. Biomimetic scaffolds based on hydroxyapatite nanorod/poly(D,L) lactic acid with their corresponding apatite-forming capability and biocompatibility for bone-tissue engineering. *Colloids Surf B*. 2015;128:506–14.
9. Lou T, Wang X, Song G, Gu Z, Yang Z. Fabrication of PLLA/ β -TCP nanocomposite scaffolds with hierarchical porosity for bone tissue engineering. *Int J Biol Macromol*. 2014;69:464–70.
10. D'Alessandro D, et al. Processing large-diameter poly(L-lactic acid) microfiber mesh/mesenchymal stromal cell constructs via resin embedding: an efficient histologic method. *Biomed Mater Bristol Engl*. 2014;9(4):045007
11. Zamparelli A, et al. Growth on poly(L-lactic acid) porous scaffold preserves CD73 and CD90 immunophenotype markers of rat bone marrow mesenchymal stromal cells. *J Mater Sci Mater Med*. 2014;25(10):2421–36.
12. Kao C-T, Lin C-C, Chen Y-W, Yeh C-H, Fang H-Y, Shie M-Y. Poly(dopamine) coating of 3D printed poly(lactic acid) scaffolds for bone tissue engineering. *Mater Sci Eng C*. 2015;56:165–73.
13. Hu Y, Zou S, Chen W, Tong Z, Wang C. Mineralization and drug release of hydroxyapatite/poly(L-lactic acid) nanocomposite scaffolds prepared by pickering emulsion templating. *Colloids Surf B Biointerfaces*. 2014;122:559–65.
14. Ding M, Henriksen SS, Wendt D, Overgaard S. An automated perfusion bioreactor for the streamlined production of engineered osteogenic grafts. *J Biomed Mater Res B*. 2015;104:532–537.
15. Lian Q, Zhuang P, Li C, Jin Z, Li D. Mechanical properties of polylactic acid/beta-tricalcium phosphate composite scaffold with double channels based on three-dimensional printing technique. *Chin J Repair Reconstr Surg*. 2014;28(3):309–13.
16. Ronca A, et al. Large defect-tailored composite scaffolds for in vivo bone regeneration. *J Biomater Appl*. 2014;29(5):715–27.
17. Hamad K. Properties and medical applications of polylactic acid: a review. *Express Polym Lett*. 2015;9(5):435–55.
18. Vidyasekar P, Shyamsunder P, Sahoo SK, Verma RS. Scaffold-free and scaffold-assisted 3D culture enhances differentiation of bone marrow stromal cells. *In Vitro Cell Dev Biol Anim*. 2016;52(2):204–17.
19. Huang J, et al. Evaluation of the novel three-dimensional porous poly (L-lactic acid)/nano-hydroxyapatite composite scaffold. *Biomed Mater Eng*. 2015;26(Suppl 1):S197–205.
20. Giordano RA, Wu BM, Borland SW, Cima LG, Sachs EM, Cima MJ. Mechanical properties of dense polylactic acid structures fabricated by three dimensional printing. *J Biomater Sci Polym Ed*. 1996;8(1):63–75.
21. Almeida CR, Serra T, Oliveira MI, Planell JA, Barbosa MA, Navarro M. Impact of 3-D printed PLA- and chitosan-based scaffolds on human monocyte/macrophage responses: unraveling the effect of 3-D structures on inflammation. *Acta Biomater*. 2014;10(2):613–22.
22. Serra T, Mateos-Timoneda MA, Planell JA, Navarro M. 3D printed PLA-based scaffolds: a versatile tool in regenerative medicine. *Organogenesis*. 2013;9(4):239–44.
23. Schlaubitz S, et al. Pullulan/dextran/nHA macroporous composite beads for bone repair in a femoral condyle defect in rats. *PLoS One*. 2014;9(10):e110251
24. Groll J, et al. Biofabrication: reappraising the definition of an evolving field. *Biofabrication*. 2016;8(1):013001
25. Sathy BN, Mony U, Menon D, Baskaran VK, Mikos AG, Nair S. Bone tissue engineering with multilayered scaffolds-part I: an approach for vascularizing engineered constructs in vivo. *Tissue Eng Part A*. 2015;21(19–20):2480–94.
26. Ren L, et al. Preparation of three-dimensional vascularized MSC cell sheet constructs for tissue regeneration. *BioMed Res Int*. 2014;2014:301279
27. Nishiguchi A, Matsusaki M, Asano Y, Shimoda H, Akashi M. Effects of angiogenic factors and 3D-microenvironments on vascularization within sandwich cultures. *Biomaterials*. 2014;35(17):4739–48.
28. Derda R, et al. Paper-supported 3D cell culture for tissue-based bioassays. *Proc Natl Acad Sci USA*. 2009;106(44):18457–62.
29. Wan W, et al. Layer-by-layer paper-stacking nanofibrous membranes to deliver adipose-derived stem cells for bone regeneration. *Int J Nanomedicine*. 2015;10:1273–90.
30. Catros S, et al. Layer-by-layer tissue microfabrication supports cell proliferation in vitro and in vivo. *Tissue Eng Part C Methods*. 2012;18(1):62–70.
31. Wen L, et al. Role of endothelial progenitor cells in maintaining stemness and enhancing differentiation of mesenchymal stem cells by indirect cell–cell interaction. *Stem Cells Dev*. 2016;25(2):123–38.

32. Eldesoqi K, et al. Safety evaluation of a bioglass-poly(lactic acid) composite scaffold seeded with progenitor cells in a rat skull critical-size bone defect. *PLoS One*. 2014;9(2):e87642
33. Vilamitjana-Amedee J, Bareille R, Rouais F, Caplan AI, Harmand MF. Human bone marrow stromal cells express an osteoblastic phenotype in culture. *In Vitro Cell Dev Biol Anim*. 1993;29A(9):699–707.
34. Thebaud NB, Bareille R, Remy M, Bourget C, Daculsi R, Bordenave L. Human progenitor-derived endothelial cells vs. venous endothelial cells for vascular tissue engineering: an in vitro study. *J Tissue Eng Regen Med*. 2010;4(6):473–84.
35. Thebaud NB, et al. Labeling and qualification of endothelial progenitor cells for tracking in tissue engineering: an in vitro study. *Int J Artif Organs*. 2015;38(4):224–32.
36. Lau KR, Evans RL, Case RM. Intracellular Cl⁻ concentration in striated intralobular ducts from rabbit mandibular salivary glands. *Pflug Arch Eur J Physiol*. 1994;427(1–2):24–32.
37. Poole CA, Brookes NH, Clover GM. Keratocyte networks visualised in the living cornea using vital dyes. *J Cell Sci*. 1993;106(Pt 2):685–91.
38. Vaughan PJ, Pike CJ, Cotman CW, Cunningham DD. Thrombin receptor activation protects neurons and astrocytes from cell death produced by environmental insults. *J Neurosci*. 1995;15(7):5389–401. Pt 2
39. Metcalf DJ, Nightingale TD, Zenner HL, Lui-Roberts WW, Cutler DF. Formation and function of Weibel-Palade bodies. *J Cell Sci*. 2008;121(Pt 1):19–27.
40. Szczurek AT, et al. Single molecule localization microscopy of the distribution of chromatin using Hoechst and DAPI fluorescent probes. *Nucl Austin Tex*. 2014;5(4):331–40.
41. Serra T, Ortiz-Hernandez M, Engel E, Planell JA, Navarro M. Relevance of PEG in PLA-based blends for tissue engineering 3D-printed scaffolds. *Mater Sci Eng C*. 2014;38:55–62.
42. Ahn S, Lee H, Kim G. Functional cell-laden alginate scaffolds consisting of core/shell struts for tissue regeneration. *Carbohydr Polym*. 2013;98(1):936–42.
43. Aguirre A, Planell JA, Engel E. Dynamics of bone marrow-derived endothelial progenitor cell/mesenchymal stem cell interaction in co-culture and its implications in angiogenesis. *Biochem Biophys Res Commun*. 2010;400(2):284–91.
44. Grellier M, Bordenave L, Amédée J. Cell-to-cell communication between osteogenic and endothelial lineages: implications for tissue engineering. *Trends Biotechnol*. 2009;27(10):562–71.

Characterization of printed PLA scaffolds for bone tissue engineering

Agathe Grémare^{1,2}, Vera Guduric¹, Reine Bareille¹, Valérie Heroguez³, Simon Latour⁴, Nicolas L'Heureux¹, Jean-Christophe Fricain^{1,2}, Sylvain Catros^{1,2,#}, Damien Le Nihouannen^{1,#,*}

¹ Univ. Bordeaux, Inserm, Tissue Bioengineering, U1026, F-33076, Bordeaux, France

² Univ. Bordeaux, Inserm, Tissue Bioengineering, U1026, CHU Bordeaux, Services d'Odontologie et de Santé Buccale, F-33076, Bordeaux, France

³ Univ. Bordeaux, IPB-ENSCBP, CNRS, Laboratoire de Chimie des Polymères Organiques, UMR5629, F-33607 Pessac, France

⁴ Univ. Bordeaux, Institut Bergonié, Inserm, ACTION, U1218, F-33076, Bordeaux, France

Equally contributed to the study

* Corresponding author: INSERM U1026, BioTiS - Tissue Engineering - Université de Bordeaux, 146 rue Léo Saignat, CS 61292, CP 45, 33076 Bordeaux Cedex, France. Email: damien.le-nihouannen@u-bordeaux.fr

Key Words:

- Fused Deposition Modeling
- PolyLactic Acid
- Scaffolds
- Physicochemical characterization
- Biocompatibility

This article has been accepted for publication and undergone full peer review but has not been through the copyediting, typesetting, pagination and proofreading process which may lead to differences between this version and the Version of Record. Please cite this article as an 'Accepted Article', doi: 10.1002/jbm.a.36289

Abstract

Autografts remain the gold standard for orthopedic transplantations. However, to overcome its limitations, bone tissue engineering proposes new strategies. This includes the development of new biomaterials such as synthetic polymers, to serve as scaffold for tissue production. The objective of this present study was to produce poly(lactic) acid (PLA) scaffolds of different pore size using fused deposition modeling (FDM) technique and to evaluate their physicochemical and biological properties. Structural, chemical, mechanical and biological characterizations were performed. We successfully fabricated scaffolds of three different pore sizes. However, the pore dimensions were slightly smaller than expected. We found that the 3D printing process induced decreases in both, PLA molecular weight and degradation temperatures, but did not change the semi-crystalline structure of the polymer. We did not observe any effect of pore size on the mechanical properties of produced scaffolds. After the sterilization by γ irradiation, scaffolds did not exhibit any cytotoxicity towards human bone marrow stromal cells (HBMSC). Finally, after three and seven days of culture, HBMSC showed high viability and homogenous distribution irrespective of pore size. Thus, these results suggest that FDM technology is a fast and reproducible technique that can be used to fabricate tridimensional custom-made scaffolds for tissue engineering.

Introduction

Orthopedic surgical procedures involving bone grafting have increased in the last few decades making bone as one of the most transplanted tissue [1]. Autografts remain the gold standard solution. However, drawbacks such as limited tissue availability, pain, donor site morbidity and difficulty in producing anatomical shapes [2] have favored the development of engineered implants. Bone tissue engineering has thus become a promising approach to fabricate bone substitutes through the association of specific bone cells, growth factors and porous biocompatible scaffold [3]. An ideal scaffold for bone reconstruction should be (i) biocompatible and porous to support cell proliferation and differentiation, (ii) biodegradable to be gradually replaced by the host tissue, (iii) osteoconductive and osteoinductive and (iv) manufactured in a specific shape to precisely match complex bone defects [1].

Solid freeform fabrication techniques, also known as additive manufacturing (AM), have emerged as a new tool for the fabrication of 3D scaffolds for bone tissue engineering with well-defined and reproducible architectures, allowing the creation of an accurate 3D anatomic model of a specific bone tissue for a particular patient. Several techniques have been developed for AM such as stereolithography (SLA) [4], selective laser sintering (SLS) [5], three-dimensional printing (3DP) [6], fused deposition modeling (FDM) [7] for the production of custom, defect-matched constructs for bone repair [8]. FDM is the most commonly used technique in which the material, a filament, is melted, extruded and deposited to generate a three-dimensional structure in a layer-by-layer fashion with the benefit of controlling both the porosity and the pore size [9]. Another advantage of FDM technology is the ease to associate cells with these thin polymeric scaffolds resulting in a better cell colonization, proliferation and differentiation compared with a larger 3D structure which often includes an inner hypoxic central area, which prevents deep cell colonization. Moreover, stacked together, these populated scaffolds can form a large 3D structure within an internal organization improving both cell communication and cell-material interactions *in vitro* and *in vivo* [10-12].

Biocompatible and biodegradable polymeric materials are commonly used for tissue engineering scaffolding [13]. Numerous degradable polymers such as poly(acrylonitrile butadiene styrene) (ABS), polycaprolactone (PCL), polylactic acid (PLA), polyglycolic acid (PGA), and chitosan can be used to fabricate 3D scaffolds [14]. In tissue engineering applications, ABS, PCL and PGA are used for bone, tendon and skin repair [15-18]. Composites polymeric materials like PCL-HA or PCL-TCP have also been produced by FDM and thus been used in bone tissue engineering for their mechanical and biochemical properties [19]. Chitosan is a well-known biodegradable polymer used to print scaffolds for tissue engineering purposes and has been shown to modulate macrophages' cytokine production *in vitro* [20, 21]. PLA is a hydrophobic aliphatic polyester approved by the US Food and Drug Administration (FDA) for different biomedical and clinical applications [22]. PLA, because of its excellent biocompatibility, thermal stability and degradation of PLA, as well as low viscosity and thermoplastic properties, has been shown through numerous studies well-suited for the FDM technology [23]. Generally, the thermal stability and degradation properties of PLA are dependent on the choice and distribution of stereoisomers within the polymers chains (L/D ratios) and molecular weights. Depending on the choice of pre-polymers and route of synthesis, a vast diversity of PLA can be achieved resulting in PLA with a broad range of physiochemical properties. The composition of PLA significantly affects crystallization kinetics and the ultimate extent of crystallinity. In turn, the level of crystallinity developed is particularly influential on the PLA glass transition temperature (T_g), melting temperature (T_m) and degradation rate [24]. T_g and T_m of PLA are approximately 55 °C and 180 °C, respectively. PLA degrades by hydrolysis and degradation products in the form of oligomers are metabolized by cells [25]. This material has often been used in skeletal tissue engineering [26, 27]. The degradation products of this polymer are not toxic. They are present in the human body and are removed by natural metabolic pathways [28]. Despite previous publications showing the possibility to associate printing PLA scaffolds with bone marrow cells, only biological properties of the printed

scaffolds are really investigated. However, it is important to know if the original material is modified through the various stages of the shaping process and how its final geometry might predict the important properties for its use in vivo. To our knowledge, no study has been conducted on the reliability of the fabrication of porous scaffolds by FDM and to explore this influence of fabrication process on materials properties.

Thus, the aim of the present study was, to print PLA scaffolds with a custom-made FDM printer at high resolution and in a reproducible manner. We have characterized the physical properties of the printed scaffolds (pore size and thread diameter) and the reproducibility of the technique. Importantly, we also assessed whether the printing process and the different porosities affected PLA chemical and mechanical properties. Finally, we investigated the biocompatibility of printed PLA scaffolds towards human bone marrow cells (HBMSC).

Materials and Methods

Scaffolds fabrication

Poly(lactic) acid filament (PLA; ESUN[®], natural, diameter 1.75mm) was used to fabricate scaffolds with a custom-made 3D printer, developed and assembled by “Technoshop” in the Technological Department at the Université of Bordeaux (IUT de Bordeaux, France). The working principle of this printer is based on FDM technology. Briefly, clump generator software[®] was used to create squared pores into a 3D object in a “stl” file format. The printing head was computer-controlled in three axes (x, y, z with a xy speed of 30 mm.s⁻¹) while extruding the PLA filament using the Repetier-Host software. A gear system guided the filament into the printing head, heated at a temperature above the PLA melting point (temperature near the nozzle was 186 °C). The melted PLA was then extruded through a 100 µm diameter stainless-steel nozzle onto a printing plate heated at 60 °C. Porous scaffolds were printed layer-by-layer in the form of squares surrounded by a dense PLA perimeter. We fabricated scaffolds with 4 different pore sizes (0, 150, 200, 250 µm). Prior to

mechanical and biological evaluations, printed scaffolds were sterilized by gamma irradiation (25 kGy, 84 hours, room temperature; Nordion[®], GC 3000).

Structural characterization of the scaffolds after printing

Printed PLA scaffolds were observed using a binocular (Leica[®], MZ10F) and a scanning electron microscope (SEM; Hitachi[®], S-2500). To confirm the reliability of the printing technique, the expected pore size and thread diameter were compared with the actual pore and thread dimensions of printed scaffolds. For each pore size (150, 200 and 250 μm), three scaffolds were printed and four pictures were then taken per scaffold using binocular microscopy. After thresholding the images with ImageJ[®] software (NIH), a plug-in was written to automatically calculate pore dimensions (pore length and pore width were pooled) and thread diameter. Both for pore length and thread diameter, more than 330 measurements were realized per scaffold resulting in a total number of more than 1200 measurements.

Physicochemical and thermomechanical characterizations of the scaffolds before and after printing

PLA molecular weight estimation (size exclusion chromatography). After solubilization of the PLA in tetrahydrofuran (THF, 0.2 %), a pumping system associated with an injector introduced the sample into the column at a constant and reproducible rate (THF flow rate of 1 $\text{ml}\cdot\text{min}^{-1}$, at 40 °C). Macromolecules were then detected by a refractive index detector at the exit of the column (Agilent Technologies, PL-GPC50 Plus; TOSOH TSK, G4000HXL) using polystyrene calibration.

Determination of the polymer thermal degradation profile (thermogravimetric analysis). The sample was placed in the balance system (under N_2 , with a heating rate of 10 $^{\circ}\text{C}\cdot\text{min}^{-1}$; TA Instruments[®], TGA Q500).

Determination of the polymer morphology (amorphous or crystalline parts) (differential scanning calorimetry). By measuring the difference in heat flow between the PLA and the reference,

the amount of heat absorbed during a fusion endothermic phase transition or released during a crystallization exothermic phase transition during a transition process can be determined. Then, glass, melting and crystallization transition temperatures, as well as the enthalpies are measured (under N₂ with a gas flow of 25 ml.min⁻¹, heating/cooling rate of 10 °C.min⁻¹; TA Instruments[®], DSC RCS).

● Mechanical evaluation of the sterilized printed scaffolds

To investigate the possible influence of pore dimensions on mechanical properties of the printed PLA mesh, a uniaxial tensile test was performed on sterilized scaffolds. Five scaffolds were tested for each pore size (150, 200 and 250 μm). Two opposite sides of PLA dense perimeter were cut with a scalpel in their midsection. PLA scaffolds were attached by the two intact opposite sides of the perimeter with pneumatic grips (4 bars in grip pressure) of an Autograph AGS-X (Shimadzu[®]). Scaffolds were stretched at a speed of 10 mm / min until failure. Maximal strength before rupture (F_{max}) was then recorded using the Trapezium X[®] software.

Biological evaluation of the sterilized printed scaffolds

Isolation and culture of human bone marrow stromal cells (HBMSC). All human samples were collected in accordance with the French Ministry of Higher Education and Research and National Institute for Health and Medical Research (agreement DC-2008-412). Human bone marrow samples were collected during orthopedic surgeries. HBMSC were isolated and cultured [29]. Briefly, a single-cell suspension was obtained by sequential passages of the aspirate through 16-, 18-, and then 21-gauge needles. After centrifugation the pellet was resuspended in Minimum Essential Medium Alpha Modification (α-MEM; Gibco[®], Cat No. A10400-02), supplemented with 10% fetal bovine serum (FBS; Biowest[®]) and 0.1% plasmocin antibiotics (Invitrogen[®], Cat No. MPP-37-02A) and plated at a density of 5 x 10⁵ cells / cm² onto 75 cm² tissue culture flasks and incubated at 37 °C in a humidified atmosphere containing 5% CO₂ in air. The culture medium was changed every 2 days, thereby removing non-adherent cells. After 11 days of culture, HBMSC were obtained [30].

Cytotoxicity evaluation. Sterile printed scaffolds cytotoxicity was evaluated according to the NF EN 30993-5 ISO 10993-5 standard, by measuring both HBMSC metabolic activity and HBMSC cellular viability using a 3-(4,5-dimethylthiazol-2-yl) diphenyl tetrazolium (MTT) assay and a Neutral Red assay, respectively. For both assays, medium extracts were prepared according to the NF EN 30993-5 ISO 10993-5 standard by incubating scaffolds in culture media with a ratio between the immersed surface of the scaffold and the volume of the medium (from 3 to 6 cm² / mL). Three scaffolds of each porosity were individually brought into contact with 1 mL of medium "Iscove's Modified Dulbecco's Medium" (IMDM) + Glutamax (Invitrogen[®], Cat No 31980-022). Scaffolds were incubated for 3 days at 37 °C in a humidified atmosphere containing 5% CO₂ in air. Medium extracts were collected after one (E1), two (E2) and three days (E3) and stored at 4 °C. For both MTT and Neutral Red assays, HBMSC were plated at 10⁴ cells / cm² in 96-well plates and cultured during 72 hours to reach sub-confluence (80%). After removal of culture media, pure medium extracts (E1, E2 and E3) were added. Being recognized to induce a cytotoxic response in a reproducible way, Triton 100X (0.1%) was used as a positive control and IMDM culture medium alone was used as negative control. Plates were incubated during 24 hours in a humidified atmosphere containing 5% CO₂ in air. After 24 hours of incubation between cells with medium extracts, the culture medium was removed and the cell layer was washed with Hank's solution (Gibco[®], Cat No. 14065-049). The stock solution of MTT (Sigma-Aldrich Co, Cat No M2128; 5 mg / mL in 0.1 M PBS, pH = 7.4) was diluted (20% in IMDM without phenol red (Gibco[®], Cat No. 21056-023)) and 125 µl of this solution was added in each well. After 3 hours of incubation at 37 °C in a humidified atmosphere containing 5% CO₂ in air, the supernatant was removed and formed formazan crystals were dissolved in adding 100 µl of dimethyl sulfoxide (DMSO; Sigma-Aldrich Co, Cat No. D5879-1L). The intensity of the staining was quantified by measuring the absorbance at 540 nm using a spectrophotometer (Perkin Elmer[®], 2030 Multilabel Reader Victor[™]X3). After 24 hours of incubation between cells with medium extracts, the culture

medium was removed and the cell layer was washed with Hank's solution. The Neutral Red (Sigma-Aldrich Co, N4638) was diluted (1.25% (w/v) in IMDM supplemented with 10% FBS) and 100 μ l of this solution was added in each well. After 3 hours of incubation at 37 °C in a humidified atmosphere containing 5% CO₂ in air, the supernatant was removed and cells were lysed with 100 μ l of a solution made of 1% acetic acid in 50% ethanol. The intensity of the staining was quantified by measuring the absorbance at 540 nm using a spectrophotometer (Perkin Elmer[®], 2030 Multilabel Reader Victor[™]X3).

Live/dead assay. Human bone marrow stromal cells were seeded onto the surface of sterile PLA printed scaffolds (3 for each pore size) into 24-well plates at a final density of 10⁵ cells / cm² and incubated at 37 °C in a humidified atmosphere containing 5% CO₂ in air. Prior to experiment, each well was coated with 1 mL of agarose (Sigma-Aldrich Co, A9539; 2% (w/v) in 1X PBS) to avoid cell adhesion on the tissue culture plastic. Each scaffold was also stabilized with a glass ring crimped by agarose. After 3 and 7 days of culture, cell viability was determined using live/dead assay (Invitrogen[®], Cat No L3224). After 3 and 7 days of culture, medium was removed and PLA printed scaffold seeded with HBMSC were washed with Hank's solution. Scaffolds were then incubated with the live/dead assay staining solution at 37 °C in a humidified atmosphere containing 5% CO₂ in air. After 15 minutes of incubation, scaffolds were rinsed with Hank's solution. Fluorescent green and red stainings were visualized at 568 nm and 488 nm respectively for excitation and 600 nm and 520 nm for emission with fluorescence confocal microscope (Leica[®], TCS DMI 4000B).

Statistical analysis

Data are presented as representative images, representative experiments or as means \pm standard deviation of the mean, with n indicating the number of independent samples or pictures. For the structural characterization (measured vs expected diameter of the thread) and the biological evaluation of the scaffolds, the differences were assessed by two-tailed one-sample t-test and accepted as

statistically significant at $p < 0.05$. For both the structural characterization (the 3 measured diameter threads) and the mechanical tests of the scaffolds, the differences were evaluated by non-parametric Kruskal-Wallis test and accepted as statistically significant at $p < 0.05$.

Results

Physical characterization of PLA printed scaffolds

PLA scaffolds were printed as a mesh with square pores in a solid frame (Fig. 1A). Scaffold total area was $0.67 \pm 0.04 \text{ cm}^2$ and the scaffold thickness was $206 \pm 4 \text{ }\mu\text{m}$ ($n = 6$). Macroscopic and microscopic observations using binocular (Fig. 1A) and scanning electron microscopy (Fig. 1B) of the scaffolds showed regular straight threads of PLA printed layer-by-layer in both horizontal and vertical directions with perpendicular crossings. To study whether the printing technology was precise and reproducible, we assessed pore size and thread diameter of printed scaffolds with predicted pore dimensions 150 (P150), 200 (P200) and 250 μm (P250) (Fig. 1C, 1D). Image analysis showed that pore sizes were statistically lower than the predicted values by $8 \pm 9 \%$ ($138 \pm 13 \text{ }\mu\text{m}$), $5 \pm 5 \%$ ($190 \pm 11 \text{ }\mu\text{m}$) and $5 \pm 5 \%$ ($237 \pm 14 \text{ }\mu\text{m}$) for P150, P200 and P250 respectively. Conversely, thread diameter was statistically higher by $16 \pm 9 \%$ ($116 \pm 9 \text{ }\mu\text{m}$), $17 \pm 8 \%$ ($117 \pm 8 \text{ }\mu\text{m}$) and $18 \pm 9 \%$ ($118 \pm 9 \text{ }\mu\text{m}$) than the predicted values (i.e. 100 μm in all cases) for P150, P200 and P250 μm respectively. Interestingly, these deviations from predicted values were not statistically different between the 3 groups ($p > 0.05$). Thus, while the printing process was reproducible (with SDs $< 10\%$ of measured values), printed scaffolds exhibited both a lower pore dimension and a higher diameter thread than the expected values.

Physicochemical and thermomechanical characterizations of the PLA printed scaffolds

Size exclusion chromatography profiles indicated a decrease in 48 % of the PLA average molecular weight from 100 kDa before printing to 54 kDa after printing (Fig. 2A). In addition, the thermal degradation curves showed a decreased in the values of both beginning and ending degradation

temperatures from 293 °C and 370 °C before printing to 250 °C (-15 %) and 363 °C after printing, respectively. The decomposition of the material (around 100% mass loss) was obtained at 400 °C. Additionally, at the specific mass loss of 5% the degradation temperature is 326°C for the PLA before printing and only 280°C for the PLA after printing (Fig. 2B). Conversely, as shown on the “heating cycle 1” curves, the printing process did not apparently affect the phase change temperature profile of PLA and the crystallinity remains similar before and after printing with a degree of crystallinity of 23% and 24%, respectively. Nevertheless, a slight modification of both the glass transition temperature and the melting temperature was observed (Fig. 2C). Therefore, the printing process induced a shortening in PLA polymer chains and a decrease in degradation temperatures but the polymer retains an amorphous and crystalline character.

Mechanical properties of the sterilized PLA printed scaffolds

A similar breaking pattern was macroscopically observed for all tested scaffolds (Fig 3A). Tensile strengths of sterilized PLA mesh were assessed after cutting the frame. Sterile scaffolds with a pore dimension of 150, 200 and 250 µm did not exhibit statistically significant differences for ultimate tensile strength with values of 8 ± 2 N, 8 ± 1 N and 8 ± 1 N respectively (Fig. 3B). Thus, pore dimension did not affect the apparent ultimate strength of sterilized PLA printed scaffolds.

Biological evaluation of the sterilized PLA printed scaffolds

Media extracts of printed scaffolds did not significantly affect either the metabolic activity or the cell viability of HBMSC, which remained significantly higher than 70% of control HBMSC cultures (Fig 4A, 4B). Thus, these results demonstrated the absence of cytotoxic effect of PLA printed scaffolds. We then examined cell viability of HBMSC plated onto printed scaffolds of different pore dimensions. After 3 and 7 days of culture, confocal microscopy pictures showed that HBMSC were predominantly alive (green fluorescence) with only rare dead (red) cells (Fig. 4C). Cells had spread throughout the mesh and moved in the pores of PLA scaffolds with pore sizes of 150, 200 and 250 µm.

On non-porous scaffolds (0 μm), cells accumulated between PLA threads to form parallel lines of green viable cells. Taken together, these data show that sterile printed PLA scaffolds are suitable substrates for HBMSC culture.

Discussion

In this study, we have shown that PLA threads can be successfully printed in scaffolds with different pore sizes. The size and the shape of the PLA printed scaffolds were maintained after cooling, and sufficient mechanical integrity was acquired to allow easy handling. We found that structural characteristics of the scaffolds measured were different from the predicted values entered in the printing software. We demonstrated that after the printing process, PLA maintained a semi-crystalline structure even if the polymer chains were shortened and thermal degradation profile was changed. Finally, we observed that not only were all sterilized printed scaffolds biocompatible, but they also allowed bone cell colonization.

In the field of solid freeform fabrication techniques, FDM is the most commonly used because of (i) its cost-effectiveness, (ii) its ability to use different materials, (iii) the printing resolution ranges from several hundred micrometers to a few micrometers and (iv) its possibility to fabricate of 3D implantable materials to exactly match patient's bone defect [31]. In our study, 200 μm thick PLA scaffolds with square pores were produced by a custom-made 3D printer based on this principle. However, because of temperatures reached during FDM printing, cells cannot be incorporated into the scaffolds during the fabrication process. For this reason, cells were seeded onto printed PLA scaffolds after the process. Numerous studies have suggested the importance of scaffold pore size in bone tissue engineering and have shown that they should be typically between 100 μm and 300 μm to allow cell penetration, migration, growth as well as an optimal tissue vascularization [32]. Thus, scaffolds with 3 different pore sizes were fabricated and scaffolds with no pore were used as a control. In this study, we demonstrate with SEM and binocular observations that all printed scaffolds exhibited statistically lower

pore dimensions compared with predicted parameters. Similarly, thread diameter increased by about 17 % at all scaffold pore sizes and was also reproducible (with SDs < 10% of measured values). We hypothesize that the decrease in the pore sizes (around 12 μm for the three conditions) was due to the increase of the thread diameter (around 16 μm for the three conditions), which was probably generated by its spreading during the printing process.

PLA is commonly used in bone tissue engineering for scaffold production and it is approved by the FDA for clinical applications [22]. As reported previously, the physicochemical properties of PLA were modified during the printing process [33]. Indeed, the use of high temperature in the printer head to melt the polymer reduced by half its molecular weight (from 100 kDa to 54 kDa). We observed that the printed PLA started to degrade at a temperature 15 % lower than before printing, which might be a direct consequence of the shortening of the polymer chains. However, the degree of crystallinity remained similar and the printed PLA retained an amorphous and crystalline character. One solution would be to reduce the temperature in order to limit the formation of short polymer chains but that requiring keeping the right solution viscosity. [14].

Mechanical properties of formed scaffolds are of important for handling during the implantation process and can influence the remodeling of the tissue. Porous designs increase usable space of the scaffolds by increasing its surface area, however, pores can also be viewed as stress concentration sites that mechanically weaken the scaffold. In our system, increasing pore size decreased the number of thread on our PLA printed scaffolds with 31, 27 and 23 threads (measured in single orientation) for P150, P200 and P250, respectively. Our results demonstrate that, regardless of the porosity, PLA printed scaffolds displayed similar ultimate tensile forces (around 9.5 N). This may seem surprising since one would expect more threads to provide more strength. We hypothesize that the breakage of the scaffolds was initiated by a single (or a few) threads breaking first, then the remaining stress was concentrated on a neighboring thread creating a sort of chain reaction. This could suggest that all

threads were not equally tensed during the test. Over all, the modification of pore size was insufficient to induce a significant difference of the mechanical properties of the scaffolds.

Thermoplastics that are widely used in biomedical applications will not survive a standard steam or dry heat sterilization. Since printing is not performed in sterile conditions all PLA printed scaffolds were sterilized by gamma irradiation (25 KGy) before their use for mechanical and biological tests. This method avoids significant degradation by PLA chain scission [34]. Possible changes of PLA properties after gamma-radiation sterilization were not studied here but the biocompatibility of sterilized PLA printed scaffolds was evaluated. Previous studies showed that PLA degradation releases acidic monomers (lactic acid) that cause inflammation and this property could affect cell attachment and behavior [9]. However, lactic acid is present in the human body and is removed by natural metabolic pathways [9]. Three methods used in this study revealed no cytotoxic effect of PLA on primary human bone marrow cells. These observations are consistent with Zhang *et al.* who showed “low” effect of PLA scaffolds on viability and metabolism of osteoblastic like cell line (MC3T3-E1) [35]. Similarly, Lee *et al.* demonstrated significant adherence and proliferation of human mesenchymal stem cells on PLA [36]. In this study, cell colonization was observed predominantly in the pits of the grooves created by the juxtaposition of the PLA threads (P0) during the printing process. Additionally, we find that cellular alignment onto non-porous scaffolds which is parallel to PLA threads.

The success of a cell-populated scaffold implantation depends on two main parameters: scaffold design and cell incorporation [12]. To date, two methods of incorporating cells into scaffolds are being explored: (i) seeding of cells onto the surface of the scaffold following fabrication (top-down approach) and (ii) the incorporation of cells into the scaffold fabrication process (bottom-up approach). The small seeded PLA scaffolds produced in this study could be assembled to produce a larger volume scaffold like in the bottom up tissue engineering approach to achieve a homogeneous cells distribution in the final 3D construct [12]. Regardless of the method used to add cells to the 3D scaffolds,

vascularization remains a great challenge in tissue engineering. The addition of endothelial progenitor cells would be a possible approach to initiate vasculogenesis before implantation [37]. Also, PLA is often used in association with calcium phosphate particles to improve bone regeneration [23]. Scaffolds loaded by calcium phosphate nanoparticles could be used to promote osteoblast activity and bone tissue formation [38].

Taken together, our results demonstrate that our method to produce scaffolds allows the printing of PLA scaffolds with a suitable and controlled pore size resolution in a highly reproducible way. Despite polymer modification induced by printing, printed scaffolds were biocompatible with HBMSC. In the context of bone regeneration, 3D printing of scaffolds has become one of the most innovative approaches in surgery to provide personalized patients treatments and our study proves the possibility of creating populated scaffolds with precise dimensions that could be later assembled in a larger tissue engineered construct for bone repair.

Acknowledgements and Funding

We are grateful to Dr. Gérard Dimier (Univ. Bordeaux, LCPO, CNRS UMR5629) for the chemical characterization of our scaffolds and to Ms Marine Garat for her technical assistance. This research was funded by “Gueules cassées” foundation (57-2015), the ANR “Sandwich” (ANR-16-CE18-0009-01).

References

1. Gomez, S., et al., Design and properties of 3D scaffolds for bone tissue engineering. *Acta biomaterialia*, 2016. 42: p. 341-50.
2. Kalk, W.W., et al., Morbidity from iliac crest bone harvesting. *Journal of oral and maxillofacial surgery* : official journal of the American Association of Oral and Maxillofacial Surgeons, 1996. 54(12): p. 1424-9; discussion 1430.
3. Langer, R., Tissue engineering. *Molecular therapy : the journal of the American Society of Gene Therapy*, 2000. 1(1): p. 12-5.

4. Lee, J.W., et al., Bone regeneration using a microstereolithography-produced customized poly(propylene fumarate)/diethyl fumarate photopolymer 3D scaffold incorporating BMP-2 loaded PLGA microspheres. *Biomaterials*, 2011. 32(3): p. 744-52.
5. Wiria, F.E., et al., Poly-epsilon-caprolactone/hydroxyapatite for tissue engineering scaffold fabrication via selective laser sintering. *Acta biomaterialia*, 2007. 3(1): p. 1-12.
6. Fielding, G.A., A. Bandyopadhyay, and S. Bose, Effects of silica and zinc oxide doping on mechanical and biological properties of 3D printed tricalcium phosphate tissue engineering scaffolds. *Dental materials : official publication of the Academy of Dental Materials*, 2012. 28(2): p. 113-22.
7. Park, S.A., S.H. Lee, and W.D. Kim, Fabrication of porous polycaprolactone/hydroxyapatite (PCL/HA) blend scaffolds using a 3D plotting system for bone tissue engineering. *Bioprocess and biosystems engineering*, 2011. 34(4): p. 505-13.
8. Chen, Q., et al., 3D Printing Biocompatible Polyurethane/Poly(lactic acid)/Graphene Oxide Nanocomposites: Anisotropic Properties. *ACS applied materials & interfaces*, 2017. 9(4): p. 4015-4023.
9. Zhang, H., et al., Three dimensional printed macroporous polylactic acid/hydroxyapatite composite scaffolds for promoting bone formation in a critical-size rat calvarial defect model. *Science and technology of advanced materials*, 2016. 17(1): p. 136-148.
10. Catros, S., et al., Layer-by-layer tissue microfabrication supports cell proliferation in vitro and in vivo. *Tissue engineering. Part C, Methods*, 2012. 18(1): p. 62-70.
11. Tiruvannamalai-Annamalai, R., D.R. Armant, and H.W. Matthew, A glycosaminoglycan based, modular tissue scaffold system for rapid assembly of perfusable, high cell density, engineered tissues. *PloS one*, 2014. 9(1): p. e84287.
12. Guduric, V., et al., Layer-by-layer bioassembly of cellularized polylactic acid porous membranes for bone tissue engineering. *Journal of materials science. Materials in medicine*, 2017. 28(5): p. 78.
13. Felfel, R.M., et al., In vitro degradation and mechanical properties of PLA-PCL copolymer unit cell scaffolds generated by two-photon polymerization. *Biomedical materials*, 2016. 11(1): p. 015011.
14. Serra, T., et al., Relevance of PEG in PLA-based blends for tissue engineering 3D-printed scaffolds. *Materials science & engineering. C, Materials for biological applications*, 2014. 38: p. 55-62.

15. Cai, H., G. Azangwe, and D.E. Shepherd, Skin cell culture on an ear-shaped scaffold created by fused deposition modelling. *Bio-medical materials and engineering*, 2005. 15(5): p. 375-80.
16. Mozdzen, L.C., et al., Increasing the strength and bioactivity of collagen scaffolds using customizable arrays of 3D-printed polymer fibers. *Acta biomaterialia*, 2016. 33: p. 25-33.
17. Groppo, M.F., et al., The effect of a hydroxyapatite impregnated PCL membrane in rat subcritical calvarial bone defects. *Archives of oral biology*, 2017. 82: p. 209-215.
18. Raeisdasteh Hokmabad, V., et al., Design and fabrication of porous biodegradable scaffolds: a strategy for tissue engineering. *Journal of Biomaterials Science, Polymer Edition*, 2017. 28(16): p. 1797-1825.
19. Chia, H.N. and B.M. Wu, Recent advances in 3D printing of biomaterials. *Journal of biological engineering*, 2015. 9: p. 4.
20. Li, G., et al., Direct writing of chitosan scaffolds using a robotic system. *Rapid Prototyping Journal*, 2005. 11(2): p. 90-97.
21. Almeida, C.R., et al., Impact of 3-D printed PLA- and chitosan-based scaffolds on human monocyte/macrophage responses: unraveling the effect of 3-D structures on inflammation. *Acta biomaterialia*, 2014. 10(2): p. 613-22.
22. Tyler, B., et al., Polylactic acid (PLA) controlled delivery carriers for biomedical applications. *Advanced drug delivery reviews*, 2016. 107: p. 163-175.
23. Senatov, F.S., et al., Mechanical properties and shape memory effect of 3D-printed PLA-based porous scaffolds. *Journal of the mechanical behavior of biomedical materials*, 2016. 57: p. 139-48.
24. Lunt, J., Large-scale production, properties and commercial applications of polylactic acid polymers. *Polymer Degradation and Stability*, 1998. 59(1): p. 145-152.
25. Hamad, K., et al., Properties and medical applications of polylactic acid: A review. *Express Polymer Letters*, 2015. 9(5).
26. Schagemann, J.C., et al., Poly-epsilon-caprolactone/gel hybrid scaffolds for cartilage tissue engineering. *Journal of biomedical materials research. Part A*, 2010. 93(2): p. 454-63.

27. Holloway, J.L., A.M. Lowman, and G.R. Palmese, Mechanical evaluation of poly(vinyl alcohol)-based fibrous composites as biomaterials for meniscal tissue replacement. *Acta biomaterialia*, 2010. 6(12): p. 4716-24.
28. Barbieri, D., et al., Controlling dynamic mechanical properties and degradation of composites for bone regeneration by means of filler content. *Journal of the mechanical behavior of biomedical materials*, 2013. 20: p. 162-72.
29. Vilamitjana-Amedee, J., et al., Human bone marrow stromal cells express an osteoblastic phenotype in culture. *In vitro cellular & developmental biology. Animal*, 1993. 29A(9): p. 699-707.
30. Guerrero, J., et al., Cell interactions between human progenitor-derived endothelial cells and human mesenchymal stem cells in a three-dimensional macroporous polysaccharide-based scaffold promote osteogenesis. *Acta biomaterialia*, 2013. 9(9): p. 8200-13.
31. Liu, A., et al., 3D Printing Surgical Implants at the clinic: A Experimental Study on Anterior Cruciate Ligament Reconstruction. *Scientific reports*, 2016. 6: p. 21704.
32. Tarafder, S., et al., Microwave-sintered 3D printed tricalcium phosphate scaffolds for bone tissue engineering. *Journal of tissue engineering and regenerative medicine*, 2013. 7(8): p. 631-41.
33. Gentile, P., et al., An overview of poly(lactic-co-glycolic) acid (PLGA)-based biomaterials for bone tissue engineering. *International journal of molecular sciences*, 2014. 15(3): p. 3640-59.
34. Farah, S., D.G. Anderson, and R. Langer, Physical and mechanical properties of PLA, and their functions in widespread applications - A comprehensive review. *Advanced drug delivery reviews*, 2016. 107: p. 367-392.
35. Zhang, Y., et al., [Biocompatibility of Porous Poly Lactic Acid/Bone Matrix Gelatin Composite Biomaterials for Bone Repair]. *Zhongguo xiu fu chong jian wai ke za zhi = Zhongguo xiufu chongjian waike zazhi = Chinese journal of reparative and reconstructive surgery*, 2016. 30(2): p. 251-7.
36. Salerno, A., et al., Bio-safe processing of polylactic-co-caprolactone and polylactic acid blends to fabricate fibrous porous scaffolds for in vitro mesenchymal stem cells adhesion and proliferation. *Materials science & engineering. C, Materials for biological applications*, 2016. 63: p. 512-21.

37. Guerrero, J., et al., The use of total human bone marrow fraction in a direct three-dimensional expansion approach for bone tissue engineering applications: focus on angiogenesis and osteogenesis. *Tissue engineering. Part A*, 2015. 21(5-6): p. 861-74.
38. Oliveira, H., et al., The proangiogenic potential of a novel calcium releasing biomaterial: Impact on cell recruitment. *Acta biomaterialia*, 2016. 29: p. 435-45.

Figure legends

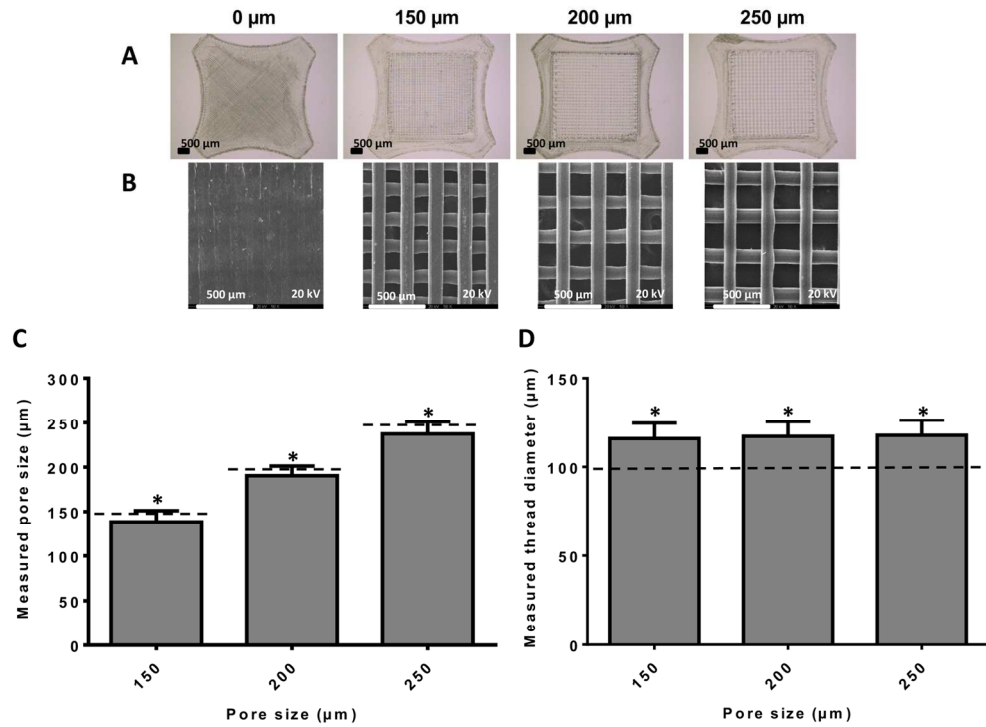
Figure 1. Structural and mechanical characterization of printed PLA scaffolds. Scaffolds with 0, 150, 200, 250 μm pore size were observed using binocular microscopy (A) and scanning electron microscopy (B). Printing reproducibility and accuracy were analyzed by quantification of both pore sizes (C) and thread diameter (D) determined by image analysis from binocular microscopy pictures. Dotted lines indicate the predicted values. Data are means \pm SD, $n = 3$ scaffolds and 4 pictures per scaffold, * $p < 0.05$ indicates significance compared to predicted values assessed by two-tailed one-sample t-test.

Figure 2. Physicochemical and thermomechanical characterizations of printed PLA scaffolds. Physicochemical and thermomechanical characterizations of PLA before and after 3D printing by FDM are displayed with red curves and with green curves, respectively. Results of size exclusion chromatographic assay (A), of thermogravimetric analysis (B) and differential scanning calorimetric assay (C).

Figure 3. Mechanical evaluation of printed PLA scaffolds. Macroscopic image of a PLA printed scaffold preparation before a uniaxial tensile test (A, left panel) and a ruptured PLA printed scaffolds (A, right panel). Green arrow indicates the PLA dense perimeter of the scaffold and red arrows indicate scalpel cuts made on two opposite sides of PLA dense perimeter. Maximal strengths before rupture of gamma-sterilized PLA printed scaffolds with pore sizes of 150 μm , 200 μm and 250 μm , were

determined using a uniaxial tensile test (after cutting sides of PLA dense perimeter) (B). Data are mean \pm SD, $n = 5$, no statistically significant difference was observed ($p > 0.05$).

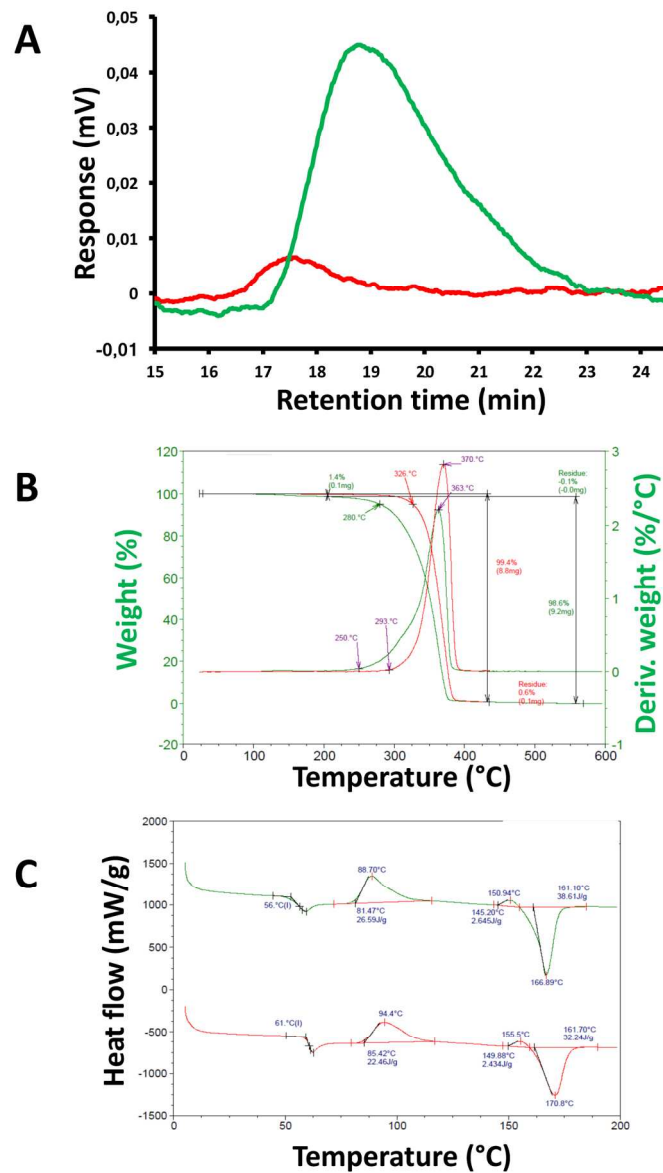
Figure 4. Biological evaluation of sterilized printed PLA scaffolds. Possible cytotoxic effect of PLA scaffolds towards HBMSC was evaluated using both MTT assay (A) and Neutral Red (NR) assay (B) and according to the NF-EN-ISO 10993-5 standard. Confluent HBMSC were cultured during 24h with medium previously incubated during 24 (D1), 48 (D2) and 72h (D3) with sterile scaffolds. Confluent HBMSC cultured during 24h with regular medium or with 0.1% Triton 100X were used as negative and positive control, respectively. Results were expressed in percentage compared to the negative control. On each graph, the dotted line indicates the limit (70%) of cytotoxicity according to NF-EN-ISO 10993-5 standard. Data are mean \pm SD, $n = 3$, * $p < 0.05$ indicates significance assessed by two-tailed one-sample t-test, compared to the limit (70%) of cytotoxicity. HBMSC colonization of sterilized PLA scaffolds was evaluated after 3 and 7 days of culture using fluorescent microscopy after live/dead staining (green/red) ($n=3$) (C). P indicates pores within the scaffolds.



Structural and mechanical characterization of printed PLA scaffolds.

148x108mm (300 x 300 DPI)

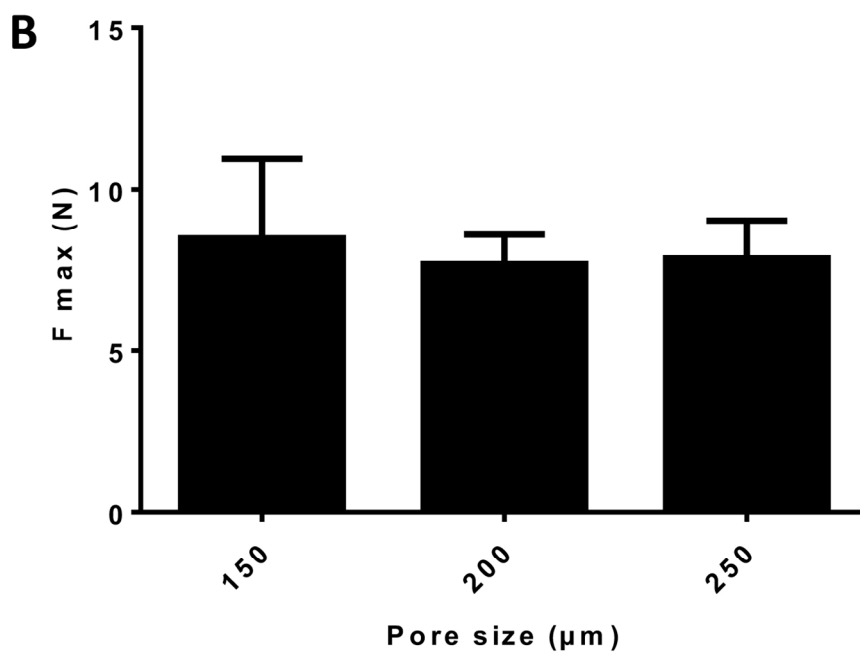
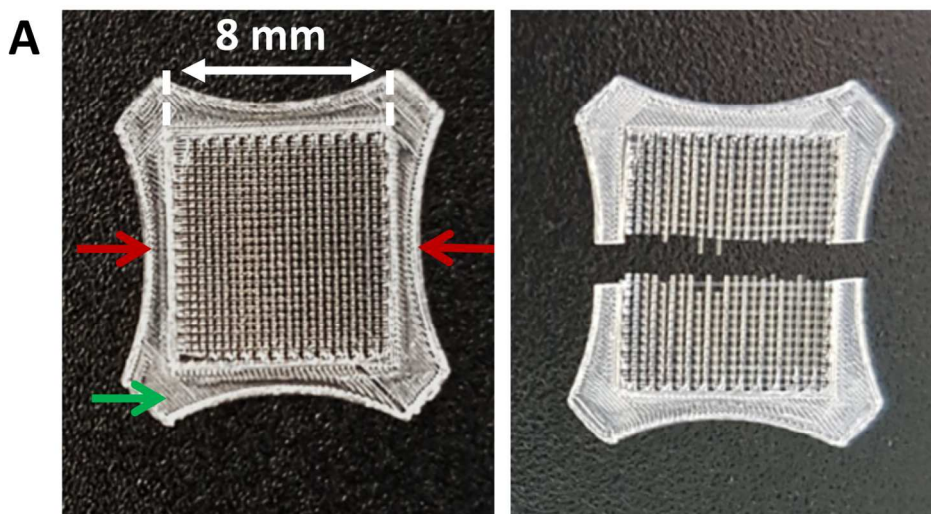
Accept



Physicochemical and thermomechanical characterizations of printed PLA scaffolds

108x189mm (300 x 300 DPI)

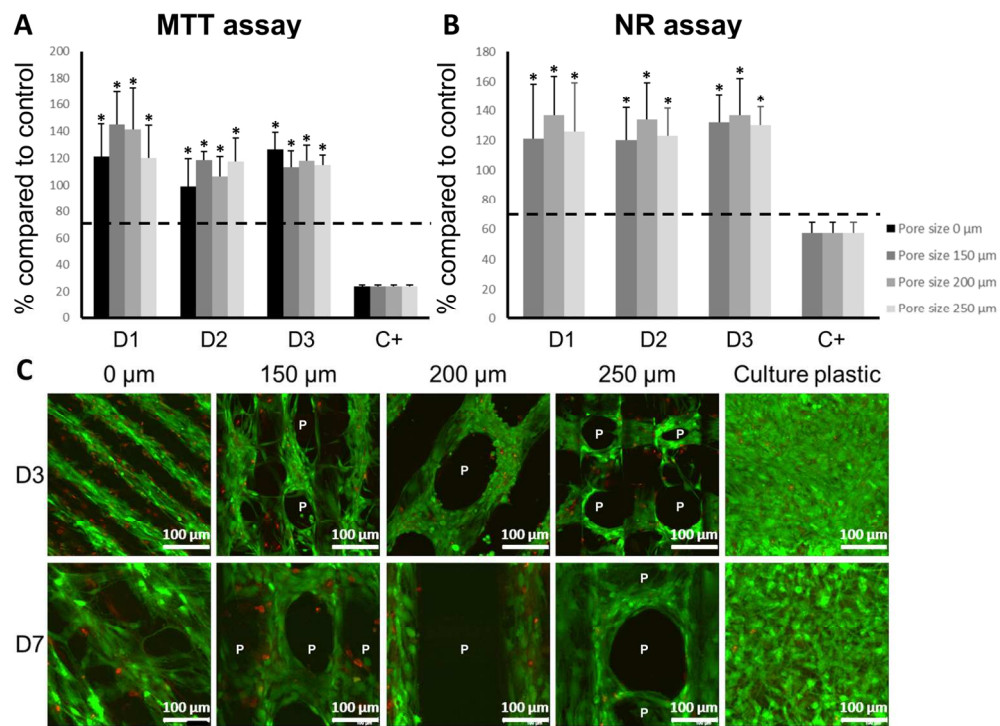
AC



Mechanical evaluation of printed PLA scaffolds

129x161mm (300 x 300 DPI)

AC



Biological evaluation of sterilized printed PLA scaffolds

150x111mm (300 x 300 DPI)

Accept



Rapid Prototyping Journal

Investigating impact of five build parameters on the maximum flexural force in FDM specimens - a definitive screening design approach

Ognjan B. Luzanin, Vera Guduric, Ivan Ristic, Simon Muhič,

Article information:

To cite this document:

Ognjan B. Luzanin, Vera Guduric, Ivan Ristic, Simon Muhič, "Investigating impact of five build parameters on the maximum flexural force in FDM specimens - a definitive screening design approach", Rapid Prototyping Journal, <https://doi.org/10.1108/RPJ-09-2015-0116>

Permanent link to this document:

<https://doi.org/10.1108/RPJ-09-2015-0116>

Downloaded on: 01 November 2017, At: 09:00 (PT)

References: this document contains references to 0 other documents.

To copy this document: permissions@emeraldinsight.com

The fulltext of this document has been downloaded 14 times since 2017*

Users who downloaded this article also downloaded:

, "Bonding quality and fracture analysis of polyamide 12 parts fabricated by fused deposition modeling", Rapid Prototyping Journal, Vol. 0 Iss ja pp. 00-00 https://doi.org/10.1108/RPJ-03-2016-0033

, "Edge quality in Fused Deposition Modeling: I. Definition and analysis", Rapid Prototyping Journal, Vol. 0 Iss ja pp. 00-00 https://doi.org/10.1108/RPJ-02-2016-0020

Access to this document was granted through an Emerald subscription provided by emerald-srm:459863 []

For Authors

If you would like to write for this, or any other Emerald publication, then please use our Emerald for Authors service information about how to choose which publication to write for and submission guidelines are available for all. Please visit www.emeraldinsight.com/authors for more information.

About Emerald www.emeraldinsight.com

Emerald is a global publisher linking research and practice to the benefit of society. The company manages a portfolio of more than 290 journals and over 2,350 books and book series volumes, as well as providing an extensive range of online products and additional customer resources and services.

Emerald is both COUNTER 4 and TRANSFER compliant. The organization is a partner of the Committee on Publication Ethics (COPE) and also works with Portico and the LOCKSS initiative for digital archive preservation.

*Related content and download information correct at time of download.

1. Introduction

Known under numerous names - Rapid Prototyping, Solid Freeform fabrication, Additive Manufacturing, 3D Printing, etc. - the technologies of layered manufacturing have been around for more than three decades. However, they have only recently gained popularity outside professional and academic circles due to explosion of affordable 3D printers on the market. The revolution was started by the expiration of patent for Fused Deposition Modeling (FDM) technology by the end of 2009 (US5121329, 2015), followed by the expiration of Deckard's patent for Selective Laser Sintering (SLS) in 2014 (US5597589, 2015) and 3D Systems' Method and Apparatus for Producing a Three-Dimensional Object by Stereolithography (SLA) in June 2015 (US5554336, 2015). Soon to follow is the expiration of patent rights for ZCorp's 3D Printing (3DP) technology, in December 2016 (US6007318, 2015).

Owing to expiration of patent rights, small start-up companies are now able to offer consumers 3D printers for as little as two to three hundred dollars. The affordability of FDM technology, for instance, spawned a host of novel applications of 3D printing. For example, a low-cost FDM printer has been recently used for building an Army/Navy surgical retractor from PLA at 1/10th the price of a stainless steel instrument (Rankin et al., 2014). Furthermore, FDM technology has also been successfully utilized in building a variety of components as part of In-situ resource utilization (ISRU) in space missions (Dunn et al, 2010), where it has been tested for zero-G capability. Many other examples like these, bring to prominence the issue of material selection, dimensional accuracy, mechanical properties, surface quality, etc. and the extent to which consumer-grade 3D printers can be used for research and business.

The phenomenon of widespread availability of FDM technology was followed by the introduction of eco-friendly Polylactic Acid (PLA) filament. Poly(lactic acid) is a linear aliphatic thermoplastic polyester, produced from renewable resources and is readily biodegradable as opposed to conventional polymers such as polyethylene (PE), polypropylene (PP), polyethylene terephthalate (PET) and polystyrene (PS) (Carrasco et al., 2010). Due to its low environmental impact, PLA has gained popularity in the domain of personal 3D printers due to several advantages. Beside eco-friendliness and renewability, it simplifies the printing equipment, since, unlike the ABS, it does not require build-platform heating, and is odour-free. PLA possesses the tensile strength and stiffness similar to polyethylene terephthalate and processing characteristics of polystyrene (Bijarimi, Ahmad and Rasid, 2012).

Considering consumer-class FDM printers and PLA as the material of choice, there is a growing body of research pertaining to various aspects of parameter selection and optimization aimed at achieving the best results in practical application. Ibrahim and Hafsa (2013) studied the dimensional accuracy and surface roughness of FDM-built part as a master pattern for Investment Casting (IC) process. The material used was Polylactic acid (PLA). They found that part orientation impacted both accuracy and surface roughness. In a similar study, Hafsa et al., 2013. evaluated dimensional accuracy and surface

roughness for hollow and solid part of FDM pattern for investment casting using Acrylonitrile Butadiene Styrene (ABS) and Polylactic acid (PLA). One of their findings was that although the ABS-built part performed better as the model, the PLA-built part produced better overall casting results. Another recent study by Afrose et al., 2014, used an open-source, low cost 3D Printer to investigate the tensile properties of the PLA thermoplastic material. The authors fabricated PLA specimens in different build orientations and reported tensile properties of PLA in different build orientations. Letcher and Waytashek (2014) also used low-cost FDM printer and PLA material to investigate the influence of raster orientation on tensile, flexural and fatigue properties of specimens. Tymrak, Kreiger and Pearce (2014) conducted a recent investigation of basic tensile strength and elastic modulus of components printed from ABS and PLA materials, in realistic (uncontrolled) environment conditions, using open-source 3D printers. The authors varied layer height and deposition pattern orientation. However, some important technological parameters, e.g., air gap, extrusion temperature and printing speed were kept at constant level. Using an open-source 3D printer, Lanzotti et al. (2015) reported on an extensive study aimed at establishing the influence of layer thickness, raster orientation and number of shell perimeters on the mechanical properties of PLA specimens. They optimized the three parameters using the Central Composite Design (CCD) as an established statistical method. However, due to sequential nature of CCD, the number of specimens used in this experiment was 60, while a number of important parameters - among which were extrusion speed, extrusion temperature and infill, were kept at a constant level.

The study presented in this paper features two important aspects. Firstly, it draws on the previous works in that it uses a consumer-priced FDM printer and PLA filament. However, it investigates the concerted influence of five key technological parameters on the flexural property of standard specimens:

- Layer height;
- Material deposition angle;
- Infill;
- Extrusion speed, and
- Extrusion temperature.

More precisely, the term extrusion speed here indicates the travel speed of extrusion head while extruding filament. Special emphasis is placed on practical implementation, thus infill is varied in the range of 10-30%, which is way less time-consuming than the usual 100% used in other reviewed experiments. Furthermore, the influence of curvature of the layer thickness effect, established in a previous study (Luzanin et al, 2014) as well as the interactions between low infill and other effects are also subject to investigation.

The second important aspect of this experiment is the application of a novel class of screening design, the Definitive Screening Design (DSD) which will allow statistical analysis and extraction of

maximum information from a relatively small number of experiments, with an important benefit of minimum aliasing.

With this in mind, the paper is organized as follows: discussed in Section 2 are some important aspect of DSD as the key statistical method which is used to organize this experiment. Section 3 presents in detail the plan of experiment, material and specimens. Selection of regression model and statistical results are presented in Section 4, while the analysis of results follows in Section 5. Concluding remarks and suggestions for future work, are given in Section 6.

2. Definitive Screening Design (DSD)

Due to its proven features, the design of experiment (DoE), in its various forms, has been the traditional statistical method of choice for numerous researchers, as it allows one to obtain maximum information with minimum number of experiments. The number of experiments is crucial when the number of input factors is large. This becomes even more prominent in cases when two-level screening designs require a second stage, i.e., additional experiments, as is typically the case with non-linear effects and response surface method.

In order to overcome the traditional separation between the screening and optimization experiments, a novel class of screening designs, called the Definitive Screening Design (DSD), have been developed (Jones and Nachtsheim, 2011). Although the initial proposal of the design allowed only numerical parameters, subsequent improvements of the method (Xiao & Lin, 2012) enabled the DSD to also include categorical parameters. As their name implies, the definitive screening designs allow users to estimate main effects, some two-factor interactions and some quadratic effects in a single experiment.

However, despite its advantages over the conventional screening designs, reports on successful application of the definitive screening design in academia and industry are still scarce. One of the reasons is its relatively novel appearance, and the fact that numerous statistical software commercially available today still do not provide support for the generation of definitive screening design tables.

According to recent literature, several studies have been performed using the DSD. Although they are not directly related to the subject of additive technologies, they deserve mentioning. Erler et al. (2013) used an augmented definitive screening design to assess the influence of 6 input parameters on protein-crosslinking reaction for a candidate vaccine product, in just 17 experimental runs.

In a study on optimization of synthesis and properties of Al-modified anatase catalyst supports, Olsen et al. (2014) successfully applied definitive screening design to separate and identify the effects of 10 variables and their interactions.

Libbrecht et al. (2015) conducted a statistically designed experiment aimed at optimization of the synthesis of soft templated mesoporous carbon. They used definitive screening design to optimize the mesoporous surface area based on 5 factors and their interactions.

2.1 Structure of Definitive Screening design

General structure of DSD is shown in Table 1. Considering m continuous factors, the table contains $2m+1$ runs. A total of m runs are fold-over pairs, plus an additional center run. As can be seen in Table 1, with the exception of the center run, all runs have one factor level at its center point, while others are at the extreme values.

Table 1 General structure of Definitive Screening Designs (Jones & Nachtsheim, 2013)

While the fold-over structure of the DSD design eliminates confounding between two-factor interactions and main effects, the center run in the last row enables user to fit a model that includes an intercept and all main and quadratic effects.

2.2 Conference matrices

Definitive screening designs can be efficiently constructed using conference matrices (Xiao & Lin, 2012). A conference matrix is an $m \times m$ matrix where m is even. The matrix C has zeros on the diagonal, off-diagonal entries equal to 1 or -1 , and satisfies (Xiao & Lin, 2012):

$$C'C = (m - 1) I_{m \times m} \quad (1)$$

where:

$$C_{ii} = 0, (i = 1, 2, \dots, m)$$

$$C_{ij} \in \{-1, 1\}, (i \neq j, i, j = 1, 2, \dots, m)$$

The design matrix D for the definitive screening design can be constructed as

$$D = \begin{pmatrix} C \\ -C \\ 0 \end{pmatrix} \quad (2)$$

where C is an $m \times m$ conference matrix and 0 is a $1 \times m$ zero matrix.

For k even and continuous factors, the number of runs is $2k+1$, while for k odd, a $(k+1) \times (k+1)$ conference matrix is used, with its last column deleted. For k odd, the total number of runs is $2k + 3$. In experiments where some factors are categorical, two additional runs are required (Jones & Nachtsheim, 2013), and they include center runs with all continuous factors set at their middle values. Similarly, with k factors and k even, the total number of runs in the design is $2k + 2$. When k is odd, the number of runs is $2k + 4$.

2.3 Advantages of Definitive Screening Design

Compared to the conventional screening designs, DSD features following advantages (Jones & Nachtsheim, 2011):

- The number of runs for continuous factors equals only twice the number of factors plus one. In the case of categorical factors, the total number of runs equals twice the number of factors plus two;
- Main effects are independent of two-factor interactions, which means that estimates of main effects remain unbiased by the presence of active two-factor interactions;
- Two-factor interactions are not completely confounded with other two-factor interactions, even though some correlation might exist;
- As opposed to designs with added centre points of resolution III, IV, and V, all quadratic effects are estimable in models comprised of any number of linear and quadratic main-effects terms;
- Quadratic effects are orthogonal to main effects and not completely confounded (though correlated) with interaction effects.

3. Materials and methods

As discussed in the introductory section, the main goal of this study is to use a consumer-priced FDM printer and PLA filament to investigate the concerted influence of five key technological parameters on the flexural property of standard specimens. The five parameters are: layer height, material deposition angle, infill, extrusion speed and extrusion temperature, while the 3D printer of choice is MakerBot Replicator 2 (*MakerBot[®] Industries*). The only modification on the original printer is the custom-made glass build plate which, due to better flatness, allows higher dimensional accuracy of prints. Original MakerBot filament (Leaf Green, 1.75 diameter) was used to build all specimens used in the study, while specimens were printed at 26 °C room temperature.

3.1 Selection of parameter boundary values

One of the key aspects of any experiment involving parameter variation is the selection of ranges within which particular parameters shall take values. Dealing with this problem gains additional importance within designs of experiments (DoE) whose fundamental property is simultaneous variation of all parameters used in experiment. Design tables require specific combinations of parameter levels which are often conflicting and therefore require careful adjustment of parameter ranges. In the case of our study, extrusion temperature was specially sensitive to variations, given its coupling with extrusion speed. More precisely, low levels of extrusion temperature in combination with high levels of extrusion speed, result in poor bonding between layers, and deteriorate surface finish, as shown in Figure 1. However, it has been previously shown that increments of 5°C in extrusion temperature lead to visible quality differences of a 3-D print, which is assumed to change mechanical strength as well (Tymrak et al, 2014). Furthermore, Drummer et al. (2012) used 235°C as the extrusion temperature of choice, because of the supposed "highest recrystallization of the subjacent layer" leading to best bonding between layers. Thus, based on previous discussion and preliminary

trial runs, a relatively narrow extrusion temperature range of 229-235°C was adopted for this experiment, which would allow us to obtain quality prints while experimenting with adverse combinations of parameter levels.

Figure 1 An example of low surface quality as the result of conflicting combination of key parameter levels - low extrusion temperature (225°C) and high extrusion speed (70 mm/s)

As regards the material deposition angle (raster orientaton), it has been shown that it causes alignment of polymer molecules along the direction of deposition, thus influencing mechanical strength of parts (Es Said et al, 2000). In this experiment, linear toolpath, i.e., raster fill was used to fill the contours in each layer. Three levels of deposition angle were 0°, 30° and 60° measured relative to X axis (horizontal) (Figure 2). Alternating layers were filled with a raster direction at 90° to one another.

Figure 2 Three levels of material deposition angle used in the experiment:
a) 0°, b) 30° and c) 60°

Other available complex geometric patterns for material deposition, such as hexagonal, catfill, etc., were not the subject of this study, since they do not allow such control over geomaterial parameters as the linear pattern, at least when speaking of desktop class 3D printers.

It is common knowledge that the infill is highly positively correlated to various aspects of mechanical strength and its reduction leads to diminishing of mechanical properties of printed parts. At the same time, printing time is radically affected by the increase of infill (3Ders, 2015). With this in mind, users of personal printers rarely resort to infills higher than 0.15, unless printing parts of very small dimensions. One of the goals of this study was to establish whether there is a significant interaction between (low) infill and the rest of the parameters varied in the experiment. Infills of 0.1, 0.2 and 0.3, were examined (Figure 3), since they are most likely to be used when printing times are of major concern.

Figure 3 Three levels of infill used in the experiment:
a) 0.1 (10%), b) 0.2 (20%) and c) 0.3(30%) infill

Finally, a custom printing script was written to enable each specimen in the DSD experiment to be printed with desired combination of layer thickness, material deposition angle (raster orientation), infill, extrusion speed and extrusion temperature (Table 2). Based on thirteen script files, thirteen print files were generated in *X3G* format and copied onto the MakerBot SD card.

3.2 Table of experiment

Table 2 shows the discussed parameters, their two-letter symbols and three levels. Based on that, a DSD table of experiment was generated. Since the number of parameters is odd and equals 5, the total number of runs is $2k+3=13$. The experiment is unreplicated, while the sufficient degrees of freedom are provided based on the *effect sparsity principle*, i.e., the fact that there are main factors and interactions which can be omitted from the regression due to lack of statistical significance. It should be noted that the center run in the last row is added to allow fitting a model that includes an intercept and all main and quadratic effects. DSD table generation and subsequent analyses were performed in *JMP 11 (SAS Institute Inc)*.

Table 2 Factors and level settings used in the experiment

DF=Degree of freedom; SS=Sum of squares; MSS=Mean sum of squares

3.3 3D printing of specimens

As mentioned in Section 3.1, 13 specimens compliant with ISO 178 (ISO 178, 2010) specification (10x4x80 mm), were built on *MakerBot 2* 3D printer. For that purpose, 13 scripts were edited to allow printing each specimen with a specific combination of five parameters levels as given in Table 4. Based on the scripts files, executable *X3G* files with machine instructions were generated automatically using *MakerBot's Makerware* software. No rafts were used, i.e., first layer was deposited directly on the Kapton tape. Printing parameters other than the varied five (Table 2) were kept at their default value and are given in Table 3.

Table 3 Vital printing parameters kept at a constant value during experiment

3.4 Flexural testing of specimens

Three-point bend testing was performed to assess variations in flexural force as the result of parameter setting combinations. Tests were completed on an *Instron 1122* testing machine, using 2 mm/min cross-head speed, at 24 °C temperature Loading edge radius, and supports radii were 5 mm, while the span was set at 64 mm to satisfy the recommended 16:1 span-to-depth ratio. The results of flexural tests are shown in Table 4. It should be noted that flexural stress values are reported for reference, but the ensuing analysis was performed based on flexural force, since none of the specimens were printed with a 100% infill. All specimens, except specimen 9, had brittle breaks.

Table 4 Experimental values of flexural force obtained for each trial, with the calculated stress and printing time as reported by the 3D printer

LT=Layer thickness; DA=Deposition angle; IN=Infill; ES=Extr. speed; ET=Extr. temperature

4. Model selection and statistical results

4.1 Model selection

Arguably one of the crucial aspects of any multi-parameter design of experiment is the selection of most adequate regression model. Such model should be parsimonious, in that it achieves a desired level of prediction with as few predictors as possible. Modern statistical softwares generally provide sufficient means to facilitate the task of identifying the model which balances under - and overfitting, while users are expected to adopt one or more available model selection criteria, depending on the specific field of application.

In our case, Bayesian Information Criterion (BIC) was used for the selection of the candidate regression model. BIC is defined as (Burnham & Anderson, 2002):

$$BIC_i = -2\log L_i + V_i \log n \quad (3)$$

where L_i , the maximum likelihood for the candidate model i , is determined by adjusting the V_i free parameters in such a way as to maximize the probability that the candidate model has generated the observed data; n is the number of observations entered into the likelihood calculation.

The BIC essentially penalizes inadequate fitting, smaller values indicating models with better prediction abilities. The procedure used in this study involved the forming of a fully quadratic model - containing all main effects, all quadratic effects and all two-factor interactions. Using the JMP stepwise regression control tool, it was possible to generate a larger number of regression models with various numbers of terms, all of which provided good fit. In the next step, models were selected on the criterion of having a maximum of 8 terms with the hierarchy restriction applied. Once the models were selected, an overlay plot was created to show the change of BIC and Root Mean Square Error (RMSE) as the function of model size (Figure 4). Generally, the idea was to select a model with lowest values of BIC and RMSE, using simplicity, i.e., low number of terms, as additional criterion.

Figure 4 Overlay plot of key indicators for model selection

Accordingly, the plot was then used to shortlist the candidate models. As shown in Figure 4, BIC and RMSE indicate models on the right end of the plot, with 6, 7 and 8 terms. These models are shown in Table 5 with the selected parameters: R^2 , R^2_{adj} , RMSE and BIC. As seen in Table 5, models 1-4 exhibit very similar characteristics in terms of R^2 , R^2_{adj} , RMSE and BIC values. Being the simplest among the four, model #4 was adopted for further analysis.

Table 5 Characteristics of the five models selected through preliminary analysis (Figure 4)

4.2 Statistical results obtained with the selected regression model

Using the regression model #4 with seven predictors selected as described in the preliminary stage, statistical analysis was performed. Tables with model summary, analysis of variance (ANOVA) and parameter estimates are given in Tables 6, 7 and 8, respectively.

Table 6 Model summary

Table 7 Analysis of Variance

Table 8 Parameter estimates sorted by statistical significance

Model adequacy is illustrated by diagrams in Figure 5, where the numbers denote actual experiments. There are no serious departures of residuals from normality (Figure 5a), which is also confirmed by the insignificance of Shapiro-Wilk test ($W=.941$, $p=.4715$). Standardized residuals are randomly scattered about zero, indicating constant variance and absence of outliers (Figure 5b).

Figure 5 Diagnostic plots showing model adequacy -
normal probability plot of residuals (a), residuals versus fitted values (b)

A plot of actual versus predicted values of Flexural force is given in Figure 6, where the numbers also correspond to actual experiments. Visual inspection reveals absence of overfitting.

Figure 6 Plot showing actual versus predicted values of Flexural force [N]

Based on Table 8, a diagram of significant two-way interactions in the model is shown in Figure 7, and further clarified by surface response plots in Figure 8. The discussion of interactions based on the surface plots is presented in the following section.

Figure 7 Diagram of significant two-way interactions in the model

Figure 8 Surface response plots illustrating two significant interactions in the regression model -
a) Infill*Layer thickness, b) Infill*Extrusion speed

A brief discussion of confounding in this design of experiment is illustrated by the colour map in Figure 9. The degree of confounding is colour-coded from pure blue (0% confounding), to pure red (100%). With this in mind, it is obvious that the main effects are completely uncorrelated with each other, the two factor interactions and the quadratic term, while there exists partial confounding between the LT^2 and $IN*ES$ (0.4655) and $LT*IN$ and $ES*IN$ (0.25). Checking of standard errors and variance inflation coefficients (VIFs) showed no unusual departures from normal values (Table 8), which indicates that the subsequent analyses and conclusions are not affected by the effect of multicollinearity.

Figure 9 Color map of correlations for the adopted regression model

5. Analysis of results

The highly significant quadratic layer thickness term (LT^2) (Table 8) is difficult to interpret in a direct way. However, it is most probably the result of anisotropy which is inherent to layered manufacturing (Ahn et al, 2002). In the case of our experiment, the anisotropy was specially emphasized in the Z-direction due to the fact that specimens in this study were printed with low infill where the roads deposited in each layer established only vertical bonds (Figure 10), while partial lateral necking was effective only at the peripheral contacts with the shell walls (Figure 11).

Figure 10 Mesostructure of PLA specimen #11 after the flexural test

Figure 11 Lateral necking between deposited roads and shell wall of the specimen

Analysis also revealed (Table 8) that the deposition angle (DA) was statistically significant and the low level of DA corresponded to higher flexural force. This is compliant with other findings which also reported that tensile and flexural strength decrease at increased deposition angles (Sood et al., 2011, Tymrak et al., 2014, Lanzotti et al., 2015).

Though not statistically significant, extrusion speed (ES) and layer thickness (LT) (Table 8) terms are each part of significant two-way interactions with infill (IN). Considering the two-way interaction between infill and layer thickness, the impact of layer thickness on the effect of infill on the mean flexural force is shown in Figure 6 and on the surface plot (Figure 8a). With layer thickness set at low level, the change in infill has no effect on the mean flexural force. However, at mid-level of layer thickness, the mean flexural force reaches maximum, dropping again as the layer thickness reaches high level. As shown at the upper-left end of the surface plot (Figure 8a), layer thickness that corresponds to maximum flexural force is somewhere past the 0.2 mm point and is pinpointed by optimization diagram given in Figure 14. Extruding minimum layer thickness of 0.1 mm with the 0.4 mm extruder nozzle also resulted in a specific cross-sectional shape of deposited roads (Figure 12) compared to that shown in Figure 10 and 11 (built with 0.3 mm layers).

Figure 12 Mesostructure of PLA specimen #4 after the flexural test

According to earlier findings (Sood et al., 2011), in order to minimize distortions due to stress accumulation during bond formation, parts should be generally built with a minimum number of layers, i.e., thicker layers, and smaller raster angles. Moreover, it was also shown by the same authors that the effect of non-uniform temperature gradient on the already deposited material becomes more prominent as the number of layers increases. This is also indicated by our results. As seen in Fig.8a, regardless on the level of *infill*, layers 0.1 and 0.15 result in significantly lower flexural forces, while layer 0.2, although better, remains sub-optimal. Quite counterintuitively, the diagram in Fig.8a shows, that for layer thickness 0.1 (i.e., higher number of passes), the increase of *infill* has no effect on flexural strength. Our present assumption is that this can be attributed to the effect of non-uniform temperature gradient, i.e., internal stresses, which quite effectively neutralize the effect of higher *infill*.

Another interesting detail revealed by ANOVA is the notably lower dispersion of standardized residuals at the middle level of the layer thickness parameter (LT) (Figure 13), which indicates the stability of the dependent variable (flexural force).

Figure 13 Scatterplot of standardized residuals
for the mean flexural force [N] versus Layer thickness [mm]

The remaining significant interaction is partly connected to our previous discussion on non-uniform temperature gradient effect. The diagram in Figure 6 shows that the increase of *infill* (IN), from 0.1 to 0.3, contributes to higher flexural forces only at higher extrusion speeds. This is better illustrated by the surface plot in Figure 8b. The finding is also supported by a previous study (Sun et al., 2008) which reported that temperature within part varies according to the motion speed of the FDM extrusion head, since its temperature is much higher than the deposited material below. This, in turn, affects the bond strength between deposited paths contributing to part strength.

The optimization plot shown in Figure 14 graphically depicts how the four investigated factors affect the predicted response. The four cells of the graph illustrate how the flexural force changes as a function of one of the variables, while all other variables remain constant. The vertical red lines on the graph represent the current settings, while the dashed, horizontal blue lines represent the current response values. The mean value of layer thickness optimized by this study equals 0.223 mm which is in accordance with the discussed results. Similar studies pertaining to tensile strength (Tymrak et al., 2014, Lanzotti et al, 2015) and compressive strength (Sood et al, 2011), reported that maximum values were obtained with a 0.2 mm and 0.254 mm layer height, respectively.

Figure 14 Optimization plot for the flexural force [N] showing optimal values of the four parameters

Printed with the optimal settings obtained by this experiment, the three 100% infill specimens showed mean flexural strength of 96.8 MPa. If we examine the results by MakerBot (whose filament was used in our study), we can see that they report flexural strength of 13731 PSI for 100% infill PLA specimens (MakerBot, 2016). This roughly corresponds to 94 MPa, which requires a flexural force of approximately 160 N, given the nominal specimen dimensions. Direct comparison of these values should be approached with caution for several reasons. First of all, the reference specimens were fabricated with 0.1 mm layer thickness, with the default extrusion speed of 90 mm/min. Secondly, the colour of the filament used in the fabrication of reference specimens is not known. However, it is of consequence to the flexural strength, bearing in mind that different-colour filaments exhibit different crystallization rates under different extrusion temperatures and cooling conditions, as discussed by Wittbrodt and Pearce (2015). Finally, there is no reference to the crosshead speed used in the reference experiment, which can also significantly alter the final result (ASTM D790, 2010).

6. Conclusions

The objective of this study was to investigate the impact of five key technological parameters and their interactions - layer thickness, deposition angle, infill, extrusion speed and extrusion temperature - on the maximum flexural force in PLA specimens built on a consumer-priced 3D printer (*MakerBot Replicator 2*). Specific detail in this experiment was the infill, which was reduced from 100% to more time-efficient values which are regularly used by everyday practitioners. This offered an additional opportunity to investigate possible interactions between infill and other parameters.

In order to allow screening and a preliminary optimization in a single experiment, a novel class of designs - Definitive Screening Design (DSD) was used. DSD allowed estimation of main effects, some quadratic effects and some two-factor interactions in just 13 runs, avoiding the traditional sequential approach of the Central Composite Design (CCD). For example, using an unblocked CCD with five continuous factors would require 52 experiments (full design) or 32 experiments (half-fractional design). The confounding of effects was minimal as shown in the discussion of results.

Through selection of a regression model that best fits the data while using minimal number of predictors, a model with seven predictors was adopted. Being the only statistically significant term without a significant interaction in the model, the effect of Deposition angle (DA) was interpreted directly, showing that the average value of flexural force was highest at the low level of deposition angle (0°). Infill (IN) was interpreted through its two-factor significant interactions with Layer thickness (LT) and Extrusion speed (ES). According to our findings, higher Infill contributed to

higher average values of flexural force only at higher levels of Layer thickness (LT) and Extrusion speed (ES).

Finally, as seen in the process of model selection, the extrusion temperature term (ET) was left out of the model used in this study. It should be noted that, due to the nature of the factorial experiment, specimens were built only individually. Since their dimensions are small, especially their thickness, FDM head movement, i.e., extrusion speed, was dominant over the extrusion temperature in terms of generating higher temperature profile of specimen layers. It should be noted that some other considered regression models (Table 5) featured extrusion temperature in some significant two-way interactions. Although not statistically significant as the main effect, at its high level, the extrusion temperature contributed to lower dispersion of the average flexural force.

With the concluding remarks in mind, further investigation shall be directed towards: (i) investigation of the phenomenon related to the mid-level layer thickness which obviously has advantages over low- and high-level values in terms of thermal history and bonding quality as shown in this and other studies; (ii) extension of the experiment to resolve ambiguity with partial confounding of two-way interaction effects and quadratic effect; (iii) realization of the design of experiment with the values of deposition angle and layer thickness fixed at optimal values, while using wider range of extrusion temperatures to investigate its interaction with extrusion speed and infill; (iv) extending the experiment to real-size objects whose dimensions overcome the discussed limitations in terms of the specific impact of extrusion head movements on the temperature profile of the deposited layers during processing.

As regards various other filament materials which are of interest for this and similar investigations, it would be usable to conduct a comparative study which, beside the omnipresent ABS, also includes polyamide, polyethylene, carbon fiber PLA, and glass filled filament. In addition to a number of interesting properties these materials exhibit, they also have printing temperatures which overlap sufficiently to allow experimentation with the unique range of settings.

References

- Afrose, M. F., Masood, S.H., Nikzad, M., Iovenitti, P. (2014) "Effects of Build Orientations on Tensile Properties of PLA Material Processed by FDM", *Advanced Materials Research*, Vols. 1044-1045, pp. 31-34.
- Ahn, S.H., Montero, M., Odell, D., Roundy, S. and Wright, P.K. (2002), "Anisotropic material properties of fused deposition modeling ABS", *Rapid Prototyping Journal*, Vol.8, No.1, pp. 248-257
- ASTM D790 (2010), "Standard test methods for flexural properties of unreinforced and reinforced plastics and electrical insulating materials", ASTM International, West Conshohocken
- Bijarimi, M, Ahmad, S., Rasid, R. (2012), "Mechanical, Thermal and Morphological properties of PLA/PP Melt Blends", International Conference on Agriculture, Chemical and Environmental Sciences (ICACES'2012), Dubai (UAE), pp.115-117.
- Burnham, K. P., Anderson, D. R. (2002), *Model selection and multimodel inference: a practical information-theoretic approach*, Springer Science & Business Media.

- Carrasco, F., Pagès, P., Gámez-Pérez, J., Santana, O. O., & Maspoch, M. L. (2010). Processing of poly (lactic acid): characterization of chemical structure, thermal stability and mechanical properties. *Polymer Degradation and Stability*, 95 (2), pp. 116-125.
- Drummer, D., Cifuentes-Cuéllar, S., Rietzel, D. (2012), "Suitability of PLA/TCP for fused deposition modeling", *Rapid Prototyping Journal*, Vol. 18(6), pp. 500 - 507
- Dunn, J. J., Hutchison, D. N., Kemmer, A. M., Ellsworth, A. Z., Snyder, M., White, W. B. and Blair, B. R. (2010), "3D printing in space: enabling new markets and accelerating the growth of orbital infrastructure," in Proc. Space Manufacturing 14: Critical Technologies for Space Settlement. Space Studies Institute.
- Erler, A., de Mas, N. and Ramsey, P. (2013), "Efficient biological process characterization by definitive-screening designs: The formaldehyde treatment of a therapeutic protein as a case study", *Biotechnology Letters*, 35, pp. 323–329.
- Es-Said, O. S., Foyos, J., Noorani, R., Mendelson, M., Marloth, R. and Pregger, B. A. (2000), "Effect of layer orientation on mechanical properties of rapid prototyped samples," *Materials and Manufacturing Processes*, 15(1), pp.107-122.
- Hafsa, M.N., Ibrahim, M., Wahab, M. S., Zahid M. S. (2013), "Evaluation of FDM Pattern with ABS and PLA Material", *Applied Mechanics and Materials*, Vols. 465-466, pp. 55-59.
- Ibrahim, M., Hafsa, M.N. (2013) "Studies on Rapid Prototyping Pattern Using PLA Material and FDM Technique", *Applied Mechanics and Materials*, Vols. 465-466, pp. 1070-1074.
- ISO 178-1:2010 (2010) "Plastics - Determination of flexural properties, International Organization for Standardization, Geneva, Switzerland.
- Jones, B., Nachtsheim, C. J. (2011), "A class of three-level designs for definitive screening in the presence of second-order effects," *Journal of Quality Technology*, 43(1), pp.1-15.
- Jones, B., Nachtsheim, C.J. (2013), " Definitive Screening Designs with Added Two-Level Categorical Factors ," *Journal of Quality Technology*, 45(2), pp.121-129.
- Lanzotti, A., Grasso, M., Staiano, G., Martorelli, M. (2015), "The impact of process parameters on mechanical properties of parts fabricated in PLA with an open-source 3-D printer", *Rapid Prototyping Journal*, Vol. 21(5), pp - available at: <http://dx.doi.org/10.1108/RPJ-09-2014-0135> (accessed 28 July, 2015)
- Letcher, T., Waytashek, M. (2014), "Material Property Testing of 3D-Printed Specimen in PLA on an Entry-Level 3D Printer", Proceedings of the ASME 2014 International Mechanical Engineering Congress & Exposition, IMECE2014, Nov. 14-20, 2014, Montreal, Quebec, Canada, pp. V02AT02A014-V02AT02A014
- Libbrecht, W., Deruyck, F., Poelman, H., Verberckmoes, A., Thybaut, J., De Clercq, J. and Van Der Voort, P. (2015), "Optimization of soft templated mesoporous carbon synthesis using Definitive Screening Design", *Chemical Engineering Journal*, Vol.259, pp. 126–134.
- Lin, C. (2015), "Construction and selection of the optimal balanced blocked definitive screening design", *Metrika*, Vol.78, Issue 4, pp.373-383
- Luzanin, O., Movrin, D. and Plancak, M. (2014), "Effect of layer thickness, deposition angle, and infill on maximum flexural force in FDM-built specimens", *Journal for Technology of Plasticity*, Vol.39, No.1., pp.49-58.
- MakerBot (2016), "PLA and ABS strength data," available at: https://eu.makerbot.com/fileadmin/Inhalte/Support/Datenblatt/MakerBot_R__PLA_and_ABS_Strenghth_Data.pdf (accessed 25 May, 2016)
- Olsen, R.E., Bartholomew, C.H., Enfield, D.B., Lawson, J., Rohbock, N., Scott, S. and Woodfield, B.F. (2014), "Optimizing the synthesis and properties of Al-modified anatase catalyst supports by statistical experimental design", *J. Porous Matter*, Vol.21(5), pp.827–837.
- Rankin, T.M., Giovinco, N.A., Cucher, D. J., Watts, G., Hurwitz, B. and Armstrong, D.G. (2014), "Three-dimensional printing surgical instruments: are we there yet?" *Journal of Surgical Research*, 30 (1), pp.193-197.
- Sood, A.K., Chaturvedi, V., Datta, S. and Mahaparta, S.S. (2011), "Optimization of process parameters in fused deposition modeling using weighted principal component analysis," *Journal of Advanced Manufacturing Systems*, 10(2), pp.241-259.
- Sun, Q., Rizvi, G. M., Bellehumeur, C. T. and Gu, P. (2008), "Effect of processing conditions on the bonding quality of FDM polymer filaments." *Rapid Prototyping Journal*, 14(2), pp.72-80.

- Turner, B. N., Gold, S. A. (2015), "A review of melt extrusion additive manufacturing processes: II. Materials, dimensional accuracy, and surface roughness", *Rapid Prototyping Journal*, Vol. 21(3), pp. 250 - 261
- Tymrak, B.M., Kreiger, M., Pearce, J.M. (2014), "Mechanical properties of components fabricated with open-source 3-D printers under realistic environmental conditions", *Materials and Design*, 58, pp. 242-246.
- US5121329 (2105), "Apparatus and method for creating three-dimensional objects US 5121329 A," available at: <https://www.google.com/patents/US5121329> (accessed 03. July, 2015)
- US5597589 (2105), "Apparatus for producing parts by selective sintering US 5597589 A," available at: <https://www.google.com/patents/US5597589> (accessed 03. July, 2015)
- US5554336 (2105), "Method and apparatus for production of three-dimensional objects by stereolithography US 5554336 A," available at: <https://www.google.com/patents/US5554336> (accessed 03 July, 2015)
- US6007318 (2105), "Method and apparatus for prototyping a three-dimensional object US 6007318 A," available at: <https://www.google.com/patents/US6007318> (accessed 03. July, 2015)
- Vijayaraghavan, V., Garg, A., Lam, J. S. L., Panda, B. and Mahapatra, S. S. (2014), "Process characterisation of 3D-printed FDM components using improved evolutionary computational approach", *The International Journal of Advanced Manufacturing Technology*, 1-13.
- Wittbrodt, B., Pearce, J. M. (2015), "The effects of PLA color on material properties of 3-D printed components", *Additive Manufacturing*, 8, pp. 110-116.
- Xiao, L., Lin, D.K.J. (2012), "Constructing definitive-screening designs using conference matrices", *Journal of Quality Technology*, Vol.44(1), pp. 2-8

Factor	Symbol	Unit	Low level (-1)	Middle level (0)	High level (+1)
Layer thickness	LT	mm	0.1	0.2	0.3
Deposition angle	DA	degree	0	30	60
Infill	IN	-	0.1	0.2	0.3
Extrusion speed	ES	mm/s	40	50	60
Extrusion temp.	ET	°C	229	232	235

Table 2 Factors and level settings used in the experiment

DF=Degree of freedom; SS=Sum of squares; MSS=Mean sum of square

Parameter	Value
Active cooling	On (starting from layer 1)
Extrusion speed (first layer)	30 mm/s
Travel speed	90 mm/s
Roof thickness	0.8 mm
Number of shells	2

Table 3 Vital printing parameters kept at a constant value during the experiment

Standard run order	Parameter level					Flexural force [N]	Flexural stress [MPa]	Printing time [min]
	LT	DA	IN	ES	ET			
1	0.2	60	0.3	60	235	160	93.12	12
2	0.2	0	0.1	40	229	155	90.21	12
3	0.3	30	0.1	60	235	130	75.66	8
4	0.1	30	0.3	40	229	125	72.75	27
5	0.3	0	0.2	40	235	140	81.48	10
6	0.1	60	0.2	60	229	135	78.57	19
7	0.3	60	0.1	50	229	120	69.84	8
8	0.1	0	0.3	50	235	142	82.64	23
9	0.3	60	0.3	40	232	140	81.48	11
10	0.1	0	0.1	60	232	135	78.57	18
11	0.3	0	0.3	60	229	158	91.96	8
12	0.1	60	0.1	40	235	135	78.57	23
13	0.2	30	0.2	50	232	150	87.31	11

Table 4 Experimental values of flexural force obtained for each trial, with the calculated stress and printing time as reported by the 3D printer

LT=Layer thickness; DA=Deposition angle; IN=Infill; ES=Extr. speed; ET=Extr. temperature

No.	Model	#Terms	R ²	R ² _{adj}	RMSE	BIC
#1	LT/DA/IN/ES/ET/LT ² /LT*IN/ES*IN	8	.9697	.9092	3.742	81.529
#2	LT/DA/IN/ES/ET/LT ² /DA ² /ET*IN	8	.9697	.9091	3.746	81.555
#3	LT/DA/IN/ES/ET/LT ² /ET ² /LT*IN	8	.9667	.9001	3.925	82.772
#4	LT/DA/IN/ES/LT ² /LT*IN/ES*IN	7	.9592	.9020	3.886	82.865
#5	DA/IN/ET/IN ² /DA*ET/IN*ET	6	.9159	.8318	5.095	89.695

Table 5 Characteristics of the five models selected through preliminary analysis (Figure 4)

Parameter	Value
R^2	0.9592
R^2_{adj}	0.9020
RMSE	3.8862
Mean of response	140.3846
Observations	13

Table 6 Model summary

Source	DF	SS	MS	F Ratio
Model	7	1775.4700	253.639	16.7735
Error	5	75.6069	15.121	Prob > F
C. Total	12	1851.0769		0.0034

Table 7 Analysis of Variance

Term	Estimate	Std Error	t Ratio		Prob> t	VIF
LT ²	-14.90462	2.919275	-5.11		0.0038	1.30
IN	5	1.229691	4.07		0.0097	1.00
LT*IN	5.1936416	1.4332	3.62		0.0152	1.09
DA	-4	1.229691	-3.25		0.0226	1.00
IN*ES	4.7254335	1.619323	2.92		0.0331	1.31
ES	2.3	1.229691	1.87		0.1204	1.00
LT	1.6	1.229691	1.30		0.2499	1.00

Table 8 Parameter estimates sorted by statistical significance

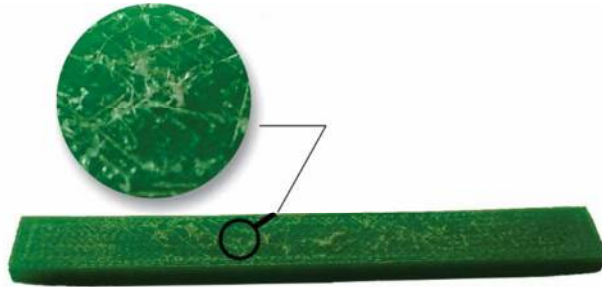


Figure 1 An example of low surface quality as the result of conflicting combination of key parameter levels - low extrusion temperature (225°C) and high extrusion speed (70 mm/s)

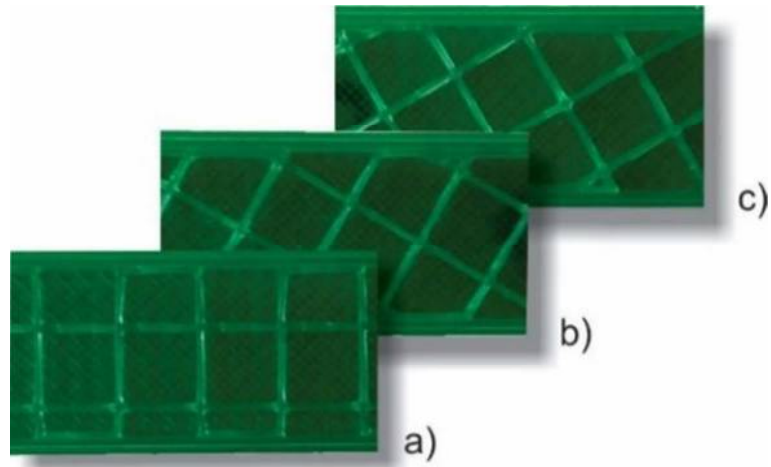


Figure 2 Three levels of material deposition angle used in the experiment:
a) 0° , b) 30° and c) 60°

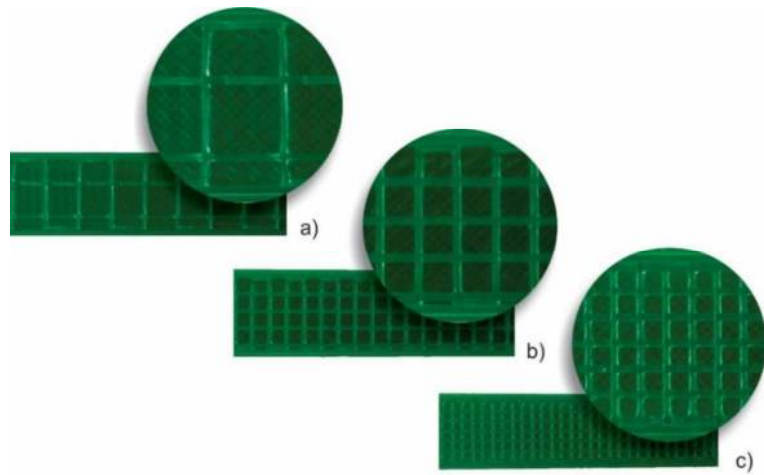


Figure 3 Three levels of infill used in the experiment:
a) 0.1 (10%), b) 0.2 (20%) and c) 0.3(30%) infill

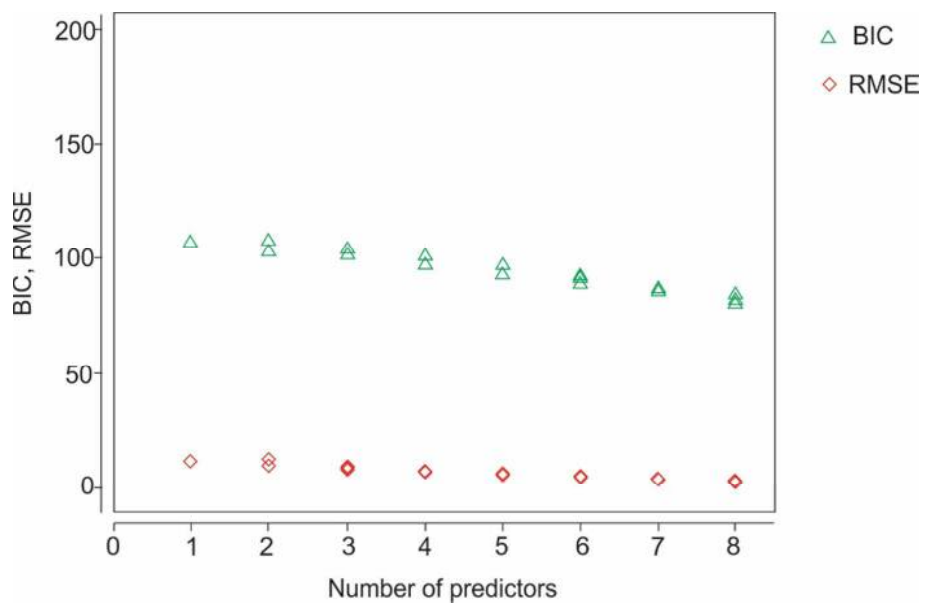


Figure 4 Overlay plot of key indicators for model selection

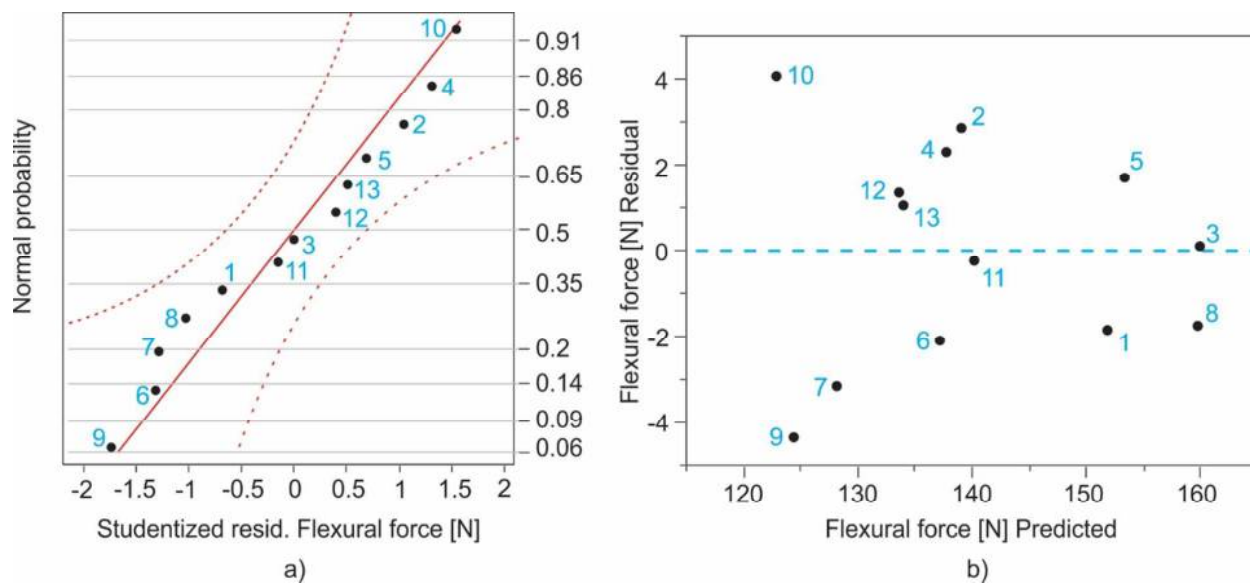


Figure 5 Diagnostic plots showing model adequacy - normal probability plot of residuals (a), residuals versus fitted values (b)

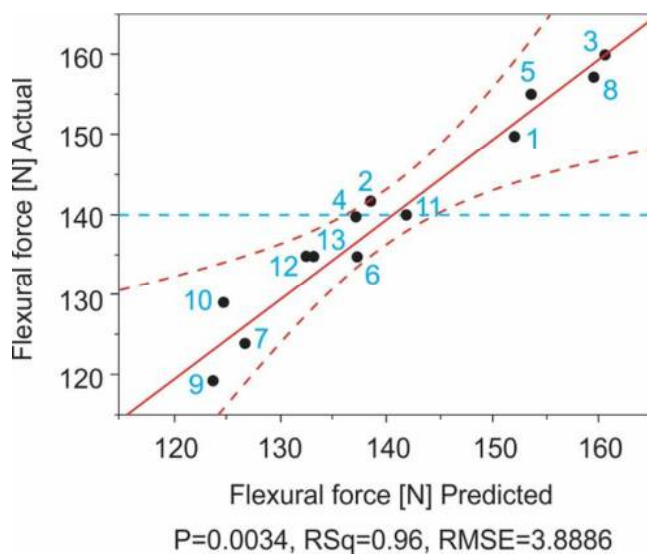


Figure 6 Plot showing actual versus predicted values of Flexural force [N]

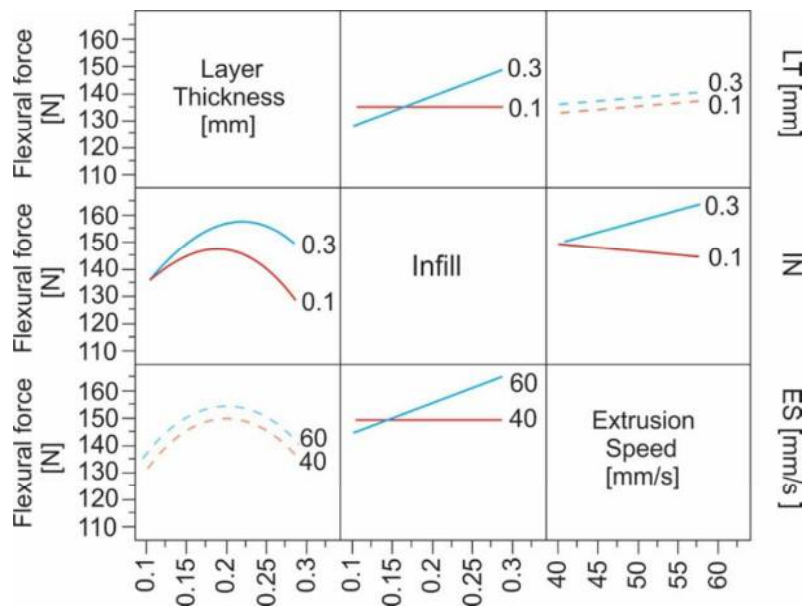


Figure 7 Diagram of significant two-way interactions in the model

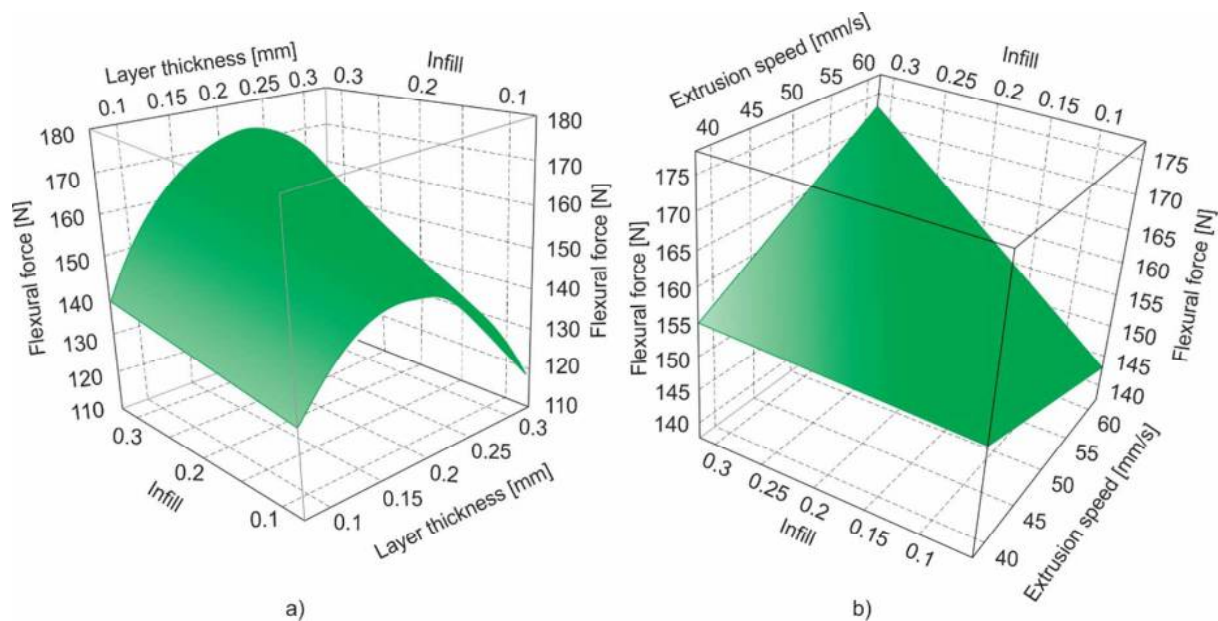


Figure 8 Surface response plots illustrating two significant interactions in the regression model - a) Infill*Layer thickness, b) Infill*Extrusion speed

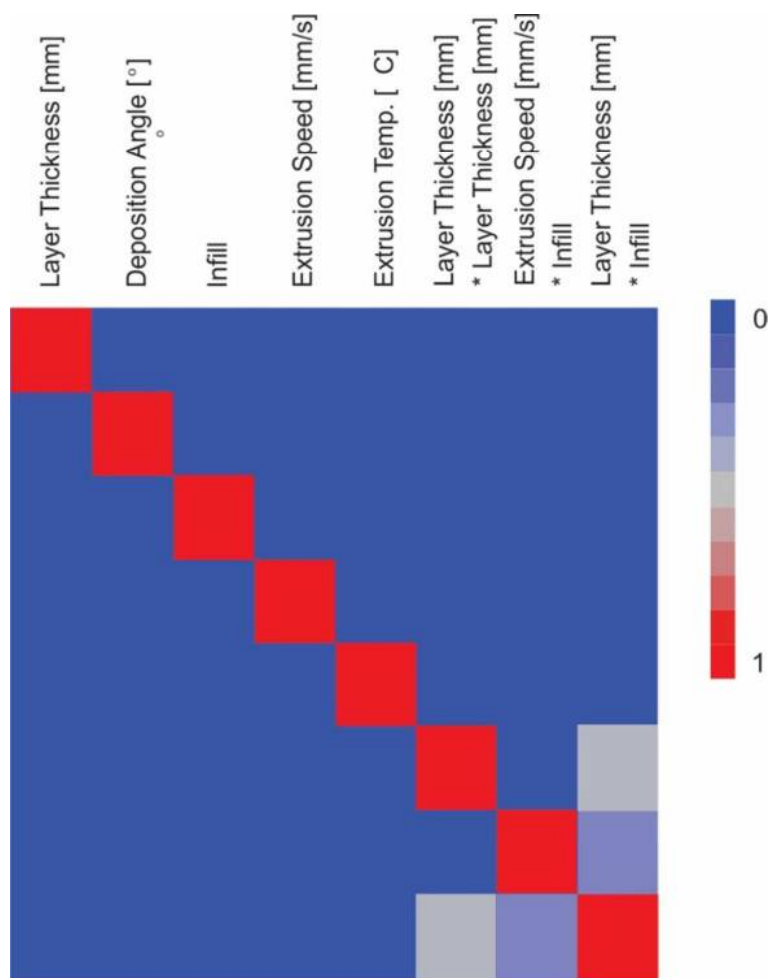


Figure 9 Color map of correlations for the adopted regression model

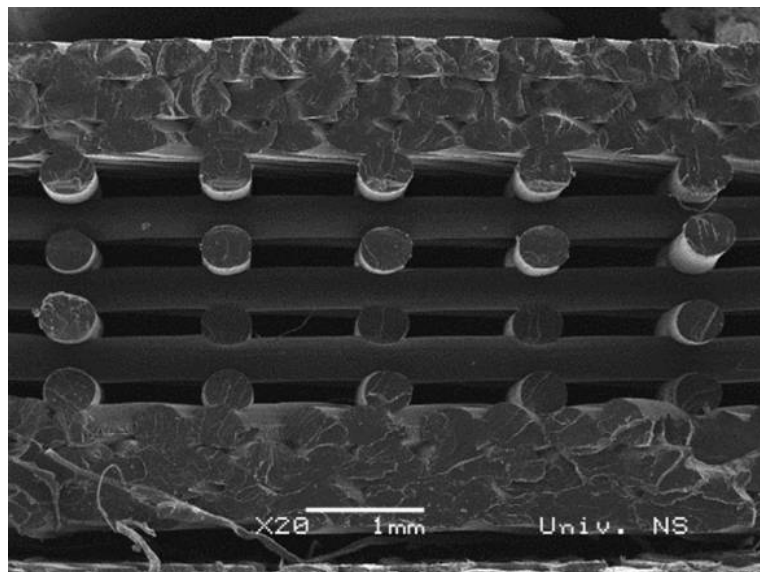


Figure 10 Mesostructure of PLA specimen #11 after the flexural test

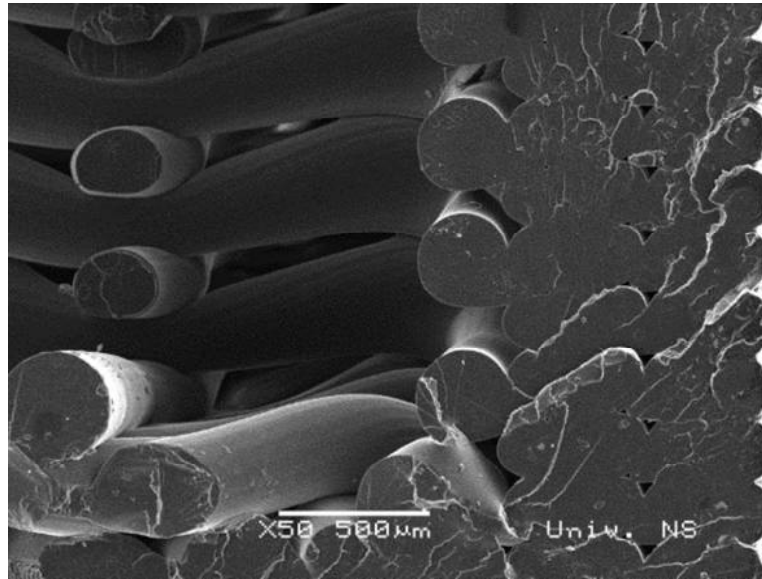


Figure 11 Lateral necking between deposited roads and shell wall of the specimen

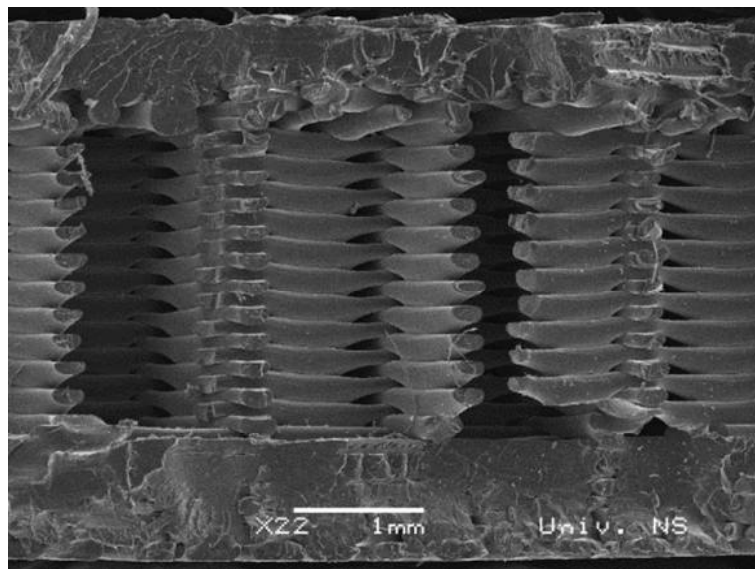


Figure 12 Mesostructure of PLA specimen #4 after the flexural test

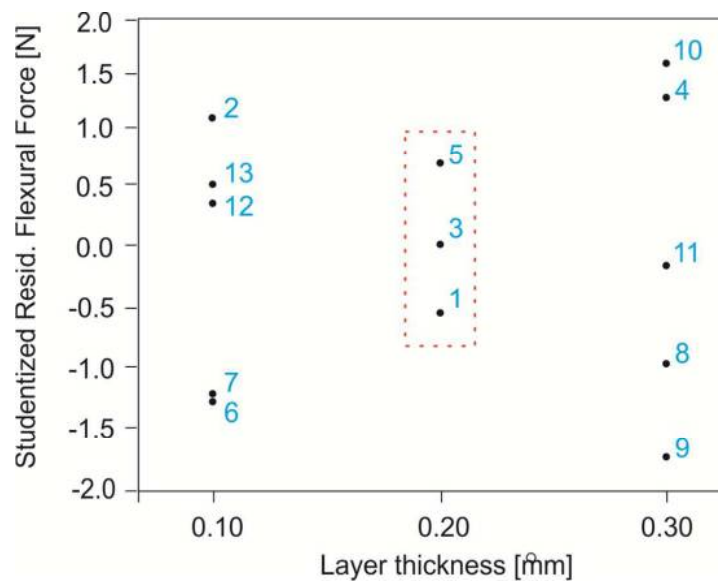


Figure 13 Scatterplot of standardized residuals for the mean Flexural force [N] versus Layer thickness [mm]

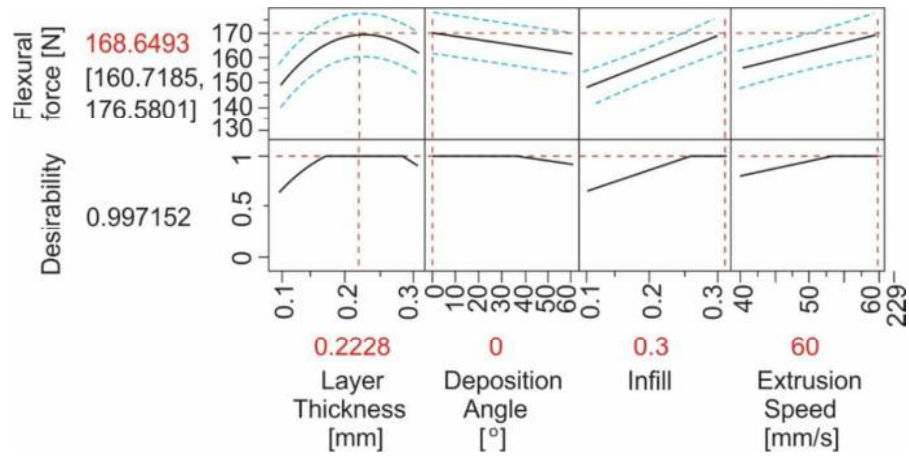


Figure 14 Optimization plot for the flexural force [N] showing optimal values of the four parameters



Au cours des dernières décennies, de nombreuses technologies ont émergé dans le domaine de l'ingénierie tissulaire osseuse. Parmi elles, la bioimpression connaît un essor considérable et pourrait constituer une alternative aux thérapeutiques actuelles.

La bioimpression au service de la régénération osseuse

Odontologie et ingénierie tissulaire

Olivia Kérourédan

AHU, UFR des Sciences Odontologiques,
Université de Bordeaux
INSERM U1026, BioTis, Université de Bordeaux

Vera Guduric

Doctorante
INSERM U1026, BioTis, Université de Bordeaux

Rawen Smirani

Interne en Médecine Bucco-Dentaire
UFR des Sciences Odontologiques,
Université de Bordeaux
INSERM U1026, BioTis, Université de Bordeaux

Murielle Rémy

Ingénieur de Recherche
INSERM U1026, BioTis, Université de Bordeaux

Hugo de Oliveira

Coordinateur de l'ART Bioimpression
INSERM U1026, BioTis, Université de Bordeaux

Jean-Christophe Fricain

PU-PH, UFR des Sciences Odontologiques,
Université de Bordeaux
INSERM U1026, BioTis, Université de Bordeaux

Adrien Naveau

MCU-PH, UFR des Sciences Odontologiques,
Université de Bordeaux
INSERM U1026, BioTis, Université de Bordeaux

Raphaël Devillard

MCU-PH, UFR des Sciences Odontologiques,
Université de Bordeaux
INSERM U1026, BioTis, Université de Bordeaux

Sylvain Catros

MCU-PH, UFR des Sciences Odontologiques,
Université de Bordeaux
INSERM U1026, BioTis, Université de Bordeaux

La chirurgie dentaire est l'une des spécialités médicales les plus concernées par la problématique des pertes osseuses. Ces dernières peuvent être liées à des traumatismes, des pathologies malignes, des lésions d'origine endodontique ou parodontale, et peuvent se révéler particulièrement problématiques dans des disciplines telles que la prothèse et l'implantologie. Différentes solutions thérapeutiques existent actuellement afin de favoriser la régénération osseuse. Parmi elles, les greffons d'origine humaine, animale ou synthétique, de même que la distraction ou la régénération osseuse guidée, offrent des taux de réussite satisfaisants [1]. Cependant, toutes ces techniques présentent des limites et des risques, comme la comorbidité au niveau du site donneur (autogreffe) ou encore le risque infectieux (allogreffe) [2, 3]. Afin de pallier ces défauts, la médecine régénérative et l'ingénierie tissulaire osseuse visent à développer de nouvelles solutions thérapeutiques permettant d'améliorer la cinétique de cicatrisation osseuse post-chirurgicale et l'intégration des substituts implantés. Ces dernières années, de nombreuses technologies se sont développées autour de l'impression 3D, notamment dans le domaine de la bioimpression, et pourraient constituer des alternatives aux techniques utilisées actuellement en pratique clinique.

Principes généraux et intérêts de la bioimpression en ingénierie tissulaire osseuse

En parallèle des applications dans des disciplines odontologiques cliniques telles que la prothèse et l'implantologie, la Conception et Fabrication Assistées par Ordinateur (CFAO) a conduit au développement de nouvelles méthodes dans le domaine de l'ingénierie tissulaire, en particulier la bioimpression.

Cette dernière peut être définie comme « l'utilisation des principes et des méthodes de modélisation et d'impression 3D pour la micro-impression d'éléments biologiques, afin de produire des assemblages biologiques complexes vivants et non vivants, à partir de matières premières d'origine biologiques telles que des cellules, des molécules signal, des matrices extra-cellulaires et/ou des biomatériaux » [4]. Ces dernières années, la bioimpression a connu un essor considérable. Cette nouvelle approche permet l'impression d'éléments biologiques nécessaires à l'élaboration de tissus implantables et fonctionnels. En ingénierie tissulaire osseuse, elle permettrait

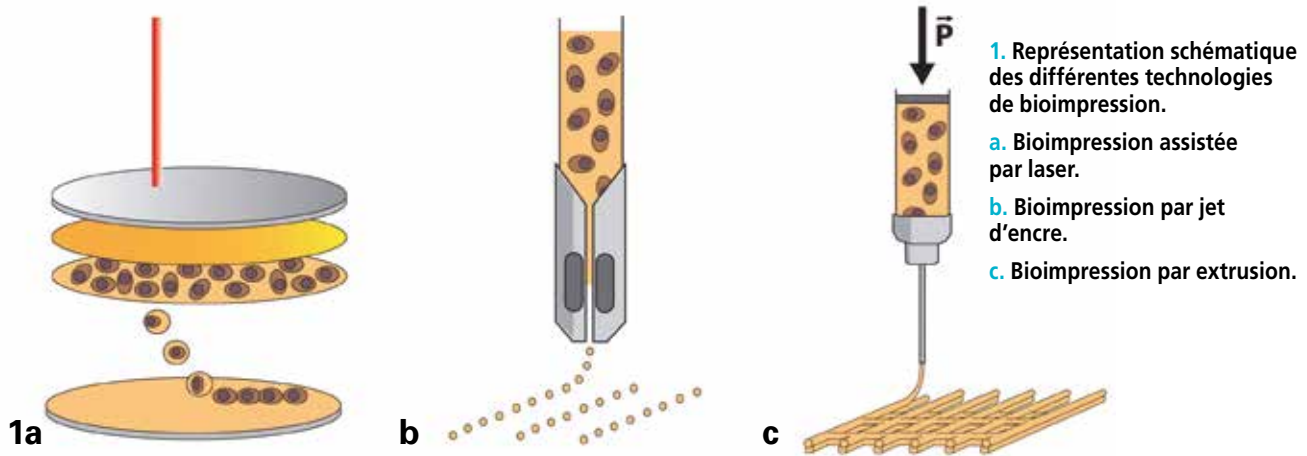
l'élaboration de substituts osseux « sur mesure », avec un meilleur contrôle de leur structure et de leur fonction, ceci de manière plus précise et sans risque de contamination croisée.

L'une des principales problématiques en ingénierie tissulaire osseuse est le contrôle de l'architecture interne des substituts à planter pour favoriser leur intégration tissulaire. Si la fabrication du substitut fait appel à l'utilisation d'un biomatériau, il sera nécessaire de pouvoir contrôler la taille et l'interconnectivité des pores afin de favoriser l'adhésion et la prolifération cellulaire, ainsi que la vascularisation du substitut. La vascularisation est en effet un point critique en ingénierie tissulaire osseuse. De nombreux échecs d'intégration de greffes sont liés à un défaut de vascularisation précoce du greffon implanté. Pour résoudre cette problématique de substitut faiblement vascularisé, des études ont aussi montré l'importance de la reproduction du micro-environnement local et de l'organisation cellulaires.

L'association de la CFAO et des méthodes d'ingénierie tissulaire a ainsi permis d'élaborer de nouvelles technologies permettant de mimer de façon fidèle l'architecture des tissus, tant au niveau macroscopique (forme de l'organe) que microscopique (organisation des composants élémentaires des tissus).

Bien que paraissant innovant dans le domaine médical, le principe de bioimpression n'est pas récent. La première expérimentation mettant en œuvre l'impression d'éléments biologiques, alors nommée « cytoscribing », a été réalisée en 1988 par Klebe [5]. Depuis cette date, plusieurs techniques ont été mises au point. À l'heure où certains parlent d'impression d'organes, il est nécessaire de se rendre à l'évidence, la bioimpression ne peut pas être utilisée aujourd'hui pour fabriquer des organes vivants fonctionnels. Mais d'autres applications sont déjà disponibles pour la recherche fondamentale ou appliquée.

Actuellement, trois technologies permettant l'impression d'éléments biologiques peuvent être distinguées : la bioimpression assistée par laser, la bioimpression par jet d'encre, et la bioimpression par extrusion (microseringues) (fig. 1). Chacune de ces méthodes peut être mise en œuvre dans des imprimantes spécifiques qui sont des prototypes ou des machines commerciales. Quel que soit le principe d'impression, on retrouve une réserve d'encre (correspondant à la cartouche), un mécanisme d'impression spécifique à la technologie (laser, jet d'encre ou pousse-seringue) et une zone réceptrice (support d'impression).



D'autres technologies basées sur les principes de la fabrication additive (impression 3D) sont régulièrement utilisées en complément des technologies de bioimpression afin d'élaborer des biomatériaux pouvant servir de support ou d'échafaudage (scaffolds), tels que les systèmes basés sur l'extrusion à chaud de fil fondu (Fused Deposition Modeling = FDM).

Ces technologies permettraient ainsi l'élaboration de substituts osseux *in vitro*, impliquant leur maturation avant implantation, voire *in vivo*, par bioimpression *in situ*, en imprimant des éléments biologiques directement au niveau du défaut osseux. L'objectif de cet article est de présenter les grands principes des technologies de bioimpression ainsi que les applications actuelles et futures dans le domaine de la régénération osseuse.

Applications des technologies de bioimpression en chirurgie orale

Prévascularisation des substituts osseux

La bioimpression assistée par laser (LAB) permet l'impression d'éléments biologiques à l'échelle micrométrique. Le prototype de station de bioimpression utilisé au laboratoire INSERM U1026 comprend un laser ($\lambda = 1064 \text{ nm}$, 30 ns) qui est focalisé sur une lame donneuse (cartouche) constitué d'une fine couche absorbante métallique et d'une couche d'encre cellulaire (bioencre). L'interaction entre le laser et la couche métallique entraîne la formation d'une bulle de vapeur puis d'un jet qui propulse une gouttelette d'encre vers le substrat receveur. Les gouttelettes sont alors imprimées selon un motif qui est prédéfini à l'aide d'une

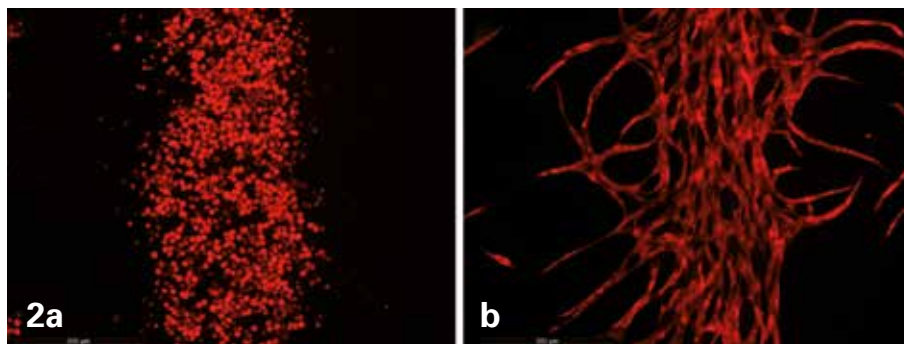
interface informatique. Des stratégies de prévascularisation des substituts osseux ont été mises au point grâce à la LAB. Ces expérimentations visaient à imprimer des motifs de cellules endothéliales sur une matrice constituée de collagène et de précurseurs de cellules osseuses, afin de favoriser la formation de réseaux vasculaires organisés selon un motif choisi (fig. 2) [6]. Cette technologie pourrait permettre de reconstituer de manière fidèle l'organisation spécifique de la vascularisation du tissu natif, et de favoriser l'intégration du substitut après implantation.

De la même manière, la bioimpression par la technologie jet d'encre permet de placer de manière contrôlée, précise et rapide des échantillons biologiques. Sa résolution est inférieure à celle de la bioimpression assistée par laser. Dans les domaines de la régénération osseuse et parodontale, cette technique permettrait d'organiser des cellules selon une configuration définie, et pourrait ainsi constituer une solution pour la construction de tissus imprimés prévascularisés, avant implantation (fig. 3).

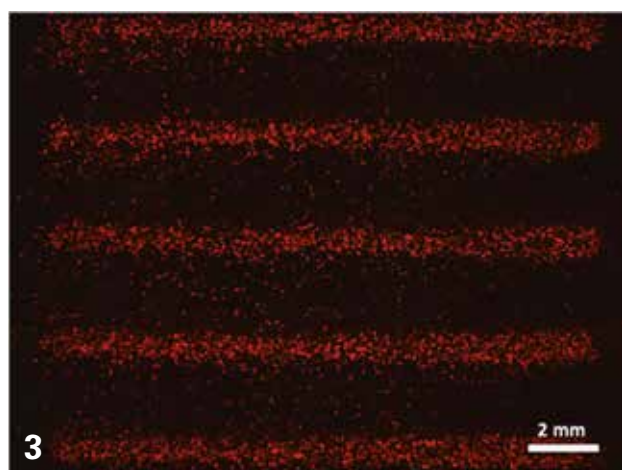
Élaboration de greffons muqueux

La bioimpression par extrusion consiste à déposer une bioencre (par exemple un gel contenant des cellules) en exerçant une pression automatisée (fig. 4) [7]. Cette technique permet de recréer, rapidement et précisément, un environnement matriciel tridimensionnel en contrôlant couche par couche la distribution spatiale de cellules et d'autres composants biologiques.

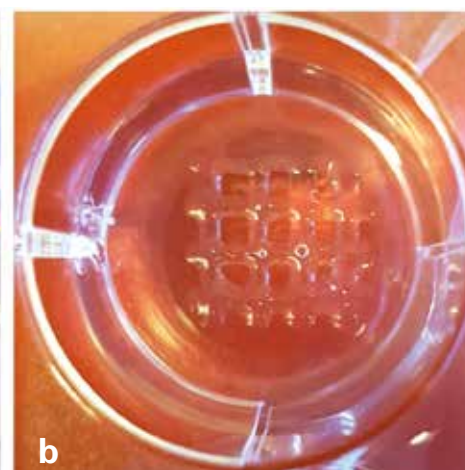
La bioimpression par extrusion est cliniquement prometteuse pour la réalisation de matrices volumineuses. En association avec la bioimpression assistée par laser, elle permet d'envisager la réalisation de greffons muqueux sur mesure pour compenser les pertes de substances orales [8].



2a. Impression par laser de cellules endothéliales humaines issues de la veine ombilicale, marquées à l'aide de la protéine fluorescente TdTomato : résultat immédiatement après impression.
b. Formation d'un réseau endothélial organisé après 5 jours de culture cellulaire.



3. Lignes de cellules endothéliales humaines issues de la veine ombilicale, marquées à l'aide de la protéine fluorescente TdTomato, imprimées par la technologie de bioimpression à jet d'encre.



4a. Exemple d'imprimante à extrusion, en cours d'impression.
b. Polymère imprimé sous forme de grille, à l'aide d'une imprimante à extrusion.

Assemblage multicouche de membranes cellularisées

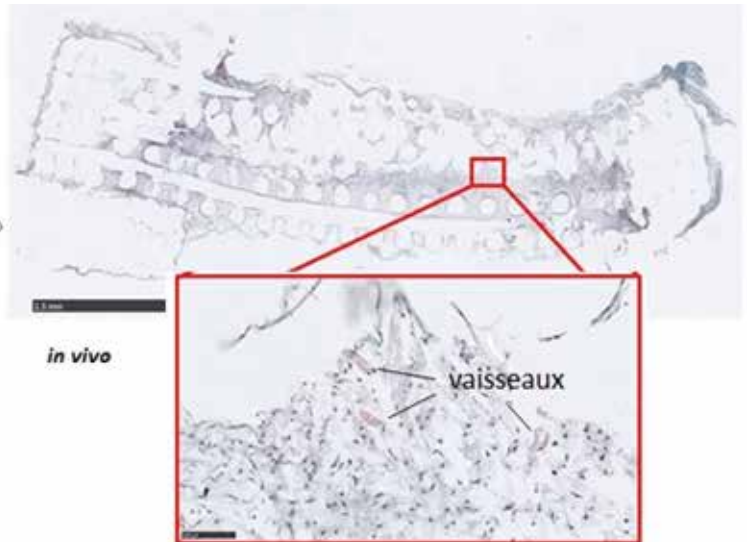
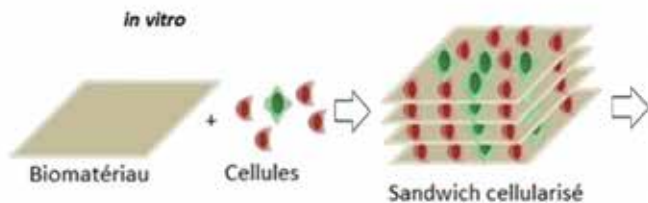
La fabrication de biomatériaux cellularisés couche par couche est très prometteuse en ingénierie tissulaire car elle permet d'obtenir une distribution cellulaire homogène et contrôlée en 3 dimensions [9]. Il s'agit d'ensemencer des cellules souches mésenchymateuses et endothéliales sur des biomatériaux sous forme de membranes poreuses et de les empiler couche par couche afin de former un assemblage tridimensionnel cellularisé. Cette méthode permet d'améliorer la prolifération et la différenciation cellulaire [10]. Ce type d'assemblage de cellules permet d'améliorer la vascularisation *in vitro* [11] et *in vivo* (fig. 5).

Bioimpression *in vivo*

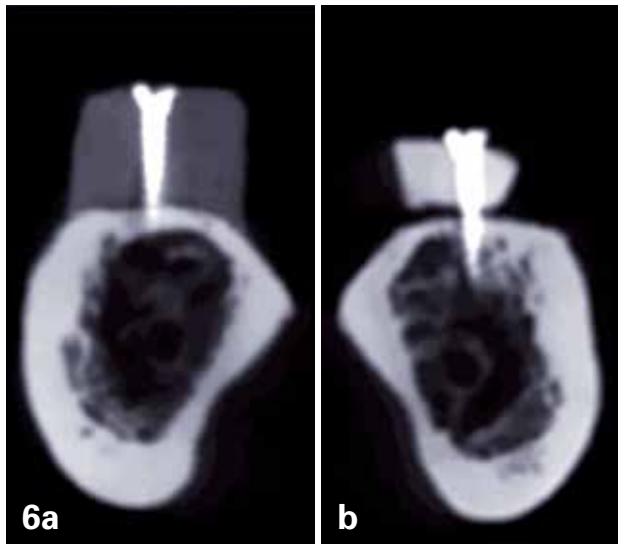
Dans la perspective d'applications cliniques de la bioimpression, l'une des principales problématiques est

de transférer au bloc opératoire les produits d'ingénierie tissulaire fabriqués au laboratoire. En effet, il faut pouvoir transférer des substituts souvent fragiles après leur fabrication et les adapter précisément sur le site opératoire. Ainsi, nous avons pu conceptualiser et mettre en œuvre la bioimpression *in vivo* et *in situ* sur un modèle de défaut osseux de calvaria chez la souris. Cette approche permet de fabriquer directement sur le site opératoire des assemblages biologiques complexes en trois dimensions afin de promouvoir la régénération tissulaire.

Nous avons pu montrer qu'il était possible d'imprimer une encre d'hydroxyapatite nano cristalline ainsi que des cellules souches mésenchymateuses par bioimpression laser sur la calvaria de souris, et que ces composants permettaient une certaine reconstruction osseuse sur le site d'impression [12].



5. Processus de fabrication des assemblages multicouche de membranes cellularisées. Résultats *in vivo* montrant les vaisseaux néoformés an sein de biomatériaux implantés chez la souris.



6. Évaluation de l'adaptation de greffes osseuses sur mandibule humaine *in vitro*. Le greffon sur mesure fabriqué en PLA par impression 3D (a) est mieux adapté que le greffon autologue préparé manuellement (b).

Biomatériaux sur mesure

Les grandes pertes de substance osseuse des maxillaires sont habituellement prises en charge par des greffes osseuses autologues [13]. Les principales limites de cette approche sont la morbidité associée au prélèvement autologue, la résorption du greffon qui est parfois

mal contrôlée dans le temps ainsi que la quantité limitée d'os disponible [14]. La méthode conventionnelle d'intégration d'un greffon implique l'adaptation manuelle de ce dernier pour obtenir un contact intime avec le site receveur. Les conséquences directes de cette technique sont un temps opératoire allongé et par conséquent un risque infectieux postopératoire plus important.

La CFAO permet aujourd'hui de dépasser certaines de ces limites avec les greffons osseux sur mesure. Il peut alors s'agir soit de l'adaptation manuelle de greffons sur des modèles en résine obtenus par impression 3D, ou bien de greffons préfabriqués par CFAO soustractive ou additive [15]. La première étape de ce processus est un examen d'imagerie 3D (scanner ou CBCT). Puis le fichier obtenu au format DICOM est traité dans des logiciels adaptés pour obtenir un modèle osseux 3D. Dans le cas de la fabrication manuelle du greffon, ce modèle du défaut va être imprimé en 3D en résine biocompatible et stérilisable et il servira de « patron » pour modeler le greffon, à distance du site opératoire. Dans le cas greffons préfabriqués sur mesure, une étape de conception informatique de la forme du greffon est nécessaire [16] avant de fabriquer la pièce par impression 3D ou par usinage.

Ces méthodes de fabrication du greffon sur mesure à partir de l'imagerie médicale permettent d'obtenir un ajustage avec le site receveur particulièrement satisfaisant (fig. 6).

Conclusion

Les avancées dans le domaine de la bioimpression donnent la possibilité d'imprimer un large choix de matériaux biologiques, cellules et biomatériaux. Ce sont des outils prometteurs, tant pour la recherche fondamentale, que pour l'ingénierie tissulaire et la médecine régénérative.

Ces technologies pourraient constituer, *via* l'élaboration *in vitro* de greffons osseux prévascularisés implantables ou la bioimpression *in situ* de composants biologiques, de nouvelles approches thérapeutiques innovantes pour favoriser la cicatrisation osseuse et le pronostic des actes chirurgicaux.

L'ensemble de ces méthodes pourrait conduire à des avancées considérables dans le domaine de la régénération osseuse, et révolutionner notre pratique clinique, notamment en parodontologie, implantologie et chirurgie orale.

POINTS ESSENTIELS

- La Conception et Fabrication Assistées par Ordinateur (CFAO) est à l'origine du développement de nouvelles technologies dans le domaine de l'ingénierie tissulaire.
- En ingénierie tissulaire osseuse, un des challenges majeurs consiste à favoriser la prévascularisation des matériaux implantés afin d'éviter les échecs d'intégration et les risques de nécrose des éléments implantés.
- La reproduction de la structure d'un tissu, à la fois à l'échelle macroscopique et microscopique, est essentielle pour garantir sa fonctionnalité.
- Les technologies de bioimpression pourraient permettre d'élaborer des substituts osseux sur mesure et aux propriétés optimisées pour optimiser la cicatrisation osseuse.
- L'ingénierie tissulaire et la médecine régénérative pourraient conduire au développement de nouvelles solutions thérapeutiques dans des disciplines comme la parodontologie, l'implantologie et la chirurgie orale.

Bibliographie

1. Chiapasco M, Casentini P, Zaniboni M. Bone augmentation procedures in implant dentistry. *Int J Oral Maxillofac Implants* 2009; 24 Suppl: 237-259.
2. Grageda E. Platelet-rich plasma and bone graft materials: a review and a standardized research protocol. *Implant Dent* 2004; 13 (4): 301-319.
3. Robertson A, Nutton RW, Keating JF. Current trends in the use of tendon allografts in orthopaedic surgery. *J Bone Joint Surg Br* 2006; 88 (8): 988-992.
4. Mironov V et al. Biofabrication: a 21st century manufacturing paradigm. *Biofabrication* 2009; 1 (2): 22001.
5. Klebe RJ. Cytoscribing: a method for micropositioning cells and the construction of two- and three-dimensional synthetic tissues. *Exp Cell Res* 1988; 179 (2): 362-373.
6. Bourget JM et al. Patterning of endothelial cells and mesenchymal stem cells by laser-assisted bioprinting to study cell migration. *BioMed Res Int* 2016; Forthcoming.
7. Ozbolat IT, Hospodiuk M. Current advances and future perspectives in extrusion-based bioprinting. *Biomaterials* 2016; 76: 321-343.
8. Smirani R. Étude de faisabilité d'un greffon biofabriqué pour traiter des récessions parodontales. *Médecine Buccale Chir Buccale* 2016; 22 (4): 331-335.
9. Groll J et al. Biofabrication: reappraising the definition of an evolving field. *Biofabrication* 2016; 8 (1): 13001.
10. Catros S et al. Layer-by-layer tissue microfabrication supports cell proliferation *in vitro* and *in vivo*. *Tissue Eng Part C Methods* 2012; 18 (1): 62-70.
11. Nishiguchi A et al. Effects of angiogenic factors and 3D-microenvironments on vascularization within sandwich cultures. *Biomaterials* 2014; 35 (17): 4739-4748.
12. Keriquel V et al. *In vivo* bioprinting for computer- and robotic-assisted medical intervention: preliminary study in mice. *Biofabrication* 2010; 2 (1): 14101.
13. Jacotti M, Barausse C, Felice P. Posterior atrophic mandible rehabilitation with onlay allograft created with CAD-CAM procedure: a case report. *Implant Dent* 2014; 23 (1): 22-28.
14. Laviv A, Jensen OT, Tarazi E, Casap N. Alveolar sandwich osteotomy in resorbed alveolar ridge for dental implants: a 4-year prospective study. *J Oral Maxillofac Surg Off J Am Assoc Oral Maxillofac Surg* 2014; 72 (2): 292-303.
15. Desobeau B, Fricain J-C, Catros S. Les greffons osseux sur mesure en chirurgie pré-implantaire. *Titane* 2016; Hors série: 49-55.
16. Plaud A. Élaboration d'un substitut osseux sur mesure par prototypage rapide [thèse d'exercice]. Université de Bordeaux; 2015.

Les auteurs n'ont pas de liens d'intérêt.

Correspondance
 Inserm U1026 - Bioingénierie Tissulaire (BioTis)
 146 rue Léo Saignat
 33076 Bordeaux

La fabrication additive recouvre un certain nombre de technologies en vogue qui suscitent l'intérêt des chercheurs en biomatériaux et en ingénierie tissulaire. La fabrication additive appliquée à la médecine régénératrice recouvre deux champs principaux : l'impression 3D de matière inerte ou bioactive et la biofabrication. Si l'impression 3D a pénétré le monde de la médecine réparatrice, les techniques de bio-assemblage et de bio-impression en sont encore à leur début. L'objectif de cet article est de faire un point non exhaustif sur ces différents aspects complémentaires de la fabrication additive au service de la médecine réparatrice, régénératrice et de l'ingénierie tissulaire. <

Impression 3D en médecine régénératrice et ingénierie tissulaire

Jean-Christophe Fricain, Hugo De Olivera, Raphaël Devillard, Jérôme Kalisky, Murielle Remy, Virginie Kériquel, Damien Le Nihounen, Agathe Grémare, Vera Guduric, Alexis Plaud, Nicolas L'Heureux, Joëlle Amédée, Sylvain Catros

Inserm U1026,
université de Bordeaux,
146, rue Léo Saignat,
33076 Bordeaux Cedex, France.
jean-christophe.fricain@inserm.fr

L'impression 3D

Reconstruire un tissu humain à la manière de la salamandre qui régénère un membre amputé est un mythe ancien déjà évoqué dans la mythologie grecque à propos d'Héraclès et l'Hydre de Lerne. Ce serpent régénérerait ses têtes à mesure qu'Hercule les tranchait. Faute de pouvoir régénérer les tissus humains, la solution la plus communément admise est le remplacement des structures lésées par une prothèse, une greffe ou une transplantation. Les premières prothèses de doigts ont été découvertes sur des momies égyptiennes datant de 900 à 700 avant Jésus Christ [1]. Classiquement, les prothèses antiques ou modernes sont fabriquées par usinage ou moulage. Cependant, depuis un peu plus de 20 ans un nouveau procédé de fabrication par empilement de couches successives a été développé : la fabrication additive qui est aujourd'hui assimilée à l'impression en trois dimensions (3D). Autrefois cantonnée à des industries de pointe comme l'aéronautique, l'impression 3D se développe et gagne le monde médical. Elle présente plusieurs avantages : faible coût de production pour des séries limitées ou la réalisation de prototypes, optimisation de la matière première qui n'est déposée que là où elle est nécessaire, fabrication

d'objets complexes, personnalisation, etc. Une des applications de l'impression 3D est la réalisation de substituts osseux [36] (→).

(→) Voir la Synthèse de F. Jordana et al., page ??? de ce numéro

sur mesure qui s'adaptent mieux aux défauts que les substituts ou greffes sculptés par le chirurgien (Figure 1). Les technologies d'impression 3D pénètrent le monde de la prothèse médicale. Récemment, un réseau de volontaires passionnés a créé un site en « open source » (libre d'accès) e-NABLE'S (<http://enablingthefuture.org/>) afin de créer des kits de prothèse de doigt et de mains sur mesure. Le principe est la mise à disposition gratuite de fichiers numériques pour « imprimer » les différentes pièces de la prothèse. Des tutoriels de montage y sont associés. Le coût des prothèses réalisées par ce type d'impression est d'environ 100 à 150 dollars contre 4 000 à 6 000 dollars pour une prothèse commerciale. Environ 1 500 de ces prothèses ont été créées [2]. Des médecins américains ont réalisé des implants trachéaux (attelles) sur mesure par impression 3D de polyester biorésorbable pour le traitement d'enfants présentant une bronchotrachéomalacie¹ sévère. Le premier enfant qui a été implanté a aujourd'hui 3 ans et son attelle est en cours de résorption sans qu'il n'y ait d'effet indésirable [3]. Les imprimantes 3D sont de plus en plus fréquentes au bloc opératoire. Elles permettent au chirurgien de préparer les interventions

¹ Ou trachéobronchomalacie (TBM) se traduit par une réduction de plus de 50 % du calibre des voies aériennes à l'expiration.

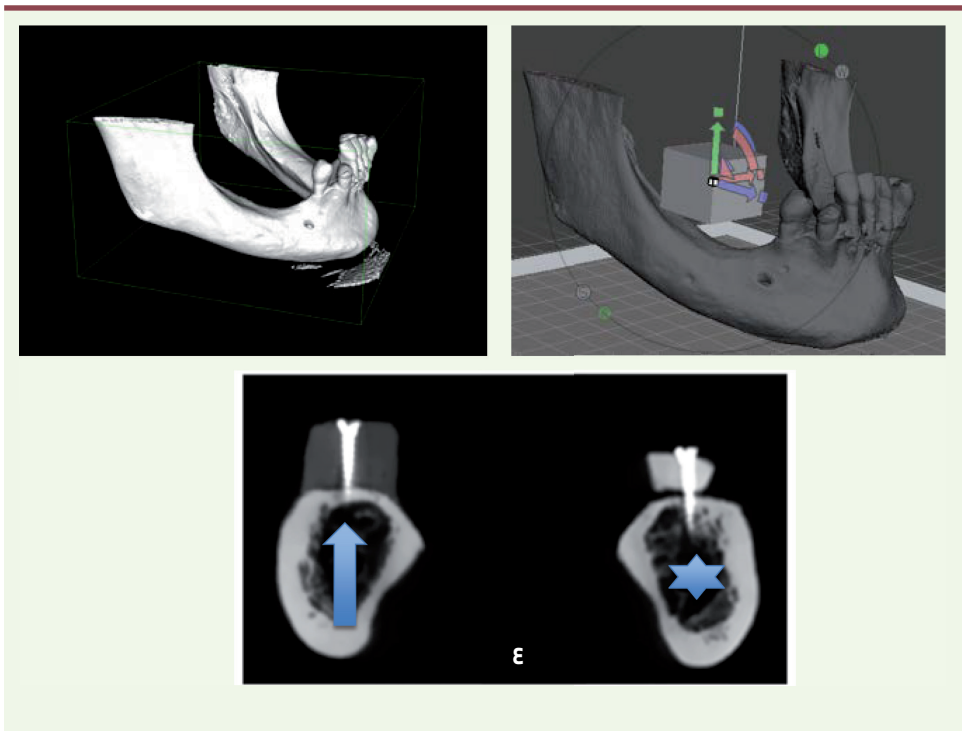


Figure 1. Réalisation d'un substitut osseux sur mesure par fabrication additive en PLA de grade médical à partir d'un fichier d'imagerie tridimensionnelle. L'adaptation du substitut créé par fabrication additive est parfaite (flèche) alors que l'autogreffe est située à distance de l'os receveur ce qui peut compromettre sa stabilité et sa bio-intégration. PLA de grade médical : matériau plastique utilisable en clinique.

planification ou des guides chirurgicaux [8].

- Les méthodes par extrusion de matériaux polymères utilisent des têtes d'impression montées sur des axes mobiles dans les trois plans de l'espace. Selon le maté-

riau, celui-ci est déposé à température ambiante ou en fusion. Après dépôt, il se solidifie par évaporation d'un solvant ou par diminution de la température. En modifiant le diamètre de la buse d'extrusion et le parcours de la tête d'impression, il est possible d'obtenir une grande variété de morphologies. Les matériaux utilisés sont principalement des polymères synthétiques [7].

En dehors des prothèses, peu de cas d'implantation de biomatériaux produits par prototypage rapide ont été décrits chez l'homme. Dans un modèle préclinique de défaut osseux alvéolaire réalisé chez le porc, Yeo *et al.* ont utilisé une greffe osseuse à base de PCL-TCP (*polycaprolactone/tricalcium phosphate*) fabriquée par un procédé d'extrusion à chaud et l'ont comparée à une autogreffe. Ils ont pu montrer que le biomatériau était très bien adapté [9] illustrant ainsi le fait que le prototypage rapide peut apporter un bénéfice en termes d'adaptation du matériau dans un défaut osseux. En revanche, ce biomatériau est peu efficace pour la régénération osseuse en l'absence de facteurs de croissance ou de cellules. Les méthodes de prototypage rapide, utilisées pour fabriquer des biomatériaux macroporeux, ont une résolution adaptée pour des applications clinique macroscopique. Cependant, cette résolution n'est pas adaptée pour contrôler le microenvironnement au niveau cellulaire. Il est probablement nécessaire de combiner plusieurs technologies pour satisfaire ces deux objectifs contradictoires : une macrostructure poreuse avec une microstructure contrôlée [10].

complexes en réalisant une réplique des tissus à opérer [4] et au chirurgien non expérimenté de préparer une intervention mais aussi de modifier l'indication de traitement grâce à une réalité qui est augmentée par rapport aux examens d'imagerie classique. Récemment, un fœtus présentant une masse susceptible de comprimer ses voies aériennes n'a pas été traité par chirurgie d'urgence, qui présentait un fort risque iatrogène pour la mère et l'enfant mais a reçu un implant facial réalisé grâce à l'impression 3D [5].

Il existe aujourd'hui de nombreuses méthodes de prototypage rapide, disponibles commercialement, pour des applications en ingénierie tissulaire : impression, extrusion, polymérisation laser.

- Les méthodes par impression utilisent l'impression d'une « colle » qui vient assembler des particules de poudre, placée dans un bac receveur. Chaque couche est assemblée progressivement pour former une structure 3D. Il persiste souvent des résidus de poudre au sein des matériaux finis, ce qui constitue une limite importante à l'utilisation de cette technique en ingénierie tissulaire [6].
- Les méthodes fondées sur l'interaction de lasers avec la matière fonctionnent sur le principe de la photopolymérisation de matériaux photosensibles. Des matériaux sous forme liquide ou solide (poudres) sont disponibles pour ces applications. Le frittage sélectif par laser utilise un laser CO₂ pour lier la poudre couche par couche. Les matériaux obtenus ont une architecture interne et externe contrôlée [7]. La stéréo-lithographie est l'une des premières méthodes de prototypage rapide utilisant cette méthode. Elle implique des résines liquides qui sont polymérisées par un laser UV, couche par couche. À la fin de la fabrication, l'objet est cuit dans un four afin de finaliser la polymérisation. La résolution obtenue est relativement faible mais cette méthode est déjà largement utilisée pour fabriquer des modèles de

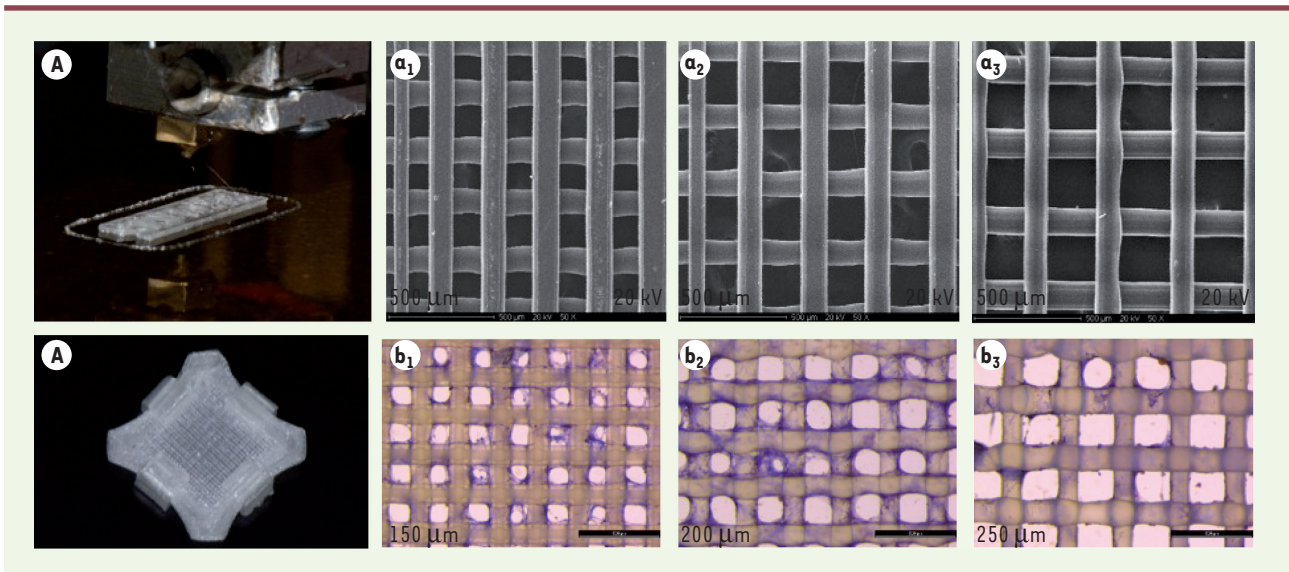


Figure 2. Procédé de biofabrication par la « technique sandwich ». Impression 3D de grilles de PLA (matériau plastique) (a) de porosités croissantes (a1, a2, a3). Ces grilles peuvent être superposées et maintenues par des clips (b) ce qui permet une cellularisation des différentes couches (b1, b2, b3) avant assemblage pour favoriser la colonisation cellulaire de la matrice imprimée selon une approche *bottom up*.

La biofabrication

Si l'on revient sur le graal de la régénération tissulaire évoqué au début de cette revue, la fabrication de prothèse n'est que palliative et ne restitue jamais la fonctionnalité du tissu *ad integrum*. C'est dans ce contexte que s'est développé l'ingénierie tissulaire, définie en 1993 par Langer et Vacanti comme « l'ensemble des techniques et des méthodes s'inspirant des principes de l'ingénierie et des sciences de la vie, utilisées pour développer des substituts biologiques pouvant restaurer, maintenir ou améliorer les fonctions des tissus » [11]. Dans l'ingénierie tissulaire classique, une matrice biologique, ou artificielle, que l'onensemence avec des cellules et/ou des facteurs de croissance est habituellement utilisée. Ce produit d'ingénierie tissulaire peut ensuite être implanté, ou avant son implantation, subir une maturation dans un bioréacteur. L'objectif de ce produit est d'être intégré dans le tissu afin de restaurer ou d'améliorer une fonction. Aujourd'hui, le concept d'ingénierie tissulaire dépasse le simple fait de la médecine régénératrice. Il tend à couvrir le champ des modèles biologiques de tissu physiologiques ou pathologiques afin de réduire le recours à l'expérimentation animale et ainsi développer des modèles pathologiques personnalisés permettant de tester différentes molécules avant de les utiliser chez un patient lui-même. L'un des verrous majeurs à l'utilisation de ces produits reste le manque de contrôle et de reproductibilité : de la matrice (géométrie, porosité, etc.), de la répartition des éléments biologiques dans cette matrice (cellules ou facteurs de croissance), de la vascularisation *in vitro* des tissus ou des organoïdes, et de la complexité des tissus à reproduire.

Une des réponses à ces verrous technologiques pourrait être la biofabrication. Cette technologie a pris depuis quelques années, une place

majeure. Le terme de *biofabrication* a été introduit en 1994, à propos de la fabrication de perles plates [12]. Au-delà des phénomènes naturels de biominéralisation, le terme de biofabrication est utilisé dans de nombreuses disciplines technologiques comme les biotechnologies ou la biologie de synthèse. La définition la plus large de la biofabrication est l'utilisation d'un procédé pour engendrer un produit présentant une fonction biologique. Dans le domaine de l'ingénierie tissulaire, la biofabrication recouvre la bio-impression et le bio-assemblage [13]. Ces deux techniques découlent d'une approche « *bottom up* », contrairement à l'ingénierie tissulaire classique qui est d'inspiration « *top down* ». L'approche *bottom up* consiste à réaliser des éléments tridimensionnels couche par couche alors que l'approche *top down* utilise des matrices 3D qui sont secondairement colonisées par des cellules ou des facteurs de croissance. La bio-impression et le bio-assemblage se différencient néanmoins par les unités assemblées et les technologies de fabrication utilisées.

Le bio-assemblage consiste à générer des unités multicellulaires sous la forme de fibres, d'agrégats ou de feuillets, ou présentant des structures complexes (organoïdes, micro-tissus) à l'aide de matrice extracellulaire (MEC). Le bio-assemblage consiste donc à fabriquer des structures hiérarchisées qui sont modulaires et possèdent une organisation en 2D ou 3D grâce à un assemblage automatisé d'éléments cellularisés. Ces éléments peuvent être fabriqués par auto-assem-

blages cellulaires ou en utilisant des briques élémentaires qui sont composées de cellules associées à des biomatériaux (Figure 2). Ces unités sont générées essentiellement à partir de techniques de micro-fluidique ou de moulage qui peuvent être couplées à l'impression 3D de matériaux [13].

La bio-impression

En 2010, Guillemot *et al.* ont défini la *bio-impression* comme « l'utilisation de technologies d'impression assistées par ordinateur permettant l'arrangement et l'assemblage de structures vivantes ou non, avec une organisation en deux ou trois dimensions, afin de produire des structures composites qui pourront être utilisées pour des applications en médecine régénératrice, pour des études pharmacocinétiques ou bien pour des travaux fondamentaux de biologie cellulaire » [14].

Principe général

La bio-impression est l'impression en deux dimensions (2D) ou trois dimensions (3D) de tissus biologiques vivants. C'est ce qui la distingue de ce que l'on nomme communément impression 3D où l'on imprime des matériaux. La bio-impression consiste donc à déposer, couche par couche, ou point par point, des cellules, des composants de la matrice extracellulaire (MEC), des facteurs de croissance et des biomatériaux grâce à une technologie d'impression pilotée par un ordinateur à partir d'un fichier numérique. Il s'agit donc d'un procédé de conception (CAO) et de fabrication (FAO) assistées par ordinateur, selon un procédé de fabrication additive grâce au couplage de l'ordinateur et d'une imprimante.

Une différence notable entre l'impression 3D qui imprime de la matière « inerte » et la bio-impression qui imprime de la matière vivante, est l'évolution du motif biologique. Il va subir des processus de fusion et de maturation qui vont évoluer en fonction du temps, de l'environnement et du motif imprimé. Cette évolution du produit biologique bio-imprimé a introduit la notion de *bio-impression 4D* où le temps représente la quatrième dimension [15]. Plus récemment, la notion de quatrième dimension a aussi été appliquée aux matériaux déformables qui évoluent dans le temps [16]. Si cette notion d'évolution est essentielle, il faut préciser qu'elle n'est pas spécifique de la bio-impression. Elle concerne également les produits d'ingénierie tissulaire, quel que soit le procédé d'élaboration.

Indépendamment de la technique utilisée, la bio-impression d'un tissu est réalisée en trois étapes : 1) conception du patron à imprimer assistée par ordinateur, 2) impression et 3) caractérisation.

Les imprimantes

Plusieurs bio-imprimantes ont été développées : imprimantes à jet d'encre, imprimantes par extrusion (les têtes d'impression sont constituées de micro-seringues) et imprimantes assistées par laser (Figure 3A). Les technologies d'impression seront plus ou moins efficaces selon le volume à imprimer et de la résolution souhaitée (Figure 3B).

La première micro-impression d'éléments biologiques (à base de fibronectine) a été réalisée par Klebe en 1988 par impression jet d'encre [16]. En 2006, Boland *et al.* ont utilisé des imprimantes de bureau modifiées afin de réaliser la micro-impression de cellules [17]. Aujourd'hui, des imprimantes thermiques (ou piézo-électriques) sont utilisées. L'impression jet d'encre thermique repose sur une cellule thermique qui produit une bulle de vapeur dont la pression génère une gouttelette au travers d'un pertuis de 30 µm à 200 µm de diamètre. Les imprimantes jet d'encre piézo-électrique utilisent sur une impulsion de tension qui génère une modification de forme d'un cristal qui contracte le réservoir d'encre. La détente du cristal piézo-électrique entraîne l'éjection de la goutte. Ces imprimantes permettent d'imprimer des cellules vivantes selon des motifs prédéfinis. Le principal inconvénient de ces imprimantes est la faible densité cellulaire utilisable (inférieure à 5 millions de cellules/mL), limite nécessaire pour prévenir l'obstruction des têtes d'impression. En ingénierie tissulaire, les imprimantes jet d'encre ont été utilisées *in situ* pour régénérer de la peau et du cartilage, ou *in vitro* pour réaliser des produits d'ingénierie tissulaire osseuse.

Des micro-seringues ont été développées pour imprimer des éléments biologiques par extrusion. Les biomatériaux (alginate, agarose, matrigel) sont extrudés de façon continue au travers de buses de quelques centaines de micromètre de diamètre. L'avantage de ces techniques est de réaliser l'impression dans le même temps des échafaudages (*scaffolds*) et des cellules. Les micro-seringues ont ainsi été utilisées pour réaliser des valves aortiques, des vaisseaux, ou des modèles tumoraux ou pharmacologiques.

Les techniques de bio-impression assistées par laser (*laser assisted bioprinting*, LAB) repose sur une source laser pulsée, une lame donneuse (cible) recouverte d'une fine couche de bio-encre à imprimer, et une lame receveuse disposée à quelques micromètres ou millimètres de la première qui reçoit les éléments imprimés. Des lasers pulsés nano ou femto-seconde² avec une longueur d'onde pouvant se situer dans l'infrarouge (1 064 nm) ou dans l'ultra-violet (193, 248, 266 et 355 nm) ont été utilisés. L'énergie laser peut être directement absorbée par l'encre (technique MAPLE-DW [*matrix assisted pulsed laser evaporation direct write*]), ce qui génère la formation d'un jet résultant de la vaporisation des premières couches moléculaires de la bio-encre au

² Type de lasers produisant des impulsions ultra-courtes dont la durée est de l'ordre de la nano ou femto-seconde.

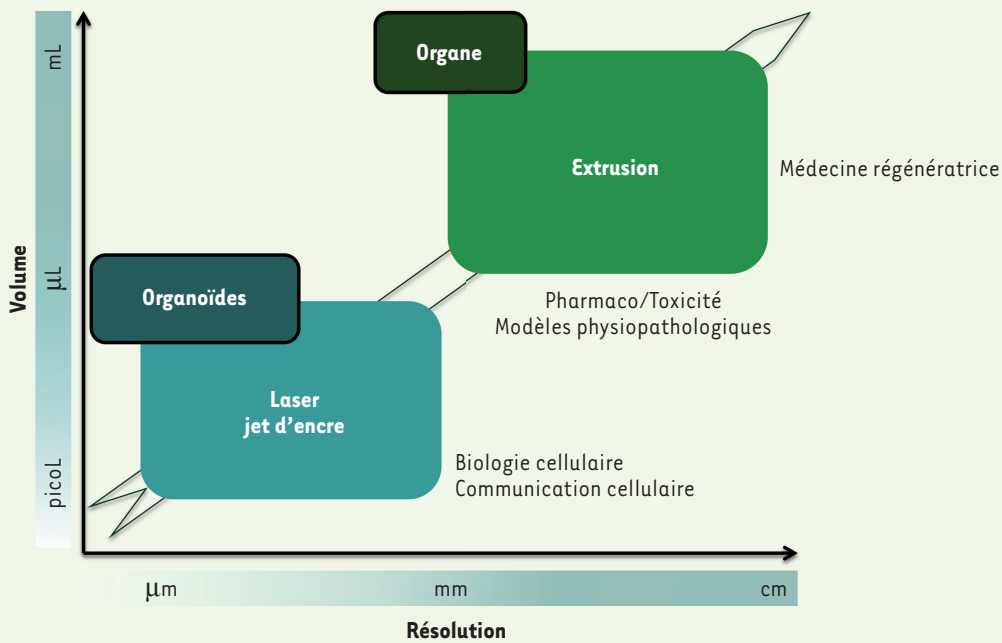
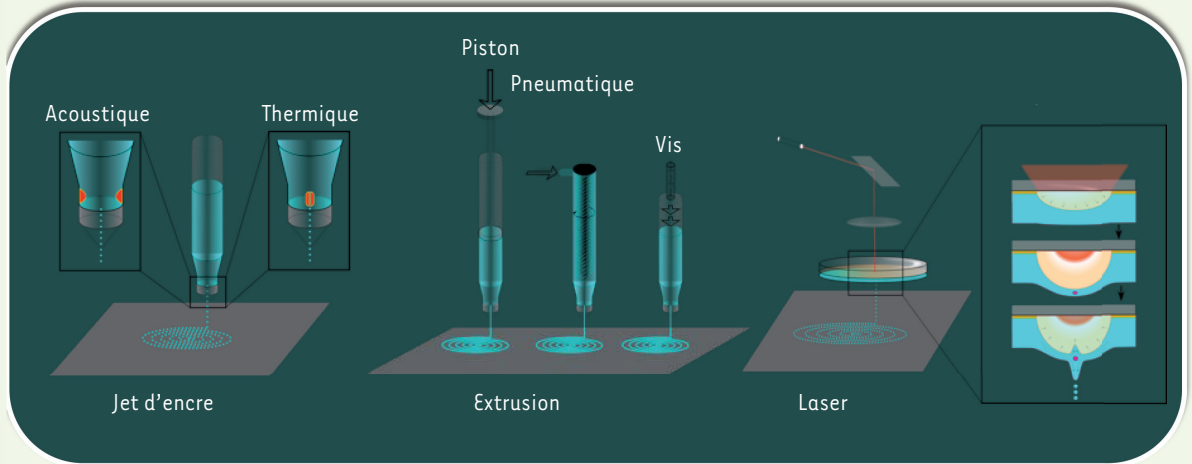


Figure 3. A. Principales technologies utilisées dans les bio-imprimantes. **B.** Le choix de la technologie dépend des impératifs de résolution et du volume à imprimer en fonction de l'application visée.

de bio-encre complexes composées d'hydroxyapatite, de cellules et de matrice extracellulaire [19-28]. Comparé à l'ensemencement d'un même

point de focalisation. Quand l'énergie laser n'est pas absorbée par la bio-encre, une couche transductrice/absorbante, qui permet de convertir l'énergie lumineuse en énergie thermique (dans le cas des BioLP, *biological laser printer*) et/ou mécanique (BA[*blister-actuated*]- et AFA[*absorbing film assisted*]-LIFT[*laser induced forward transfer*]), doit être utilisée. La couche absorbante est constituée de métal (or, titane, argent) de quelques dizaines de nm pour le BioLP, alors qu'elle est en polyimide pour le BA-LIFT. Le principe de l'éjection des gouttes par LAB dépend de la formation d'une poche de gaz secondaire à l'interaction de l'énergie laser avec la couche absorbante. En 2002, Ringeisen *et al.* ont mis en évidence la possibilité d'imprimer des protéines par MAPLE-DW sans que soient endommagés les épitopes qu'elles présentent, la structure de double brin d'ADN, ou la fonctionnalité de la phosphatase alcaline [18]. Le procédé a été amélioré par l'impression

nombre de feuillet par simple dépôt (approche *top-down*), l'impression de motifs cellulaires, couche par couche, sur des feuillets de polycaprolactone (approche *bottom-up*), augmente la prolifération des cellules *in vitro* et *in vivo* [21]. Les recherches actuelles s'orientent vers la bio-impression *in situ* assistée par laser qui consiste à imprimer directement, sur le patient, les composants cellulaires et matriciels selon une organisation définie pour favoriser la régénération tissulaire.

Les applications de la bio-impression 3D

La bio-impression de tissus vise deux types d'application : la création de modèle cellulaires et tissulaires, et la fabrication de produit d'ingénierie tissulaire pour la médecine régénératrice et réparatrice.

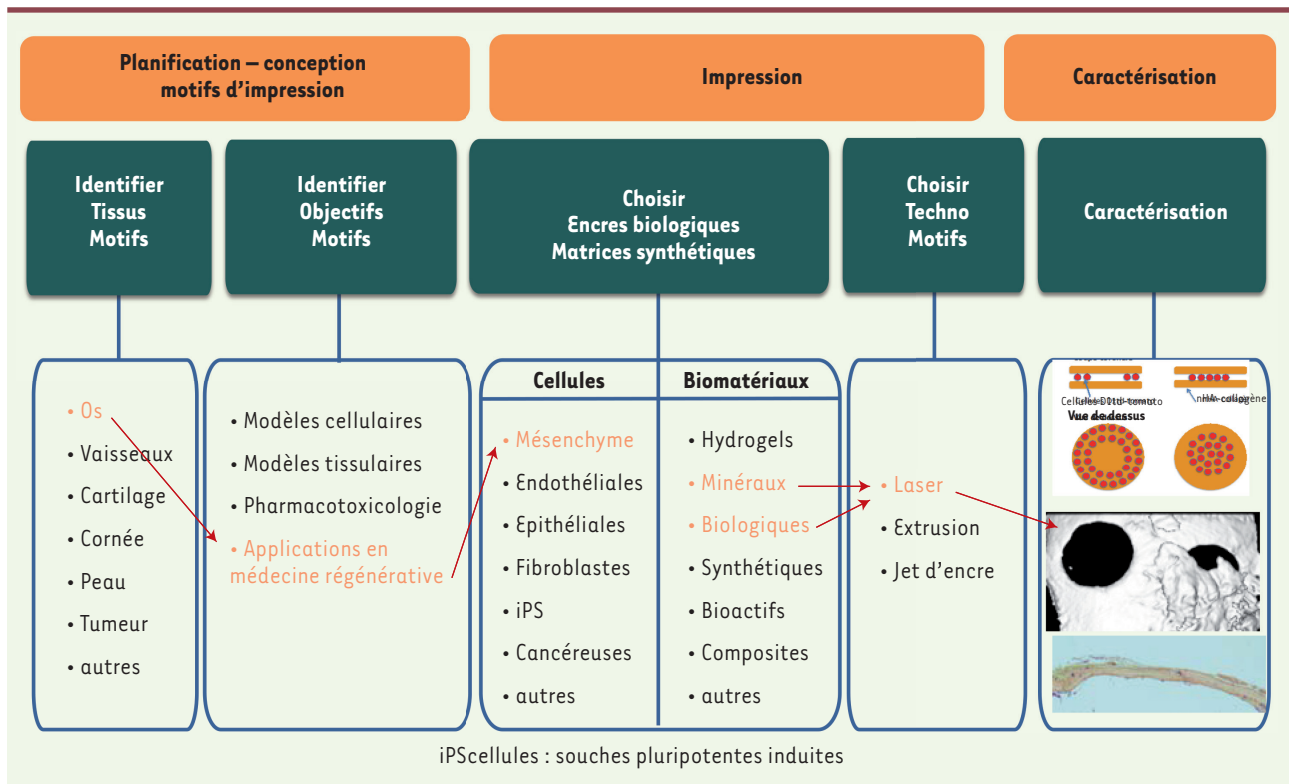


Figure 4. De la conception à la caractérisation du processus de bio-impression. Exemple de la bio-impression *in situ* de cellules souches (D1), d'une matrice d'hydroxyapatite et de collagène. L'impression des cellules sous forme de disque favorise la cicatrisation du défaut critique de calvaria sur la totalité de la surface alors que la cicatrisation est limitée à la périphérie pour les impressions en anneau.

Des modèles d'organe ou de tissu

Les modèles d'organe ou de tissu sont des outils permettant de tester, de façon reproductible et répétée, l'action pharmacologique de drogues. Ils représentent un enjeu important dans la sélection de molécules en fonction de leur efficacité et leur toxicité. Le développement de modèles tridimensionnels complexes est un enjeu important pour la recherche en pharmacologie du XXI^e siècle. Aujourd'hui, la plupart des modèles disponibles ne reproduisent que très partiellement la situation *in vivo* car leur architecture ne prend pas en compte la complexité des interfaces tissulaires et la perfusion vasculaire. Les puces de microfluidique permettent de résoudre partiellement l'exposition des tissus aux stimulations mécaniques des fluides et à la perfusion, mais elles ne reproduisent pas, en trois dimensions, la complexité des tissus. Dans ce contexte, des recherches sont développées pour bio-imprimer en 3D de façon reproductible des organoïdes complexes qui soient perfusables. Un autre espoir concerne l'impression d'organoïdes de tissus différents pour étudier leurs interactions. Peu de résultats sont actuellement disponibles. En 2008, R. Chang [29] a publié un modèle associant la microfluidique à l'impression 3D. La société Organovo, aux États-Unis, a commercialisé, en 2014, son premier modèle de foie qui intègre des hépatocytes, des cellules stellaires et des cellules endothéliales, imprimés dans une matrice. Ce modèle serait, selon la société, plus discriminant que les cultures 2D. La principale limite est le faible volume des structures hépatiques qui ne dépasse

pas quelques centaines de microns. Elles sont donc loin du modèle réel. Les modèles tumoraux en trois dimensions sont actuellement le plus souvent réalisés avec des techniques de sphéroïdes en suspension dans des gels (collagène, alginate, matrigel), reproduisant l'environnement extracellulaire, dans des structures de support (chitosane, polycaprolactone). Elles présentent comme limite l'absence d'interaction avec l'immunité et l'angiogenèse ainsi qu'un apport en nutriments insuffisant, ce qui a été partiellement résolu par les systèmes de microfluidique. Xu *et al.* ont imprimé des cellules d'ovaire cancéreuses et des fibroblastes dans du matrigel mais ils n'ont pas pu montrer la supériorité de leur modèle [30]. Un modèle de cancer du sein a été réalisé par impression 3D de cellules cancéreuses et de fibroblastes. Ce modèle a été validé en termes de réponse au traitement [31]. Plus récemment (cellules HeLa) ont été imprimées avec de la gélatine, du fibrinogène et de l'alginate, mimant ainsi l'environnement 3D. Après assemblage, 90 % des cellules étaient vivantes et avaient tendance à former des sphéroïdes alors que les cellules cultivées en 2D restaient en monocouches. Par comparaison aux cellules cultivées en 2D, ces cellules exprimaient plus de métallo-protéases et présentaient

une plus grande résistance à la chimiothérapie, les rapprochant de la situation clinique [32]. Les recherches actuelles tentent de modéliser le comportement des cellules tumorales dans leur environnement. Le développement de ces modèles 3D de tumeur par bio-impression représente donc un grand espoir pour la recherche pharmaceutique et le développement de traitements personnalisés.

La médecine régénératrice et réparatrice

Le deuxième domaine d'application concerne la médecine régénératrice et réparatrice. Dans ce domaine, on distingue la bio-impression *ex vivo* et la bio-impression *in situ*.

La bio-impression *ex vivo* consiste à créer des produits d'ingénierie tissulaire à l'aide de bio-imprimantes. Plusieurs tissus, de complexité variable, ont pu être reconstruits en utilisant ces technologies. Elle nécessite le recours à des bio-imprimantes complexes multi-têtes pour imprimer différentes encres biologiques afin de satisfaire à la complexité des tissus. La réalisation d'organes complexes comme le rein est une réalité qui reste lointaine, mais plusieurs groupes sont actuellement capables de produire de la peau. À moyen terme, les vaisseaux pourront partiellement être bio-imprimés. Un des défis actuels de l'ingénierie tissulaire est la production d'un réseau veineux, artériel et capillaire associé aux organes imprimés. Des vaisseaux ont pu être créés par impression 3D en imprimant des cellules endothéliales, des fibroblastes et de la fibrine dans un gel de collagène tunnelisé, à l'aide d'une encre thermolabile. Un réseau capillaire s'est développé entre les vaisseaux endothélialisés. La deuxième approche consiste à imprimer directement un réseau vasculaire de forme tubulaire autour d'un tube ou sur un matériau support (l'agarose) [33]. La maturation et la fusion des agrégats cellulaires en quelques jours forment les vaisseaux. Récemment, Atala *et al.* ont fait la démonstration qu'il était possible d'imprimer des tissus humains de taille compatible avec une utilisation clinique. Cela a été rendu possible grâce à la combinaison de plusieurs techniques : imagerie du défaut anatomique et conception assistée par ordinateur du tissu à reconstruire, réalisation d'un moule acellulaire dégradable pour donner la forme au tissu, impression d'hydrogels cellularisés réticulés après impression, et création d'un réseau de microtunnels pour favoriser le passage des nutriments [34]. Ils ont ainsi pu démontrer par des techniques combinées, intégrées dans une seule bio-imprimante, qu'il était possible de reconstruire : 1) une portion de mandibule de morphologie adaptée à la perte de substance (3,6 × 3,2 × 1,6 cm), et la fabrication d'un os de calvaria qui permet la régénération osseuse chez le rat ; 2) un muscle strié squelettique (15 × 1 × 5 mm) innervé et répondant à des stimulations électriques après implantation *in vivo* chez le rat ; le cartilage de l'oreille (3,2 × 0,9 × 1,6 cm), qui présente une forme complexe, qui a été maintenue deux mois après implantation pour maturation en site sous cutané chez des rats athymiques [34].

La bio-impression *in situ* consiste à bio-imprimer des cellules, de la matrice, des facteurs de croissance directement au niveau de la perte de substance du tissu pour favoriser sa régénération. Les bio-imprimantes pour imprimer le tissu ou l'organe manquant *in situ* au bloc opératoire est évidemment une perspective à long terme qui nécessitera de coupler

les imprimantes à des systèmes d'imagerie afin de visualiser le défaut tissulaire. L'avantage de cette approche est cependant de se dispenser des étapes de maturations *in vitro* qui sont longues, coûteuses et favorisent les risques de contamination. La limite actuelle de la bio-impression *in situ* est qu'elle ne peut être utilisée que pour des pertes de substance localisée en superficie comme la peau ou la calvaria³). Cette approche a été utilisée avec des imprimantes jet d'encre pour imprimer des cellules souches issues du liquide amniotique pour le traitement de brûlures [35]. Notre groupe a été utilisé une imprimante laser par pour imprimer de l'hydroxyapatite dans des défauts de calvaria [25]. Plus récemment nous avons pu imprimer du collagène, de l'hydroxyapatite et des cellules souches mésenchymateuses et nous avons observé que le motif cellulaire imprimé pouvait guider la cicatrisation (Figure 4). ♦

SUMMARY

3D biprinting in regenerative medicine and tissue engineering

Additive manufacturing covers a number of fashionable technologies that attract the interest of researchers in biomaterials and tissue engineering. Additive manufacturing applied to regenerative medicine covers two main areas: 3D printing and biofabrication. If 3D printing has penetrated the world of regenerative medicine, bioassembly and bioimprinting are still in their infancy. The objective of this paper is to make a non-exhaustive review of these different complementary aspects of additive manufacturing in restorative and regenerative medicine or for tissue engineering. ♦

LIENS D'INTÉRÊT

Les auteurs déclarent n'avoir aucun lien d'intérêt concernant les données publiées dans cet article.

RÉFÉRENCES

1. Finch J. The ancient origins of prosthetic medicine. *Lancet* 2011 ; 377 : 548-9.
2. Kuehn BM. Clinicians embrace 3D printers to solve unique clinical challenges. *JAMA* 2016 ; 315 : 333-5.
3. Zopf DA, Hollister SJ, Nelson ME, *et al.* Bioresorbable airway splint created with a three-dimensional printer. *N Engl J Med* 2013 ; 368 : 2043-5.
4. Malik HH1, Darwood AR2, Shaunak S3, *et al.* Three-dimensional printing in surgery: a review of current surgical applications. *J Surg Res* 2015 ; 199 : 512-22.
5. VanKoeveering KK, Morrison RJ, Prabhu SP, *et al.* Antenatal three-dimensional printing of aberrant facial anatomy. *Pediatrics* 2015 ; 136 : e1382-5.
6. Billiet T1, Vandenhoute M, Schelfhout J, *et al.* A review of trends and limitations in hydrogel-rapid prototyping for tissue engineering. *Biomaterials* 2012 ; 33 : 6020-41.
7. Leong KF, Cheah CM, Chua CK. Solid freeform fabrication of three-dimensional scaffolds for engineering replacement tissues and organs. *Biomaterials* 2003 ; 24 : 2363-78.

³ Partie supérieure de l'enveloppe osseuse du crâne.

RÉFÉRENCES

8. Bai S, Bo B, Bi Y, et al. CAD/CAM surface templates as an alternative to the intermediate wafer in orthognathic surgery. *Oral Surg Oral Med Oral Pathol Oral Radiol Endod* 2010 ; 110 : e1-7.
9. Yeo A, Cheok C, Teoh SH, et al. Lateral ridge augmentation using a PCL-TCP scaffold in a clinically relevant but challenging micropig model. *Clin Oral Implants Res* 2012 ; 23 : 1322-32.
10. Ovsianikov A, Mironov V, Stampf J, Liska R. Engineering 3D cell-culture matrices: multiphoton processing technologies for biological and tissue engineering applications. *Expert Rev Med Devices* 2012 ; 9 : 613-33.
11. Langer R, Vacanti JP. Tissue engineering. *Science* 1993 ; 260 : 920-6.
12. Fritz M, Belcher AM, Radmacher M, et al. Flat pearls from biofabrication of organized composites on inorganic substrates. *Nature* 1994 ; 371 : 49-51.
13. Groll J, Boland T, Blunk T, et al. Biofabrication: reappraising the definition of an evolving field. *Biofabrication* 2016 ; 8 : 013001.
14. Guillemot F, Mironov V, Nakamura M. Bioprinting is coming of age: report from the International Conference on bioprinting and biofabrication in Bordeaux (3B'09). *Biofabrication* 2010 ; 2 : 010201
15. Gao B, Yang Q, Zhao X, et al. 4D bioprinting for biomedical applications. *Trends Biotechnol* 2016 ; 34 : 746-56.
16. Klebe RJ Cytoscribing: a method for micropositioning cells and the construction of two- and three-dimensional synthetic tissues. *Exp Cell Res* 1988 ; 179 : 362-73.
17. Boland TI, Xu T, Damon B, Cui X. Application of inkjet printing to tissue engineering. *Biotechnol J* 2006 ; 1 : 910-7.
18. Ringeisen BR1, Chrisey DB, Piqué A, et al. Generation of mesoscopic patterns of viable *Escherichia coli* by ambient laser transfer. *Biomaterials* 2002 ; 23 : 161-6.
19. Ali M, Pages E, Ducom A, et al. Controlling laser-induced jet formation for bioprinting mesenchymal stem cells with high viability and high resolution. *Biofabrication* 2014 ; 6 : 045001.
20. Devillard R, Pagès E, Correa MM, et al. Cell patterning by laser-assisted bioprinting. *Methods Cell Biol* 2014 ; 119 : 159-74.
21. Catros S1, Guillemot F, Nandakumar A, et al. Layer-by-layer tissue microfabrication supports cell proliferation *in vitro* and *in vivo*. *Tissue Eng Part C Methods* 2012 ; 18 : 62-70.
23. Guillotin B, Guillemot F. Cell patterning technologies for organotypic tissue fabrication. *Trends Biotechnol* 2011 ; 29 : 183-90.
24. Mézel C, Souquet A, Hallo L, Guillemot F. Bioprinting by laser-induced forward transfer for tissue engineering applications: jet formation modeling. *Biofabrication* 2010 ; 2 : 014103.
25. Keriquel V1, Guillemot F, Arnault I, et al. *In vivo* bioprinting for computer- and robotic-assisted medical intervention: preliminary study in mice. *Biofabrication* 2010 ; 2 : 014101.
27. Guillotin B, Souquet A, Catros S, et al. Laser assisted bioprinting of engineered tissue with high cell density and microscale organization. *Biomaterials* 2010 ; 31 : 7250-6.
28. Guillemot F, Souquet A, Catros S, et al. High-throughput laser printing of cells and biomaterials for tissue engineering. *Acta Biomater* 2010 ; 6:2494-500.
29. Chang R, Nam J, Sun W. Direct cell writing of 3D microorgan for *in vitro* pharmacokinetic model. *Tissue Eng Part C Methods* 2008 ; 14 : 157-66.
30. Xu F1, Celli J, Rizvi I, et al. A three-dimensional *in vitro* ovarian cancer coculture model using a high-throughput cell patterning platform. *Biotechnol J* 2011 ; 6:204-12.
31. Wang C, Tang Z, Zhao Y, et al. Three-dimensional *in vitro* cancer models: a short review. *Biofabrication* 2014 ; 6 : 022001.
32. Zhao Y, Yao R, Ouyang L, et al. Three-dimensional printing of HeLa cells for cervical tumor model *in vitro*. *Biofabrication* 2014 ; 6 : 035001.
33. Ozbolat IT. Bioprinting scale-up tissue and organ constructs for transplantation. *Trends Biotechnol* 2015 ; 33 : 395-400.
34. Kang HW, Lee SJ, Ko IK, et al. A 3D bioprinting system to produce human-scale tissue constructs with structural integrity. *Nat Biotechnol* 2016 ; 34 : 312-9.
35. Skardal A, Mack D, Kapetanovic E, et al. Bioprinted amniotic fluid-derived stem cells accelerate healing of large skin wounds. *Stem Cells Transl Med* 2012 ; 1 : 792-802.
36. Jordana F, Le Visage C, Weiss P. Substituts osseux. *Med Sci (Paris)* 2017 ; 33 : ???.

TIRÉS À PART
J.C. Fricain

Subject Fwd: R: A kind request (from Prof. Angelo Basile)
From Sylvain Catros <sylvain.catros@u-bordeaux.fr>
To <vera.guduric@inserm.fr>
Date 26-07-2017 16:19



- Five Easy Steps for Using EMSS.DOCX (~221 KB)
- Permissions- AuthorInstructionsAUTHOR.DOCX (~19 KB)
- Permission Request Form.doc (~33 KB)
- Author-Permission-Log.xlsx (~21 KB)
- Abstract and keyword guide.pdf (~125 KB)
- ST Style Guide.doc (~92 KB)
- Basile-RenewableEnergy_Contributor_ST_Books_Manuscript_Guidelines.doc (~179 KB)

Sylvain Catros

Début du message transféré :

Expéditeur: "A. BASILE" <a.basile@itm.cnr.it>
Date: 1 juin 2017 à 09:52:06 UTC+2
Destinataire: "Sylvain Catros" <sylvain.catros@u-bordeaux.fr>
Cc: <V.Piemonte@unicampus.it>
Objet: R: A kind request (from Prof. Angelo Basile)
Répondre à: <a.basile@itm.cnr.it>

Dear Sylvain Catros,

I am very happy that you accepted my invitation.
I am sure taht with your also contribute we will have an excellent book!

You'll find all you need in attached.
Anyway, please do not hesistate to contact me incase of any problem/question.

Meanwhile you are going toreceive the official contract from Elsevier, my suggestioni s to start to prepare it. There are 8-9 months (for the final version) but the time runs very quickly!

Have a nice time with all my best wishes and regards,
Angelo

Da: Sylvain Catros [mailto:sylvain.catros@u-bordeaux.fr]
Inviato: mercoledì 31 maggio 2017 22:18
A: a.basile@itm.cnr.it
Oggetto: Re: A kind request (from Prof. Angelo Basile)

Dear Pr Basile
I will be glad to write this book chapter concerning the membrane scaffold that we are producing in our group for 3D culture experiments.
Could you please send me the full authors guidelines for this chapter?
Best Regards

--

Dr Sylvain CATROS

MCU-PH, Chirurgie Orale

UFR d'Odontologie et Inserm U1026

Université de Bordeaux

<http://www.biotis-bordeaux.com/>

Le 31/05/2017 12:06, A. BASILE a écrit :

Dear Prof. Sylvain Castros,

My name is Angelo Basile, senior researcher and previous director at the ITM-CNR, the research institute created by Prof. Enrico Drioli.

Prof. Vincenzo Piemonte (Italy), Prof. Mariacristina Annesini (Italy), Prof. Catherine Charcosset (France) and I have had approved by Elsevier the book-proposal "**Membrane applications in the Artificial Organs and Tissue Engineering**".

Being one of the chapters of our book strictly related to your specific expertise, it is my big pleasure to invite you and your research group to contribute in writing this one:

➤ **Ch. 1. Membrane scaffolds for 3D cell Culture**

The deadline for the final version, will be, more or less, 8-9 months.

The length of the chapter should be in the range 4.500-9.000 words (excluding tables, figures and references).

The number of co-writers of the chapter is up to you.

Could you please let me know if you are interested or not on it?

Thanks a lot in advance.

With all my best regards,

Angelo Basile

=====

Dr. Eng. Angelo Basile, Ph.D.

Full Prof. in Chem. Eng. Principles

Associate Editor of the *International Journal of Hydrogen Energy* - IJHE

Editor-in-chief of the *Int. J. of Membrane Science and Technology* - IJMST

Editor-in-chief of *Membrane Processes (Applications)*, a section of the international journal *Membranes*.

Senior Scientist

Institute on Membrane Technology of

the Italian National Research Council, ITM-CNR

c/o University of Calabria

via P. Bucci, cubo 17/C

87036 Rende (CS, Italy)

Ph.: +39 0984 49 2013 / 2011

Fax: +39 0984 402103

E-mail: a.basile@itm.cnr.it

Web-site: www.itm.cnr.it